Structural and functional analysis of CpBs4C, a *Xanthomonas* activated resistance protein from *Capsicum pubescens*

Dissertation

der Mathematisch-Naturwissenschaftlichen Fakultät

der Eberhard Karls Universität Tübingen

zur Erlangung des Grades eines

Doktors der Naturwissenschaften

(Dr. rer. nat.)

vorgelegt von

Danalyn R. Holmes

aus Ajax, Kanada

Tübingen

2023

Gedruckt mit Genehmigung der Mathematisch-Naturwissenschaftlichen Fakultät der Eberhard Karls Universität Tübingen.

Tag der mündlichen Qualifikation:	15.09.2023
Dekan:	Prof. Dr. Thilo Stehle
1. Berichterstatter:	Prof. Dr. Thomas Lahaye
2. Berichterstatter:	Prof. Dr. Suayb Üstün

TABLE OF CONTENTS

LIST OF PUBLICATIONS

Parts of this work have been published:

Danalyn R. Holmes, Robert Morbitzer, Markus Wunderlich, Hequan Sun, Farid El Kasmi, Korbinian Schneeberger, Thomas Lahaye.
A shortcut in forward genetics: concurrent discovery of mutant phenotype and causal mutation in Arabidopsis M2 families via MAD-mapping.
bioRxiv, published 2020. https://doi.org/10.1101/2020.06.29.177808

Moritz K. Nowack, Danalyn R. Holmes, Thomas Lahaye.
TALE-induced cell death executors: an origin outside immunity?
Trends in Plant Science, published 2022. https://doi.org/10.1016/j.tplants.2021.11.003

From the work presented in this thesis, the following manuscript is in preparation:

Danalyn R. Holmes, Robert Morbitzer, Kaltra Xhelilaj, Markus Wunderlich, Shouguang Huang, Rainer Hedrich, Julien Gronnier, Thomas Lahaye.
Xanthomonas activated resistance protein Bs4C has homologues in Solanaceous species and utilises calcium movement for cell death.
In preparation

From work not presented in this thesis, the following manuscripts have been published:

Yuan You, Grzegorz Koczyk, Maria Nuc, Robert Morbitzer, Danalyn R. Holmes, Edda von Roepenack-Lahaye, Shiji Hour, Axel Giudicatti, Carin Gris, Pablo A. Manavella, Laurent D. Noël, Paweł Krajewski, Thomas Lahaye.
The eINTACT system dissects bacterial exploitation of plant osmosignalling to enhance virulence.
Nature Plants, published 2023. https://doi.org/10.1038/s41477-022-01302-y

Deepak Shanthara, Gerald V. Minsavage, Vladmir Orbović, Gloria A. Moore, Danalyn R. Holmes, Patrick Römer, Diana M. Horvath, Thomas Lahaye, Jeffery B. Jones.
A promoter trap in transgenic citrus mediates a broad spectrum *Xanthomonas citri* pv. *citri* TALEs, including *in planta*-evolved derivatives.
Plant Biotechnology Journal, published 2023. https://doi.org/10.1111/pbi.14109

LIST OF ABBREVIATIONS

35S	Cauliflower mosaic virus 35S promoter
A. thaliana	*Arabidopsis thaliana*
A. tumefaciens	*Agrobacterium tumefaciens*
aa	amino acid
ABA	abscisic acid
AD	activation domain
An	anthesis
ANOVA	analysis of variance
ATP	adenosine triphosphate
BLAST	basic local alignment search tool
BN-PAGE	blue native polyacrylamide gel electrophoresis
bp	base pairs
Br	breaker
Ca^{2+}	calcium ion
$[Ca^{2+}]$	calcium ion concentration
$[Ca^{2+}]_{cyt}$	calcium ion concentration in the cytosol
$[Ca^{2+}]_{ER}$	calcium ion concentration in the endoplasmic reticulum
C. annuum	*Capsicum annuum*
C. pubescens	*Capsicum pubescens*
CaM	calmodulin
cDNA	complementary DNA
CDPKs	calcium dependent protein kinases
CDS	coding sequence
CFU	colony forming unit
coIP	co-immunoprecipitation
Col-0	Columbia-0
CPA	cyclopiazonic acid
CRISPR	Clustered Regularly Interspaced Short Palindromic Repeats
DALI	distance matrix alignment
DMSO	dimethyl sulfoxide
DNA	deoxyribunucleic acid
dNTPs	deoxyribonucleotide triphosphate
DPA	days post anthesis
dPCD	developmental programmed cell death
dpi	days post infection

dTALE	designer transcription activator-like effector
E. coli	*Escherichia coli*
EBE	effector binding element
ECA	ER-type Ca^{2+}-ATPases
ECW	Early Calwonder
EDTA	ethylenediaminetetraacetic acid
EMS	ethyl methanesulphonate
ER	endoplasmic reticulum
Estr	estradiol
ETI	effector triggered immunity
ETS	effector triggered susceptibility
EV	empty vector
FLIM-FRET	fluorescence lifetime imaging - Förster resonance energy transfer
FMO	flavin monooxygenase
GFP	green fluorescent protein
GO	gene ontology
GUS	β-Glucuronidase
HA	human influenza hemagglutinin
HCl	hydrochloric acid
HF	high fidelity
hpi	hours post infection
HR	hypersensitive reaction
HRP	horseradish peroxidase
hrp	hypersensitive response and pathogenicity
IP	immunoprecipitation
IP-MS	immunoprecipitation mass spectrometry
kb	kilo base pairs
kDa	kilo Dalton
KO	knockout
$LaCl_3$	lanthanum chloride
LB	Luria-Bertani
LR	light red
LRR	leucine-rich repeat
MES	2-Morpholinoethanesulphonic acid
MG	mature green
$MgCl_2$	magnesium chloride
MS	Murashige and Skoog

N. benthamiana	*Nicotiana benthamiana*
NaClO	sodium hypochlorite (bleach)
NB	nucleotide binding
NLR	nucleotide-binding domain leucine-rich repeat
NYG	nutrient yeast glycerol
OD_{600}	optical density at wavelength 600 nm
PAGE	polyacrylamide gel electrophoresis
PAMP	pathogen associated molecular pattern
PCD	programmed cell death
PCR	polymerase chain reaction
PDB	protein database
Pk	pink
pLGIC	pentameric ligand gated ion channel
PM	plasma membrane
PRRs	pattern recognition receptors
PTI	PAMP-triggered immunity
qPCR	quantitative polymerase chain reaction
R gene	resistance gene
Ref	reference
RFP	red fluorescent protein
RMSD	root mean square deviation
RNA	ribonucleic acid
RNA-seq	RNA sequencing
ROS	reactive oxygen species
RR	ripe red
RVD	repeat variable diresidue
S gene	susceptibility gene
S. lycopersicum	*Solanum lycopersicum*
SA	salicylic acid
SDS-PA	sodium dodecyl sulfate polyacrylamide
SEC	size exclusion chromatography
SNP	single nucleotide polymorphism
T-DNA	transfer DNA
T3SEs	type III secreted effectors
T3S	type III secretion system
T3SS	type III secretion signal
TALE	transcription activator-like effector

TFs	transcription factors
UV	ultraviolet
WT	wild type
Xcc	*Xanthomonas campestris* pv *campestris*
Xe	*Xanthomonas euvesicatoria*
Xops	*Xanthomonas* outer proteins
YEB	Yeast extract beef
C	Celsius
g	gravity
Hz	hertz
RT	room temperature
V	volts
v/v	volume per volume
w/v	weight per volume
M	molar
mM	millimolar
nM	nanomolar
µM	micromolar
pM	picomolar
cm	centimetre
mm	millimetre
nm	nanometre
L	litre
mL	millilitre
µL	microlitre
g	gram
mg	milligram
ng	nanogram

ABSTRACT

Since the identification of bacterial spot disease on pepper in the 1920s (Higgins, 1922), extensive research has been undertaken to identify mechanisms within the plant to counteract this disease. The resistance (R) protein CpBs4C in *Capsicum pubescens* was first identified through activation by AvrBs4 from *Xanthomonas euvesicatoria* (Strauß et al., 2012). Previous work discovered that CpBs4C induces cell death when ectopically overexpressed in *Nicotiana benthamiana*, localises to the endoplasmic reticulum, and there are homologues of CpBs4C in *Capsicum annuum* (Elsaesser, 2014; Wang et al., 2018). In this work, there were multiple CpBs4C homologues found in myriad different plant species, mainly within the order Solanales. The homologues found in *Solanum lycopersicum, C. annuum, C. pubescens,* and *N. benthamiana* all had a similar tertiary structure within the predicted transmembrane region of the proteins. By contrast, the non-transmembrane region of the Bs4C homologues proteins had a very diverse tertiary structure. It was found that there were three homologues in *N. benthamiana,* and they could be divided into two classes: cell death-inducing homologues and non-cell death-inducing homologues. Further investigation highlighted that the amino acid composition of the transmembrane region of the protein was the differentiating factor between the cell death-inducing homologues and the non-cell death-inducing homologues. Structural analysis of this transmembrane region of the Bs4C homologues identified a strong structural homology to the transmembrane regions of neurotransmitter receptors, which are pentameric ligand-gated ion channels. Structural prediction of the Bs4C transmembrane region in a pentameric fashion showed a striking similarity to the pentameric ring of neurotransmitter receptors. Similarly to neurotransmitter receptors, the Bs4C homologues from both *C. pubescens* and *N. benthamiana* were able to homo- and hetero-oligomerize, and CpBs4C was able to form a higher-order complex of at least 640 kDa. Proteomic analysis identified that the CpBs4C complex has a strong indication of binding to calcium-ATPases and that CpBs4C-induced cell death was able to be suppressed by a calcium channel inhibitor, indicating that the movement of calcium ions is vital for the induction of CpBs4C cell death. CpBs4C is also able to induce growth arrest in *Arabidopsis thaliana*, and the generation of a novel method for a forward genetic screen identified the exoribonuclease *AtXRN4* to be required for CpBs4C-induced growth arrest. The work presented herein identifies new mechanisms of action for the cell death induction of CpBs4C and hypothesises the native function of CpBs4C and its true origin.

ZUSAMMENFASSUNG

Seit der Entdeckung der bakteriellen Fleckenkrankheit bei Paprika in den 1920er Jahren wurden umfangreiche Forschungsarbeiten durchgeführt, um Mechanismen innerhalb der Pflanze zu identifizieren, die dieser Krankheit entgegenwirken. Das Resistenz (R)-Protein *CpBs4C* aus *Capsicum pubescens* wurde erstmals aufgrund seiner transkriptioneller Aktivierung durch das AvrBs4 Protein des bakteriellen Erregers *Xanthomonas euvesicatoria* identifiziert (Strauß et al. 2012). In früheren Arbeiten wurde festgestellt, dass *CpBs4C* eine Zelltodreaktion induziert, wenn es in *Nicotiana benthamiana* überexprimiert wird, das CpBs4C am endoplasmatischen Retikulum lokalisiert ist, und das es in *Capsicum annuum* CpBs4C Homologe gibt (Wang et al. 2018; Elsaesser 2014). In dieser Arbeit wurden mehrere CpBs4C-Homologe in verschiedenen Pflanzenarten, hauptsächlich innerhalb der Ordnung *Solanales*, gefunden. Die in *Solanum lycopersicum*, *C. annuum*, *C. pubescens* und *N. benthamiana* gefundenen Homologe wiesen alle eine ähnliche Tertiärstruktur innerhalb der vorhergesagten Transmembranregion der Proteine auf, während die Nicht-Transmembranregion der Proteine eine sehr unterschiedliche Tertiärstruktur aufwies. Es wurde festgestellt, dass es in *N. benthamiana* drei Homologe gibt, die in zwei Klassen eingeteilt werden können: Zelltod-induzierende Homologe und nicht Zelltod-induzierende Homologe. Die Strukturanalyse dieser Transmembranregion der Bs4C-Homologen ergab eine starke strukturelle Homologie zu Transmembranregionen von Neurotransmitter-Rezeptoren, die pentamere Liganden-gesteuerte Ionenkanäle sind. Die strukturelle Vorhersage der Bs4C-Transmembranregion in pentamerer Form zeigte eine auffällige Ähnlichkeit mit dem pentameren Ring von Neurotransmitter-Rezeptoren. Ähnlich wie bei Neurotransmitterrezeptoren waren die Bs4C-Homologe aus *C. pubescens* und *N. benthamiana* in der Lage, zu Homo- und Heterooligomeren zu assemblieren, und CpBs4C war in der Lage, einen Komplex höherer Ordnung von mindestens 640 kDa zu bilden. Proteomanalysen ergaben, dass der CpBs4C-Komplex eine Bindung an Kalzium-ATPasen aufweist und dass der durch CpBs4C ausgelöste Zelltod durch einen Kalziumkanal-Inhibitor unterdrückt werden konnte. Dies deutet darauf hin, dass die Bewegung von Kalziumionen für die Auslösung des CpBs4C-Zelltods entscheidend ist. CpBs4C ist auch in der Lage, einen Wachstumsstillstand in *Arabidopsis thaliana* zu induzieren, und über einen neu-entwickelten genetischen Ansatz wurden fünf neue Mutationen in der Exoribonuklease AtXRN4 identifziert, die in der Lage waren, den CpBs4C-induzierten Wachstumsstillstand zu unterdrücken. In der hier vorgestellten Arbeit wurden Wirkmechanismen der CpBs4C-vermittelten Zelltodinduktion identifiziert und Hypothesen zur Funktion von CpBs4C und seinen Ursprung aufgestellt.

1. INTRODUCTION

By the year 2050, the world population is projected to reach 9.7 billion inhabitants and exceed 10.4 billion in the mid-2080s, presenting a monumental challenge to global food security (United Nations, n.d.). The challenge of feeding an ever-growing population is compounded by the daunting reality of a rapidly changing climate and its looming threat to crop resilience. Crop failure is one of the most significant challenges to achieving food security, which can be caused by various biotic and abiotic factors, including pests, diseases, and unfavourable weather conditions (Seppelt et al., 2022). It is evident that plant immunity plays a vital role in mitigating and overcoming these challenges, and extensive research has been conducted using various approaches to identify components of plant immunity that can be translated into improving crop resilience. This thesis aims to unravel the underlying mechanisms that plants use to defend themselves against biotic challenges, like pests, the potential evolutionary development of these mechanisms, and explores innovative genetic techniques to rapidly identify novel components of these defence pathways.

1.1. The plant immune system and the Zig-Zag model

There is an ongoing struggle between pathogens and their hosts, known as an evolutionary arms race, where both pathogen and host are constantly escalating adaptations and counter-adaptations against each other in hopes of defeating the other. Pathogens rapidly evolve to overcome their hosts, and the hosts evolve to overcome their pathogen. The ability to surmount a response and protect oneself against an invading threat is a universal practice across all kingdoms of life.

Both animals and bacteria have two broad categories of immune responses, the innate immune system and the adaptive immune system. The innate immune system is typically a broad first line of defence that is genetically encoded within the host and acts effectively at defending itself without having any previous exposure to a pathogen in that lifetime (Kimbrell & Beutler, 2001). Adaptive immunity, on the other hand, can be thought of as immune memory or trained immunity that builds upon innate immunity, meaning that after the host is presented with a pathogen, it can remember this pathogen and develop a specific immune response towards it if it ever tries to infect the host again, ultimately preventing future recurring disease (Janeway et al., 2001). Plants, however, lack this adaptive immune system and rely solely on each cell's genetically encoded innate immune system to detect and defend against the

infection of pathogens (Jones & Dangl, 2006). It is generally accepted that there are two different branches of the plant immune system, the first being the ability to sense pathogens outside of the cell, and the second being the ability to act upon pathogen-injected molecules inside the cell.

As a framework for explaining the ever-evolving compatibility and incompatibility in plant-microbe interactions, the Zig-Zag model was proposed by Jones and Dangl, 2006 (Figure 1.1). This model fits well to plant pathogens with a biotrophic or hemibiotrophic lifestyle, for example, *Pseudomonas syringae* pv. *tomato* (*Pst*) and *Xanthomonas euvesicatoria* (*Xe*). In a simplified version, the first stage, PAMP-triggered immunity (PTI), enables the plant to sense a pathogen via pathogen-associated molecular patterns (PAMPs) at the cell periphery using pattern recognition receptors (PRRs). This PTI response typically involves a burst of extracellular reactive oxygen species (ROS), an increase in cytosolic calcium, and the activation of PTI-defence-related genes, resulting in transcriptional reprogramming of the cell, ultimately to curtail pathogen invasion (Couto & Zipfel, 2016). During the second stage, called effector-triggered susceptibility (ETS), pathogens establish virulence by injecting a suite of effector proteins into the host plant cell, which act as virulence factors to dampen or abolish the host plant's basal defence response and make way for colonisation (Nomura et al., 2006). The third stage, effector-triggered immunity (ETI), includes specific recognition of these effectors by the plant, either directly or indirectly, thereby leading to cell death of the infected tissue. The ability to sense effectors is mainly through a type of resistance (*R*) gene that encodes for nucleotide-binding leucine-rich repeat receptors (NLRs) (Jones et al., 2016). Upon sensing the action of an effector, NLRs initiate a rapid and robust immune response, known as the hypersensitive response (HR), which is a localised induction of programmed cell death (PCD) to limit pathogen growth (Greenberg, 1997). Over evolutionary time, the pathogen then evolves the ability to evade these NLRs, and then to counteract this, the plant host evolves new *R* genes to be able to sense and defend against these newly evolved effectors, which essentially is the initiation of the evolutionary arms race (Jones & Dangl, 2006). It has been recently highlighted that both plant immune responses, PTI and ETI, share many overlapping downstream responses and require each other for optimal immune response activation, eluding to the fact that the distinction between PTI and ETI is much more blurred than previously thought (Yuan et al., 2021). One central component linking PTI and ETI is the induced flux of calcium and the resulting signalling cascades that initiate further downstream responses (Köster et al., 2022).

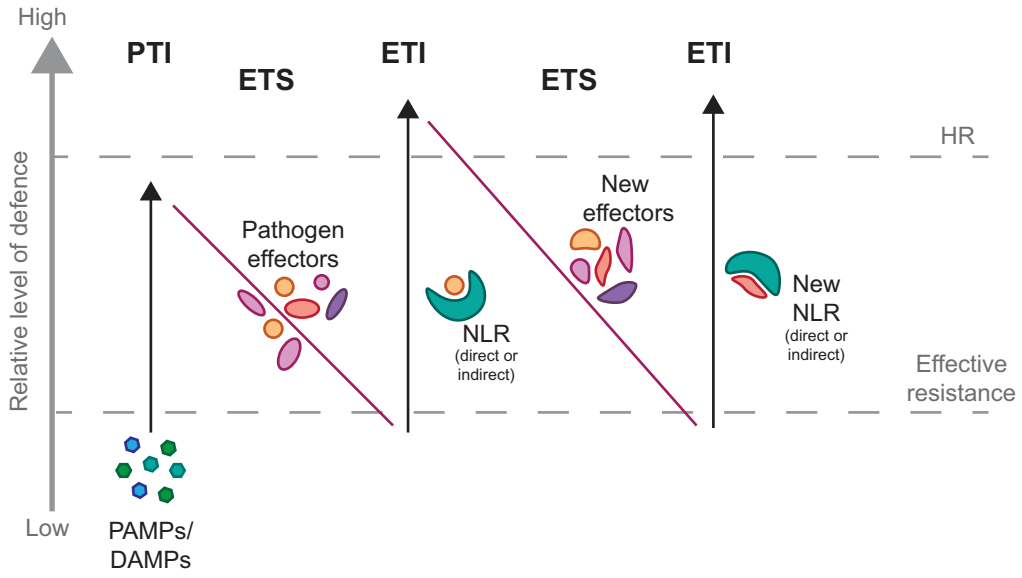

FIGURE 1.1. Zig-Zag model of the plant immune system.

This model represents the host's response to pathogenesis. In the first stage, plants are able to detect PAMPs which triggers an effective immune response, called PTI. In the second stage, pathogens deliver effector proteins into the plant to circumvent PTI responses, and this is called ETS. In the third stage, the bacterial effector is recognised by host plant NLRs, which induce a strong immune response, resulting in HR cell death, which is called ETI. PTI, Pattern-triggered immunity; ETS, Effector-triggered susceptibility; ETI, Effector-triggered immunity; NLR, nucleotide-binding leucine-rich repeat receptor; HR, hypersensitive response. Adapted from Jones and Dangl, 2006.

1.2. Calcium as a universal secondary messenger

Calcium (Ca^{2+} hereafter) is an essential component for the growth and development of plants and functions as a critical signalling molecule in various physiological processes. In plants, Ca^{2+} acts as a secondary messenger, transmitting signals to regulate multiple cellular processes such as gene expression, cell division, differentiation, and nutrient sensing, as well as responses to both abiotic and biotic stresses (Thor, 2019). The Ca^{2+} concentration within the cell is tightly regulated by a number of Ca^{2+} permeable channels, transporters, and pumps that enable the rapid and precise rises or reductions in the [Ca^{2+}], which are referred to as transients (Dodd et al., 2010). To be able to sense these transients, plants have evolved a wide range of various Ca^{2+} sensors, including calmodulins (CaM) and CaM-like proteins, calcineurin B-like proteins, and Ca^{2+}/CaM-dependent protein kinases (CDPKs), which are able to decode the Ca^{2+} signal and initiate a downstream response (Ranty et al., 2016). Ca^{2+}-mediated signalling pathways ultimately play crucial roles in plant adaptation and survival in rapidly changing environments, as well as in plant immunity.

1.2.1. The role of Ca^{2+} in immunity

Ca^{2+} signalling plays a crucial role in the initiation and propagation of PTI. One of the earliest immune responses that occurs in plants after the detection of a pathogen is an increase in Ca^{2+} into the cytosol via Ca^{2+} permeable channels, transporters, and pumps (Seybold et al., 2014). Membrane-bound Ca^{2+} permeable channels allow for a rapid increase in cytosolic [Ca^{2+}] ([Ca^{2+}]$_{cyt}$ hereafter) which is then interpreted by various Ca^{2+} sensor proteins that initiate downstream responses (DeFalco et al., 2009). This moderate increase in [Ca^{2+}]$_{cyt}$ is perceived by CDPKs, which are then able to phosphorylate target proteins in the desired PTI pathways. For example, in *Arabidopsis thaliana* (Arabidopsis hereafter), the activation of CDPKs transmits the signal to activate a ROS burst, and they are also able to activate transcription factors that induce the expression of immunity-related genes (Boudsocq et al., 2010; Dubiella et al., 2013). Moreover, the Ca^{2+}-dependent phosphorylation cascade leads to the closure of the plant stomata to close off key points of entry for pathogens (Thor et al., 2020). In addition to the vital role that Ca^{2+} has in the multitude of downstream responses to PRR activation, it also has a critical role in the induction of ETI.

ETI signalling typically involves a longer and more sustained increase in [Ca^{2+}]$_{cyt}$ levels, as opposed to the rapid transient induced by elicitors in PTI (Köster et al., 2022). Recent breakthroughs in the NLR field confirmed the long-predicted hypothesis that NLRs form large multimeric complexes and act as ion channels (Dangl & Jones, 2019; Jones et al., 2016). With structural analysis of the Arabidopsis NLR ZAR 1 (HOPZ-ACTIVATED RESISTANCE 1), it was shown that upon detection of the bacterial effector AvrAC-mediated changes in the cell, ZAR1 is activated and forms a symmetrical pentameric structure, termed the ZAR1 resistosome (Wang et al., 2019). The ZAR1 resistosome pentamer encircles a central funnel and was hypothesised to embed itself into membranes. Further analysis indeed confirmed that the ZAR1 resistosome, upon activation, forms a pentamer and inserts itself in the plasma membrane, where it becomes a Ca^{2+} permeable ion channel. This Ca^{2+} channel activity and passive movement of Ca^{2+} into the cell causes ZAR1-mediated cell death (Bi et al., 2021).

Another subfamily of NLRs, called helper NLRs because they aid in the activation of NLRs that sense effector action, were also found to be Ca^{2+} permeable channels (Jacob et al., 2021). Precisely, the Arabidopsis helper NLRs NRG1.1 (N REQUIREMENT GENE 1) and ADR1 (ACTIVATED DISEASE RESISTANCE 1) both form higher-order homo-oligomeric complexes and form Ca^{2+} permeable ion channels at the plasma membrane. The negatively charged glutamic acid (E) in the inner lining of the central pore of the ZAR1 resistosome, E11, the E in the predicted inner ring of NRG1.1, E14, and the aspartic acid (D) in the predicted ring of

ADR1 (D11), are all believed to be the selective negative filter for the positively charged Ca^{2+} ion to induce a rapid Ca^{2+} influx into the cell and initiate a swift cell death response (Bi et al., 2021; Jacob et al., 2021).

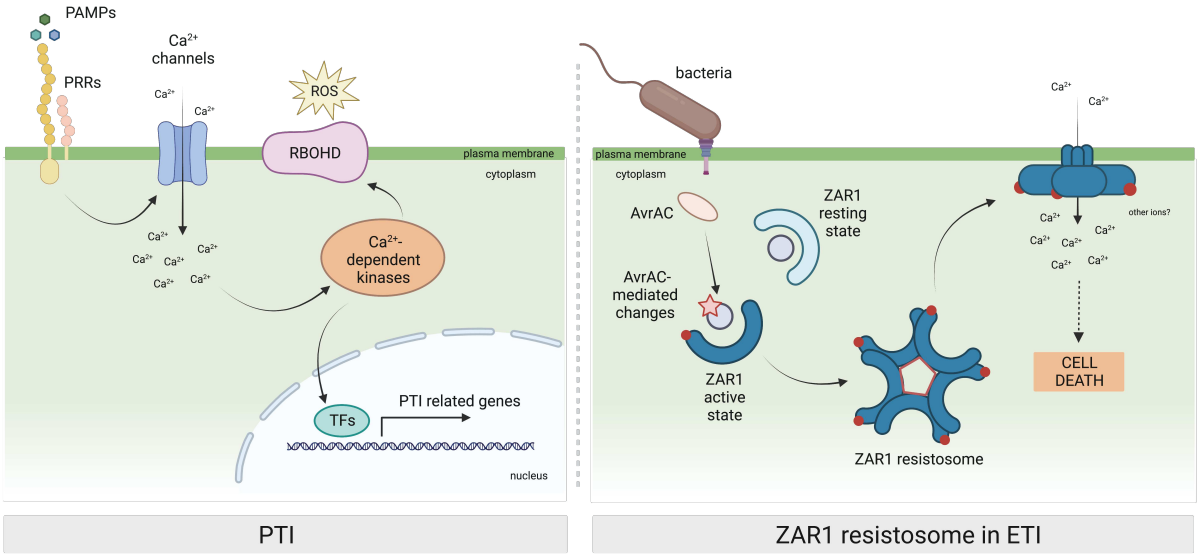

FIGURE 1.2. Ca^{2+} signalling in PTI and ETI.

LEFT PANEL | Ca^{2+} signalling in PTI. Upon the perception of PAMPs, the PRRs initiate a downstream signalling cascade, starting with an increase in cytosolic Ca^{2+} concentrations. This increase in Ca^{2+} intracellularly activates Ca^{2+}-dependent protein kinases, which go on to phosphorylate RBOHD, triggering the production of an extracellular ROS burst, in addition to the phosphorylation of transcription factors that activate PTI-related genes, ultimately changing the transcriptional landscape of the cell.
RIGHT PANEL | Ca^{2+} signalling in ZAR1 resistosome mediated ETI. Bacteria inject effectors into the host cell, specifically AvrAC, which alters the composition of host proteins. This AvrAC-mediated change in host proteins is detected by ZAR1, which then becomes active and forms a pentameric ring structure. This pentameric ring structure then inserts itself into the plasma membrane, where it acts as a Ca^{2+} permeable channel that induces an increase in cytosolic Ca^{2+} concentrations, with the possibility of other cations making their way inside the cell as well. This sustained increase in cytosolic Ca^{2+} causes the cell to undergo cell death.
PTI, PAMP-triggered immunity; PAMPs, pathogen-associated molecular patterns; PRRs, pattern recognition receptors; ROS, reactive oxygen species; RBOHD, respiratory oxidase homologue D; TFs, transcription factors; ZAR1, HOPZ-ACTIVATED RESISTANCE1; ETI, effector-triggered immunity. Figures from Köster et al., 2022 were used as inspiration for this figure. Image created using Biorender.com.

Moreover, lanthanum chloride, $LaCl_3$, a broad Ca^{2+} channel blocker that was found to inhibit the cell death induction of the NLR RPM1 (RESISTANCE TO PSEUDOMONAS SYRINGAE PV. MACULICOLA1), was also found to inhibit the induction of cell death by ZAR1, NRG1.1, and ADR1, suggesting a relatively simple pharmacological proxy to test the use or requirement of Ca^{2+} channels in both NLR and *R* gene-mediated resistance (Bi et al., 2021; El Kasmi et al., 2017; Jacob et al., 2021). The resulting action of this prolonged sustained increase in $[Ca^{2+}]_{cyt}$ in the cell has yet to be elucidated. However, there have been speculations that either

the $[Ca^{2+}]_{cyt}$ is too high and becomes toxic to the cell, that this increase in $[Ca^{2+}]_{cyt}$ could induce further Ca^{2+} signalling processes, or that this channel within the plasma membrane causes the cell to lose the electrochemical gradient of Ca^{2+} with its surroundings, ultimately causing cell death (Köster et al., 2022).

1.2.2. The role of Ca^{2+} in plant organelles

Within the cell, the fluctuation of $[Ca^{2+}]$ in different organelles varies in spatiotemporal parameters in a stimulus-specific manner, and lays the foundation for organelles to generate their own Ca^{2+} signals independent of the change in $[Ca^{2+}]_{cyt}$ (Pirayesh et al., 2021). The endoplasmic reticulum (ER) has the highest resting concentration of Ca^{2+}, which is why it is referred to as a Ca^{2+} store, followed by the vacuole, the mitochondria, then the apoplast, then the nucleus, and the cytoplasm having the lowest concentration (Pirayesh et al., 2021). The tight regulation of $[Ca^{2+}]$ in each organelle is critical to the health of the cell, and the fine-tuned movement of Ca^{2+} between the plant cell's organelles allows for the function of signal transduction networks to appropriately respond to specific stresses (Stael et al., 2012).

The flux of Ca^{2+} from an area of high concentration to a place of low concentration is conducted via Ca^{2+} permeable ion channels that facilitate the passive transport along the electrochemical gradient, and the movement of Ca^{2+} from an area of low concentration to a place of high concentration is conducted via Ca^{2+} pumps (Ca^{2+}-ATPases) and Ca^{2+}/H^{+} transporters (Demidchik et al., 2018). Ca^{2+} permeable channels are finely tuned and tightly regulated, only becoming active for a specific reason, to avoid an uncontrolled flow of Ca^{2+}. For example, the flux of Ca^{2+} into the cytosol after PAMP perception is controlled via the plasma membrane localised proteins CNGC2 and CNGC4 (CYCLIC NUCLEOTIDE-GATED CHANNEL) which form a functional Ca^{2+} channel, facilitating the passive flux of Ca^{2+} from the apoplast into the cytoplasm upon activation, and initiating the aforementioned downstream processes (Pirayesh et al., 2021; Tian et al., 2019). Where on the other hand, Ca^{2+}-ATPases, like ER-type Ca^{2+}-ATPases (also referred to as ECAs), actively transport Ca^{2+} from the cytosol, an area with low $[Ca^{2+}]$, into the ER, which has a very high $[Ca^{2+}]$, and has proven to have an important function in the control of PCD during innate immune responses against a fungal pathogen (Zhu et al., 2010). However, the specifics and downstream responses of this Ca^{2+} influx into the ER have yet to be explained. Ca^{2+}-ATPases have further been implicated in a wide range of developmental and stress responses both as an inducer of Ca^{2+}-dependent signal transduction networks but also as a termination mechanism for increases in $[Ca^{2+}]_{cyt}$ to restore basal $[Ca^{2+}]_{cyt}$ following a stress response (García Bossi et al., 2020). The function and

utilisation of ER-type Ca^{2+}-ATPases has not yet been investigated in great detail, however, the identification of Ca^{2+}-regulating genes and subsequent encoded proteins in recent years has highlighted the vital role that Ca^{2+}-regulating proteins have in plant stress responses and underscores the fact that there are many more that have yet to be identified.

1.3. The identification of causal mutations using EMS-based forward genetic screens

Numerous signalling components mentioned in the previous sections were identified using forward genetic screens in Arabidopsis. Forward genetic screens in Arabidopsis are powerful tools to identify components of biological pathways without prior knowledge of their molecular function. The Arabidopsis genome is diploid, sequenced, and well-defined, with many resources easily accessible (Arabidopsis Genome Initiative, 2000). Mutagenesis of Arabidopsis largely relies on ethyl methanesulphonate (EMS) induced mutations due to the high mutagenesis rate and accessibility of the chemical (Page & Grossniklaus, 2002). EMS mutagenesis often leads to mutations in alleles that ultimately translates into a dramatic change in phenotype. The mutations generated by EMS can be dominant, however, recessive EMS mutations are most prevalent. The M0 generation is where the EMS-induced mutation is introduced, the M1 generation has the mutation in a heterozygous fashion, and the M2 generation is ultimately segregating for this mutation. After the identification in the M2 generation of an individual plant that has a change in phenotype, it is typically backcrossed to the parental non-mutagenized plant, and then allowed to self-cross until the F2 generation is reached. The established F2 population is likely segregating for the potential recessive causal mutation, and individual plants within the F2 segregating population with the change in phenotype are collectively studied by next-generation sequencing (NGS) of DNA from the bulked mutants. Observed DNA sequences can be used for genetic mapping of the phenotype and to potentially discover the causal mutation (Schneeberger et al., 2009). From the mutagenesis of the parental seeds (M0 generation) to identifying a potential causal mutation in the F2 segregating population, the average time of this traditional process is at least one year.

For example, a forward genetic screen was used to identify specific components in the signalling cascade of a PAMP-induced increase of $[Ca^{2+}]_{cyt}$: The wildtype (WT) Arabidopsis line, Columbia-0 (Col-0) was transformed with a fluorescence-based Ca^{2+} sensor for visual screening and termed the Col-0^{AEQ} reporter line (Knight et al., 1991). This Col-0^{AEQ} line was EMS-mutagenized and mutants that showed an alteration in $[Ca^{2+}]_{cyt}$ after PAMP treatment

were sought out and investigated (Tian et al., 2019). This screen identified multiple *CNGC* genes, specifically *CNGC2* and *CNGC4*, which are now considered vital to the Ca^{2+}-based PTI response. Similarly, the NLR protein RPM1 was also identified in an EMS-based forward genetic screen (Tornero et al., 2002), ultimately showing the successful nature of EMS screens in identifying immunity-related signalling components.

The employment of EMS-based forward genetic screens has endless possibilities for identifying important signalling components in biological pathways *in planta*. However, the workload and time required to establish populations segregating for the causal mutation is substantial. Traditional identification methods can take a minimum of one year, from EMS mutagenesis of WT seeds (generating M0 seeds) to the isolation of F2 bulked DNA. Faster methods are currently being developed and utilised, such as identifying mutations in the M3 generation, negating any backcrossing to the parental line (Hodgens et al., 2020). Nevertheless, there is still room for improvement with this time frame, and potentially identifying mutations in an earlier generation. EMS-based forward genetics screens using the time-consuming traditional methods, like genetic mapping with PCR-based markers followed by complementation analysis of candidate genes, have been used in Solanaceous species of pepper and tomato to identify causal mutations (Arisha et al., 2015; Garcia et al., 2016). The development of faster methods of identifying causal mutations will be beneficial for Arabidopsis, and it will be especially vital for the application in agriculturally essential crops with a longer generation time, like tomato and pepper, to identify and produce more climate- and pathogen-resilient crops.

1.4. Origins of *Capsicum* species and bacterial spot caused by *Xanthomonas*

The genus *Capsicum* is commonly referred to as pepper, chilli pepper, and paprika and belongs to the *Solanaceae* family. The distribution origins of *Capsicum* are believed to have originated in Mexico, extending south to Columbia. The domestication of this genus resulted in five major species, *C. annuum, C. frutescens, C. chinense, C. baccatum, and C. pubescens* (Basu & De, 2003). *Capsicum* species are typically well adapted to hotter climates with an optimal growing temperature between 21 – 29 ^{o}C. However, both *C. pubescens* and *C. baccatum* were cultivated from a natural habitat with average daily temperatures ranging between 11 – 12 ^{o}C (De Swart et al., 2006). Due to their multitude of uses in both food and non-food products, *Capsicum* species are grown in most countries worldwide and cover 1.93 million hectares of crop-growing land across the world, with China being the largest producer (Penella & Calatayud, 2018).

1.4.1. Bacterial spot of pepper caused by *Xanthomonas*

As the cultivation of pepper species increased in popularity, so did the emergence of pests and diseases that hindered the viability of the pepper yield. Many pathogens pose a threat to *Capsicum*, including fungi, viruses, insects, and bacteria. Bacterial spot, caused by species of the bacterial genus *Xanthomonas*, was first described on pepper in 1922 after being found in the state of Georgia, in the United States of America (Higgins, 1922). Bacterial spot is a disease of pepper which can be characterised by necrotic lesions found on the fruit, leaves, stems, petals, and flowers, ultimately causing a reduction in fruit quality and yield losses in both greenhouses and in the field (Potnis et al., 2015). Fruit yield losses can range between 23% to 44% caused by severe cases of bacterial spot, and indirect losses caused by severe infection can be observed through leaf shedding and exposing the fruit to direct sunlight (Bashan et al., 1985).

There are three distinct species of *Xanthomonas* that bacterial spot of pepper can be incited by: *X. euvesicatoria, X. vesicatoria,* and *X. gardneri* (Jones et al., 2004; Osdaghi et al., 2021). *Xanthomonas* species are widely distributed in different geographical areas due to their transmission via contaminated seeds, rain, and wind (Gitaitis & Walcott, 2007). The optimal range of temperatures for *Xanthomonas* to grow and proliferate is in a humid environment between 24 ºC and 27 ºC (Shu & Yang, 1990), and overlaps quite nicely with the optimal growing conditions of most *Capsicum* species. In these humid and warm conditions, it is ultimately more favourable for the pathogen to proliferate, causing the devastating crop losses mentioned previously.

1.4.2. Type III secreted effectors and *Xanthomonas* virulence

Xanthomonas infection begins on healthy leaf tissue by entering the plant via natural openings and wounds and invading the host plant by colonising the apoplastic space (Ryan et al., 2011). Here, they use the type III secretion system (T3S), which is encoded by the *hrp* (*hypersensitive response and pathogenicity*) gene cluster*,* to translocate proteins into the host plant cells (Bonas et al., 1991; White et al., 2009). These proteins are classified as type III-secreted effectors (T3SEs) and are typically named *Xanthomonas* outer proteins (Xops), except for a particular class of effectors, the transcription activator-like effectors (TALEs). T3SEs were first identified due to the fact that they act as avirulence (Avr) proteins that trigger immune reactions *in planta* (Klement, 1982; Staskawicz, 2001). To date, there are 79 T3SEs identified from *Xanthomonas* (Koebnik, 2023), many with independent or redundant virulence functions,

however, many of these mechanisms have yet to be characterised. By definition, the virulence mechanisms of these effectors have a role in helping the bacteria to colonise the host plant and to promote disease. These effectors can localise to different subcellular compartments of host cells and often aim to interfere with host immune responses (Büttner & He, 2009). For example, XopS from *X. euvesicatoria* (*Xe* hereafter) targets and stabilises the transcriptional regulator WRKY40 in *C. annuum,* inhibiting the activation of defence-related genes. This subdues the plant's ability to fight off the pathogen and prevents the plant's stomata from closing, ultimately making it easier for more bacteria to colonise the plant and proliferate (Raffeiner et al., 2022). Plants that are unable to surmount an effective immune response against these bacterial virulence mechanisms are classified as susceptible plants and ultimately result in crop devastation and yield losses. Identifying how to overcome such a harvest reduction due to this susceptibility of crops has been a significant focus of disease control research since the first identification of bacterial spot.

1.4.3. Host resistance to bacterial spot causing *Xanthomonas*

Currently, control of bacterial spot of pepper in the field typically still relies on copper-containing bactericides, however, *Xanthomonas* populations within the field developed copper resistance, making this management strategy unsustainable (Stall et al., 2009). Genetic resistance within pepper species infected by *Xanthomonas* has proven to be an effective, sustainable, and economic strategy for limiting bacterial disease. If a plant is resistant, the plant induces an immune response that usually correlates with HR, causing rapid necrosis of the infected tissue (Klement & Goodman, 1967). As *Xanthomonas* is prone to a hemibiotrophic lifestyle, this necrotic HR will limit *Xanthomonas* proliferation and not allow the bacteria to spread and cause further damage to the plant. The HR response in a resistant plant is typically induced by dominantly inherited *R* genes, which have been deployed in agricultural settings as a successful tool for managing crop diseases.

To date, there have been five dominant resistances reported against bacterial spot on pepper that rely on the function of the following *R* genes: *Bs1 (Bacterial spot resistance gene number 1)*, coming from *C. annuum* accession PI 163192 (Cook & Stall, 1963), *Bs2* coming from *C. chacoense* PI 260435 (Cook & Guevara, 1984), *Bs3* from *C. annuum* PI 271322 (Kim & Hartmann, 1985), *Bs4C* derived from *C. pubescens* PI 235047 (Sahin & Miller, 1998), and *Bs7* from *C. baccatum* var. *pendulum* line 1556 (Potnis et al., 2012). As opposed to dominant *R* genes, recessive resistance does not elicit an HR after infection but reduces the infecting bacteria's ability to proliferate. There are three identified recessive resistances against

bacterial spot on pepper coming from the following genes: *bs5* from *C. annuum* PI 271322, *bs6* derived from *C. annuum* PI 163192, and *bs8* coming from *C. annuum* PI 163192 (Jones et al., 2002; Sharma et al., 2023).

Host resistance against bacterial infection was hypothesised to be regulated according to the gene-for-gene resistance model, meaning that resistance is controlled by an *R* gene in the host plant and an avirulence (*avr*) gene in the pathogen (Flor, 1955). After the creation of near-isogenic lines of the *C. annuum* cultivar Early Calwonder (ECW), ECW-10R, ECW-20R, and ECW-30R, where each of the dominant *R* genes *Bs1*, *Bs2*, and *Bs3* were introgressed, respectively, the cognate *avr* genes *avrBs1*, *avrBs2*, and *avrBs3*, were able to be identified in *Xe* (Minsavage et al., 1990). These *avr* genes were some of the first T3SEs identified from *Xanthomonas* and ultimately established a gene-for-gene response in the pepper and bacteria interaction.

1.4.4. TALE-mediated susceptibility

Of the *avr* genes mentioned above, *avrBs3* encodes for one of the most well-studied T3SEs from *Xe*, AvrBs3 (Bonas et al., 1989). AvrBs3 belongs to the TALE class of effectors, which upon injection from the bacteria into the plant cell, translocates to the nucleus and transcriptionally activates host plant genes (Bogdanove et al., 2010). Functionally, TALEs have hallmark domains such as a type III secretion signal, nuclear localisation signal, a DNA binding domain, a transcription factor binding domain, and an activation domain (Figure 1.3) (Nowack et al., 2022). The DNA binding domain is located within the centre of the TALE structure and consists of anywhere between 15-20 repeats, with each repeat comprising a nearly identical sequence of 33-35 amino acids. Each of these TALE repeats have specific binding to one DNA nucleotide in a target sequence, and this specificity is determined by the repeat variable diresidue (RVD), which are two amino acid residues located at positions 12 and 13 of each TALE repeat (Boch et al., 2009; Moscou & Bogdanove, 2009). Therefore, each TALE has a given target DNA sequence, called an effector binding element (*EBE*), that can be predicted based on the RVD prediction (Doyle et al., 2012). TALEs scan the host genome until they find a compatible *EBE*, bind to this *EBE*, and transcriptionally activate the plant gene directly downstream of the binding site. Compatible *EBE*s can be found upstream of a wide variety of genes, however, the consensus is that TALEs only target susceptibility (*S*) genes to promote disease, and all other TALE-induced genes are likely off-targets (Nowack et al., 2022).

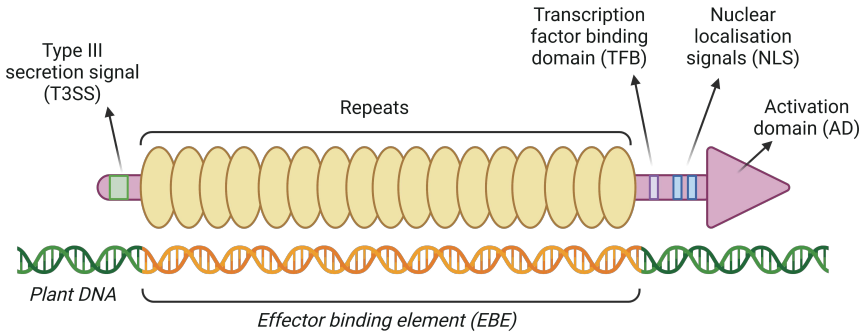

FIGURE 1.3. Structure of a transcription activator-like effector (TALE) protein.

The N-terminal T3SS tags TALEs to travel from the bacteria into the plant host cell. The NLS targets the TALE to the host plant's nucleus so the search for the target *EBE* can begin. The repeat sequences are located near the centre of the protein, with each repeat corresponding to a specific base-pair so that the TALE can bind to the *EBE* in the host plant DNA. The TFB facilitates the interaction with the host's transcription initiation complex. The AD on the C-terminal portion of the protein facilitates transcriptional activation downstream of the target *EBE* once the TALE has found its target *EBE* sequence. T3SS, type III secretion signal; NLS, nuclear localisation signal; *EBE*, effector binding element; TALE, transcription factor-like effector; TFB, transcription factor binding domain; AD, activation domain. Inspiration for this figure was taken from Nowack et al., 2022. Image created using BioRender.com.

In a TALE virulence scenario, the target *EBE* is upstream of an *S* gene that generally would promote disease and bacterial proliferation, like for example, the *SWEET (Sugars Will Eventually be Exported Transporter)* genes in *Oryza sativa* (Bezrutczyk et al., 2018). *Xanthomonas oryzae* pv. *oryzae* (*Xoo*) specific TALE induction of three *OsSWEET* genes were proven to be *bona fide* host virulence targets, promoting bacterial proliferation in the host upon infection (Streubel et al., 2013). However, during plant-pathogen co-evolution, some plants have established the ability to sense these *S* gene-inducing TALEs and trigger a defence reaction to employ host resistance. There are two functionally distinct classes of *R* genes in TALE-induced resistance. The first is an *R* gene that encodes a type of receptor that is constitutively present in the host cell and can sense the structure of TALEs and induce an immune reaction. The second class are *R* genes that are transcriptionally activated by the TALEs and subsequently trigger a cell death response.

1.4.5. TALE-mediated resistance

There are over 314 cloned plant *R* genes, with the majority encoding proteinaceous receptors (Kourelis & van der Hoorn, 2018). Some of these *R* genes encode NLR-type receptors, whereby the leucine-rich repeat (LRR) domain could be sensing the TALE either directly or indirectly (Zhang et al., 2022). Specifically, the *R* gene *Bs4* from *Solanum lycopersicum* (previously named *Lycopersicon esculentum*) encodes an NLR protein that triggers HR upon

perceiving the TALE AvrBs4 from *Xe* (Schornack et al., 2004) and several other TALEs. Knocking out *Bs4* in *S. lycopersicum* not only suppresses the induction of HR after the delivery of TALEs by *Xe* into the plant, but it also uncovered Bs4-dependent non-HR immune responses masking AvrBs3-induced virulence in *S. lycopersicum* (Schenstnyi et al., 2022). This finding gave further credibility to the Nowack et al., 2022 statement that TALEs only target *S* genes, and that *S. lycopersicum* established a mechanism to sense and defend against *Xanthomonas* virulence.

The second class of *R* genes are cell death-inducing genes that have a TALE-compatible *EBE* within the 5' upstream DNA region and are called executor *R* genes (Zhang et al., 2015). It is hypothesised that these cell death-inducing executor *R* genes were already present in the plant performing a function that is not immunity-related. A TALE-compatible *EBE* in the upstream region ultimately traps the TALEs to induce transcription of the downstream cell death-inducing executor gene (Nowack et al., 2022). While it has often been stated that the *EBE* evolved upstream of the cell death-inducing gene to trap the TALE, this statement remains questionable since there is typically little sequence diversity at the *EBE* when different genotypes of one species are compared. This type of *R* gene is termed executor due to the fact that as soon as it is transcribed, it induces a cell death response, unlike NLRs, which are constitutively expressed but require activation to induce a cell death response. Executors are commonly classified into two groups solely based on the characteristics of the encoded proteins (Zhang et al., 2015). Group 1 executor has one sole member, Bs3, from *C. annuum* PI 271322 and introgressed into ECW to make cv. ECW-30R (Römer et al., 2007). Upon infection of *Xe* on *C. annuum* cv. ECW-30R, AvrBs3 binds to a 19-bp *EBE* located in the promoter of *Bs3* and activates its transcription (Bonas et al., 1989; Römer et al., 2007). *Bs3* encodes a protein with 342 amino acids and high sequence similarity to an enzyme family called flavin-containing monooxygenases (FMOs), and is localised in the cytoplasm and nucleus when ectopically expressed in *Nicotiana benthamiana* (Krönauer et al., 2019; Römer et al., 2007). To date, this is the only identified executor that localises to the cytoplasm/nucleus and likely requires enzymatic activity to induce a cell death reaction (Krönauer et al., 2019). It has been revealed that Bs3 causes an increase in the hormone salicylic acid (SA) *in planta* and that Bs3 can induce apoptosis in humans cells and limit the proliferation of yeast cells, proving that the mechanism of action that Bs3 uses to induce cell death is conserved from single-celled eukaryotes to complex multi-cellular eukaryotes (Krönauer, 2019). The specific mechanism and mode of action that Bs3 employs to induce cell death is still unknown.

Group 2 executors contain Bs4C coming from *C. pubescens*, which has an AvrBs4-compatible *EBE* trap in the 5' upstream DNA region (Strauß et al., 2012), Xa7 derived from *O. sativa* with

an upstream AvrXa7 compatible *EBE* trap (Chen et al., 2021; Luo et al., 2021; Wang et al., 2021), Xa10 coming from *O. sativa* with an upstream AvrXa10 compatible *EBE* trap (Tian et al., 2014), Xa23 from *Oryzae rufipogon* with an upstream AvrXa23 compatible *EBE* trap (Wang et al., 2015), and Xa27 from *Oryza minuta* that has an upstream AvrXa27 compatible *EBE* trap (Gu et al., 2005).

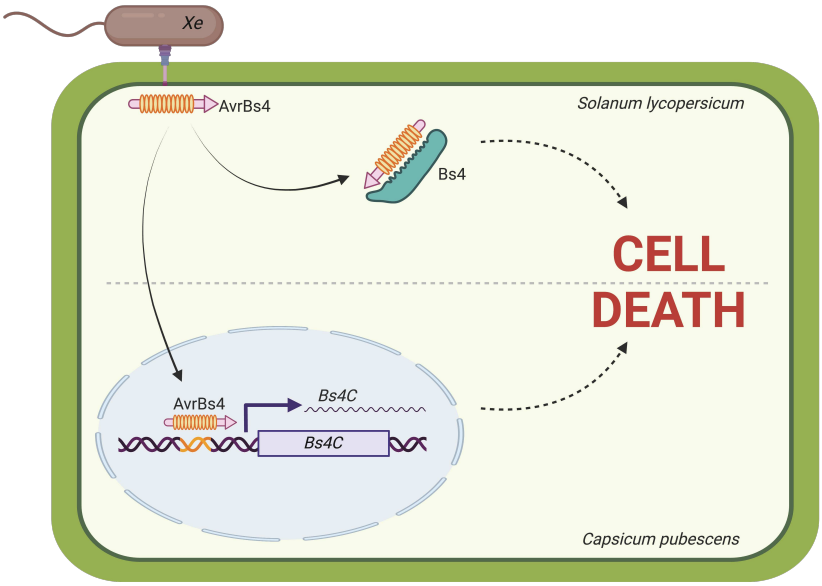

FIGURE 1.4. Tomato and pepper species have distinct resistance mechanisms against AvrBs4.

Xanthomonas euvesicatoria (*Xe*) injects the TALE protein AvrBs4 into the host plant cytoplasm. In the upper panel, AvrBs4 is injected into the tomato species *Solanum lycopersicum*. Once injected, AvrBs4 is sensed by the constitutively expressed NLR protein Bs4. Upon the sensing of AvrBs4, Bs4 activates a rapid and robust immune response, leading to cell death. In the pepper species *Capsicum pubescens*, AvrBs4 translocates to the nucleus after being injected, where it scans the genome for a compatible *EBE*, which is located upstream of the executor *R* gene *Bs4C*. Upon binding of AvrBs4 to the compatible *EBE*, *Bs4C* is transcriptionally activated and subsequently induces a fast immune response, culminating in cell death. Image created using BioRender.com.

There are two different mechanisms for recognition and subsequence cell death induction after AvrBs4 insertion in tomato and pepper. Tomato developed the use of Bs4, the TALE-sensing NLR, and pepper utilises Bs4C with an AvrBs4-trapping *EBE* in the upstream DNA region (Figure 1.4) (Schornack et al., 2004; Strauß et al., 2012). The likely scenario, as described in Nowack et al., 2022, is that tomato has evolved the ability to sense AvrBs4 through the NLR Bs4, to negate its virulence mechanism and limit disease progression of *Xe* and that the AvrBs4 compatible *EBE* upstream of *Bs4C* in pepper is only there by chance.

All of these group 2 executors are relatively small in their molecular weight, ranging from 11 to 20 kDa, induce cell death when ectopically expressed in *N. benthamiana* aside from Xa27,

have between two to four transmembrane domains, and are localised to the ER, except for Xa27 which localises to the apoplast (Ji et al., 2022; Nowack et al., 2022; Wu et al., 2008) (Figure 1.5). It has also been proposed that all group 2 executors likely form ion channels within their respective membranes and are likely to be Ca^{2+} channels, releasing Ca^{2+} from their organelle stores into the cytoplasm (Ji et al., 2022). Thus far, all group 2 executors have been identified as transcriptionally activated by a TALE coming from a *Xanthomonas* pathogenic species (Nowack et al., 2022).

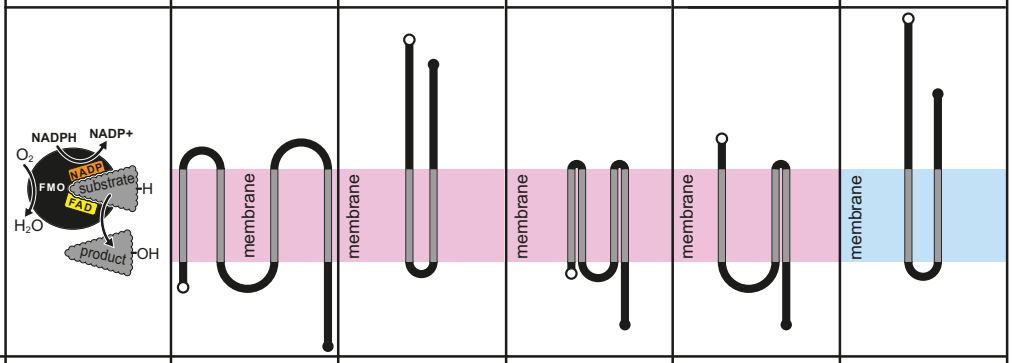

	Bs3 [342aa]	**Bs4C** [164aa]	**Xa7** [113aa]	**Xa10** [126aa]	**Xa23** [113aa]	**Xa27** [113aa]
Executor *R* gene donor species	*Capsicum annuum* PI271322	*Capsicum pubescens* PI235047	*Oryza sativa* DV85	*Oryza sativa* Cas 209	*Oryzae rufipogon*	*Oryza minuta* Acc. 101141
HR in *N. benthamiana*	Yes	Yes	Yes	Yes	Yes	No
Transmembrane domains	0	4	2	4	3	2
Subcellular localisation	cytoplasm/nucleus	endoplasmic reticulum	endoplasmic reticulum	endoplasmic reticulum	endoplasmic reticulum	apoplast
References	Römer et al., 2007; Krönauer et al., 2019	Strauß et al., 2012; Wang et al., 2018	Chang et al., 2021; Wang et al. 2021	Tian et al., 2014	Wang et al., 2015	Gu et al., 2005; Wu et al., 2008

FIGURE 1.5. Features of executor R proteins.

The name of each R protein is given at the top, with the number of amino acids (aa) that make up the protein. The number of transmembrane domains and structure is given by predicted topology either from the corresponding reference or from TMHMM (https://services.healthtech.dtu.dk/services/TMHMM-2.0/).
Figure has been adapted from Nowack et al., 2022.

All of these executor *R* gene transcripts have only been found in plant tissue after their transcriptional activation via TALEs and have not been detected under any other conditions. This tight control of a transcriptional profile of these executor *R* genes has been hypothesised to resemble features of developmentally programmed cell death (dPCD) (Nowack et al., 2022). dPCD has similarly tightly controlled expression, both spatially and temporally, and is typically confined to specific cells at a distinct time in a specific organ (Daneva et al., 2016). The commonalities between pathogen-induced PCD and dPCD have been investigated on a transcriptional level previously in Arabidopsis, however, a functional core machinery that is shared between these two PCD pathways remains unidentified (Huysmans et al., 2017;

Olvera-Carrillo et al., 2015). Nowack et al., 2022 speculate that because of this tight transcriptional regulation of cell death-inducing genes, executor genes could actually be transcriptionally regulated activators of dPCD but have been repurposed to provide resistance to *Xanthomonas*, by putting an *EBE* trap upstream of these genes that are then compatible with TALEs.

1.5. Identification and previous characterisation of Bs4C

The aforementioned *R* gene, *Bs4C,* identified from *C. pubescens,* is the main focus of the work herein. The observation of *Xanthomonas* resistance in the *C. pubescens* accession PI 235047 was first reported in Sahin & Miller, 1998, with an observation of HR development described as collapsed tissue at the inoculation site 24 hours after *Xe* 17b (race P6) infiltration. It was found that another strain of *Xe*, 116 (race P1), was unable to elicit an immune response on PI 235047 plants, implying that *C. pubescens* PI 235047 plants carry an *R* gene that is specific to an avirulence gene in the P6 strain of *Xe* (Sahin & Miller, 1998). The pathogen avirulence gene was first termed *avrBsP* and *avrBs3-2* but was then renamed to *avrBs4*, and the cognate plant *R* gene was originally termed *Bs4* (Ballvora et al., 2001; Sahin & Miller, 1998). This designation of *Bs4* in *C. pubescens* was done prior to the identification of the *R* gene *Bs4* in tomato, and upon the identification of the specific gene that *Bs4* encodes in *C. pubescens*, it was renamed to *Bs4C*, the *C* representing *Capsicum*.

1.5.1. Isolation and cloning of *Bs4C*

The isolation of *Bs4C* was performed using a comparative approach between two different *C. pubescens* accessions, PI 235047 (resistant) and PI 585270 (susceptible), which either showed the presence or absence of an AvrBs4-triggered HR, respectively (Strauß et al., 2012). Bs4C-induced cell death was dependent upon the transcriptional activation capabilities of AvrBs4, and it was therefore believed that the resistant accession of *C. pubescens*, PI 235047, would have *Bs4C* transcriptionally activated, and the susceptible accession, PI 585270, would not. Indeed, upon RNA-sequencing of each accession after Xe^{AvrBs4} and subsequent transcriptome profiling, a *Bs4C* candidate gene, with a direct AvrBs4 target *EBE* in the upstream sequence, was identified to be transcriptionally activated in PI 235047 and not in PI 585270 and was confirmed to be the *Bs4C* resistance gene (Strauß et al., 2012). After further investigation, Strauß et al. 2012 discovered that the coding sequence (CDS) of *Bs4C* in the resistant accession PI 23507 was also found in the susceptible accession PI

585270, with only a few amino acid differences between the two, and were named *Bs4C-R* and *Bs4C-S*, respectively. Furthermore, the upstream sequences of both genes were found to be nearly identical, barring a few base pairs, and specifically, two base pairs were different within the AvrBs4 targeted *EBE*. Putting both *Bs4C-R* and *Bs4C-S* under the control of a strong promoter (35S, Cauliflower Mosaic Virus), they both induced cell death in *N. benthamiana*. However, placing both *Bs4C-R* and *Bs4C-S* under control of their endogenous upstream 5' DNA sequence (~250 base pairs) and co-infiltrating with AvrBs4, only *Bs4C-R* was able to induce a cell death reaction. Indeed, this finding confirmed that this two base pair polymorphism in the AvrBs4 targeted *EBE* was what differentiated the resistance of *Bs4C-R* in PI 23507 and susceptibility of *Bs4C-S* in PI585270 (Elsaesser, 2014; Wang et al., 2018).

1.5.2. Previous characterisation of Bs4C-R

To understand how Bs4C-R was inducing a cell death response, the functional characterisation of Bs4C-R was initially undertaken by a previous student in Prof. Dr. Thomas Lahaye's lab. Janett Elsaesser was the first to predict the transmembrane regions of Bs4C-R (J. Elsaesser, 2014, unpublished), and J. Elsaesser's findings were supported in Wang et al., 2018, in that Bs4C-R likely has four transmembrane domains, consisting of membrane-spanning alpha helices (Figure 1.6).

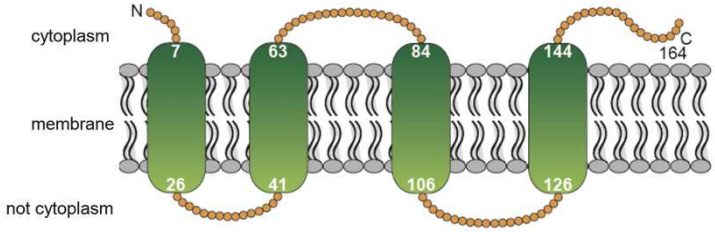

FIGURE 1.6. Bs4C-R structural prediction.

Prediction of transmembrane regions of Bs4C-R using TMHMM prediction and probability of localisation within the cytoplasm, not in the cytoplasm or in a transmembrane domain. The first and last amino acid positions are indicated by N or C, respectively. Image generated by J. Elsaesser.

J. Elsaesser found that Bs4C-R likely localises to the ER (Figure 1.7A). Furthermore, J. Elsaesser also noted that Bs4C-R formed aggregates along the ER and that these aggregates are able to move (Figure 1.7B). This subcellular localisation of Bs4C-R was confirmed in Wang et al., 2018, which found Bs4C-R was able to co-localise to the ER marker RcDGAT2, however, J. Elsaesser was able to exhibit much greater confocal resolution and able to define Bs4C-R along the network of the ER clearly.

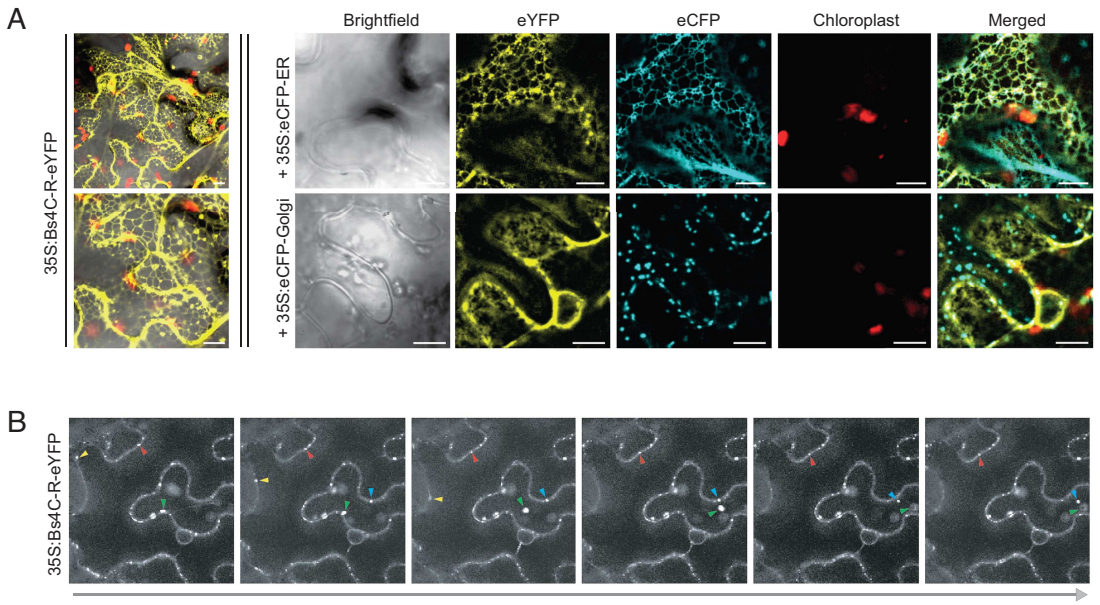

FIGURE 1.7. Bs4C-R likely localises to the endoplasmic reticulum.

A | Confocal images of the *Agrobacterium tumefaciens*-mediated ectopic expression and subcellular localisation of Bs4C-R in *N. benthamiana*. All constructs were under control of the 35S promoter. Bs4C-R-eYFP, left most panels, and Bs4C-R-eYFP co-infiltrated with the indicated subcellular markers. Pictures of independent Bs4C-R-eYFP infiltration were taken 24 hours post-inoculation. The images for the co-infiltrations were taken 24 hours post Bs4C-R-eYFP infiltration and 48 hours post Golgi/ER marker infiltration. Scale bar indicates 10 µm. Images taken by Janett Elsaesser, unpublished.
B | Temporal serial imaging of Bs4C-R-eYFP. Fluorescence signals transported through the cells can be observed. Coloured arrows indicate moving signals. Grey arrow at bottom indicates passage of time through images. Images taken by Janett Elsaesser, unpublished.

Bs4C-R-like genes have been identified in other *Capsicum* species (Elsaesser, 2014; Wang et al., 2018). J. Elsaesser identified many potential *Bs4C-R*-like genes in *C. annuum*, but could only successfully clone three, all of which came from chromosome one. These were termed *Ca01gBs4C.1*, *Ca01gBs4C.2*, and *Ca01Bs4C.5*, and their encoded amino acid sequence had 54.4%, 69% and 83.9% similarity to Bs4C-R, respectively. *Ca01Bs4C.1* and *Ca01Bs4C.5* were the only *Bs4C-R*-like genes that were able to surmount a cell death reaction when overexpressed in *N. benthamiana* (Supplementary Information S1). In Wang et al., 2018, the authors identified only one *Bs4C-R*-like gene from *C. annuum* and designated the corresponding protein as CaBs4C, which upon comparison to the three identified by J. Elsaesser, CaBs4C is the same as Ca01Bs4C.1. Wang et al., 2018 had a similar observation in that CaBs4C also induced cell death when ectopically overexpressed in *N. benthamiana*.
For simplicity, Bs4C-R will hereafter be referred to CpBs4C (*Capsicum pubescens* Bs4C), and the name *Bs4C* will refer to the broader family of *Bs4C-R*-like genes that have been identified. It is clear that with the identification of *Ca01gBs4C.1, .2,* and *.5* in addition to the identification of *CaBs4C* between the years of 2014 and 2018, there are some discrepancies and weak points in the identification of *Bs4C*-like genes in other species.

1.6. Working objectives

Executor *R* genes counteract the virulence of *Xanthomonas* TALEs. The executor *R* gene *CpBs4C* was found to be transcriptionally activated by AvrBs4 in a non-native infection scenario, where it localises to the ER and induces a rapid cell death response (Figure 1.8).

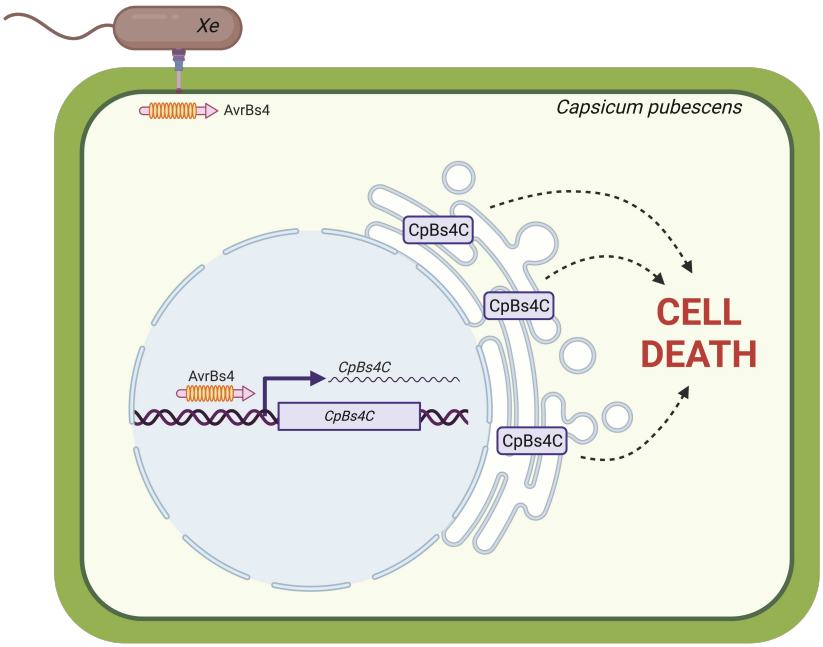

FIGURE 1.8. *CpBs4C* is activated by AvrBs4, localises to the endoplasmic reticulum, and induces cell death by unknown means.

Xanthomonas euvesicatoria (*Xe*) injects the TALE AvrBs4 into a cell of the host plant, *Capsicum pubescens*. AvrBs4 translocates to the nucleus, where it binds to a 19-base pair target DNA sequence upstream of the resistance gene *CpBs4C*. AvrBs4 activates the transcription of *CpBs4C*, where it is then translated and localises to the ER and induces a cell death reaction that has yet to be elucidated. Image created using BioRender.com.

Other than these pieces of information, how CpBs4C works in the plant cell has yet to be clarified. Therefore, this work aims to characterise the structure and function of CpBs4C and how it induces cell death, by answering these questions:

1. Are there other *Bs4C*-like genes in other plant species and do they behave similarly to CpBs4C?
2. What is the mechanism of action of CpBs4C *in planta* and how does CpBs4C induce cell death?
3. Are there downstream signalling components of CpBs4C, and can they be isolated and identified using a more rapid technique than conventional methods?

2. MATERIALS AND METHODS

2.1. Materials

Table 2.1. Composition of media.		
Media name	**Organism used**	**Composition**
Luria-Bertani (LB)	*Escherichia coli*	1% (w/v) tryptone 1% (w/v) NaCl 0.5% (w/v) yeast extract
YEB	*Agrobacterium tumefaciens*	0.5% (w/v) beef extract 0.5% (w/v) peptone 0.5% (w/v) saccharose 0.1% (w/v) yeast extract 2 mM $MgSO_4$
NYG	*Xanthomonas euvesicatoria*	0.5% (w/v) peptone 0.3% (w/v) yeast extract 0.2% (v/v) glycerine
½ MS	*Arabidopsis thaliana*	0.4% (w/v) MS Salts (Gibco) 1% (w/v) sucrose 0.05% (w/v) MES pH 5.8

Table 2.2. Antibiotics.			
Antibiotic	**Organism used**	**Stock concentration**	**Dilution**
Ampicillin (Amp)	*E. coli*	100 mg/mL	1:1000 in plate 1:2000 in liquid
Basta®	*A. thaliana*	200 g/L	1:500 in liquid
Cefotaxim	*A. thaliana* *N. benthamiana*	200 mg/mL	1:1000
Gentamycin (Gent)	*E. coli* *A. tumefaciens* *X. euvesicatoria*	15 mg/mL	1:1000 for *X. euvesicatoria* *E. Coli* 1:300 for *A. tumefaciens*
Kanamycin (Kan)	*E. coli* *A. tumefaciens* *A. thaliana*	25 mg/mL	1:1000 for *E. coli* 1:250 for *A. tumefaciens* 1:500 for *A. thaliana*
Rifampicin (Rif)	*A. tumefaciens* *X. euvesicatoria*	100 mg/mL	1:1000
Spectinomycin (Spec)	*E. coli* *A. tumefaciens*	100 mg/mL	1:1000

Table 2.3. Bacterial strains.		
Organism	**Strain**	**Reference**
E. coli	Top10	Invitrogen™
A. tumefaciens	GV3101	Holsters et al., 1980
X. euvesicatoria	85-10 *ΔxopQ*	Adlung et al., 2016

Table 2.4. Antibodies.			
Antibody	**Organism**	**Concentration used**	**Manufacturer**
Anti-GFP-HRP (monoclonal)	Mouse	1:5000	SantaCruz Biotechnology
Anti-HA-HRP (monoclonal)	Rat	1:5000	Roche
Anti-RFP 6G6 (monoclonal)	Mouse	1:5000	ChromoTek
Anti-FLAG (monoclonal)	Mouse	1:5000	Sigma-Aldrich
Anti-mouse-HRP (whole molecule)	Rabbit	1:5000	Sigma-Aldrich

2.2. Methods

2.2.1. Plant methods

Plant growth conditions

Arabidopsis thaliana seedlings were put at 4 °C and left to stratify in complete darkness for 2 days. Seeds were then put to long-day conditions (16 hours light and 8 hours dark) at 20 °C in light and 18 °C dark. *Nicotiana benthamiana* plants were grown at 20 ± 2 °C on a photoperiod of 16 hours light and 8 hours dark with relative humidity between 30-50%.

Stable transformation of *A. thaliana*

Agrobacterium tumefaciens containing the indicated plasmid was struck on YEB plates containing the appropriate antibiotics and left to incubate at 28 °C for 2 days. On Day 1, a 5 mL overnight culture of YEB + appropriate antibiotics + *A. tumefaciens* was inoculated and shaken overnight at 28 °C. On Day 2, a 25 mL culture of YEB + appropriate antibiotics + 5 mL culture from Day 1 was created and shaken overnight at 28 °C. On Day 3, a 300 mL culture of YEB + appropriate antibiotics + 25 mL culture from Day 2 was created and shaken overnight at 28 °C. On Day 4, the 300 mL culture was spun down at 4 000 x *g* for 10 min. The supernatant was removed, and the pellet was resuspended in a sucrose solution (50 g / L) and set to an optical density (OD_{600}) of 0.8 in 500 mL. To this 500 mL solution, 250 µL of Sylwet L-77 was added. Approximately 6-week-old *A. thaliana* plants had their flowers placed in the *A. tumefaciens* for 30 seconds, making sure every flower was dipped into the solution. The pot of *A. thaliana* was then placed horizontally in a tray lined with wet paper towels and covered with another tray for 1 day. After 1 day, the lids of the trays were removed, and the plants were stood upright. Once the sucrose solution had dried off of the flowers, the flowers were bagged. Protocol has been adapted from Zhang et al., 2006.

Transient transformation of *N. benthamiana*

A. tumefaciens containing the indicated plasmid was struck on YEB plates containing the appropriate antibiotics and left to incubate at 28 °C for 2 days. The day before infiltration, a 5 mL overnight culture of YEB + appropriate antibiotics + *A. tumefaciens* was inoculated and shaken overnight at 28 °C. On the morning of infiltration, the culture was spun down at 10 000 x *g* for 2 minutes. The supernatant was discarded, and the pellet was resuspended in 1 mL ddH_2O and spun down again at 10 000 x *g* for 2 minutes. Unless indicated otherwise, the pellet was resuspended in infiltration buffer (10 mM MES, 10 mM $MgCl_2$) and the OD_{600} was set to 0.4. Using a blunt-end needle-less syringe, the *A. tumefaciens* was infiltrated into 4-5 week-

old *N. benthamiana*, on the 3rd or 4th leaf on the abaxial side. The plants were then placed on the bench in the lab in a shaded area (away from direct overhead light) until harvest.

A. thaliana seed sterilisation using gas

A. thaliana seeds were placed in a 1.5 mL tube with the lid open and put in a rack in a desiccator (chamber) in the fume hood. 80 mL of NaOCl solution was put into a 100 mL bottle and then placed in the desiccator. 3.2 mL of 32% HCl solution was put into the 100 mL bottle containing the NaOCl, and then the desiccator was immediately closed and sealed. After an overnight incubation, the desiccator seal was broken and then the rack containing the seeds was placed in the clean bench for at least 30 minutes. 500 µL of 0.1% (w/v) phytoagar (Duchefa Biochemie) was put on the seeds, and the seeds were allowed to stratify at 4 °C for 3 days.

A. thaliana seed sterilisation using liquid

A. thaliana seeds were placed in a 1.5 mL tube. 1 mL of sterilisation solution (80% (v/v) EtOH, 0.05% (v/v) Triton X-100) was added to the seeds and mixed. The sterilisation solution was removed, and another 1 mL of sterilisation solution was added and incubated for 15 minutes on an end-over-end rotation wheel. Following this, the supernatant was removed and 100% EtOH was added and mixed thoroughly. The supernatant was again removed, and 100% EtOH was then added and mixed. The seeds were placed on a sterilised filter paper and then left to dry in the clean bench. 500 µL of 0.1% (w/v) phytoagar (Duchefa Biochemie) was put on the seeds, and the seeds were allowed to stratify at 4 °C for 2 days.

Seedling growth assay

A. thaliana seeds were sterilised in a solution with 80% ethanol and 0.05% Triton X-100 (as indicated above) and then left to stratify at 4 °C in the dark for 2 days on ½ MS plates containing Cefotaxim and the appropriate antibiotics. Plates containing sterilised seeds were put into a long day chamber (16 hr light/8 hr dark) at 20 °C in light and 18 °C in dark for five days. On the 5th day, seedlings were then transplanted to a 48-well plate containing either 20 µM estradiol or mock treatment (1 % (v/v) DMSO) and left for 10 days. 14 days post germination, seedling growth was analysed.

A. thaliana seedling immunodetection

Four 14-day-old *A. thaliana* seedlings of the indicated genotype were put in either 20 µM estradiol or 1% DMSO (mock), vacuum infiltrated, and then left at room temperature for 24 hours. The seedlings were then taken out of their solution, briefly dried off and flash frozen, and then used for immunoblotting, as described below.

EMS mutagenesis

Approximately 200 mg of *A. thaliana* seeds were put in water for 3 days to swell. The seeds were then put in 50 mL of 0.3% (w/v) ethyl methanesulfonate (EMS) solution, shaking for 6 hours. Then the seeds were transferred to a filter unit and subsequently washed 6 times with water. The seeds were then resuspended in 0.1% (w/v) phytoagar and sowed onto soil. 10 days later, the seedlings were then transplanted to individual pots in an outdoor greenhouse (16 hr light/8 hr dark, minimum temperature 18 ^{o}C, no humidity control). These plants now individually generate the M1 population. After 6 weeks, seeds from each individual M1 plant were collected, thus creating 4000 individual M2 families.

Screening of M2 families

100 seeds from each of the 4000 M2 families were put in individual wells in a 96-well plate, and were gas sterilised overnight, as described above. The next day, 200 µL of 1% (w/v) phytoagar was placed in each well and the plate was then sealed with an adhesive plate cover. The plate was then placed in the dark at 4 ^{o}C for 2 days to stratify. The seeds were then plated in rows on ½ MS plates containing 20 µM estradiol and put to long day chamber conditions (described previously). The seeds were left on the plates for 14 days, and then analysed. Suppressing families were selected and the survivors were transplanted to soil.

Adult *A. thaliana* plant immunodetection

Three 4 mm punches were taken from 5-week-old surviving plants and then vacuum infiltrated with 20 µM estradiol, and then left to rest at room temperature for 24 hours. The punches were then flash frozen in liquid N_2 and used for subsequent immunoblotting, as described below.

N. benthamiana plant immunodetection

Four 6 mm punches were taken at the indicated time points and flash frozen in liquid N_2. Samples were ground to a fine powder using the RetschMill (Qiagen) at 16 Hz for 30 seconds. Samples were then proceeded using the immunoblotting protocol below.

Photosynthetic measurements

Photosynthetic measurements served as a proxy for cell death, which was measured via chlorophyll fluorescence using a PAM fluorometer (IMAG-MAX/L; Walz GmbH, Effeltrich, Germany) and IMAGINGWIN software (Maxi version; v.2-46), which has been previously described in Bresson et al., 2018. 4 days post infiltration of *A. tumefaciens* with the indicated plasmid, *N. benthamiana* leaves were detached and placed in darkness for 30 minutes. Then, the leaves were exposed to a super pulse in a dark chamber, and a minimum fluorescence

F_0, maximum fluorescence F_m, and a maximum quantum yield of photosystem II, F_v/F_m (photosynthetic efficiency) was determined.

2.2.2. Bacterial methods

Transformation of *E. coli*

Approximately 100 ng of plasmid was mixed with 25 µL of *E. coli* Top10 cells that were put on ice to thaw, and the mixture was left on ice for 10 minutes. The cells were then placed in a water bath at 42 °C to for heat shock for 45 seconds. The cells were then placed on ice for 1 min and 300 µL of 1X LB was added. The cells were then placed on a shaker at 37 °C for 1 hour, and then plated on LB plates with the appropriate antibiotics. The plates were placed in the 37 °C incubator overnight.

Transformation of *A. tumefaciens*

50 µL of electro-competent *A. tumefaciens* GV3101 cells were put in a 2 mm electrocuvette, and approximately 100 ng of plasmid was mixed in. The electrocuvette was placed in the MicroPulser Electroporator (BioRad), and the *Agr* setting was used. After electroporation, 300 µL of 1X YEB was immediately put on the cells and shaken at 28 °C for 1 hour for recovery. The cells were then plated on YEB plates containing the appropriate antibiotics, and then placed in the 28 °C incubator for 2 days.

Xanthomonas euvesicatoria competent cells

5 mL *ΔxopQ* overnight cultures were prepared with NYG and the appropriate antibiotics. The following morning, 1-2 mL of the overnight culture was put in 50 mL of fresh NYG containing the appropriate antibiotic. The culture was grown in the 28 °C incubator shaking, until the OD_{600} reached 0.4. The culture was then spun down at 4 000 x *g* for 15 min at room temperature (RT). The supernatant was discarded, and the pellet was resuspended in 50 mL ice-cold autoclaved water and then spun down at 4 000 x *g* for 15 min at RT. The supernatant was then discarded and resuspended in 20 mL of ice-cold autoclaved water and then spun down at 4 000 x *g* for 15 min at RT. Next, the supernatant was discarded, and the pellet was resuspended in 5 mL of ice-cold 10% glycerol. This was then spun down at 4 000 x *g* for 20 min at RT. The supernatant was discarded, and the remaining pellet was resuspended in 2 mL of ice-cold 10% glycerol and then aliquoted into 50 µL tubes and flash frozen in liquid N_2 and then stored at -80 °C. The aliquots were tested on different combinations of antibiotics to ensure that there was no contamination or antibiotic resistance.

Transformation of *X. euvesicatoria*

50 µL aliquot of electro-competent *X. euvesicatoria* cells were placed in a 2 mm electrocuvette. At least 100 ng of the desired plasmid was mixed into the 50 µL of competent cells. The *EC2* setting was used on the MicroPulser Electroporator (BioRad). After electroporation, 300 µL of 2X NYG was immediately put on the cells, and they were allowed to recover by shaking at 28 ^{o}C for 1 hour. The cells were then plated on NYG containing the appropriate antibiotics, and the plates were put in the 28 ^{o}C incubator for 2 days.

Infection of *X. euvesicatoria*

5 mL overnight cultures were prepared with NYG containing the appropriate antibiotics for both the bacteria and the plasmid. The following morning subcultures were prepared in a 1:10 (v/v) dilution and allowed to grow for 5-6 hours until the bacteria doubled in their OD_{600}, twice. The bacterial cells were spun down at RT for 10 min at 4 000 x *g*. The supernatant was discarded, and the pellet was resuspended in 10 mM $MgCl_2$. The culture was spun down again at RT for 10 min at 4 000 x *g*, and the supernatant was discarded. The OD_{600} was adjusted to 0.0001 using 10 mM $MgCl_2$ and infiltrated into *N. benthamiana* on the 3rd or 4th leaf on the abaxial side. The leaves were allowed to dry fully after being infiltrated before two 6mm punches were collected from the infiltrated area and put into a 2 mL tube containing 1 mM $MgCl_2$ and a ceramic bead. The tubes were homogenized using the RetchMill (Qiagen) at 22 Hz for 20 seconds. This homogenization was performed twice. Then the indicated dilutions were created using 1 mM $MgCl_2$ and 10 µL was plated. The colonies were counted 2 days later at the indicated dilution.

2.2.3. Molecular methods

Cloning

To produce most of the constructs listed in Appendix Table 6.1, Golden Gate Assembly cloning was used. To amplify genes of interest, primers found in Appendix Table 6.2 were used. Cloning into all Level II vectors was performed using *BsaI-HF®v2* from NEB. Constructs were confirmed using Sanger sequencing.

Plasmid isolation

6 mL liquid cultures containing LB, the appropriate antibiotics, and a colony of *E. coli* Top10 were placed in the 37 ^{o}C shaker overnight. The following morning, the cultures were then spun down and the plasmid DNA was isolated using the NucleoSpin® Plasmid DNA purification kit from Machery-Nagel according to the manufacturer's manual. Plasmid DNA was assessed for

quality and quantity using the NanoDrop® ND-1000 UV-Vis Spectrophotometer (ThermoFisher Scientific).

Genomic DNA extraction for genotyping

Small portions of a leaf from individual plants were pressed into an FTA Card (Whatman®-FTA™, Qiagen) using parafilm and the back of a test tube. The card was left to rest at RT for at least 1 hour. 50 µL of 1X FTA buffer (10 mM Tris pH8, 2 mM EDTA pH 8, 0.1% (v/v) Tween-20) was put into each well of a 96 well plate, and then 1.2 mm punches from the FTA card were placed directly into the well with the 1X FTA, and left at RT for 5 min. The 1X FTA was removed, and then each punch was washed with 100 µL TE^{-1} (10 mM Tris pH 8, 0.1 mM EDTA pH 8), and left at RT for 5 min. The TE^{-1} was removed and then another 100 µL TE^{-1} was added and left at RT for 5 min. The remaining TE^{-1} was removed. The punch was then directly used in a PCR reaction.

Genomic DNA extraction for next-generation sequencing

Roughly 100-150 mg of leaf material was collected. 600 µL of CTAB buffer (100 mM Tris-HCl pH 8, 20 mM EDTA, 1.4 M NaCl, 2% (w/v) cetyltrimethyl ammonium bromide) was added, and vortexed until homogenized. Samples were then incubated at 65 °C for 30 minutes. After samples were heated, they were spun down at RT at 15 000 x *g* for 5 minutes. 2.5 µL of RNAse A (10 mg/mL, ThermoFisher) was added, vortexed gently, and then incubated for 40 min at 37 °C. 500 µL of chloroform was added and then mixed. Samples were then spun down at RT at 15 000 x *g* for 7 minutes, and 450 µL of the aqueous phase was transferred to a new tube. 450 µL of 100% isopropanol was added and then gently mixed. The tubes were spun down at 15 000 x *g* until a pellet was formed, and then the supernatant was discarded. 500 µL of 70% ethanol was added and mixed, and then spun down at RT at 15 000 x *g* for 10 minutes. The supernatant was then discarded. This process was repeated twice. The final pellet was then dried at 35 °C, and then dissolved in 35 µL of 10 mM Tris-HCl pH 8.0 and quantified using a Qubit (ThermoFisher). These samples were then sent for next-generation sequencing (NGS).

Next-generation sequencing and mapping populations

Raw reads of each sample were aligned to Col-0 reference genome (The Arabidopsis Genome Initiative 2000; www.arabidopsis.org) using *GenomeMapper* (Choi et al., 2009), where short-read alignments were corrected for read-pair information and consensus bases were called with *shore*. After eliminating common single nucleotide polymorphisms (SNPs) between each mutant and the corresponding parental line, the causal mutation of each mutant was predicted with SHOREmap by analysing allele frequencies (Schneeberger et al., 2009; Sun &

Schneeberger, 2015). Next generation sequencing and mapping analysis was performed by Dr. Hequan Sun.

Polymerase chain reaction (PCR)

For the amplification of plant genetic material, the following reaction mixture in Table 2.5 was used.

Table 2.5. Reaction mixture for PCR.	
Amount/volume	**Component used**
4 µL	Forward primer (1 pmol/µL)
4 µL	Reverse primer (1 pmol/µL)
4 µL	5 X HF Buffer (NEB)
1 µL	dNTPs (2 mM)
0.5 µL	Phusion polymerase
1 µL/1 FTA punch	Template DNA
To make 20 µL	ddH_2O

After the reaction mixture was made, the following PCR program in Table 2.6 was used:

Table 2.6. Program for PCR.		
98 °C	2 minutes	
98 °C	20 seconds	35 cycles
62 °C *	20 seconds	
72 °C	1 minute/kb	
72 °C	3 minutes	
* temperature is dependent on the annealing temperature of the primers, kb is 1000 base pairs		

Isolation of RNA

Four 6 mm punches of plant tissue were flash frozen in liquid N_2 and ground to a fine powder using the RetschMill (Qiagen) at 16 Hz for 30 sec. The GeneMATRIX Universal RNA Purification Kit from EURx® (Roboklon) was used, with modifications to the manufacturer's protocol. 400 µL of RL buffer (adjusted with 1% (v/v) β-mercaptoethanol) was added to the ground tissue and homogenized using a vortex. The samples were centrifuged for 2 min at 14 000 x *g* at RT. The supernatant was then transferred to the homogenization spin column and

centrifuged at 14 000 x *g* at RT for 2 minutes. Then 350 µL 70% (v/v) of ethanol was added to 350 µL of the flow through and mixed thoroughly by pipetting up and down. The mixture was then transferred to the RNA binding spin column and centrifuged at 11 000 x *g* for 1 minute. The flow-through was discarded, and then 400 µL of Wash DN1 buffer was added to the spin column and centrifuged at 11 000 x *g* for 1 minute. The flow-through was discarded and 50 µL DNR buffer with DNaseI added (2µL/50µL) was placed directly on the membrane and incubated at RT for 15 minutes. Then 400 µL of RB1 buffer was added and then centrifuged at 11 000 x *g* for 1 minute. The flow through was discarded and then 650 µL of RBW wash buffer was added to the column and centrifuged for 1 minute at 11 000 x *g*. The flow through was then discarded and 350 µL of RBW wash buffer was added to the column and centrifuged at 11 000 x *g* for 1 minute. 40 µL of RNA/DNAse-free water was added to the column, and centrifuged. The final product was assessed for quality and concentration of RNA using the NanoDrop (ThermoFischer Scientific).

Reverse transcription

The following protocol in Table 2.7 was used to generate cDNA from the RNA isolated in the previous section, using a 10 µL sample reaction with the RevertAid First Strand cDNA Synthesis Kit from ThermoFisher Scientific.

Table 2.7. Reaction mixture for cDNA synthesis.

Amount/volume	**Component used**
± 500 ng (up to 5.5 µL)	RNA template
0.25 µL	Oligo $(dT)_{18}$
2 µL	5 X Reaction Buffer
0.5 µL	RiboLock RNase Inhibitor
1 µL	10 mM dNTP Mix
0.5 µL	RevertAid Reverse Transcriptase
To make 10 µL	ddH_2O

The reaction mixture was incubated at 42 ^oC for 60 minutes and then the reaction was terminated by heating to 70 ^oC for 5 minutes. The final product was diluted 1:4 by adding 30 µL RNase-free ddH_2O, and then used for real-time quantitative PCR.

Real-time quantitative PCR

To quantify gene expression of specific genes in *N. benthamiana*, an 8µL reaction mixture as described in Table 2.8 was used in a 384 well plate:

Table 2.8. Reaction mixture for RT-qPCR.	
Amount/ volume	**Component used**
4 µL	2X MESA BLUE qPCR MasterMix Plus for SYBR Assay No Rox (Eurogentec SA)
0.25 µL	F primer (10 pmol/µL)
0.25 µL	R primer (10 pmol/µL)
1 µL	cDNA (1:4 dilution)
2.5 µL	DNase-free H_2O

The following protocol in Table 2.9 was used for RT-qPCR cycling in a BioRadCFX384 Touch Real-Time PCR Detection System:

Table 2.9. Program for RT-qPCR.		
95 °C	5 minutes	
95 °C	15 seconds	39 cycles
59 °C	45 seconds	
59 – 95 °C	Melt curve in 0.5 °C increments	

The Ct value is the threshold cycle when an amplification signal is detected through fluorescence. The Ct value for the targeted gene was compared to the Ct value of the same cDNA samples for the indicated reference gene, which determined the relative expression of the gene of interest.

2.2.4. Protein methods

Immunoblotting

Samples were flash frozen in liquid N_2 with a ceramic bead in a 2 mL tube. Samples were then ground to a fine powder using a RetschMill (Qiagen) at 16 Hz for 30 seconds. 75 µL of SDS extraction buffer (3% (w/v) SDS, 100 mM Tris-HCl pH 7.5) was added to the sample and then vortexed to homogenize. 25 µL of 4X loading buffer (20 mM Tris-HCl pH 8.6, 40% (v/v) glycerol, 10% (v/v) β-mercaptoethanol, 0.1% (w/v) bromophenol blue) was then added to the sample, and vortexed again. Samples were then boiled at 90 °C for 10 min. Samples were loaded onto an SDS-polyacrylamide gel (4% stacking, and either 10% or 12% resolving, as indicated) and run at 180V until the loading dye was 1 cm from the bottom of the gel. The

proteins were then transferred to a PVDF-membrane (Immobilon®-P, 0.45 µm pore size) using a TurboTransfer (BioRad) at 1.0 mA and 25 V for 30 min. The membrane was then blocked in 5% milk/1X TBST (50 mM Tris-HCl, 150 mM NaCl, 0.05% Tween-20) for at least 1 hour, and then the indicated primary antibody was then applied. The following day, if a secondary antibody was required, then the membrane was washed 3 X with 1X TBST, and then placed in the conjugated secondary antibody for at least 2 hours. The membrane was then washed 3 X with 1 X TBST for 10 minutes with shaking, and then once with 1X TBS (1X TBST, but no Tween-20 added). The Clarity ECL Substrate (BioRad) and the Amersham™ Imager 600 (GE Life Sciences) machine were used to reveal the membranes. After imaging, the membranes were stained with Ponceau (5% (v/v) glacial acetic acid, 0.1% (w/v) Ponceau S), and left to dry before imaging.

Co-immunoprecipitation

Approximately 1-2 g of *N. benthamiana* leaves were weighed out and flash frozen in liquid N_2. Two 6 mm punches were taken from the leaves for input before weighing the sample. Samples were ground to a fine powder using a mortar and pestle and put on ice to slowly thaw. 5 times the amount of tissue in weight was calculated and converted to mL. This quantity of mL of ice-cold extraction buffer (10% (v/v) glycerol, 25 mM Tris pH 7.5, 1 mM EDTA, 150 mM NaCl, 0.5% (v/v) Triton, 2% (w/v) PVPP) was added to the thawed leaf powder, and vortexed. The sample was then placed on an end-over-end rotating shaker in the 4 ^{o}C cold room for 10 minutes. The samples were then centrifuged at 4 000 x *g* for 30 min at 4 ^{o}C, and then put on ice. The supernatant was poured slowly over 2 pieces of Miracloth (Millpore) into a funnel leading into a 15 mL Falcon tube and put on ice. GFP-Trap® Agarose beads (ChromoTek) were resuspended in the resin, and then 20 µL of the resin was pipetted into a 2 mL tube, and 40 µL of IP buffer (10% (v/v) glycerol, 25 mM Tris pH 7.5, 1 mM EDTA, 150 mM NaCl, 0.5% (v/v) Triton) was added to make the bead slurry. 60 µL of the slurry was added to the sample in the 15 mL falcon tube and turned end-over-end for 2 hours at 4 ^{o}C. The sample was kept on ice as continuously as possible and centrifuged at 1 000 x *g* for 1 minute and then the supernatant was discarded. 1 mL of fresh IP buffer was added to the beads and then centrifuged again at 1 000 x *g* for 1 minute. The supernatant was discarded, and the washing step was repeated 4 more times until the supernatant was clear. After the last wash, as much liquid as possible was removed. 4 X SDS loading buffer was added to the beads (as described above) so that the final volume was 40 µL. The samples were then prepared according to the immunoblotting protocol, as described above. To continue with IP-MS analysis, see protocol as described below.

IP-MS analysis

Samples prepared using the GFP-Trap® as described above were given to the Proteomic Centre Tübingen in collaboration with Irina Droste-Borel, where the sample running took place. The eluates were analysed by SDS gel electrophoresis and were run on the Q Exactive™ HF-X Hybrid Quadrupole-Orbitrap™ Mass Spectrometer (ThermoScientific). Analysis of protein groups was performed by Gautier Langin. Significant enrichment for protein groups was assessed on Rstudio through analysis of associated spectral counts using the R package lPinquiryv4 (Kuhn et al., 2023). For each *N. benthamiana* protein group, the closest *A. thaliana* orthologue was retrieved using BlastP software, with an E value < e^{-10} (https://blast.ncbi.nlm.nih.gov/Blast.cgi?PROGRAM=blastp&PAGE_TYPE=BlastSearch&LINK_LOC=blasthome). *N. benthamiana* protein sequences were extracted from Kourelis et al., 2019 and blasted against the *A. thaliana* proteome Araport 11 (Cheng et al., 2017). In the case of protein groups matching with multiple *N. benthamiana* proteins, each individual protein was blasted and the *A. thaliana* protein with the highest occurrence as a top hit was considered. Downstream gene ontology (GO) analysis was performed using the list of *A. thaliana* genes on ShinyGO v0.77 (http://bioinformatics.sdstate.edu/go/).

FLIM-FRET

Leaf discs from *N. benthamiana* plants expressing the indicated protein were used for fluorescence lifetime imaging microscopy (FLIM) experiments. The experiments were conducted using a Leica SP8 confocal laser scanning microscope equipped with time-correlated single photon counting (TCSPC) electronics, photon-sensitive detectors (HyD SMD detector), and a pulsed white light laser. The abaxial side of the leaves were imaged using a Leica C-APOCHROMAT 63x/1.2 water immersion objective lens. Green fluorescent protein (GFP) was excited at 488 nm, and fluorescence emission was collected between 500-540 nm. mCherry was excited at 580 nm and the corresponding fluorescence emission was collected between 590-640 nm. FLIM data sets were captured using the Leica LASX FLIM wizard, which was linked to the PicoQuant SymPhoTime 64 software (Picoquant GmbH). The FLIM GFP images were acquired by exciting the samples with a 470 nm pulsed laser (LDH-P-C-470, Picoquant GmbH) for 35 repetitive scans at 20 MHz, with an image resolution of 256 x 256 and a pixel dwell time of approximately 20 µs. The corresponding emission was detected with HyD SMD from 455 nm to 505 nm, and images were collected until 1500 counts were achieved for each pixel. The fluorescence lifetime calculations were performed using the PicoQuant SymPhoTime 64 software. A two-exponential decay fit was used for GFP. Microscope calibration and measurements were taken in collaboration with Kaltra Xhelilaj.

Size exclusion chromatography (SEC)

17 mg of *N. benthamiana* leaf tissue was collected and flash-frozen in liquid N_2 and ground to a fine powder using a mortar and pestle. To approximately 600 µL of leaf powder in volume, 700 µL of extraction buffer (50 mM Tris pH 8, 150 mM NaCl, 2.5 mM EDTA, 10% (v/v) glycerol, 5 mM DTT, 0.1% (v/v) NP-40) was added and homogenized by mixing up and down with a pipette. The sample was then centrifuged at 16 000 x *g* for 15 min at 4 ^{o}C. 650 µL of the supernatant was transferred to a fresh tube and then centrifuged at 16 000 x *g* for 15 min at 4 ^{o}C. 600 µL of the remaining supernatant was transferred to a fresh tube and then subjected to SEC on a Superdex 200 Increase 10/300 GL (Cytiva) using the ÄKTA Pure^{TM} protein purification system (Cytiva) using running buffer (50 mM Tris pH 8, 150 mM NaCl, 2.5 mM EDTA, 10% (v/v) glycerol). 500 µL fractions were collected from the column, and samples with a peak using the indicated UV filter were subjected to immunoblotting, as described above.

Blue native PAGE

55 mg of *N. benthamiana* leaf tissue was collected and flash-frozen in liquid N_2. Samples were ground to a fine powder using the RetchMill (Qiagen) at 16 Hz for 30 seconds. 198 µL of GTEN-DDM buffer (10% (v/v) glycerol, 100 mM Tris-HCl pH 7.5, 1 mM EDTA, 150 mM NaCl, 5 mM DTT, 1X plant protease inhibitor cocktail tablet (Sigma), 0.5% (w/v) DDM (nDodecyl β Dmaltoside)) was added to the tissue and vortexed. The samples were centrifuged at 20 000 x *g* at 4 ^{o}C for 30 minutes. The supernatant is the sample that is used for BN-PAGE. 3 parts of the 4X NativePAGE sample buffer (ThermoFisher Scientific) was added to the supernatant. NativePAGE 5% G250 Sample Additive (ThermoFisher Scientific) was added to the sample at 0.5 µL / 20 µL ratio and mixed. The wells of a Novex NativePAGE 3-12% Bis-Tris Protein Gel (ThermoFisher Scientific) were rinsed with NativePAGE Dark Blue Cathode Buffer (ThermoFisher Scientific) thrice, and then filled with the NativePAGE Dark Blue Cathode Buffer. The outer chamber was filled with the NativePAGE Anode Buffer (ThermoFisher Scientific), and the inner chamber was filled with the NativePAGE Dark Blue Cathode Buffer. The samples were loaded into the wells and then 5 µL of the Native Mark Protein Standard (ThermoFisher Scientific) was loaded. The tank was run at 150 V for 30 minutes, then the inner chamber buffer was changed to the NativePAGE Light Blue Cathode Buffer (ThermoFisher Scientific). The tank was run at 150 V for 30 minutes, then increased to 250 V for 90 minutes, or until the proteins reached the bottom of the gel. The gel was removed from the cassette and the protein ladder was cut out and stained with Coomassie Brilliant Blue (50% (v/v) methanol, 10% (v/v) acetic acid, 0.5% (x/v) CBB-R250, 40% (v/v) ddH_2O). The remaining well of the gel was removed and a wet transfer using a PVDF membrane, filter paper, and 1 X Transfer Buffer (ThermoFisher Scientific) was done. The transfer was run for 1 hour at 30V, with a maximum current of 500 mA. The PVDF membrane was then taken to

proceed with the immunoblotting blocking and imaging as described above. The membrane was stained using CBB, and then both the membrane and the protein ladder gel were de-stained using de-staining solution (50% (v/v) methanol, 10% (v/v) acetic acid, 40% (v/v) ddH_2O).

Cytosolic Ca^{2+} measurements

The R-GECO1-mTurquoise plasmid (Waadt et al., 2017) was co-infiltrated with the indicated plasmid via *A. tumefaciens* into *N. benthamiana* in a 1:1 ratio, for a final OD_{600}=0.5. Protein expression was verified by GFP fluorescence under a stereo-microscope and Ca^{2+} imaging was conducted 24 hours post infiltration. Fluorescence signals of Ca^{2+} experiments were conducted utilising a charge-multiplying CCD camera (QquantEM; Photometrics) affixed to a CARV (Crestoptics) confocal spinning disc unit. Within the CARV mechanism, three filter wheels were employed while concurrently displacing the spinning disc from the light trajectory. Excitation of the R-GECO1 and mTurquoise subunits was achieved through the implementation of an LEC illumination system (pE4000; CoolLED) at wavelengths of 435 nm and 580 nm, respectively. Emission signals passed through dichroic mirrors with cut-off wavelengths of 450 nm (T450 LPXR; Chroma Technology Corp.) and 590 nm (FF593 BrightLine; Semrock) and band filters at 475/28 nm (BrightLine HC; Semrock) and 628/40 nm (BrightLine; Semrock). Image processing and subsequent analysis were executed using the ImaheJ/Fiji software package. Experimental procedure and analysis were performed by Dr. Shouguang Huang.

Ca^{2+} channel inhibition

3 mM of $LaCl_3$ (final concentration) was added to the *A. tumefaciens* culture immediately before infiltration into *N. benthamiana*. Samples were taken for immunoblot 24-40 hours post infiltration, as indicated, and cell death photos were taken 3 days post infiltration.

Confocal microscopy

Punches were taken of *N. benthamiana* leaves after *A. tumefaciens* infiltrations at the indicated time point. The abaxial side of the leaves were imaged using the LSM 880 confocal microscope (ZEISS) with a 40x objective lens. Excitation/emission was 488 nm/498-530 nm for GFP and 561/571-610 nm for mCherry. Image processing and analysis was performed in the Fiji software (Schindelin et al., 2012).

2.2.5. *In silico* methods

Cloning

All *in silico* cloning was performed using CLC Main Workbench (Qiagen).

Blast

The CpBs4C protein sequence indicated in Appendix 6.2 was used in the tblastn webpage (https://blast.ncbi.nlm.nih.gov/Blast.cgi?PROGRAM=tblastn&PAGE_TYPE=BlastSearch&LINK_LOC=blasthome) which searches for translated protein from nucleotides in the genomes of all plant species, using taxid:3193. Then, individual genomes were taken from Published plant genomes (https://www.plabipd.de/plant_genomes_pa.ep), and were used to perform a targeted tblastn search using CpBs4C as a protein query in CLC Main Workbench (Qiagen).

Protein structure prediction and comparison

The 3D structures of the Bs4C homologues, Xa10, and Xa23 were predicted using AlphaFold2 (Jumper et al., 2021) via ColabFold x1.5.2 (Mirdita et al., 2022) without structure template. Multiple sequence alignments (MSA) were generated using a many-against-many sequence searching MMseqs2 (Steinegger & Söding, 2017) homology search using Uniref sequences (Suzek et al., 2015). Structural models presenting the lowest predicted alignment error (PAE) and predicted local-distance different test (pLDDT) (Jumper et al., 2021), were kept for further analyses. Structural analogues of CpBs4C were searched via DALI (Holm, 2022), for which the AlphaFold2 predicted structure of CpBs4C (amino acids 1-110) was used as an input to search against the Protein Data Bank (PDB). A predicted pentameric model of CpBs4C (amino acids 1-110) was determined using ColabFold Multimer (Evans et al., 2022) via ColabFold v1.5.2 (Mirdita et al., 2022). Structural analyses were made using Chimera X-1.5 (Pettersen et al., 2021). Structural analysis and predictions were performed by Dr. Julien Gronnier.

Multiple sequence alignment

Sequences (either protein or DNA) were put into Clustal Omega Multiple Sequence Alignment server (https://www.ebi.ac.uk/Tools/msa/clustalo/), and the output ClustalW parameter was selected. The resulting alignment was then put into pyBoxShade program (https://github.com/mdbaron42/pyBoxshade, Michael Baron).

Data visualization and statistical analysis

Bar charts were generated in Excel. Box and whisker plots were generated in R. All statistical analyses were performed in R. The following scripts were used in R:

```
#Load packages
library(readxl)
library(ggplot2)
library(tidyverse)
library(paletteer)
library(dplyr)
library(gapminder)
library(egg)
library(gdata)
library(ggsignif)
library(RColorBrewer)

#call a file
f <- file.choose()
DATA <- read.csv(f)

#Plot data
gg <- ggplot(DATA, aes(x = sample, y = CFU, col=sample))+
  theme_classic()+
  geom_boxplot(width = 0.5, alpha = 0.2, notch = FALSE) +
  #geom_boxplot(stat="identity") +
  geom_point(alpha = 0.4, position = position_jitterdodge(dodge.width = 0.5))+
  theme(text=element_text(family="Helvetica", face="bold", size=12))
plot(gg)

#Plot data with t-test
gg <- ggplot(DATA, aes(x = sample, y = Fm, col=sample))+
  theme_classic()+
  geom_boxplot(width = 0.5, alpha = 0.2, notch = FALSE) +
  #geom_boxplot(stat="identity") +
  geom_point(alpha = 0.4, position = position_jitterdodge(dodge.width = 0.5))+
  theme(text=element_text(family="Helvetica", face="bold", size=12))+
  geom_signif(comparisons = list(c("CpBs4C -","CpBs4C +")), test = "t.test", y_position =
c(0.85))+
  geom_signif(comparisons = list(c("NbBs4C.1 -","NbBs4C.1 +")), test = "t.test", y_position =
c(0.9))+
  geom_signif(comparisons = list(c("NbBs4C.2 -","NbBs4C.2 +")), test = "t.test", y_position =
c(0.95))+
  geom_signif(comparisons = list(c("NbBs4C.3 -","NbBs4C.3 +")), test = "t.test", y_position =
c(1))
plot(gg)

#ONE-WAY ANOVA

#Load packages
library(ggplot2)
```

```
library(ggpubr)
library(tidyverse)
library(broom)
library(AICcmodavg)
library(multcompView)

#Run the anova
one.way <- aov (CFU ~ sample, data = DATA)
summary(one.way)

#Tukey's test
tukey <- TukeyHSD(one.way)
print(tukey)

#compact letter display
cld <- multcompLetters4(one.way, tukey)
print(cld)
```

3. RESULTS

3.1. Structural and molecular characterisation of CpBs4C

The transcription activator-like effector (TALE) AvrBs4, from *Xanthomonas euvesicatoria* (*Xe* hereafter), was found to transcriptionally activate a resistance (*R*) gene in *Capsicum pubescens* called *Bs4C* (designated as *CpBs4C* hereafter). The translation of CpBs4C induces a cell death reaction, and ultimately limits the proliferation of *Xe* (Strauß et al., 2012). The underlying mechanism of CpBs4C cell death and other TALE-induced executor proteins has been a topic of interest for many research groups, including ours, for the last several years. Until now, there has been little to no clarity regarding the native function of CpBs4C aside from its TALE-triggered function in the context of plant immunity and how it activates cell death.

3.1.1. Homologues of CpBs4C are found in other Solanaceous species

A previous PhD student, Janett Elsaesser, identified homologues of CpBs4C in species other than *C. pubescens*, including *C. annuum* (Elsaesser, 2014). However, the updated genomes of numerous species have been released since her findings in 2014, providing a basis to screen up-to-date genomes for *CpBs4C*-like genes across plant species. Accordingly, CpBs4C was re-blasted to these new genomes and analysed in the context of J. Elsaesser's original findings. Using BLAST (Basic Local Alignment Search Tool) with tblastn (translated protein to nucleotide) search, the CpBs4C full-length protein was used as a protein query against the nucleotide translated genomes of all plant species (taxid:3193). There were multiple hits for potential homologues in a wide variety of plant species, as shown in Table 3.1. The constraints used to define a potential CpBs4C homologue were based on three parameters: 1. There was an ATG at the beginning of the potential protein-coding region, 2. the predicted protein was similar in length to that of CpBs4C (ranging from 120 to 180 amino acids) and 3. the identity cover was greater than 20%. This dramatically reduced the number of potential homologues that were investigated and essentially only included BLAST hits from the order Solanales.

Table 3.1. Hits from CpBs4C tblastn against all plants.

Scientific species	% ident	Accession
Capsicum pubescens	87.8	JX944826.1
Capsicum pubescens	81.21	JX944827.1
Solanum pinnatisectum	63.22	CP047564.1
Solanum tuberosum	53.89	CP055241.1
Solanum dulcamara	53.85	OX359256.1
Solanum tuberosum	49.09	CP046701.1
Solanum tuberosum	46.84	CP046686.1
Solanum pennellii	36.52	HG975447.1
Solanum lycopersicum	35.59	AK247974.1
Solanum lycopersicum	35.59	HG975520.1
Solanum lycopersicum	35.59	CP023764.1
Solanum lycopersicum	35.59	OU640351.1
Jasminum sambac	34.17	CP073640.1
Misopates orontium	34.07	OX326953.1
Jasminum sambac	32.52	CP073649.1
Fraxinus pennsylvanica	32.26	OU503049.1
Misopates orontium	31.54	OX326946.1
Ipomoea trifida	31.25	CP025656.1
Ipomoea triloba	31.25	CP025672.1
Scutellaria galericulata	31.17	OX335791.1
Misopates orontium	30.77	OX326948.1
Fagus sylvatica	30.62	OU015764.1
Quercus robur	29.66	OW028776.1
Fraxinus pennsylvanica	29.17	OU503046.1
Jasminum sambac	28.85	CP073641.1
Misopates orontium	27.78	OX326949.1
Sesamum indicum	27.5	XM_011083825.2
Vitis vinifera	27.5	AM452480.1
Andrographis paniculata	26.22	XR_007842008.1

Hits of CpBs4C homologues using tblastn of the taxid:3193. Scientific species is the species from which the hit was identified, % ident is the percent identity of the blast hit to full length CpBs4C protein sequence, Accession is the protein accession number of the blast hit.

The BLAST tool gives a very broad search of the genomes within the database; however, it is often the case that proteins are missed, not annotated, or an old version of a species' genome is used. To dive deeper to see if any additional hits in the families and subfamilies of the Solanales order were not found in the broad tblastn search, and to confirm the hits found in the broad search, we used a targeted tblastn search. The most up-to-date versions of the genomes from Published plant genomes (https://www.plabipd.de/plant_genomes_pa.ep)

were downloaded into CLC Main Workbench, and CpBs4C was used as a protein query to directly search for homologous translated protein sequences. In essentially all the genomes examined within the order Solanales, at least one hit within the tblastn search suggested a CpBs4C-like protein.

It was decided that the focus would be on the homologues from *C. annuum, C. pubescens, Nicotiana benthamiana*, and *Solanum lycopersicum*, because of the accessibility of plant material and relevance to the broader work conducted in the lab. Only one homologue was identified in *S. lycopersicum*; therefore, it was named SlBs4C. Three homologues were identified in *N. benthamiana*, and they were termed NbBs4C.1, NbBs4C.2, and NbBs4C.3, based on their similarity to CpBs4C, meaning that the potential protein coding sequence for NbBs4C.1 has the closest % amino acid similarity to CpBs4C (Table 3.2, Figure 3.1). Furthermore, the homologues from *C. annuum* were previously annotated in the lab, so they were named CaBs4C.1, CaBs4C.2, CaBs4C.3, and CaBs4C.4, also numbered in order of their % amino acid similarity to CpBs4C. One important note, however, is that upon re-blasting and subsequent stringent parameters of what a potential CpBs4C homologue could be, CaBs4C.2 was eliminated from our analysis due to the fact that it was less than 120 amino acids and had less than 20% identity to CpBs4C.

Table 3.2. CpBs4C homologues used herein.

Species	Name of protein	Length of protein	% identity to CpBs4C	Annotated in genome?
Capsicum pubescens	CpBs4C	164 aa	100%	No
Nicotiana benthamiana	NbBs4C.1	157 aa	38.42%	No
Nicotiana benthamiana	NbBs4C.2	164 aa	21.58%	No
Nicotiana benthamiana	NbBs4C.3	164 aa	23.16%	No
Solanum lycopersicum	SlBs4C	178 aa	34.48%	No
Capsicum annuum	CaBs4C.1	164 aa	82.14%	No
Capsicum annuum	CaBs4C.3	161 aa	69.84%	No
Capsicum annuum	CaBs4C.4	154 aa	54.76%	No

CpBs4C homologues used for the remainder of the study. Protein sequences can be found in Appendix 6.2. % identity refers to the percentage of amino acid identity similarity between the indicated protein and CpBs4C.

As *CpBs4C* was originally found to be activated by AvrBs4, the upstream sequences of all homologues were analysed for an AvrBs4 specific effector binding element (*EBE*). The AvrBs4 specific repeat variable diresidue (RVD) composition, as determined in Strauß et al., 2012 (NI NG NI NI NG NG NI NS NG NI NS NG HD HD NS HD NG NG), was used as the query to

search for potential compatible *EBEs* in the 1000 base pairs (bp) upstream of the ATG of each potential homologue. This search was performed using TAL Effector Nucleotide Targeter 2.0 (Doyle et al., 2012). None of the homologues from *N. benthamiana*, *C. annuum*, and *S. lycopersicum* were found to have an AvrBs4 compatible *EBE* upstream of their predicted ATG start codon, indicating that these genes are probably not activated by AvrBs4 and likely have a function lying elsewhere.

Taking the homologues found from *C. annuum, C. pubescens, N. benthamiana*, and *S. lycopersicum*, we can see that their amino acid composition is quite diverse by looking at their per cent identity towards one another. The lowest % identity between the homologues was between CaBs4C.1 and NbBs4C.2, at 21.35%, and the highest % identity was between NbBbs4C.2 and NbBs4C.3, at 89.63% (Figure 3.1).

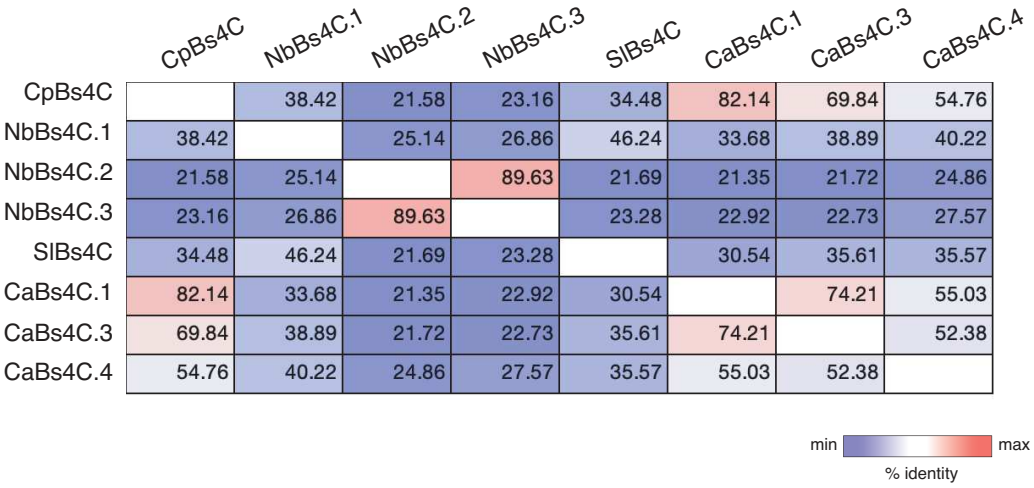

FIGURE 3.1. CpBs4C homologues from *C. annuum*, *S. lycopersicum*, and *N. benthamiana* are very diverse at the amino acid level.

Pairwise comparison of full-length amino acid composition of Bs4C homologues. Percent identity between two amino acid sequences is given in the corresponding box. Pink colour scale for % identity above 50%, and purple colour scale for % identity below 50%.

There is generally a higher similarity within a species than between two different species. For example, between NbBs4C.2 and NbBs4C.3 there was the highest similarity, in addition to CaBs4C.1 and CaBs4C.3 having a high similarity of 74.21%, whereas between species, like between CaBs4C.1 and NbBs4C.2 there was the lowest similarity of 21.35%. The exception to this, however, is between CpBs4C and CaBs4C.1, which had the highest cross-species percent similarity at 82.14%, which could be explained by the fact that they belong to the same genus, *Capsicum*. Looking into two other *Capsicum* species' genomes, specifically *Capsicum baccatum* and *Capsicum chinense*, multiple CpBs4C homologues can also be found with a similarly high % identity, ranging from around 50% to 80% identity (Supplementary Table 6.4).

While these homologues range from very similar at the amino acid level to very diverse, J. Elsaesser saw that CpBs4C had four predicted transmembrane domains and that CpBs4C localised to the endoplasmic reticulum (ER) (Figure 1.6 and Figure 1.7). Using TMHMM transmembrane topology prediction software (Krogh et al., 2001), J. Elsaesser also found that *C. annuum* homologues had zero to four transmembrane domains (data not shown). However, since the inception of AlphaFold (Jumper et al., 2021), there has been a renaissance of protein structure prediction using previously resolved structures to predict what new structures might look like with striking accuracy. Dr. Julien Gronnier took our CpBs4C homologues to see if their structures could be predicted with a high degree of probability and if the homologues looked similar or different. Their structures were predicted using AlphaFold and visualised using Chimera X (Pettersen et al., 2021). Taking the entire protein sequence of each homologue and superimposing them onto one another to determine if they are structurally similar was met with some challenges. The last 45-55 amino acids kept falling back on the structure, which affected the predicted model of all homologues (Figure 3.2).

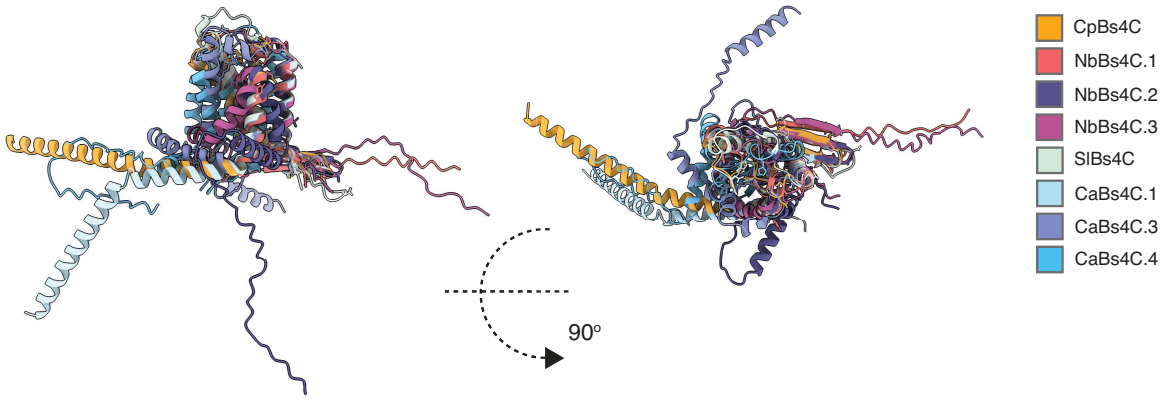

FIGURE 3.2. Structures of full length Bs4C homologues are not topologically similar.

Structural overlay of the Bs4C homologues in comparison to CpBs4C. Structures were visualised using ChimeraX.

Looking more closely at the individual structural predictions of each protein, the last 45-55 amino acids had a poor prediction score. From what could be predicted, each of the C-terminal tails from the homologues was very distinct and different from one another. Therefore, for structural prediction, these last amino acids were termed the “C-terminal tail” and deleted from further *in silico* predictions. This left us with a conserved N-terminal region, composed of four alpha helices, two that span the entirety of the predicted membrane, and two that only partially span the predicted membrane (Figure 3.3A). This conserved region had a generally high prediction score, and when all the conserved N-terminal regions were superimposed on top of one another, they were strikingly similar (Figure 3.3B). Alignment with the previously identified

localisation of CpBs4C (Elsaesser, 2014; Wang et al., 2018), the longest alpha helices are similar in length to the width of the ER, which has been calculated to be around 40 to 55 nm wide (Pain et al., 2019; Stephenson & Hawes, 1986).

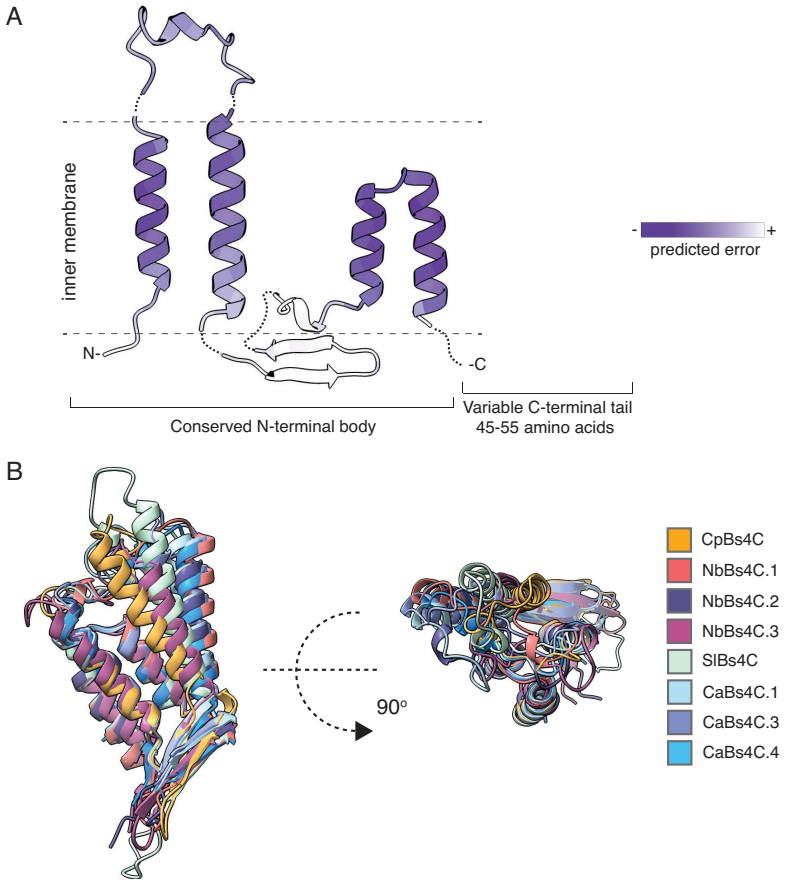

FIGURE 3.3. All Bs4C homologues have a topologically similar core structure.

A | The conserved core structure of CpBs4C. N and C indicate position within the protein. Dashed grey lines indicate membrane boundaries. Colour score is for the predicted error of the structure in Alphafold. Figure created by Dr. Julien Gronnier.

B | Structural overlay of the conserved N-terminal body of all Bs4C homologues, as indicated by their colour. All structures were visualised using ChimeraX.

Naturally, the next step was to test the homologues to see if they had a similar subcellular localisation and function to that of CpBs4C; however, cloning of all these genes and expressing them in a higher-order vector proved to be a challenge. We were unable to detect any protein expression for the *C. annuum* and the *S. lycopersicum* homologues, when infiltrated into *N. benthamiana* using *Agrobacterium tumefaciens* (agroinfiltration hereafter). The only species that successfully had all homologous genes expressing detectable protein ectopically in *N. benthamiana* were the homologous genes coming from *N. benthamiana*, *NbBs4C.1, NbBs4C.2*, and *NbBs4C.3*, which are the genes that were decided to move forward with.

3.1.2. The homologues from *N. benthamiana* have two different cell death phenotype classes

The homologues from *N. benthamiana* were placed under the control of a strong constitutive promoter (Cauliflower mosaic virus 35S promoter; 35S), and then were ectopically agroinfiltrated into *N. benthamiana*. It was found that there were two different classes of cell death phenotypes. NbBs4C.1 has a cell death phenotype similar to that of CpBs4C, which can be seen both visually with cell death upon the leaf and the timing of the cell death (visible cell death symptoms can be seen as early as 36 hours post infiltration), but also quantifiably with a significant reduction in photosynthetic ability (Figure 3.4). The two homologues from *N. benthamiana* that are the farthest in amino acid similarity to CpBs4C, NbBs4C.2 and NbBs4C.3, do not induce a cell death phenotype and do not cause a reduction in photosynthetic capacity (Figure 3.4). Notably, when these proteins were ectopically overexpressed, they had different accumulation levels of protein, with CpBs4C, NbBs4C.2, and NbBs4C.3 all having similar levels of expression, and NbBs4C.1 having a visibly dramatic reduction in protein accumulation (Figure 3.4B).

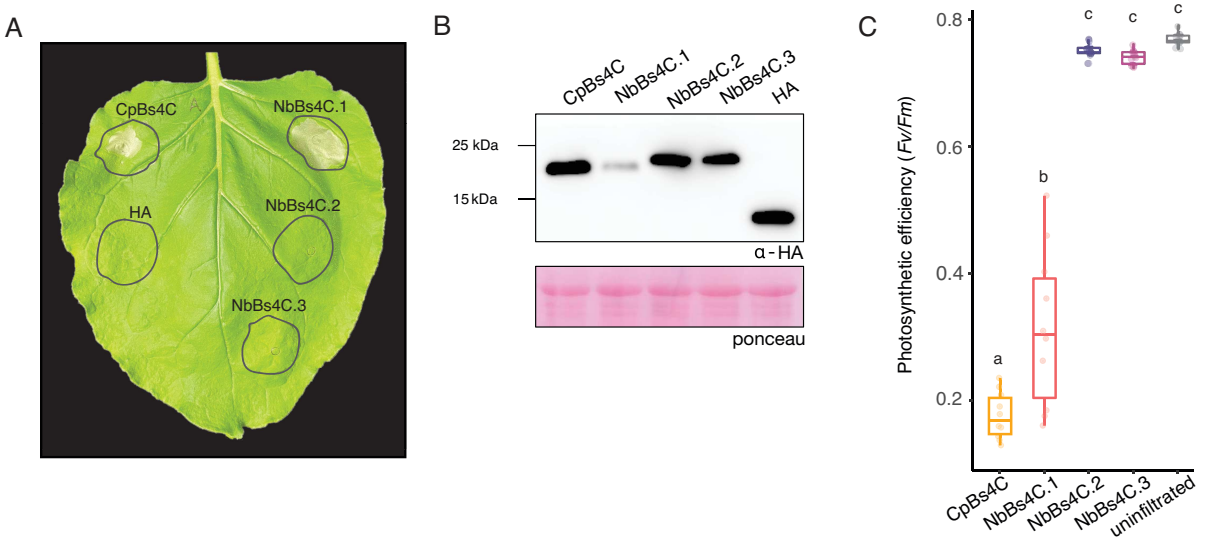

FIGURE 3.4. NbBs4C.1 has a similar cell death phenotype to CpBs4C.

A | Overexpression constructs agroinfiltrated into *N. benthamiana*. All constructs are driven by *35S* promoter and have a C-terminal HA tag. Photo taken three days post infiltration.
B | Immunoblot of protein accumulation of homologues in *N. benthamiana*. Sample taken 24 hours post agroinfiltration. Samples were run on a 12% SDS-PA gel. Anti-HA-HRP antibody was used to detect protein. Ponceau stained membrane serves as a loading control. The numbers on the left side of each blot indicate the molecular weight (kDa) determined by protein ladder.
C | Photosynthetic capacity of tissue after agroinfiltration into *N. benthamiana.* Sample taken at four days post infiltration. Values are presented in a box and whisker plot to show variation in samples, n=10 leaves, statistically significant groups ($p<0.05$) are presented with letters resolved by a one-way ANOVA with post hoc Tukey's test.

After observing that the homologues fell into two different categories: cell death or no cell death, but have such striking structural similarity to each other, we next tested whether this difference in phenotype is due to a difference in the localisation or localisation pattern of the homologues. The C-terminally GFP-tagged CpBs4C and *N. benthamiana* homologues showed a similar localisation pattern under the confocal microscope, in that they all localised to the ER (Figure 3.5). An mCherry-tagged ER marker (HDEL-mCherry) was used to determine the structural network of the ER. Consistently, CpBs4C, NbBs4C.1, NbBs4C.2, and NbBs4C.3 all localised along the tubules of the ER, but they also formed these rather dense aggregates found at intersections of the ER tubules, which is reminiscent of the localisation of AtLNP1 (Arabidopsis LUNAPARK1) at the ER 3-way junctions (Kriechbaumer et al. 2018). ER 3-way junctions are the points at which ER tubules come together to stabilise and shape the network of the ER (Chen et al., 2013). Interestingly, these Bs4C dense aggregates can be stable at ER 3-way junctions, but they can also be very mobile (refer to Figure 1.7B). Taken together, these results suggest that while the Bs4C homologues have two different classes cell death phenotypes, they all have a similar localisation pattern within the ER.

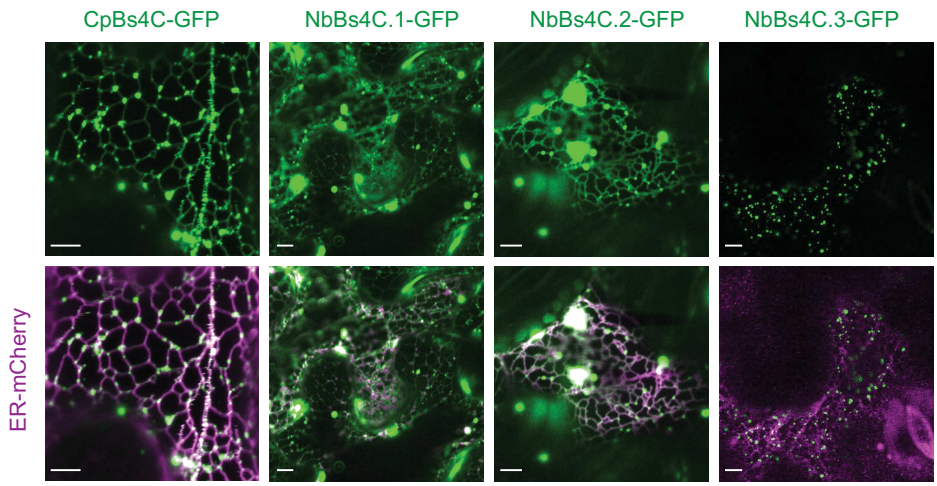

FIGURE 3.5. CpBs4C, NbBs4C.1, NbBs4C.2, and NbBs4C.3 localise to the ER.

Co-expression of indicated Bs4C homologue tagged with GFP and ER-mCherry 24 hpi in *N. benthamiana*. Top panel is GFP filter alone, bottom panel is GFP and mCherry filter merged. White scale bar in bottom left corner of each image represents 5 µm.

One could argue that this cell death phenotype of the NbBs4C.1 homologue is due to ectopic overexpression from a T-DNA (transfer DNA) insertion via agroinfiltration. To rule this out, designer TALEs (dTALEs) were constructed to bind upstream of the *N. benthamiana* homologues and activate the transcription of these endogenes (Morbitzer et al., 2010). The dTALEs were arranged to bind to a region of DNA approximately 100 bp upstream of the ATG of the homologues to activate transcription (Figure 3.6A, Supplementary Information S3).

Indeed, qPCR-based quantification of NbBs4C transcripts induced by agroinfiltration of the dTALEs into *N. benthamiana* revealed that the dTALEs were able to specifically activate the intended endogenes. The dTALE activating *NbBs4C.1* (dT779) was the only dTALE that induced a cell death response and reduced the photosynthetic capacity of the infiltrated area (Figure 3.6). It was also found that the dTALEs activating *NbBs4C.2* and *NbBs4C.3* (dT780 and dT782, respectively) did not have a visible cell death reaction or a reduction in photosynthetic capability when activated by a matching dTALE (Figure 3.6).

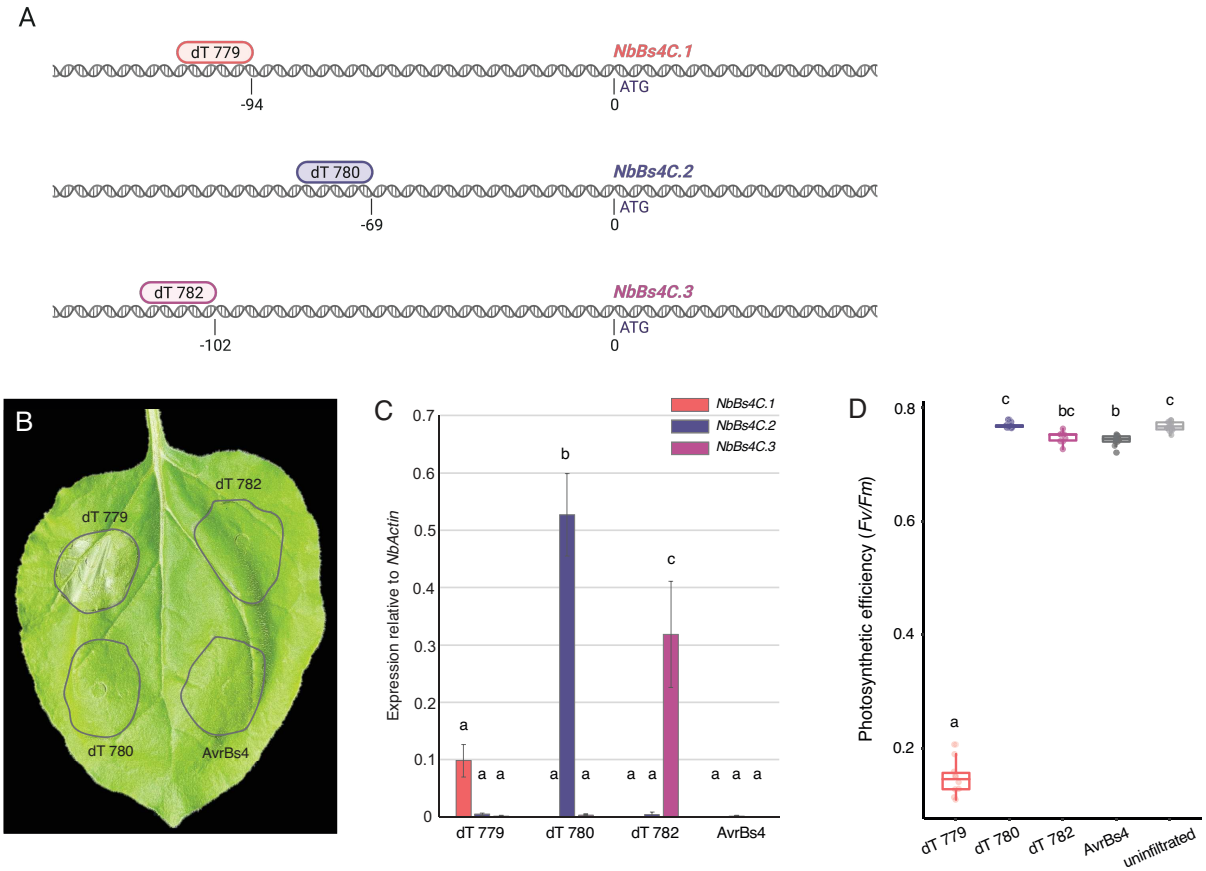

FIGURE 3.6. dTALE 779 activates *NbBs4C.1* and induces cell death.

A | Schematic of where the dTALEs bind. dTALE 779 (dT 779) binds 94 bp (-94) upstream of the ATG of *NbBs4C.1*. dTALE 780 (dT 780) binds 69 bp (-69) upstream of the ATG of *NbBs4C.2*. dTALE 782 (dT 782) binds 102 bp (-102) upstream of the ATG of *NbBs4C.3*. Image created using BioRender.com.
B | dTALE constructs agroinfiltrated into *N. benthamiana*. Photo taken three days post infiltration.
C | Quantitative real-time PCR was used to determine the activation of each targeted gene by the corresponding dTALE. Samples were taken 40 hours post agroinfiltration. Values are means + standard deviations. n=3 technical replicates coming from the same cDNA, each gene was normalized again the expression of *NbActin* from the same sample, statistically significant groups ($p<0.05$) are presented with letters resolved by a one-way ANOVA with post hoc Tukey's test.
D | Photosynthetic capacity of tissue after agroinfiltration into *N. benthamiana.* Sample taken at four days post infiltration. Values are presented in a box and whisker plot to show variation in samples n=10 leaves, statistically significant groups ($p<0.05$) are presented with letters resolved by a one-way ANOVA with post hoc Tukey's test.

3.1.3. *NbBs4C* homologues have an impact on bacterial growth

As it was previously determined that *CpBs4C* plays a role in limiting bacterial growth when activated by AvrBs4 (Strauß et al., 2012), we thought it would be interesting to see if cell death induced by *NbBs4C.1* would also reduce bacterial *in planta* growth, and also if the non-cell death-inducing homologues had any impact on bacterial growth *in planta*.

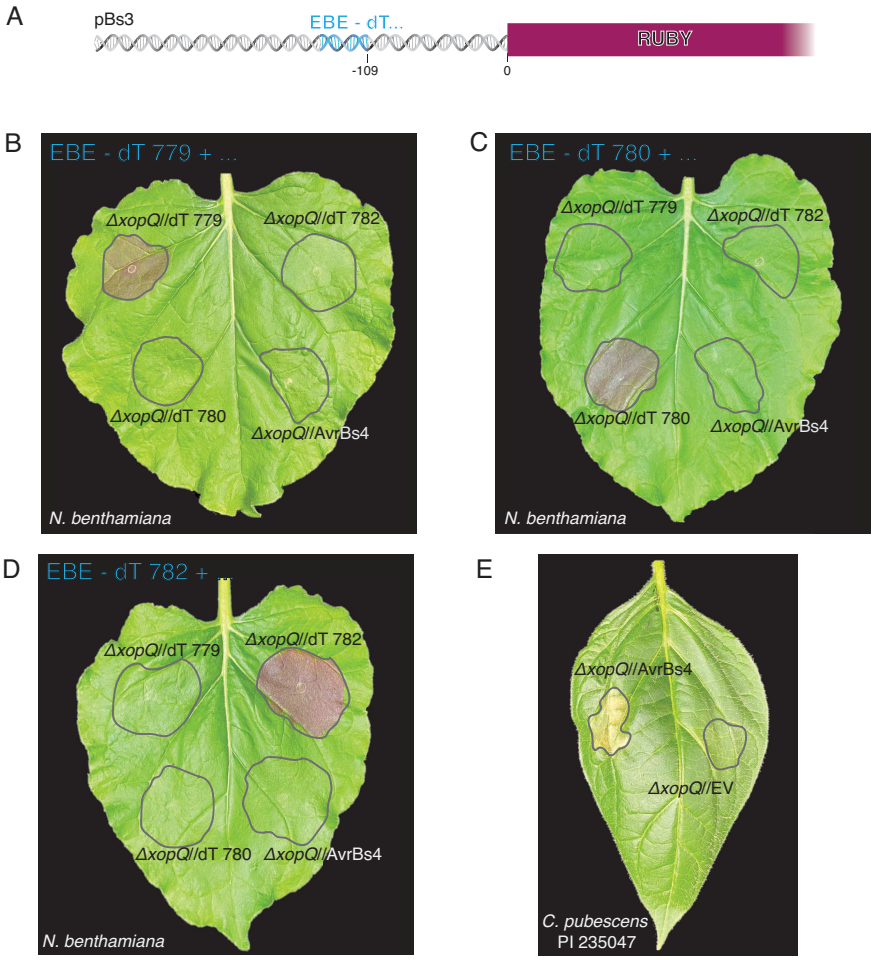

FIGURE 3.7. dTALEs are functional in *Xe ΔxopQ*.

A | Schematic of *Bs3* promoter with the desired *EBE* integrated 109 bp before (-109) the ATG of the RUBY cassette.
B | Co-infiltration of *A. tumefaciens* containing the pBs3-EBE:RUBY construct with the *EBE* for dTALE 779 (dT 779) and the *ΔxopQ* strains, individually the indicated TALE, into WT *N. benthamiana*. Photo taken three dpi.
C | Co-infiltration of *A. tumefaciens* containing the pBs3-EBE:RUBY construct with the *EBE* for dTALE 780 (dT 780) and the *ΔxopQ* strains, carrying the indicated TALE, into WT *N. benthamiana*. Photo taken three dpi.
D | Co-infiltration of *A. tumefaciens* containing the pBs3-EBE:RUBY construct with the *EBE* for dTALE 782 (dT 782) and the *ΔxopQ* strains, carrying the indicated TALE, into WT *N. benthamiana*. Photo taken three dpi.
E | Infiltration of *ΔxopQ* either containing AvrBs4 or empty vector (EV) into *C. pubescens* PI 235047. Photos taken three dpi.

To test this, the dTALEs in Figure 3.6 were put into the *Xanthomonas* compatible expression vector, pSKX1 (Tran et al., 2018), and then transformed into the *Xe ΔxopQ* (ΔxopQ hereafter) mutant bacterial strain, so that bacterial growth curves could be performed in WT *N. benthamiana* (Adlung et al., 2016). The ΔxopQ strain was used because the effector XopQ is recognised in *N. benthamiana* by ROQ1 (RECOGNITION OF XOPQ 1) and would affect the bacterial growth phenotype that the *NbBs4C* homologues could have (Schultink et al., 2017). To confirm that the dTALEs in *Xanthomonas* could still bind to their compatible *EBE* and activate the cognate downstream genes, the corresponding *EBE* was placed into the promoter of *C. annuum* executor *Bs3* (Römer et al. 2007), upstream of the RUBY reporter gene, which consists of the triple gene-block encoding enzymes of the betalain biosynthesis pathway that produces betalain, a visible purple pigment (He et al. 2020) (Figure 3.7A). The Bs3promoter_dTALE-EBE:RUBY construct was transformed into *A. tumefaciens*, and then co-infiltrated with the dTALE-containing ΔxopQ strains. If the appropriate dTALE binds to its corresponding *EBE*, then the downstream RUBY reporter is transcriptionally activated. Wherever RUBY is transcribed, it induces the synthesis of betalain, a purple pigment. Three days post-infiltration, each dTALE only activated RUBY with its corresponding *EBE* by developing a purple pigment in the infiltrated region, and no cross-activation was found with the other *EBEs* (Figure 3.7B-D). For example, the ΔxopQ/dT779 strain only showed a RUBY phenotype on *N. benthamiana* leaf when the pBs3_EBE-dT779:RUBY construct was co-infiltrated with it. Furthermore, we used AvrBs4 as a TALE control because it does not activate any of the tested *N. benthamiana Bs4C* homologues. We confirmed the functionality of AvrBs4 in ΔxopQ by infiltrating it into *C. pubescens* PI 235047, as AvrBs4 *EBE* is upstream of the *CpBs4C* gene and causes a visible cell death reaction (Figure 3.7E).

After the dTALEs were deemed functional in the ΔxopQ strain, their bacterial growth phenotypes were tested in WT *N. benthamiana*. Each strain was syringe-infiltrated into the leaves of the plant and allowed to grow for six days. After six days of allowing the bacteria to grow and proliferate in the plant, it was found that the dTALE targeting the endogenous activation of the cell death-inducing *NbBs4C.1* gene did indeed have an impact on bacterial growth and reduced bacterial growth by tenfold compared to AvrBs4 and one hundred-fold compared to empty vector (EV) (Figure 3.8). It can also be seen that the activation of *NbBs4C.2* and *NbBs4C.3* also had reduced bacterial growth by tenfold compared to EV but had slightly similar growth to AvrBs4. The difference in bacterial growth between the activation of *NbBs4C.1* and the activation *NbBs4C.*2 and *NbBs4C.3* was also tenfold, indicating that *NbBs4C.1* had the greatest reduction in bacterial growth upon its activation. Even though NbBs4C.2 and NbBs4C.3 had no visible cell death or reduction in photosynthetic ability (Figure 3.6), the activation of these genes still had an impact on bacterial growth. Ultimately, this

allows for the conclusion that these genes likely have a function within the plant, however, this specific function has yet to be clarified.

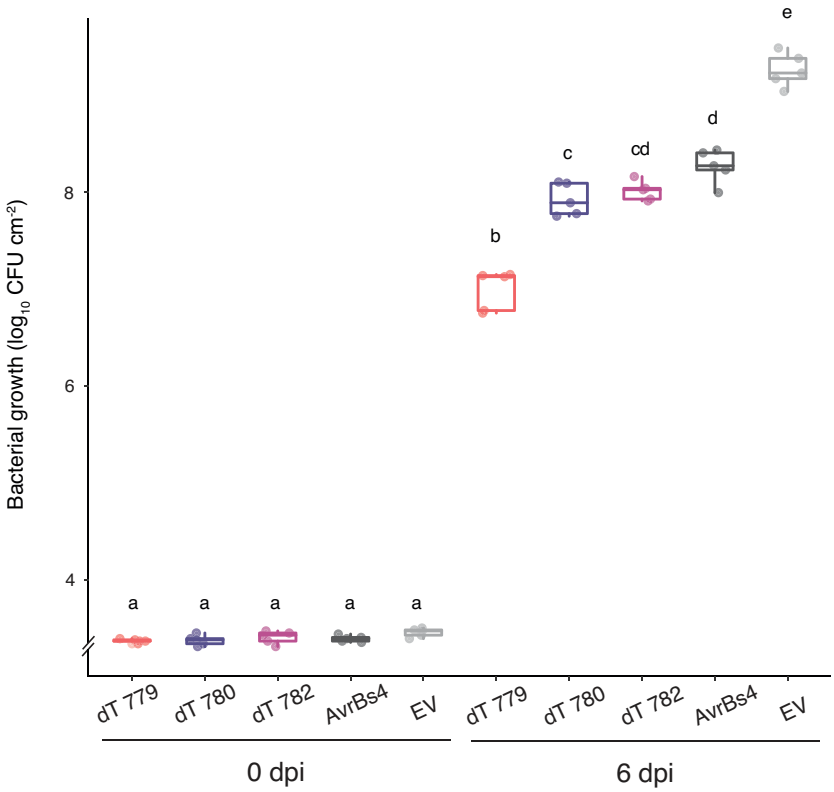

FIGURE 3.8. *NbBs4C* homologues negatively impact bacterial growth.

WT *N. benthamiana* were inoculated with the indicated strains via syringe infiltration. CFU (colony forming units) were determined both on the day of inoculation (0 dpi) and 6 days after infection (6 dpi). Bar and whisker plot shows the variance of n=5 biological replicates. Statistically significant groups ($p<0.01$) are presented with letters resolved by a one-way ANOVA with post hoc Tukey's test.

To verify that it is indeed *NbBs4C.1* which causes impaired bacterial growth and no other dTALE off-target genes, a triple knockout (KO) of all three *NbBs4C* homologues (*NbBs4C.1, NbBs4C.2*, and *NbBs4C.3*) was generated using CRISPR (Clustered Regularly Interspaced Short Palindromic Repeats) (Feng et al., 2013; Jinek et al., 2012; Stuttmann et al., 2021) mutagenesis and termed *ΔNbBs4C.1-3* (Figure 3.9). In *ΔNbBs4C.1-3*, a single A insertion in *NbBs4C.1* generated an early stop codon, a two base pair deletion and a single T insertion in *NbBs4C.2* also generated an early stop codon, and a 13 base pair deletion in *NbBs4C.3* generated an early stop codon (Figure 3.9). Hereafter, these mutant alleles will be referred to as *nbbs4c.1, nbbs4c.2,* and *nbbs4c.3*. It should also be noted that there were no obvious visible developmental or morphological discrepancies between the *ΔNbBs4C.1-3* plants and WT.

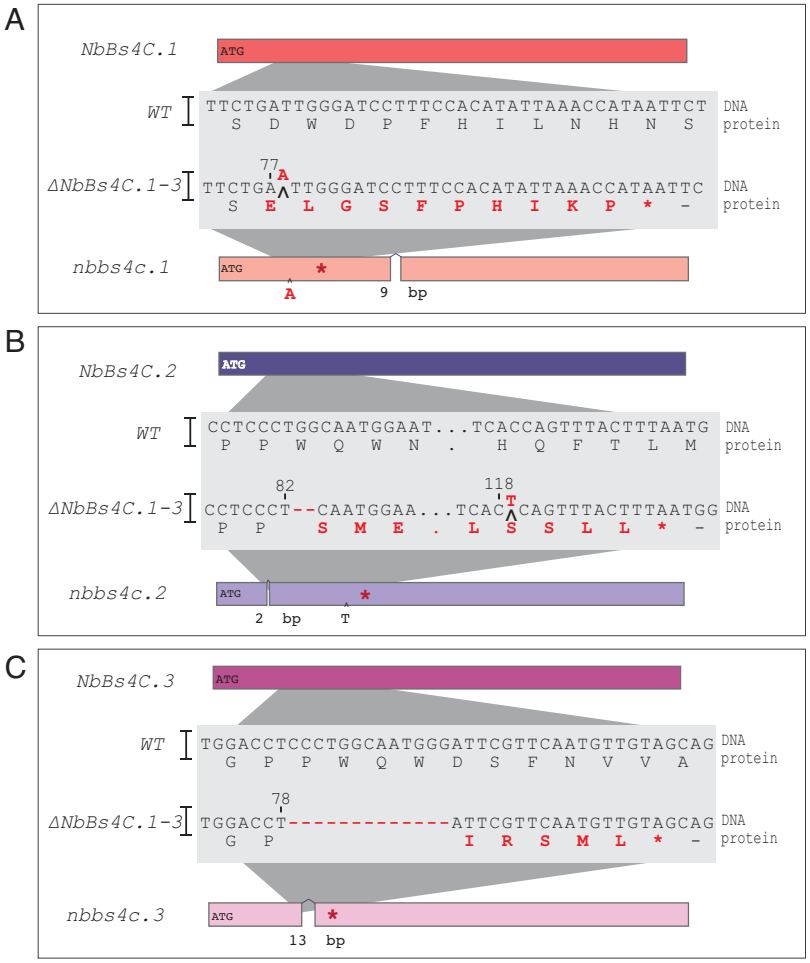

FIGURE 3.9. *ΔNbBs4C.1-3* CRISPR-induced mutations in *NbBs4C.1, NbBs4C.2,* and *NbBs4C.3*.

Gene schematic of CRIPSR induced mutations on the three homologues in *N. benthamiana, NbBs4C*.1 (A)*, NbBs4C.2* (B), *NbBs4C.3* (C). Red letters indicate changes induced via CRISPR mutagenesis. Number above DNA indicates base pair number near the mutation. Small arrow with a letter underneath indicates single base pair insertion. Large arrow with a break in the rectangle below represents a deletion, with the size of the deletion in bp directly below it. Red star indicates an early translational stop codon generated via the insertion/deletion. Dashes indicate deleted nucleotides.

Agroinfiltration of the previously used dTALEs from Figure 3.6 were used in *ΔNbBs4C.1-3* to see if there was a difference in cell death phenotype when all *N. benthamiana* homologues were knocked out. In *ΔNbBs4C.1-3*, *nbbs4c.1* was still transcriptionally activated, but there was no cell death and no reduction in photosynthetic capability (Figure 3.10). This indicates that it is indeed *NbBs4C.1* causing these cell death phenotypes, and it is neither a result of ectopic overexpression from agroinfiltration nor the consequence of dTALE off-target sites. *nbbs4c.2* and *nbbs4c.3* were also activated using the corresponding dTALEs, but there was no difference in their visible symptoms of cell death or photosynthetic capacity between the WT and the mutant. It should also be noted that in *ΔNbBs4C.1-3*, dTALE 782 was able to activate *nbbs4c.3* significantly ($p<0.001$) more than dTALE 782 was able to activate *NbBs4C.3* in WT (Figure 3.10B).

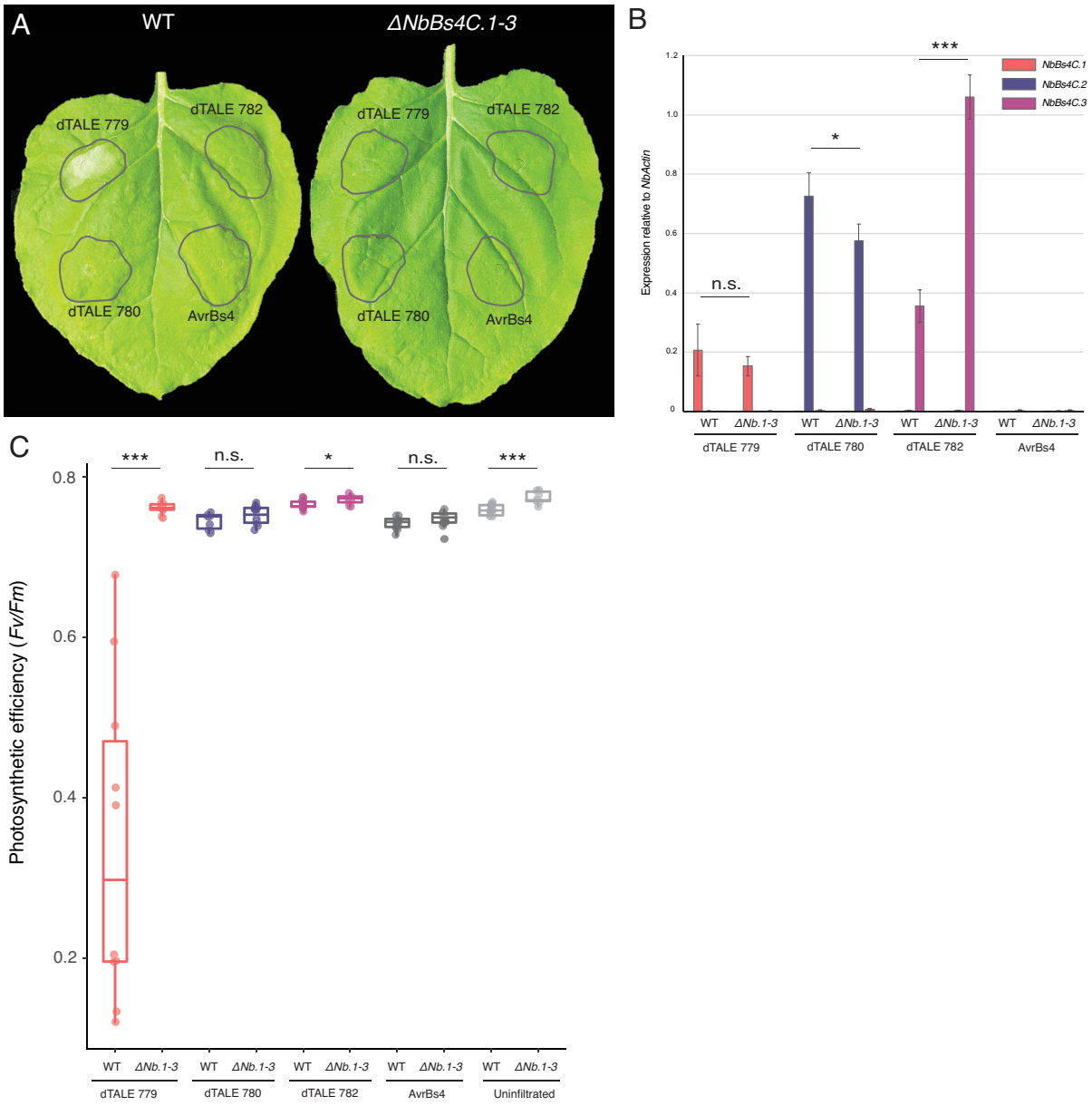

FIGURE 3.10. *ΔNbBs4C.1-3* abolishes cell death.

A | dTALE constructs agroinfiltrated into *N. benthamiana*. Photo taken three days post infiltration.
B | Quantitative real-time PCR was used to determine the activation of each targeted gene by the corresponding dTALE. Samples were taken 40 hours post agroinfiltration. Values are means + standard deviations. The same primer pairs are used to amplify both the WT and mutated alleles of the indicated gene. n=3 technical replicates coming from the same cDNA, each gene was normalised against the expression of *NbActin* from the same sample.
C | Photosynthetic capacity of tissue after agroinfiltration into *N. benthamiana.* Sample taken at four days post infiltration. Values are presented in a box and whisker plot to show variation in samples n=10 leaves. Statistical significance was determined between the indicated gene/dTALE in the WT sample versus *ΔNbBs4C.1-3* using a student's T-test, * $p < 0.05$, ** $p < 0.01$, *** $p < 0.001$, n.s. = no significance. *ΔNb.1-3* is the short form for *ΔNbBs4C.1-3*.

The same dTALEs in the *ΔxopQ* mutant were then infiltrated into both WT and *ΔNbBs4C.1-3* *N. benthamiana*, to see if knocking out the *NbBs4C* genes also had an impact on bacterial

growth. It was found that transcriptional activation of the non-functional *nbbs4c.1* gene indeed did not affect bacterial growth, with bacteria activating *nbbs4c.1* growing one hundred-fold better than the bacteria activating *NbBs4C.1* (Figure 3.11).

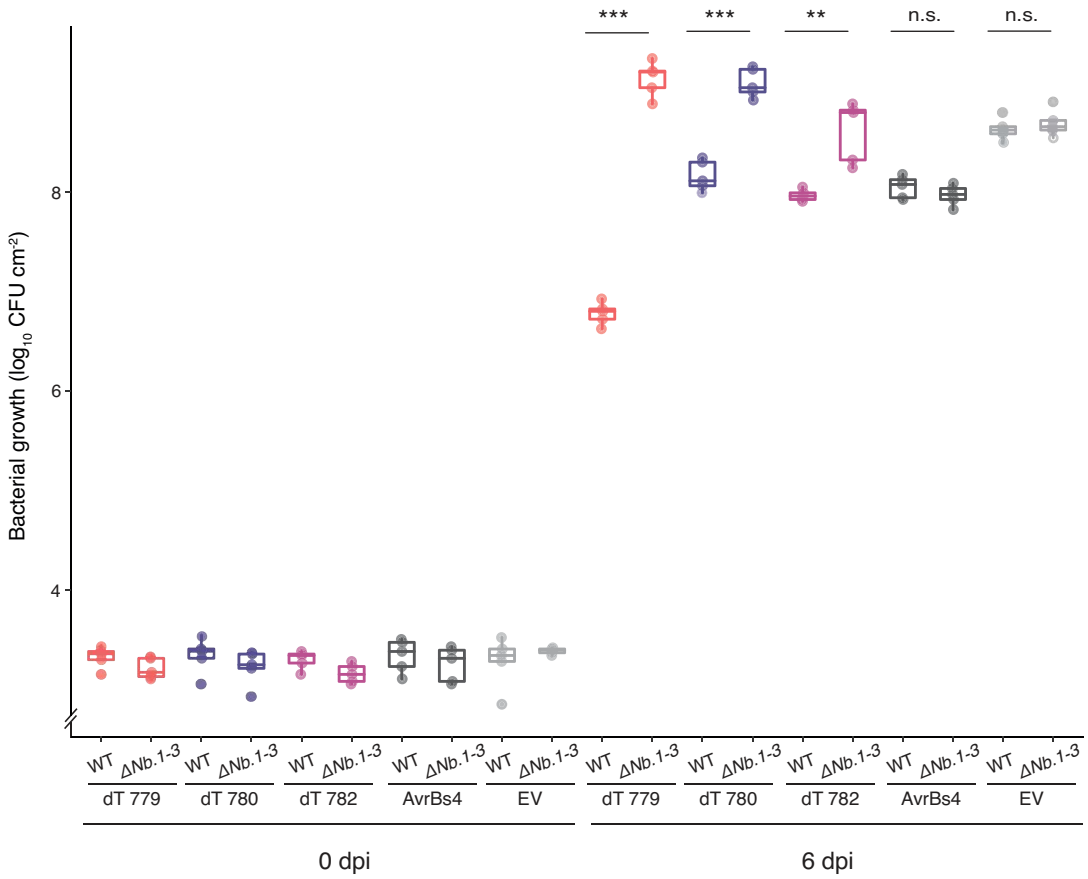

FIGURE 3.11. Activation of mutated *nbbs4c* alleles do not have a negative impact on bacterial growth.

WT and *ΔNbBs4C.1-3 N. benthamiana* were inoculated with the indicated strains via syringe infiltration. CFU (colony forming units) were determined both on the day of inoculation (0 dpi) and six days after infection (6 dpi). Bar and whisker plot shows the variance of n=5 biological replicates. Statistical significance was determined between the bacterial growth of the same strain in the WT sample versus *ΔNbBs4C.1-3* using a student's T-test, * $p < 0.05$, ** $p < 0.01$, *** $p < 0.001$, n.s. = no significance. *ΔNb.1-3* is the short form for *ΔNbBs4C.1-3.*

Even more, the bacteria activating *nbbs4c.1* grew slightly better (threefold better) than the EV control. Furthermore, the bacterial growth when *nbbs4c.2* and *nbbs4c.3* were activated, was greater than the bacterial growth when *NbBs4C.2* and *NbBs4C.3* were activated, by tenfold. There were no significant differences in bacterial growth between WT and *ΔNbBs4C.1-3* plants when either ΔxopQ//AvrBs4 or ΔxopQ//EV were infiltrated, indicating that *NbBs4C.1*, *NbBs4C.2*, and *NbBs4C.3* only have an impact on bacterial growth when they are specifically activated. With this, it is evident that *NbBs4C.1* has a clear and dramatic impact on limiting bacterial growth. Taken together with Figure 3.8, it is clear that the activation of *NbBs4C.2* and

NbBs4C.3 indeed have an impact on bacterial growth, due to the fact that when the null alleles of each gene are similarly activated, the bacterial growth is at least tenfold greater. Therefore, it stands to reason that all *NbBs4C* homologues do indeed have a function when they are activated, as shown by a change in bacterial growth when the homologues are knocked out, however, the function of such genes have yet to be elucidated.

3.1.4. CpBs4C has strong structural homology to neurotransmitter receptors

Looking at other proteins with a similar topological structure can provide insight into the potential mechanism that CpBs4C, and ultimately the Bs4C homologues, utilise to execute cell death. When the CpBs4C project was being worked on back in 2014 by J. Elsaesser, the bioinformatic tools that are around today were not available. As such, only some predictions could be made about CpBs4C's structure and function. Frequently in the literature, and also in previous studies done within the Lahaye lab, CpBs4C gets grouped with two other executor proteins Xa10 and Xa23, coming from *Oryza sativa* and *Oryza rufipogon*, respectively, mainly due to their relatively short sequence length, the number of predicted transmembrane regions, and that they all localise to the ER (Elsaesser, 2014; Nowack et al., 2022; Wang et al., 2018; Zhang et al., 2015). Once the predicted structure of CpBs4C was resolved by Dr. J. Gronnier, as seen in Figure 3.3, it was an obvious step to check if the predicted structures of Xa10 and Xa23 were similar to the structure of CpBs4C.

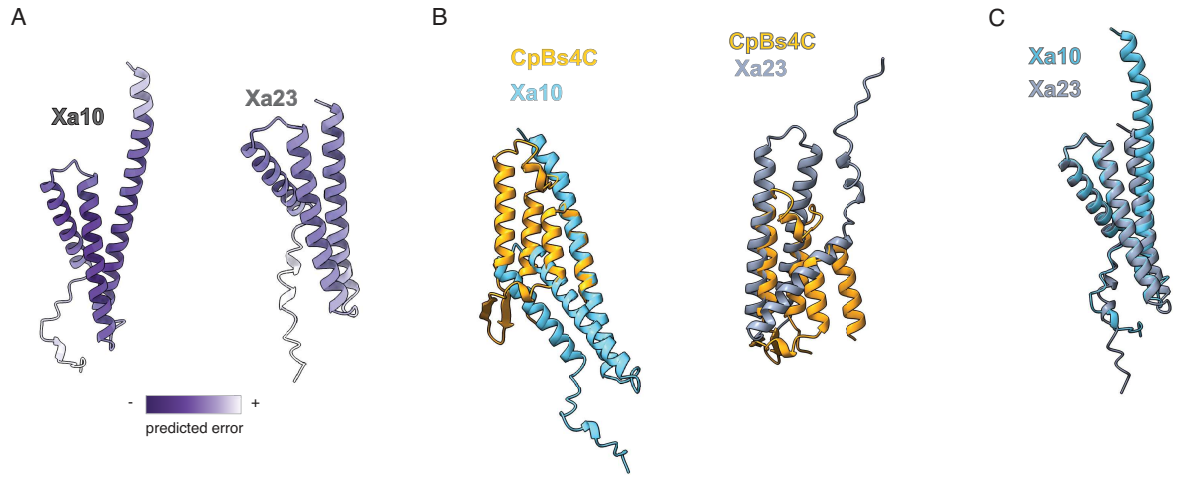

FIGURE 3.12. Xa10 and Xa23 are not structural homologues of CpBs4C.

A | Predicted structure of Xa10 and Xa23. Colour scale indicates the error likelihood of predicted error.
B | Structural overlay of CpBs4C (orange) with Xa10 (light blue) and CpBs4C with Xa23 (grey).
C | Structural overlay of Xa10 and Xa23. All structures were visualised using ChimeraX.

The structural predictions of Xa10 and Xa23 had a high confidence, which can be seen by their relatively low predicted error (Figure 3.12A). In this new structural prediction, Xa10 has three transmembrane regions, similar to the new structure (and previously hypothesised structure) of Xa23, as opposed to Xa10 previously thought to have four transmembrane domains (Nowack et al., 2022). To identify if Xa10 and/or Xa23 are similar to CpBs4C, the structural predictions were superimposed onto one another. When the CpBs4C structure was superimposed onto both Xa10 and Xa23, there were few topological similarities between them (Figure 3.12B). For example, in Figure 3.12B, it can be seen that the four alpha helices of CpBs4C do not align with the three alpha helices of Xa10 or Xa23, in either their size or in their angle of conformation. Furthermore, when comparing Xa10 and Xa23 together, they are quite structurally similar, with all of their alpha helices aligning in their angle of conformation, and the first two alpha helices aligning in their size (Figure 3.12C). Ultimately, this indicates that Xa10 and Xa23 are structurally similar and could indeed be acting in a similar manner. It also stands to reason that CpBs4C can no longer be grouped together with Xa10 and Xa23 due to their diverse structural topology, and also that CpBs4C likely has a distinct mechanism of inducing cell death compared to Xa10 and Xa23.

Seeing as Xa10 and Xa23 are not structural homologues of CpBs4C, the next step was to see if there were any other structural homologues of the conserved N-terminal region of CpBs4C (and as they have the same well-defined core structure, essentially all Solanaceous Bs4C homologues) in other organisms. Taking this well-defined core structure, Dr. J. Gronnier compared this structure to the AlphaFold database that was available as of March 2022, where all proteins with a resolved well-defined structure were deposited. The proteins that came back with high structural homology were all subunits of neurotransmitter receptors, including the GABA (gamma-aminobutyric acid) receptor alpha subunits ($GABA_A$) from *Homo sapiens* (Protein Data Bank #: 6x3xB (Kim et al., 2020)), the subunits from the serotonin receptor from *Mus musculus* (PDB#: 6y5bA (Zhang et al., 2021)), and the nicotinic receptor subunits from *Torpedo californica* (PDB#: 6uwzB (Rahman et al., 2020)) (Figure 3.13). The N-terminal core structure of CpBs4C aligned with the transmembrane regions of the neurotransmitter receptors, both being the domains that are inserted into a membrane. However, a major difference between CpBs4C transmembrane regions and the identified neurotransmitter receptor transmembrane domain regions is that CpBs4C is localised to the ER membrane, whereas the identified neurotransmitter receptors are localised to the plasma membrane (Blanco & Blanco, 2017).

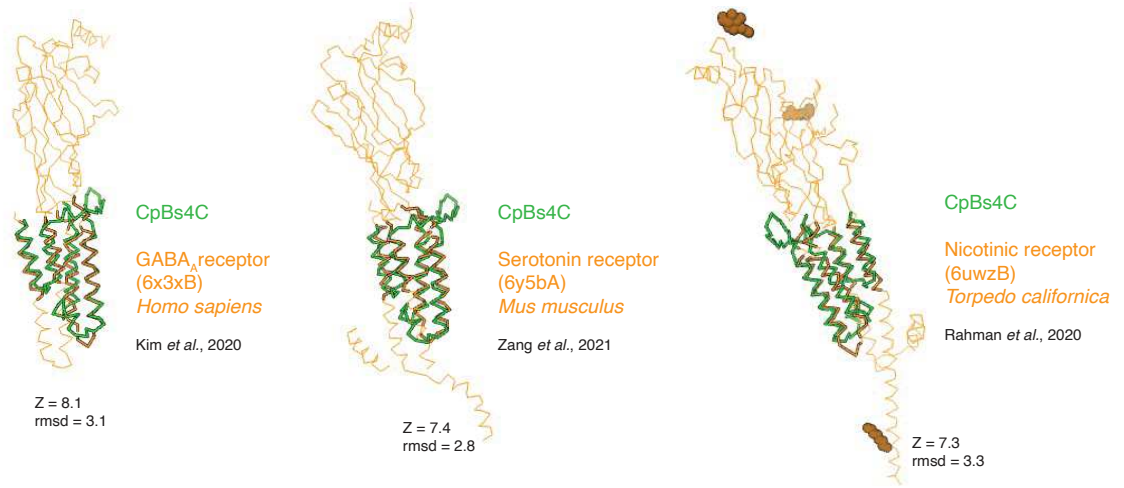

FIGURE 3.13. CpBs4C has strong structural homology to neurotransmitter receptors.

Structural homology prediction using the DALI server. Green structure is CpBs4C and the orange structure is the predicted homologue, with the host organism, and the corresponding protein data bank reference. Z-score is the DALI Z-score, and rmsd is the room mean square deviation.

Two different scoring methods were used to identify the degree of structural homology between CpBs4C and the neurotransmitters, RMSD (root mean square deviation of atomic positions), which measures the average distance between the atoms of two superimposed protein model structures (Kufareva & Abagyan, 2012), and DALI (Distance matrix alignment), which measures the residue-residue intramolecular distances between two superimposed protein segments (Holm & Sander, 1993; Holm, 2020).

Table 3.3. Scoring of structural similarity between CpBs4C and neurotransmitter receptors.

Protein	Protein ID	Species	DALI score	RMSD Score
$GABA_A$ receptor	6x3xB	*Homo sapiens*	8.1	3.1
Serotonin receptor	6y5bA	*Mus musculus*	7.4	2.8
Nicotinic receptor	6uwzB	*Torpedo californica*	7.3	3.3

DALI = distance matrix alignment score, RMSD = root mean square deviation of atomic positions score.

For the DALI Z-score, a score between 2 and 8 is a grey area, and 8 to 20 means that the two are probably homologous (Holm, 2020), and for RMSD, the smaller the value, the more similar they are (Kufareva & Abagyan, 2012). As seen in Table 3.3, for CpBs4C compared to the $GABA_A$ receptor, the DALI score and RMSD score were Z=8.1 and rmsd=3.1, respectively. For CpBs4C compared to the serotonin receptor, Z=7.4 and rmsd=2.8, and for CpBs4C compared to the nicotinic receptor, Z=7.3 and rmsd=3.3. Given the values scored for the comparison of CpBs4C to the neurotransmitter receptors, it is fair to say that the structural homology is quite strong.

The neurotransmitters mentioned above are in a specific group of receptors known as fast-acting pentameric ligand-gated ion channels (pLGICs). As suggested by their name, they are composed in a heteromeric fashion with five distinct but structurally homologous subunits, which are organised in pseudo-symmetry to encircle a central pore (Salari et al., 2014). The $GABA_A$ receptor modelled from Kim et al. 2020 was taken as inspiration for what the Bs4C homologues might look like if they formed a similar pentameric structure (Figure 3.14). As all the Bs4C homologues have a similar core structure, it is plausible that all of the Bs4C homologues could form a similar pentameric structure. The similarity between the $GABA_A$ receptor and the CpBs4C putative pentamer is visually quite similar, which laid the foundation for identifying if CpBs4C could act in a similar manner to neurotransmitter receptors.

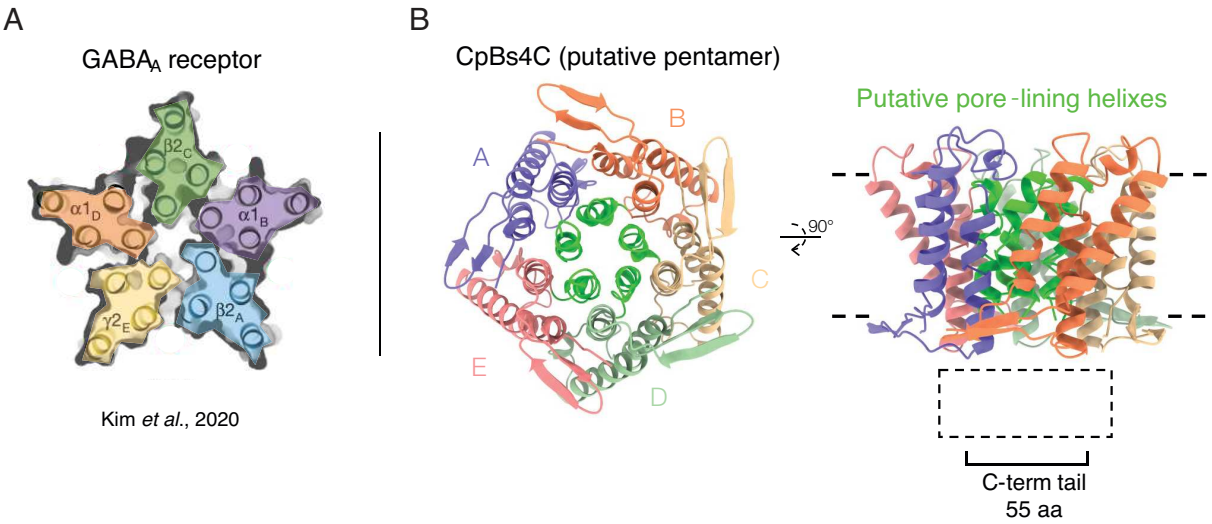

FIGURE 3.14. Putative CpBs4C pentamer has striking similarity to the $GABA_A$ receptor.

A | Resolved $GABA_A$ receptor modified from Kim *et al.,* 2020, with the five different subunits highlighted in a different colour.

B | The predicted putative pentamer of CpBs4C in a top view, and a side view, with the putative pore-lining helices on each individual unit highlighted in green. The dotted box beneath the structure in the far right panel indicates where the C-terminal tail would be.

3.1.5. CpBs4C can self-associate and form a higher-order complex

The first test to see if this putative pentamer is even a possibility was to see if CpBs4C can associate with itself. To do this, a coimmunoprecipitation (coIP) was performed, where CpBs4C with either an HA or a GFP epitope tag on the C-terminus was placed under the control of 35S promoter and was agroinfiltrated into *N. benthamiana.* Another executor, Bs3 served as a cell death-inducing protein control. After immunoprecipitation with anti-GFP beads, the anti-HA immunoblot shows that CpBs4C can be pulled down with itself, and not with GFP alone or Bs3 (Figure 3.15). Furthermore, it can be seen in the top right panel of the

coIP, that the monomeric form of CpBs4C (approximately 17 kDa) is not the only form of CpBs4C that was pulled down in the assay. The ladder effect of this lane shows that there are multiple sizes of CpBs4C being pulled down. One band at the 17 kDa range suggests that there are at least two CpBs4Cs forming a complex (one from CpBs4C-GFP, which is being pulled down, and CpBs4C-HA being immunoblotted for). However, the fact that there are multiple bands indicates that a higher-order complex could be formed.

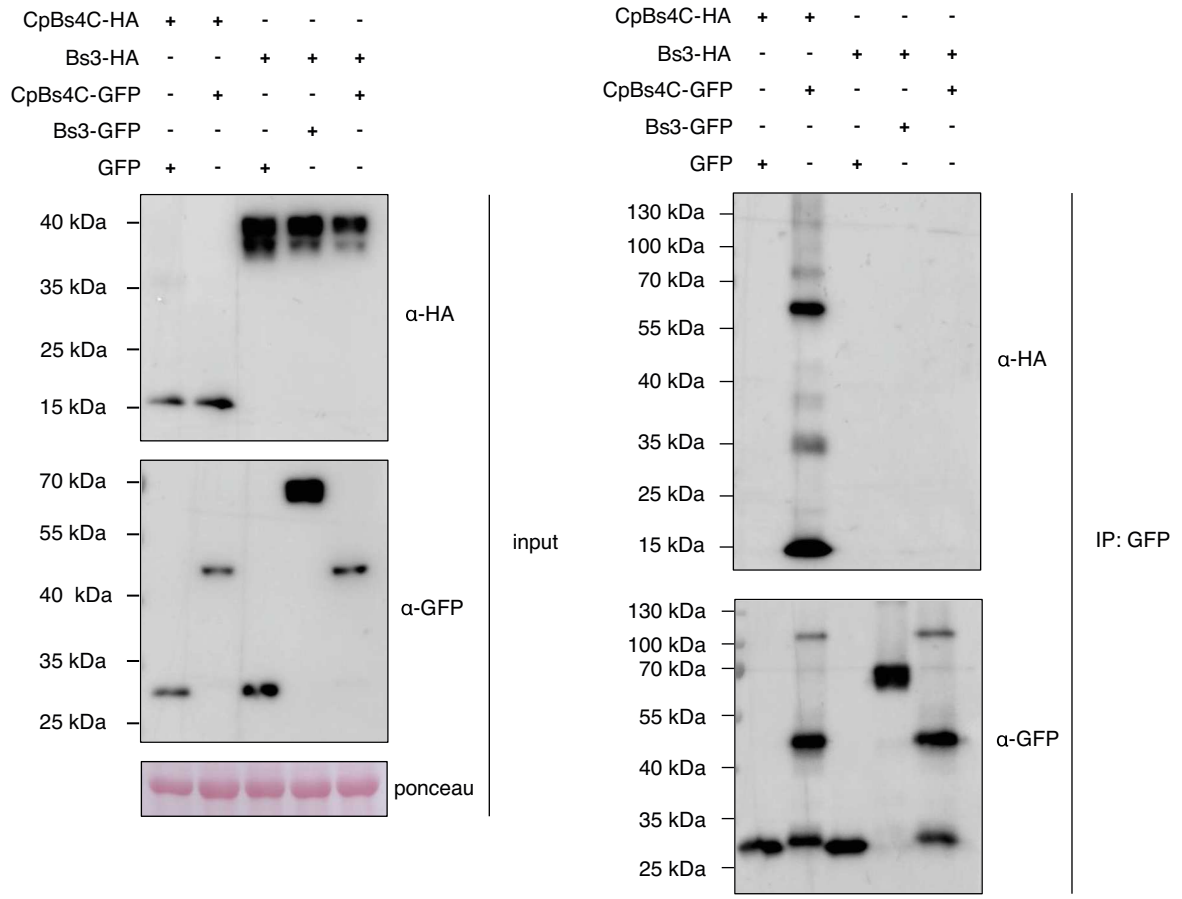

FIGURE 3.15. CpBs4C can associate with itself and might form a higher order complex.

Coimmunoprecipitation of overexpression constructs of the indicated gene and tag, where total proteins were extracted at 24 hpi. IP was used using anti-GFP beads, and then the co-immunoblot was used using anti-HA antibody. Both input and IP samples were run on a 10% SDS-PA gel. The left panel shows the input immunoblots, and the right panel shows the immunoprecipitation and subsequent co-immunoblot. The numbers on the left side of each blot indicate the molecular weight (kDa) determined by protein ladder. Ponceau stained membrane serves as a loading control.

Once it was seen that CpBs4C likely forms a higher-order complex, we wanted to resolve the number of units that might come together to form this complex. The first approach to resolving this was to run CpBs4C on a Blue Native PAGE (BN-PAGE) which follows similar principles of SDS-PAGE, but does not use denaturing detergents so that the native oligomerization state of proteins can be determined by their size (Wittig et al., 2006). It can be seen on the BN-

PAGE gel that there is a large smear starting below 1048 kDa and extends upwards past the 1236 kDa marker and towards the top threshold of the gel (Figure 3.16A). If this complex exclusively consisted of CpBs4C-HA in the BN-PAGE, then this would make CpBs4C form at least a 50-unit oligomer. This does fall within an order of the pentamer prediction that was made in Figure 3.14, making at least 10 pentameric complexes, but it could be that other proteins are sticking to the CpBs4C complex, giving the complex a higher molecular weight.

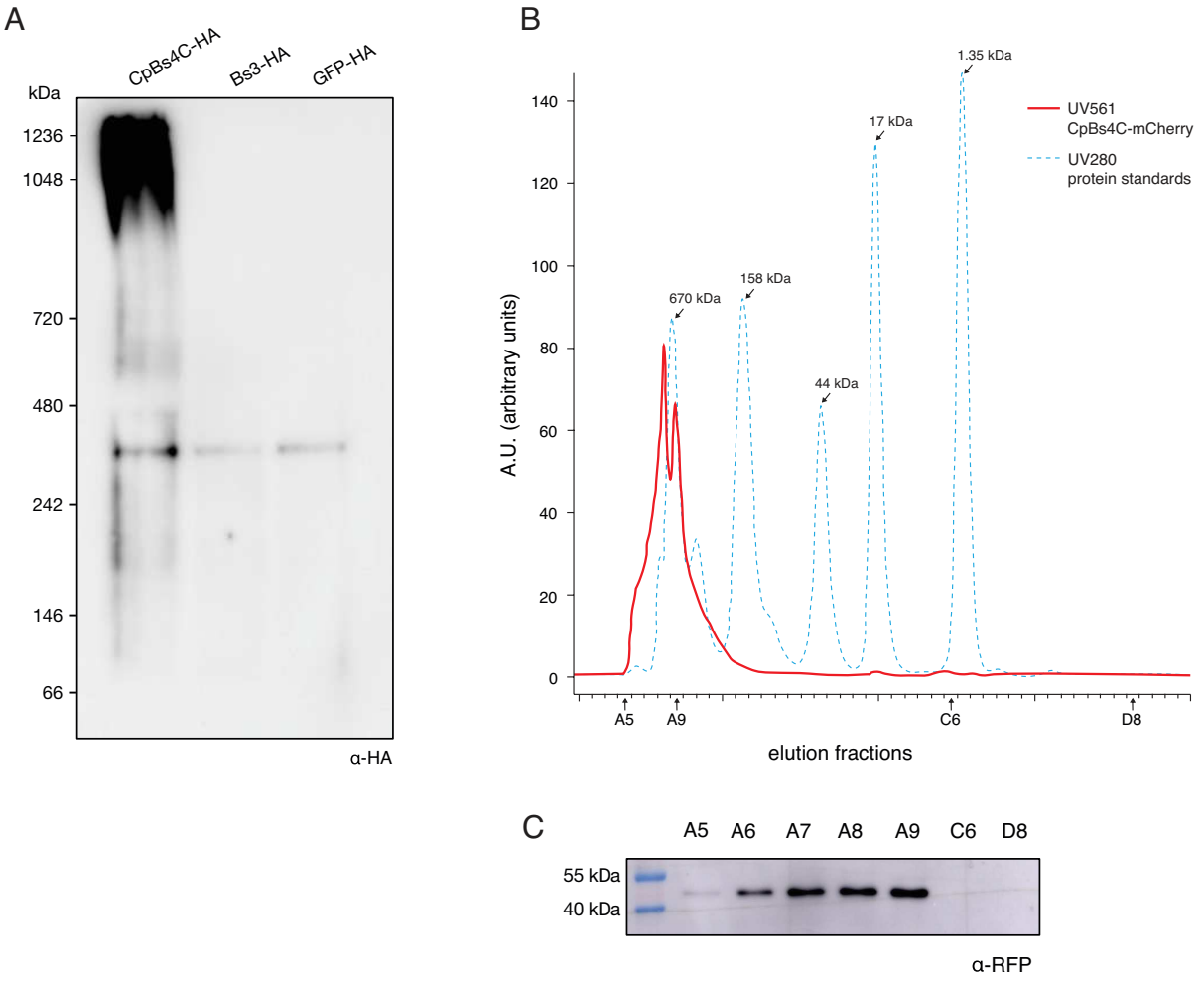

FIGURE 3.16. CpBs4C forms a higher order complex.

A | Detection of higher molecular weight CpBs4C complexes using a 3-12% bis-tris blue native polyacrylamide gel electrophoresis (BN-PAGE). After agroinfiltration of CpBs4C-HA into *N. benthamiana*, tissue was collected 24 hpi and total protein was extracted. Anti-HA antibody was used for detection. Numbers on the left hand side indicate molecular weight specified by an unstained native protein ladder.

B | Analytical size exclusion chromatography (SEC) of crude protein extracted from CpBs4C-mCherry agroinfiltrated into *N. benthamiana*, 24 hpi. Red line indicates observation through UV561 filter when the CpBs4C-mCherry sample was eluted, and the blue dotted line indicates observation through UV280 filter when the protein standard was eluted. Black arrows with molecular weight (kDa) indicate protein standard size. Letter and number in elution fraction indicates which fraction was used for immunoblot in (**C**).

C | Immunoblot of indicated fractions from (**B**) using anti-RFP antibody on a standard 10% SDS-PA gel. Numbers on the left-hand side indicate molecular weight (kDa) determined by protein ladder.

We tried another method to resolve the oligomeric state of CpBs4C, which was using a crude extract from *N. benthamiana* in combination with size exclusion chromatography (SEC). Overexpressing CpBs4C-mCherry in *N. benthamiana,* and then extracting total crude protein from these leaves then running this extract on the SEC column, is a quick way to see if there is a larger complex of your protein of interest being formed, by using a UV filter (UV561) that is specific to mCherry. It was found that there was only one bi-modal peak in the CpBs4C-mCherrry sample, and this bi-modal peak occurred around the same elution fraction as the 670kDa peak from the protein standard (Figure 3.16B). Immunoblotting of the eluted fractions confirmed that this peak indeed contains CpBs4C-mCherry, and that elution fractions that do not have a UV561 peak, like elution fractions C6 and D8, do not contain CpBs4C-mCherry (Figure 3.16C). This indicates that the CpBs4C-mCherry complex found *in planta* is at least 670 kDa, and if this complex only contains CpBs4C-mCherry and no other binding partners, then the CpBs4C complex could be making at least a 15-mer.

If CpBs4C can self-associate and form a higher-order complex, then the next logical experiment was to test if the other Bs4C homologues from *N. benthamiana* could also self-associate. Using a different technique this time to validate the coIP result in Figure 3.15 and test the association of the other homologues, we used a FLIM-FRET (fluorescence lifetime imaging of Förster resonance energy transfer) approach. In this experiment, the protein of interest is tagged on independent constructs with FRET (Förster resonance energy transfer) compatible fluorophores (Bajar et al., 2016). Their compatibility is determined by the fact that if these two compatible fluorophores are in close enough proximity (1-10 nm), then the excited donor fluorophore is able to transfer energy to the acceptor fluorophore, and then the acceptor fluorophore is put into an excited state (Vogel et al., 2014). This transfer of energy can then be measured by the average lifetime of the donor fluorophore, where the average lifetime is the time that a molecule can remain in the excited state (Wallrabe & Periasamy, 2005). Essentially, if these two fluorophores are in close enough proximity, then the donor will excite the acceptor, and the average lifetime (τ) of the donor will be dramatically decreased, indicating that the proteins with which the fluorophores are tagged, are associating.

In our study, we tagged CpBs4C, NbBs4C.1, NbBs4C.2, and NbBs4C.3 to both eGFP and to mCherry, and we also used ER-targeted GFP and mCherry as subcellular localization controls. The average lifetime of ER-targeted GFP (ER-GFP hereafter) ranges between 2.8 and 3.0 ns, and co-infiltrated ER-GFP with ER-targeted mCherry did not change that average lifetime range of 2.8 to 3.0 ns, allowing us to determine that these two fluorophores on their own do not associate within the ER (Figure 3.17).

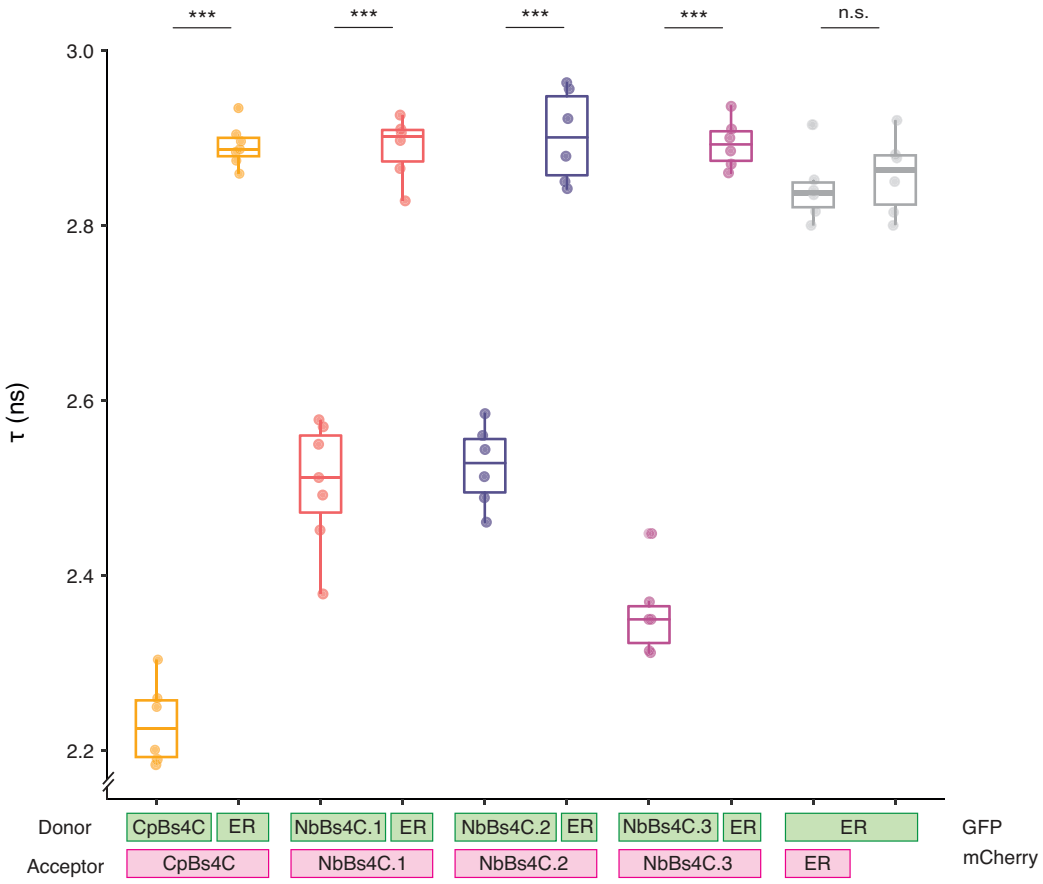

FIGURE 3.17. NbBs4C homologues can self-associate using FLIM-FRET.

FLIM-FRET measurements, as quantified through τ (ns) of the indicated protein tagged with GFP when co-infiltrated with the indicated protein tagged with mCherry. Values are represented in a box and whisker plot, n=6, statistical significance was determined between the protein of interest tagged with GFP when co-infiltrated with protein of interest tagged to mCherry and ER-GFP when co-infiltrated with the protein of interest tagged to mCherry, using a student's T-test, *** $p < 0.001$, n.s. = no significance.

The average lifetime of CpBs4C-GFP when co-infiltrated with CpBs4C-mCherry is significantly reduced ($p<0.001$) compared to the average lifetime of ER-GFP when co-infiltrated with CpBs4C-mCherry, indicating that these two proteins are in close enough proximity to one another (1-10 nm) to facilitate a transfer of energy, and ultimately a reduction in the lifetime of the GFP fluorophore (Figure 3.17). This reduction in GFP lifetime suggests that CpBs4C-GFP and CpBs4C-mCherry associate. A similar significant reduction ($p<0.001$) in the lifetime of NbBs4C.1-GFP when co-infiltrated with NbBs4C.1-mCherry, as compared to ER-GFP being co-infiltrated with NbBs4C.1-mCherry (Figure 3.17). The same pattern is exhibited for both NbBs4C.2-GFP and NbBs4C.3-GFP, ultimately indicating that all Bs4C homologues from *N. benthamiana* can self-associate.

3.1.6. NbBs4C homologues and CpBs4C can hetero-associate and NbBs4C.1 can dominate their phenotype

Since all of the studied Bs4C homologues can associate with themselves (homo-association) (Figure 3.17), and all of their structures are highly similar (Figure 3.3), we wanted to see if they would associate with each other (hetero-association). This would allow us to determine if there is specificity within the amino acid sequence that allows for the homologues to homo-associate, or if it is just the structure of the homologues that makes way for the association. As can be seen from a hetero-associative coIP, all of the homologues from *N. benthamiana* and CpBs4C can associate with one another (Figure 3.18).

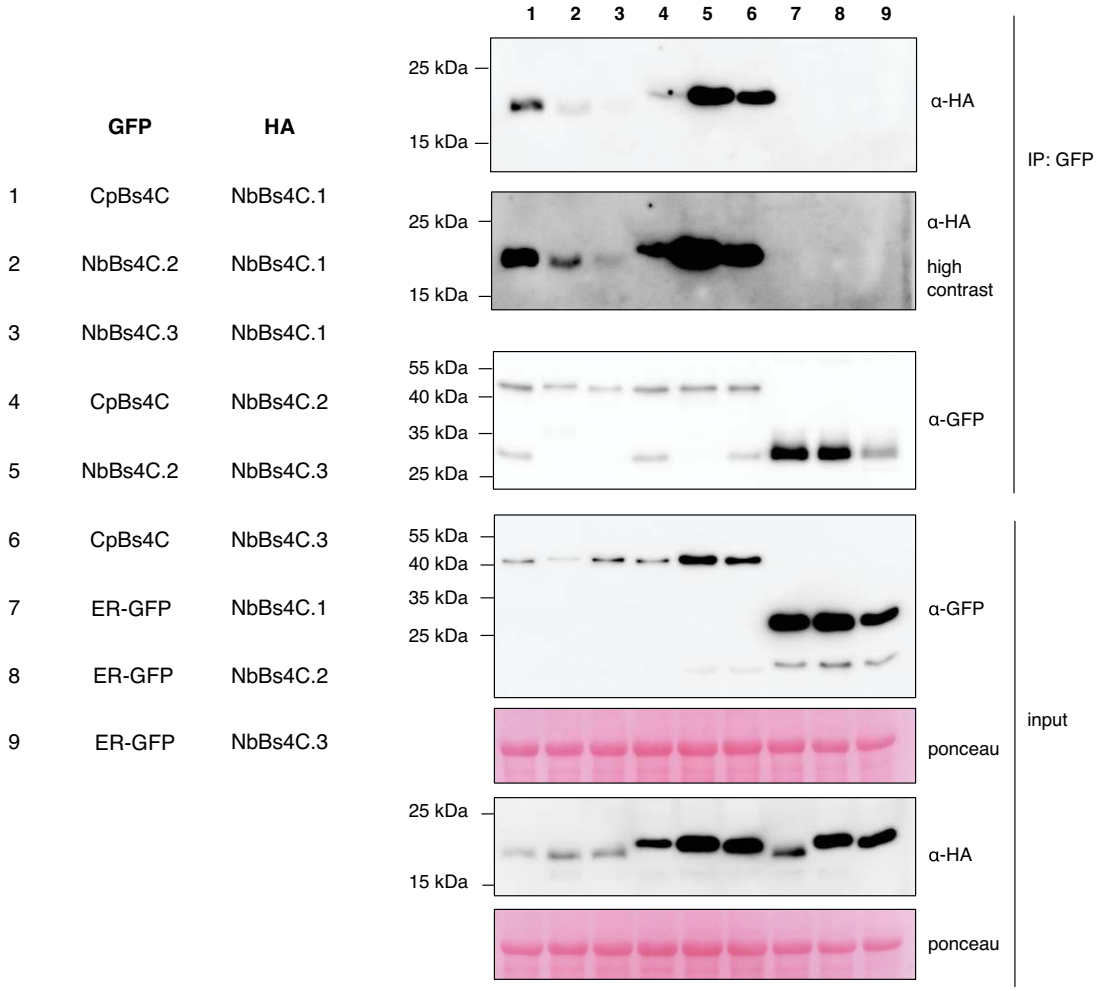

FIGURE 3.18. CpBs4C, NbBs4C.1, NbBs4C.2, and NbBs4C.3 can all associate with each other.

coIP of all homologues under 35S promoter in hetero-association in *N. benthamiana*, using ER-GFP as a negative control. Sample taken 24 hours post agroinfiltration. IP was performed using anti-GFP beads. Both input and IP samples were run on a 12% SDS-PA gel. Immunoblots were performed using anti-HA-HRP or anti-GFP-HRP antibodies, as indicated. Ponceau stained membrane serves as a loading control. Numbers on the left-hand side indicate molecular weight (kDa) determined by protein ladder.

Even further, this interaction is specific with the Bs4C homologues themselves, and not just associating with anything in the ER, as can be seen when ER-GFP is pulled down, none of the homologues associate with it.

A

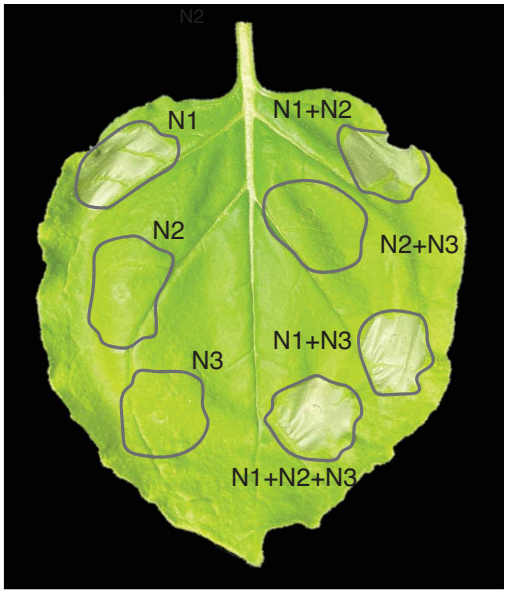

N1	dT779 targeting *NbBs4C.1*
N2	dT780 targeting *NbBs4C.2*
N3	dT782 targeting *NbBs4C.3*
N1+N2	dT779 + dT780 targeting *NbBs4C.1* and *NbBs4C.2*
N2+N3	dT780 + dT782 targeting *NbBs4C.2* and *NbBs4C.3*
N1+N3	dT779 + dT782 targeting *NbBs4C.1* and *NbBs4C.3*
N1+N2+N3	dT779 + dT780 + dT782 targeting *NbBs4C.1*, *NbBs4C.2* and *NbBs4C.3*

B

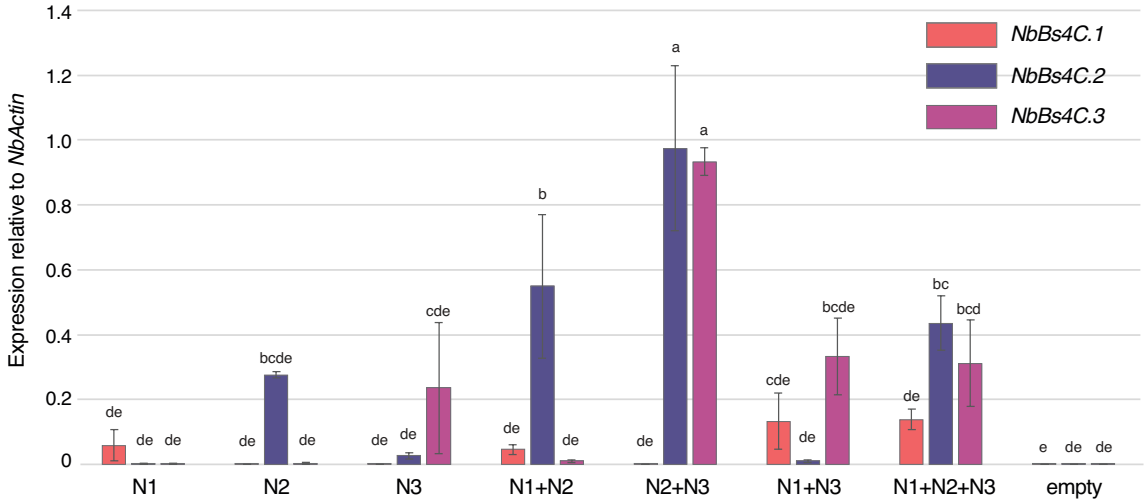

FIGURE 3.19. *NbBs4C.2* and *NbBs4C.3* are not able to suppress *NbBs4C.1* induction of cell death.

A | Overexpression constructs agroinfiltrated into *N. benthamiana*. Photo taken three days post infiltration. Right panel indicates the abbreviations used for the left panel in the combination of dTALEs infiltrated.

B | Quantitative real-time PCR was used to determine the activation of each targeted gene by the corresponding dTALE combination. Samples were taken 40 hours post agroinfiltration. Values are means + standard deviations. Three technical replicates coming from the same cDNA, each gene was normalised against the expression of *NbActin* from the same sample, statistically significant groups ($p<0.05$) are presented with letters resolved by a one-way ANOVA with post hoc Tukey's test.

Once it was determined that all of the Bs4C homologues can both homo- and hetero-associate, we wanted to see if perhaps one of the NbBs4C phenotypes could suppress the other, meaning that if we co-infiltrate an NbBs4C homologue that induces cell death with a homologue that does not induce cell death, what would the resulting phenotype be? To test this, we co-infiltrated *A. tumefaciens* containing the dTALEs of the NbBs4C homologues in a pair-wise fashion to see which homologues' phenotype would be dominant in the context of cell death. In all of the combinations of the dTALEs that were infiltrated, in every instance where the dTALE activating *NbBs4C.1* was present, there was cell death (Figure 3.19). The only instances where there was no cell death present, were when the two dTALEs activating the non-cell death-inducing *NbBs4C.2* and *NbBs4C.3* were infiltrated either on their own or together. This ultimately allows us to determine that the activation of *NbBs4C.1* has the most dominant phenotype regarding cell death, and that *NbBs4C.2* and *NbBs4C.3* are not able to suppress *NbBs4C.1* induction of cell death.

3.1.7. Bs4C might be disrupting calcium homeostasis within the cell

Seeing as Bs4C homologues from *C. pubescens* and *N. benthamiana* can homo-associate (Figure 3.17) and a predicted model of a pentameric ring of Bs4C subunits looks very similar to the $GABA_A$ receptor channel, it is conceivable that Bs4C might be working as a channel. At the beginning of this work on Bs4C, there was no indication of what Bs4C might be doing in the cell. We therefore took a very broad approach to identify potential binding partners of CpBs4C *in planta* to gain insight into how CpBs4C might be inducing cell death. We immunoprecipitated CpBs4C-GFP and GFP as a control and studied these samples by mass spectrometry to identify peptides of proteins that were pulled down in the CpBs4C sample. An analysis of the proteomics data set was analysed by Gautier Langin, a PhD student in Prof. Dr. Suayb Üstün's lab. After cutting-off MS/MS counts that had a 0 count in the GFP samples, and an MS/MS count of greater than 1 in the CpBs4C-GFP samples, *N. benthamiana* proteins were blasted against the Arabidopsis proteome (Cheng et al., 2017), and a comparative analysis was done between the remaining proteins of CpBs4C-GFP and the proteins of the ER-localised transcription factors NAC53 and NAC78, previously performed by Gautier Langin (Figure 3.20A). This analysis was performed to ensure the specificity of CpBs4C binding partners, and because free GFP was used as the control in the IP/MS experiment instead of a more suitable ER-localised protein, and non-specific ER proteins needed to be ruled out. Only 64 proteins identified in the CpBs4C proteomics overlapped with the NAC53 and NAC78 transcription factors, leaving 336 proteins remaining that were specific to CpBs4C (Figure 3.20A).

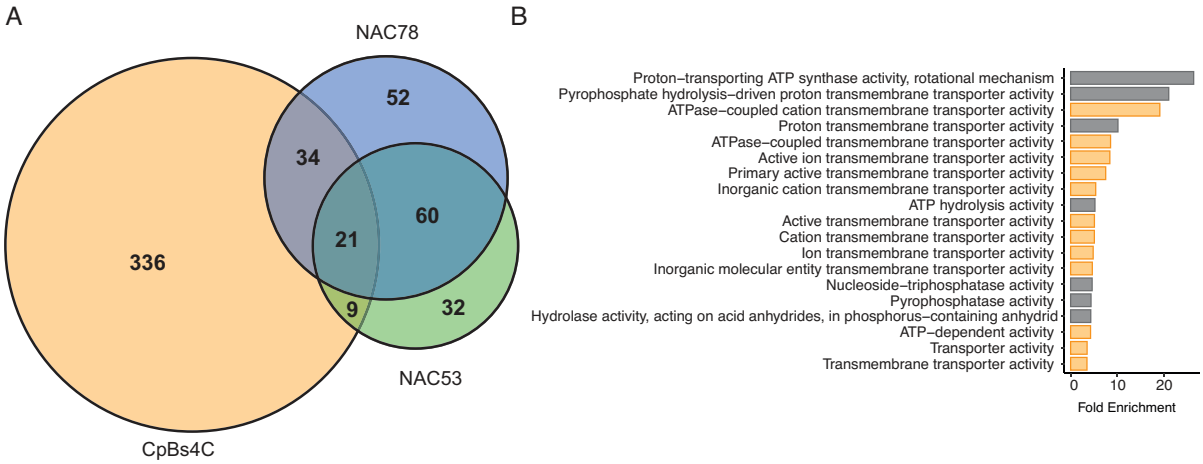

FIGURE 3.20. CpBs4C proteomic dataset is unique and indicates ion binding and transporter activity.

A | Comparison of overlapping proteins identified in the CpBs4C (light orange) proteomic data set and the Arabidopsis NAC78 (blue) and NAC53 (green) mock-treated proteomic data set. Comparison was performed on the *N. benthamiana* protein homologues in Arabidopsis.
B | Top 20 GO Molecular Function terms of the 336 proteins found exclusively in CpBs4C data set, ranked based on their fold enrichment using ShinyGO v0.77. False discovery rate (FDR) < 0.05. Ion transmembrane transporter activity categories related to Ca^{2+} are highlighted in orange.
Analysis performed by Gautier Langin.

A gene ontology (GO) molecular function enrichment analysis of the Arabidopsis homologues of CpBs4C-specific proteins revealed a strong indication of ion transport, ion-binding proteins, and transmembrane transporter activity in the CpBs4C interactome (Figure 3.20B). Taking a closer look at the ion-binding protein hits, there are many calcium-transporting ATPases, either ER type or plasma membrane type, that are specific to the CpBs4C-GFP samples (Table 3.4).

Table 3.4 Potential in planta interaction partners of CpBs4C.

Identified protein	**MS/MS Count**					
	Cp 1	Cp 2	Cp 3	GFP 1	GFP 2	GFP 3
CpBs4C	7	6	5	0	0	0
Calcium-transporting ATPase 2, plasma membrane-type-like (NbD017236.1)	3	3	2	0	0	0
Calcium-transporting ATPase 2, plasma membrane-type-like (NbE03060505.1)	0	5	10	0	0	0
Calcium-transporting ATPase 10, plasma membrane-type-like (NbE05067716.1)	1	2	3	0	0	0
Calcium-transporting ATPase 4, endoplasmic reticulum-type-like (NbD018366.1)	1	4	15	0	0	0
Calcium-transporting ATPase 2, plasma-membrane-type-like (NbE03056943.1)	1	1	1	0	0	0
Calcium-transporting ATPase 4, plasma membrane-type-like (NbD012761.1)	0	4	8	0	0	0

Cp refers to the MS counts found for the potential CpBs4C-GFP interaction partners. GFP refers to the peptides found in the GFP samples. Nb# after identified protein indicates protein ID.

After finding many calcium-transporting proteins in the CpBs4C IP-MS analysis, the logical next step was to see if calcium (Ca^{2+} hereafter) was somehow involved in CpBs4C-induced cell death. Recent studies have found that NLR resistance proteins form a Ca^{2+}-permeable ion channel, and their induction of cell death can be inhibited by the Ca^{2+} channel blocker, lanthanum chloride ($LaCl_3$) (Bi et al., 2021; El Kasmi et al., 2017; Jacob et al., 2021).

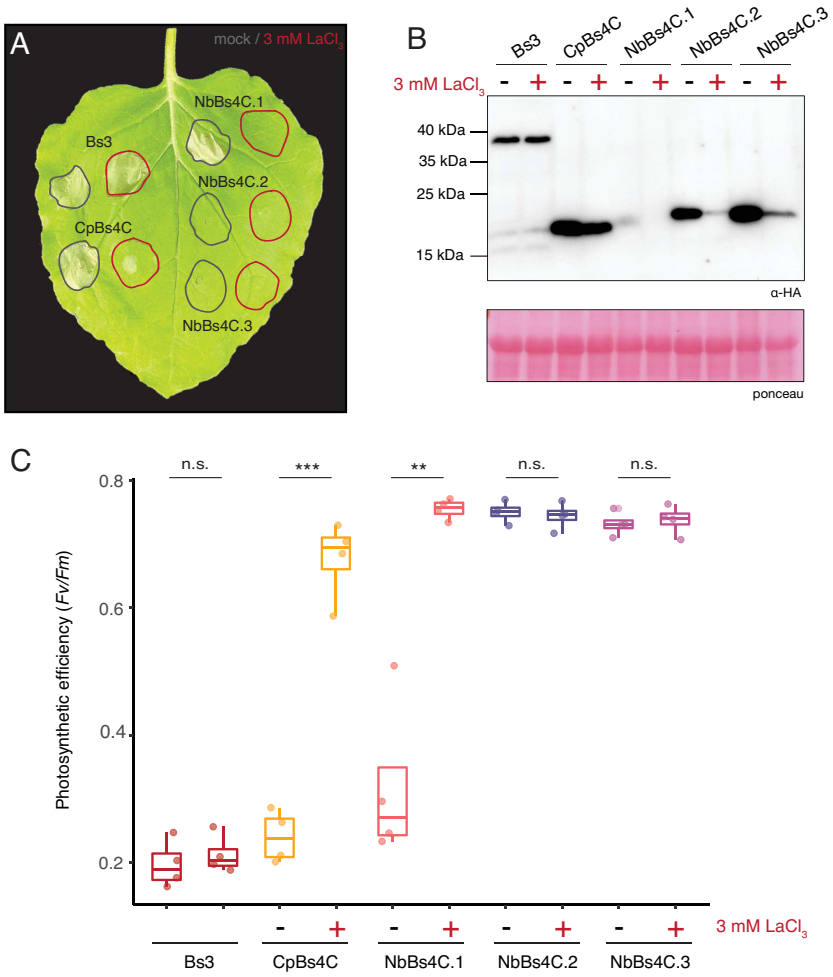

FIGURE 3.21. Ca^{2+} channel inhibitor suppresses CpBs4C and NbBs4C.1 cell death.

A | Overexpression constructs agroinfiltrated with or without 3 mM $LaCl_3$ into *N. benthamiana*. Grey – indicates mock treatment and red + indicates co-infiltration with 3 mM $LaCl_3$. Photo taken three days post infiltration.

B | Immunoblot to show protein accumulation at the expected molecular weight. CpBs4C, NbBs4C.1, NbBs4C.2 and NbBs4C.3 samples taken 24 hours post-agroinfiltration, Bs3 samples taken 40 hours post-agroinfiltration. Grey – indicates mock treatment and red + indicates co-infiltration with 3 mM $LaCl_3$. Samples were run on a 12% SDS-PA gel. Anti-HA-HRP antibody was used to detect protein. Ponceau stained membrane serves as a loading control. The numbers on the left side of the blot indicate the molecular weight (kDa) determined by the protein ladder.

C | Photosynthetic capacity of tissue after agroinfiltration with or without 3 mM $LaCl_3$ into *N. benthamiana.* Sample taken three days post infiltration. Values are presented in a box and whisker plot to show variation in samples, n=4 leaves. Statistical significance was determined using a student's T-test between the indicated infiltrated construct with or without 3 mM $LaCl_3$, ** $p < 0.01$, *** $p < 0.001$, n.s. = no significance.

It was found that 3 mM $LaCl_3$, when co-infiltrated with CpBs4C, suppressed the visible cell death induction in *N. benthamiana* leaves three days after infiltration in addition to restoring photosynthetic capability (Figure 3.21A and C). By contrast, $LaCl_3$ co-infiltration did not suppress Bs3 cell death induction, which was used as a non-ER localised cell death-inducing executor control, making the suppression of cell death using this Ca^{2+} channel inhibitor specific to CpBs4C. Both NbBs4C.2 and NbBs4C.3 had no change in lack of cell death or photosynthetic ability with or without co-infiltration of 3 mM $LaCl_3$. Furthermore, there was an equal level of protein accumulation when Bs3 was infiltrated with or without 3 mM $LaCl_3$, and a somewhat similar level of protein accumulation when CpBs4C was infiltrated with or without 3 mM $LaCl_3$, confirming that the action of $LaCl_3$ is inhibiting the function of CpBs4C and does not have a great effect on CpBs4C protein accumulation (Figure 3.21B). It should be noted, however, that there was a dramatic reduction in NbBs4C.1, NbBs4C.2, and NbBs4C.3 protein accumulation when co-infiltrated with 3 mM $LaCl_3$, which might be the reason why there was no NbBs4C.1 cell death when infiltrated with 3 mM $LaCl_3$ (Figure 3.21B). Ultimately, however, this confirms that CpBs4C is somehow using the movement of Ca^{2+} to induce a cell death response.

Since ER-like Ca^{2+}-ATPases were abundant in the IP-MS analysis, and the Ca^{2+} channel inhibitor was able to suppress CpBs4C cell death, we wanted to test if CpBs4C had an impact on the Ca^{2+} homeostasis within the plant cell, and more specifically, the Ca^{2+} homeostasis within the cytosol, as an increase in concentration of cytosolic Ca^{2+} ($[Ca^{2+}]_{cyt}$ hereafter) is a hallmark indicator of pathogen-induced immunity in plants, specifically PTI and ETI (Köster et al., 2022). A collaborator, Dr. Shouguang Huang from Prof. Dr. Rainer Hedrich's lab used a ratiometric Ca^{2+} sensor (Waadt et al., 2017) to determine the increase in $[Ca^{2+}]_{cyt}$ after CpBs4C had been expressed. Interestingly, it was found that Bs3-GFP actually had a significant increase in $[Ca^{2+}]_{cyt}$ after 24 hpi compared to GFP, while CpBs4C had no significant increase in $[Ca^{2+}]_{cyt}$ after 24 hpi (Figure 3.22C). Even though Bs3-GFP had a lower GFP signal of the infiltrated construct (Figure 3.22B), it still had an increase in $[Ca^{2+}]_{cyt}$. An immunoblot was performed to confirm that the Bs3-GFP and CpBs4C-GFP constructs were expressing at the correct molecular weight (CpBs4C-GFP, 47 kDa, and Bs3-GFP, 65 kDa) (Figure 3.21D). This was rather peculiar because we found that Ca^{2+}-ATPases were highly represented in the CpBs4C interactome and that CpBs4C cell death was able to be suppressed with the co-expression of the broad Ca^{2+} channel inhibitor, $LaCl_3$. We therefore hypothesised that since CpBs4C is localised to the ER (Figure 3.5) and we saw no increase in $[Ca^{2+}]_{cyt}$ (Figure 3.22), then it could be possible that CpBs4C is using Ca^{2+} transporting proteins to move Ca^{2+} in a different manner than from the ER to the cytosol.

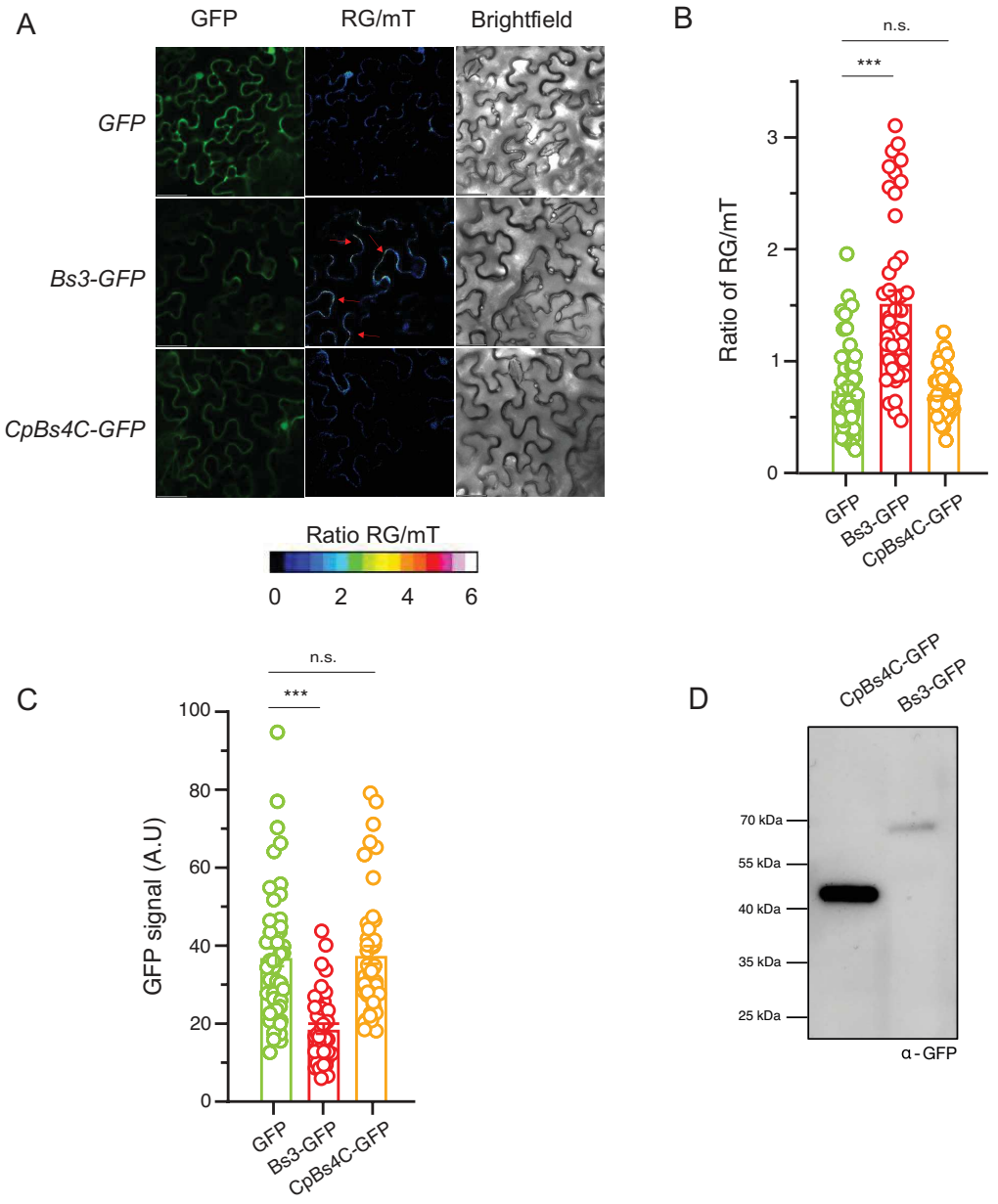

FIGURE 3.22. CpBs4C does not cause an increase in $[Ca^{2+}]_{cyt}$, but Bs3 does.

A | Images showing protein expressing levels (left: GFP), the cytosolic Ca^{2+} concentration (middle: r-GECO/mTurquoise ratio), and bright-field (right) in epidermal cells of *N. benthamiana* after agroinfiltration. Red arrows mark the position where a pronounced increase in cytosolic Ca^{2+} signals were detected.

B | Average cytosolic Ca^{2+} signals (ratio of indicated constructs under control of 35S promoter) in *N. benthamiana* epidermal cells.

C | Average expression levels of indicated constructs under control of 35S promoter in *N. benthamiana* epidermal cells.

D | Immunoblot to show protein accumulation at expected molecular weight. Sample taken 24 hours post agroinfiltration. Samples were run on a 10% SDS-PA gel. Anti-GFP-HRP antibody was used to detect protein. The numbers on the left side of the blot indicate the molecular weight (kDa) determined by the protein ladder.

Values are represented in a bar graph with individual data points in a circle, n=52, statistical significance was determined between GFP and either Bs3-GFP or CpBs4C-GFP using a student's T-test, *** $p < 0.001$, n.s. = $p > 0.05$, no significance. **A-C** was performed by Dr. Shouguang Huang.

3.1.8. The conserved N-terminal body confers cell death, but the C-terminal tail limits protein accumulation

To understand the function and potential mechanisms of the cell death-inducing Bs4C homologues, we looked deeper into their structure and amino acid sequence. As seen in Figure 3.3B, the N-terminal body is quite conserved structurally between the homologues, but the C-terminal tail is very diverse. The first thought upon seeing this was since there is strong diversity between all of the C-terminal tails, even between the two that have cell death, CpBs4C and NbBs4C.1, and between the two that do not have cell death, perhaps the C-tail is what is causing the protein to induce cell death.

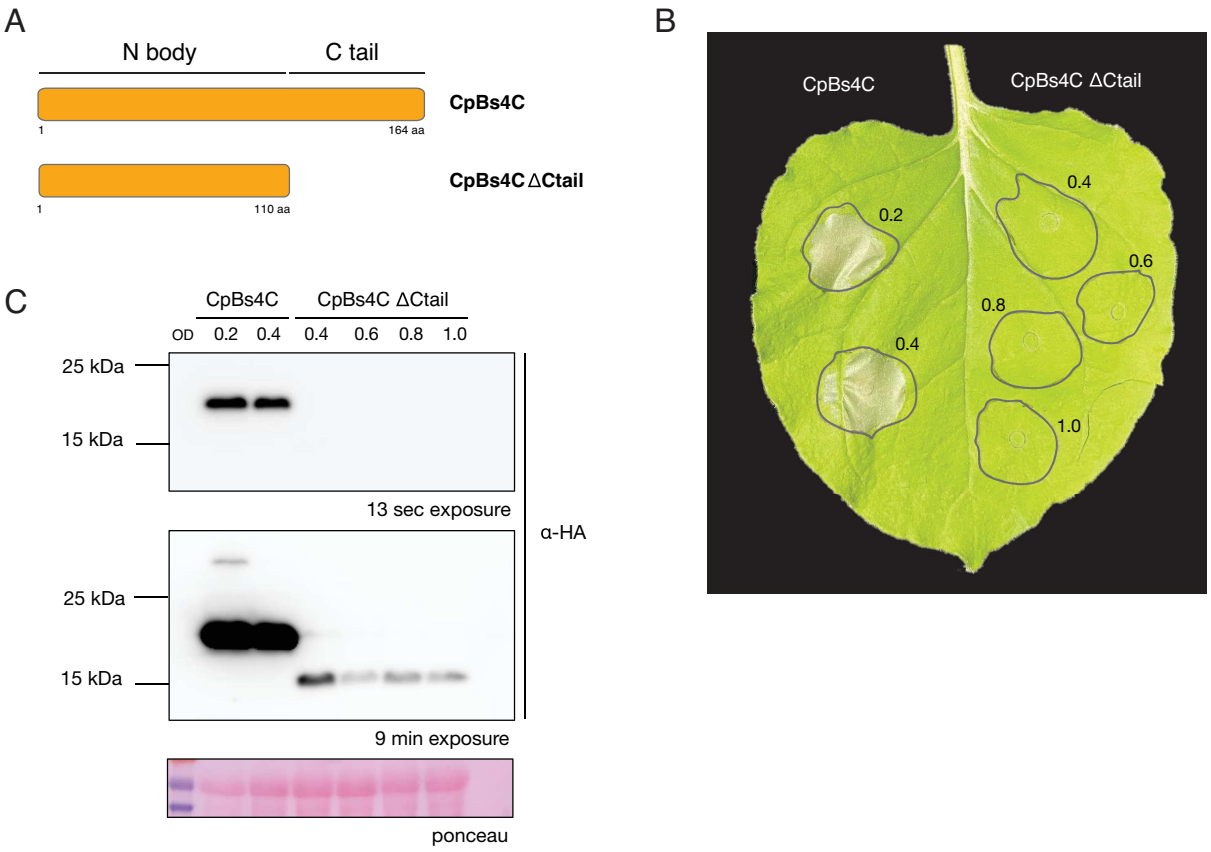

FIGURE 3.23. Deletion of the C-terminal tail affects CpBs4C protein accumulation.

A | Schematic of truncated protein.
B | Overexpression constructs agroinfiltrated into *N. benthamiana*. Photo taken three days post infiltration. Numbers on the leaf indicate the OD_{600} of *A. tumefaciens* that was infiltrated.
C | Immunoblot to show protein accumulation of truncated protein. Sample taken 24 hours post agroinfiltration. Sample taken 24 hours post agroinfiltration. Samples were run on a 12% SDS-PA gel. Anti-HA-HRP antibody was used to detect protein. Ponceau stained membrane serves as a loading control. The numbers on the left side of blot indicate the molecular weight (kDa) determined by protein ladder.

The first test was to see if CpBs4C even requires the C-terminal tail to function. To do this, a truncated version of CpBs4C was generated where the entire C-terminal region was deleted, and an HA epitope tag was translationally fused immediately after the last alpha helix in the protein (see Figure 3.3A for reference) and was termed CpBs4C ΔCtail. It was found that CpBs4C ΔCtail not only has no cell death but also has a vast decrease in protein accumulation, which can be seen via immunoblot (Figure 3.23). The standard for *A. tumefaciens* infiltration into *N. benthamiana* is to have an *A. tumefaciens* optical density (OD_{600}) of 0.4 when infiltrating the leaves. As there was such a dramatic decrease in protein accumulation between the full-length CpBs4C and CpBs4C ΔCtail, the OD_{600} of CpBs4C ΔCtail was increased from 0.4 to 1.0 in 0.2 increments. Interestingly, it can be seen that when the OD_{600} is increased, there is actually a reduction in the protein accumulation of CpBs4C ΔCtail (Figure 3.23C). This ultimately allows for the conclusion that the CpBs4C C-terminal tail is required for adequate protein accumulation and subsequent cell death.

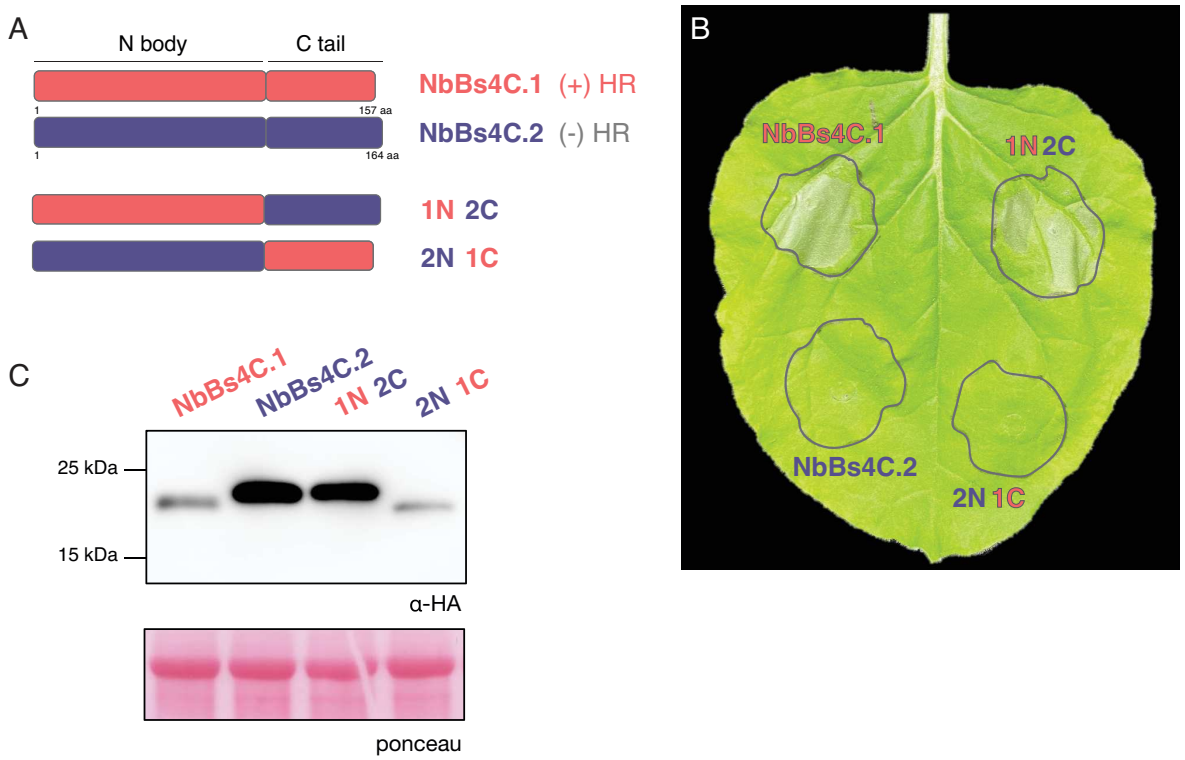

FIGURE 3.24. C-terminal tail of NbBs4C.1 is not responsible for cell death.

A | Schematic of chimeras generated using the N-body and C-terminal tail of both NbBs4C.1 and NbBs4C.2. 1N refers to the N-body of NbBs4C.1, 2N refers to the N-body of NbBs4C.2, 1C refers to the C-terminal tail of NbBs4C.1, and 2C refers to the C-terminal tail of NbBs4C.2.
B | Overexpression constructs agroinfiltrated into *N. benthamiana*. Photo taken three days post infiltration.
C | Immunoblot to show protein accumulation of chimeras. Sample taken 24 hours post agroinfiltration. Samples were run on a 12% SDS-PA gel. Anti-HA-HRP antibody was used to detect protein. Ponceau stained membrane serves as a loading control. The numbers on the left side of each blot indicate the molecular weight (kDa) determined by protein ladder.

Now that we have determined that the C-terminal tail is vital for adequate accumulation of protein, the next logical question is to test if it is indeed the C-tails of the cell death-inducing homologues that are actually causing cell death. As previously mentioned, the Bs4C homologues have a very similar core structure, but quite diverse C-terminal tails. These structures lend themselves nicely towards the generation of chimeras where we can take the C-terminal tail of a cell death-inducing homologue and put it on the N-terminal body of a non-cell death-inducing homologue and see if this chimera induces cell death. Taking the N-terminal bodies and C-terminal tails from both NbBs4C.1 and NbBs4C.2 (the two homologues that have cell death and no cell death, respectively, and are closest in their structure), chimeras were generated to have 1N2C, whereby the N-terminal body of NbBs4C.1 was translationally fused to the C-terminal tail of NbBs4C.2, and 2N1C, whereby the N-terminal body of NbBs4C.2 was fused to the C-terminal tail of NbBs4C.1 (Figure 3.24A). Placing these chimeras under control of the 35S promoter, the constructs were put into *A. tumefaciens* and infiltrated into *N. benthamiana* and examined for both cell death development and protein accumulation. Surprisingly, it was found that 1N2C had visible cell death, and 2N1C had no cell death (Figure 3.24B). This allows us to determine that the N-terminal bodies of NbBs4C.1/.2 are what govern functional differences in their capability to induce cell death. It can also be seen in Figure 3.24C that the C-terminal tail is also the part of the protein that is responsible for protein accumulation, specifically when NbBs4C.1 full length is expressed, it has less protein accumulation than NbBs4C.2, and similarly, 2N1C, which has the NbBs4C.1 C-tail, and NbBs4C.2 N-body, has a reduced protein accumulation compared to 1N2C, which has the NbBs4C.2 C-tail and the NbBs4C.1 N-body. Taken together, we can conclude that the C-tail is required for the protein to accumulate to adequate levels and to induce cell death, yet the C-tail does not dictate whether the protein will induce cell death; in fact, the N-terminal body is what dictates if a homologue induces cell death or not.

To narrow down the region of the N-terminal body that causes the functional difference in cell death between NbBs4C.1 and NbBs4C.2, we looked at the pentameric ring prediction from Figure 3.14. Looking closely, one of the alpha helices from the N-terminal core structure is what lines the inner ring of the potential pore, which is the green highlighted alpha helices in Figure 3.14B. This alpha helix is the last alpha helix in the transmembrane region of the Bs4C homologues (Figure 3.3A for reference) and will now be termed the pore-lining helix.

FIGURE 3.25. Multiple sequence alignment of CpBs4C and NbBs4C homologues.

Degree of conservation is shown with grey or black shading. Names and lines above the alignment indicate the domains. Blue indicates the structurally conserved N-body. Green indicates the last helix within the N-body termed the pore-lining helix. Pink indicates the variable C-terminal tail. Numbers on the right hand side indicate the amino acid position.

Comparing the amino acids that compose the pore-lining helices of cell death-inducing and non-cell death-inducing homologues, there is no obvious charge within these pore-lining alpha helices that would indicate selectivity for a potential ion that might be able to pass through (Figure 3.25). Specifically meaning that there are no negatively charged amino acids like aspartic acid (D) or glutamic acid (E) within the pore-lining helix (highlighted in green in Figure 3.25), that would select for positively charged ions, like Ca^{2+}. However, we still swapped this pore-lining helix to see if it had an impact on cell death. The pore-lining helix of NbBs4C.1 (cell death-inducing homologue) and the pore-lining helix of NbBs4C.2 (non-cell death-inducing homologue) were swapped to generate chimeras. These chimeras were named 1N2P1C (N-terminal body of NbBs4C.1, pore-lining helix of NbBs4C.2, and C-terminal tail of NbBs4C.1) and 2N1P2C (N-terminal body of NbBs4C.2, pore-lining helix of NbBs4C.1, and C-terminal tail of NbBs4C.2). These chimeras were placed under control of the 35S promoter and tagged with an HA epitope tag at the C-terminus, and then transformed into *A. tumefaciens* and infiltrated into *N. benthamiana*. Interestingly, neither chimera produced a visible cell death reaction, but they both did have visible protein accumulation (Figure 3.26). This indicates that the integrity of the last two alpha helices within the N-terminal body of the protein are required for cell death.

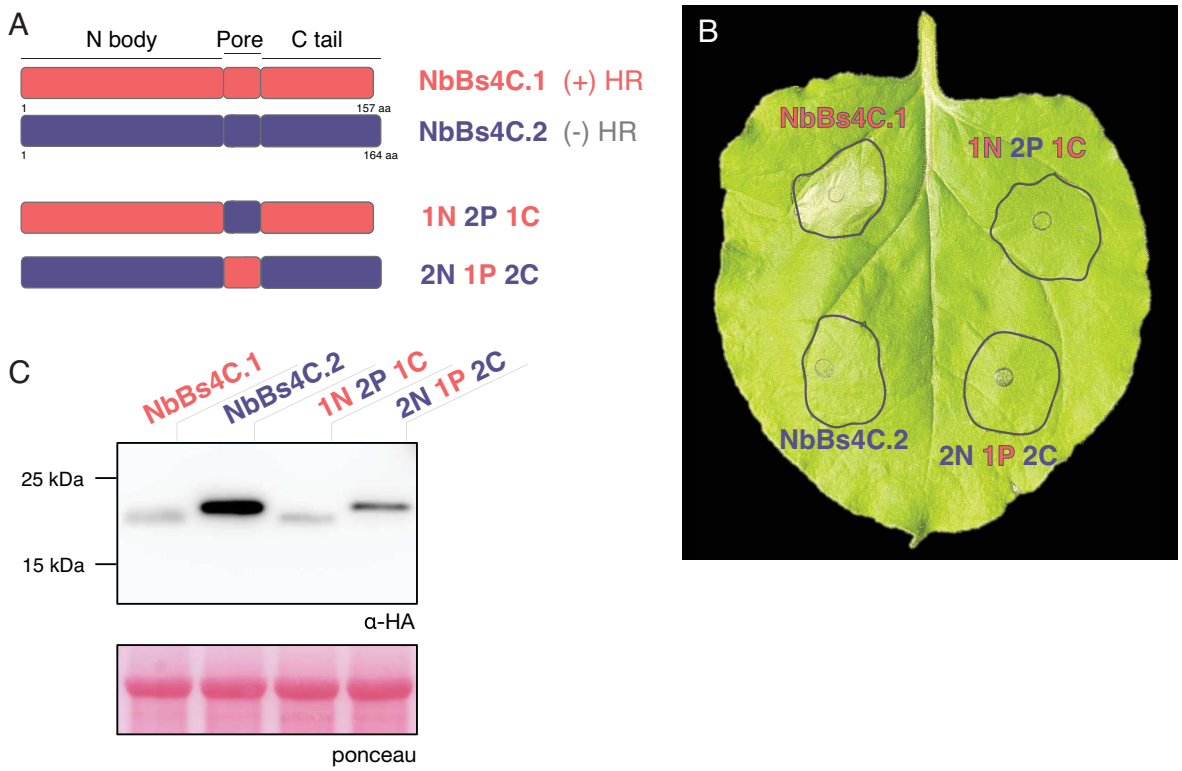

FIGURE 3.26. Pore-lining helix of NbBs4C.1 is not responsible for cell death.

A | Schematic of chimeras generated using the N-body, pore lining helix, and C-terminal tail of both NbBs4C.1 and NbBs4C.2. 1N refers to the N-body of NbBs4C.1, 2N refers to the N-body of NbBs4C.2, 1P refers to pore lining helix of NbBs4C.1, 2P refers to the pore lining helix of NbBs4C.2. 1C refers to the C-terminal tail of NbBs4C.1, and 2C refers to the C-terminal tail of NbBs4C.2.
B | Overexpression constructs agroinfiltrated into *N. benthamiana*. Photo taken three days post infiltration.
C | Immunoblot to show protein accumulation of truncated protein. Sample taken 24 hours post agroinfiltration. Samples were run on a 12% SDS-PA gel. Anti-HA-HRP antibody was used to detect protein. Ponceau stained membrane serves as a loading control. The numbers on the left side of each blot indicate the molecular weight (kDa) determined by protein ladder.

3.1.9. $GABA_A$ subunit does not mimic Bs4C homologue phenotype

It was determined in Figure 3.24 that the conserved N-terminal body is responsible for the functional difference between NbBs4C.1 and NbBs4C.2. Seeing as the conserved core N-terminal body is the region of CpBs4C (and the other homologues) that is structurally homologous to the transmembrane regions of the $GABA_A$ subunits as seen in Figure 3.13, we sought to test if the homologous transmembrane part of the $GABA_A$ subunits could functionally replace the NbBs4C.1 transmembrane region. The most structurally homologous subunit of the $GABA_A$ receptor to CpBs4C, $GABA_A$ subunit α, was used for the generation of the GABA-Bs4C chimeras (Figure 3.27A).

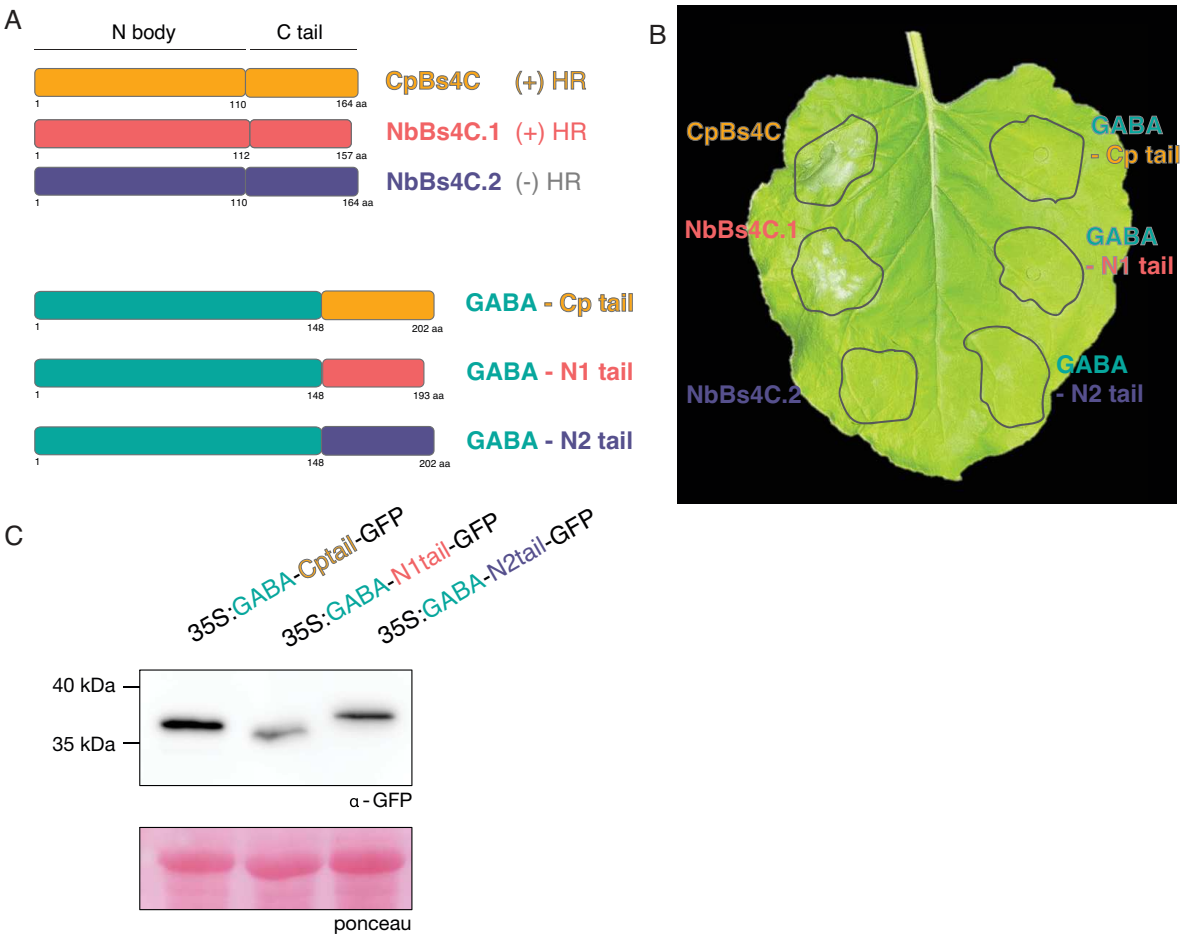

FIGURE 3.27. $GABA_A$ chimeras do not induce cell death.

A | Schematic of chimeras generated using the membrane bound domain of $GABA_A$ receptor and C-terminal tail of CpBs4C (Cptail), NbBs4C.1 (N1tail), and NbBs4C.2 (N2tail).
B | Overexpression constructs agroinfiltrated into *N. benthamiana*. Constructs driven with 35S promoter and a C-terimal GFP tag. Photo taken three days post infiltration.
C | Immunoblot to show protein accumulation of chimeras. Sample taken 3 days post agroinfiltration. Samples were run on a 12% SDS-PA gel. Anti-GFP-HRP antibody was used to detect protein. Ponceau stained membrane serves as a loading control. The numbers on the left side of each blot indicate the molecular weight (kDa) determined by a protein ladder.

Specifically, the first 148 amino acids of the $GABA_A$ α subunit were used as a swap for the N-terminal body of the Bs4C homologues, as this is the part of the protein that lies within the membrane. The C-terminal tails from CpBs4C, NbBs4C.1, and NbBs4C.2 were used to generate the GABA-Cptail, GABA-N1tail, and GABA-N2tail chimeras, respectively (Figure 3.27A). Three days after these chimeras were agroinfiltrated into *N. benthamiana*, none of the chimeras generated a cell death reaction similar to CpBs4C or NbBs4C.1 (Figure 3.27B). Typically, samples for Bs4C immunoblots are collected 24 hpi due to the fact that cell death is visible at 40 hpi. Samples for the GABA chimeras were taken at 24 hpi, but no protein was visible via immunoblot (data not shown). Only after three days post infiltration was protein able to be seen on an immunoblot (Figure 3.27C), but CpBs4C, NbBs4C.1, and NbBs4C.2 protein

samples were not taken due to cell death of the former two. This ultimately further confirms the notion that the cause of cell death in the Bs4C homologues is indeed the amino acid composition of the N-terminal body, and not the structural topology that it presents.

Next, the localisation of these chimeras was inspected to see if they localised to the plasma membrane as the complete $GABA_A$ receptor does, or if they localise to the ER as the Bs4C homologues do. For all three of the chimeras tested, they were found to localise to the ER, and in a similar fashion to that of their corresponding full-length Bs4C homologues (Figure 3.28). GABA-Cptail, GABA-N1tail, and GABA-N2tail all had a similar pattern of faint diffusion along the ER but scattered large aggregates stable at the ER 3-way junctions. Furthermore, these aggregates were also mobile, moving very quickly along the ER, in a similar fashion to the full-length Bs4C homologues. Taken together, it can be concluded that while these chimeras localise to a similar subcellular compartment as the Bs4C homologues, the chimeras are unable to induce cell death in a similar fashion to CpBs4C or NbBs4C.1.

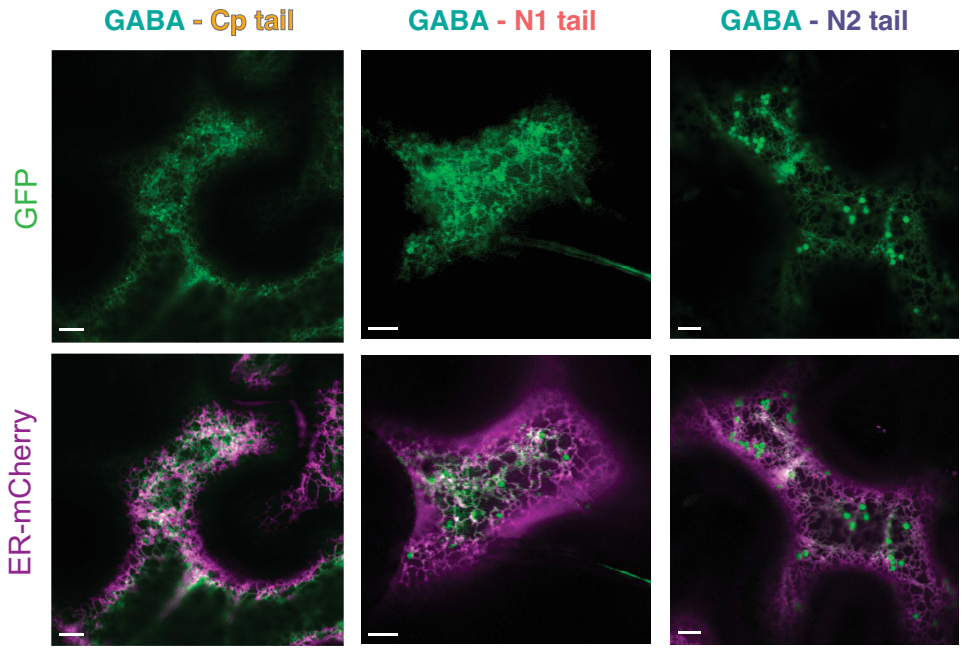

FIGURE 3.28. $GABA_A$ chimeras localise to the ER.

Co-expression of indicated $GABA_A$ chimera tagged with GFP and ER-mCherry 3 dpi in *N. benthamiana*. Top panel is GFP filter alone, bottom panel is GFP and mCherry filter merged. White scale bar in bottom left corner of each image represents 5 µm.

3.1.10. *SlBs4C* transcripts found in raw RNA-seq data set in early ripening stages of fruit development

Seeing as we got no indication from the publicly available plant transcriptome databases where and when *Bs4C* homologue transcripts might be present, we sought out collaborators to check raw RNA-seq datasets. As previously mentioned, *Bs4C* homologues are not annotated in any of the published RNA-seq datasets, so we asked Dr. Zhangjun Fei from Dr. Jocelyn Rose's group to search the sequence of *SlBs4C* against the raw spatiotemporal transcriptome dataset of *S. lycopersicum* fruit development and ripening (Shinozaki et al., 2018). There were 84 different combinations of tissue type and developmental stage, starting from the anthesis of the fruit, through fruit expansion, and across fruit ripening (Figure 3.29A). The different tissue types were not only limited to the different types within the cross-section of the middle of the fruit (Figure 3.29B), but also the different tissue types at the top of the fruit (stem), the middle of the fruit (equatorial), and the bottom of the fruit (stylar) (Figure 3.29C). There is an increase in *SlBs4C* expression at the beginning stages of fruit ripening, mainly at the mature green and breaker stage, on the stem part of the fruit (top part), most notably within the total pericarp and the septum (Figure 3.29D). This could possibly indicate that *SlBs4C* plays a role in tomato fruit ripening, however, this needs to be experimentally validated.

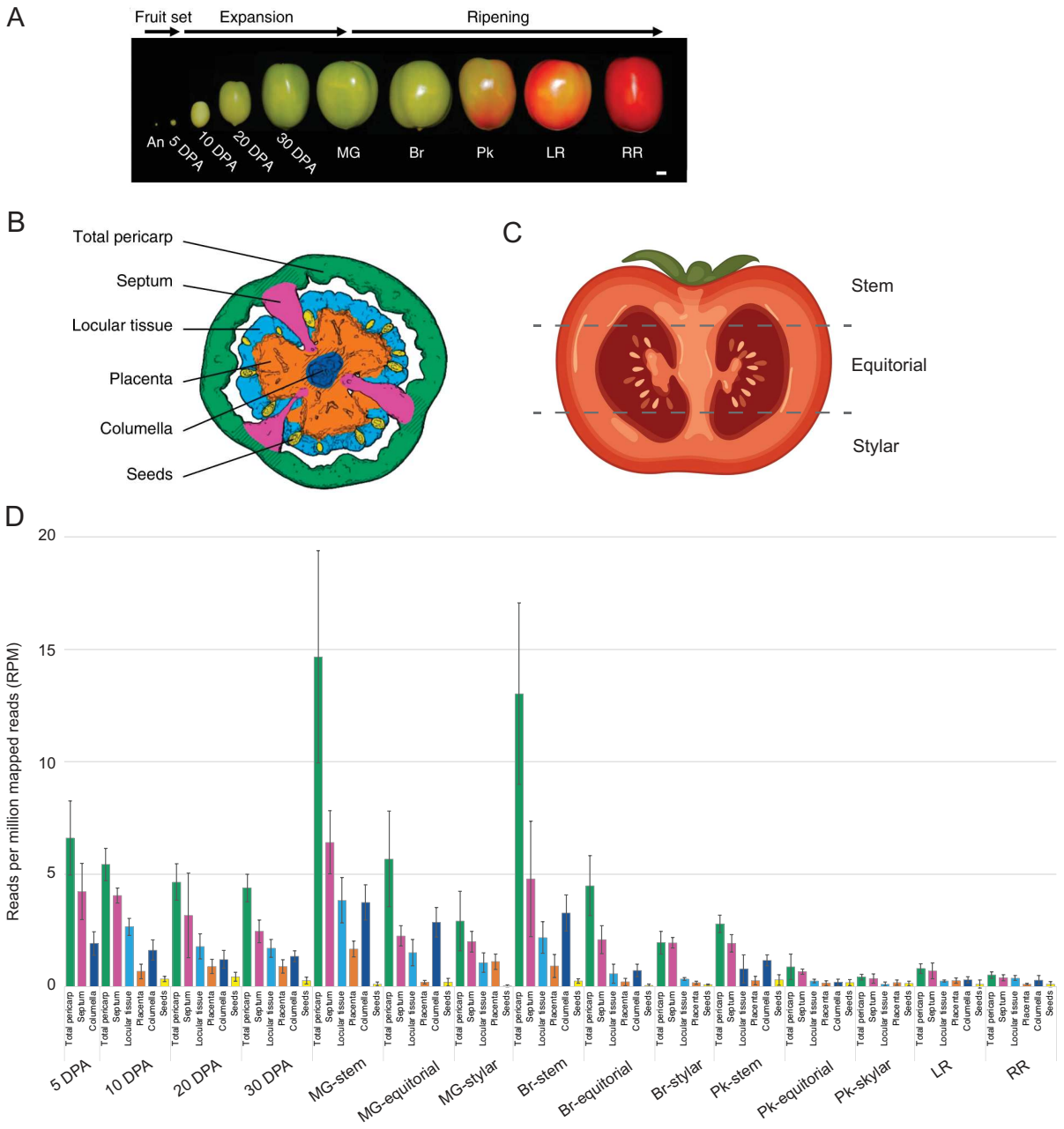

FIGURE 3.29. *SlBs4C* transcript found in early stages of fruit ripening.

A | Pictures represent harvested fruit at 10 different developmental stages. Image taken from Shinozaki et al., 2018. An = anthesis, DPA = days post anthesis, MG = mature green, Br = breaker, Pk = pink, LR = light red, RR = ripe red.

B | Horizontal cross-section of tomato fruit indicating specific tissue types taken for sampling. Image taken from Shinozaki et al., 2018.

C | Vertical cross-section of tomato fruit indicating the region of fruit where specific tissue types were taken. Image created using BioRender.com.

D | Expression of *SlBs4C* at the indicated tissues at the specific time points from the RNA-seq data set from Shinozaki et al., 2018. Values are represented as a bar graph, with the average of four biological replicates (n=4), and the error bars displaying the standard deviation.

3.1.11. Bs4C has structural homologues in bacteria

Towards the end of this project, the company Meta released the predicted structures for over 617 million proteins coming from bacteria, viruses, and other organisms whose proteins had previously not been structurally characterised (Lin et al., 2022). We were previously limited to identifying CpBs4C structural homologues to protein structures that had already been predicted or resolved (Figure 3.13). However, with this massive number of new predicted protein structures, we were able to see if there were any other proteins in Meta's databank that had structural similarity to CpBs4C. The protein comparison analysis, completed by Dr. J. Gronnier, found that CpBs4C had structural homology to several bacterial proteins (Figure 3.30, Table 3.5).

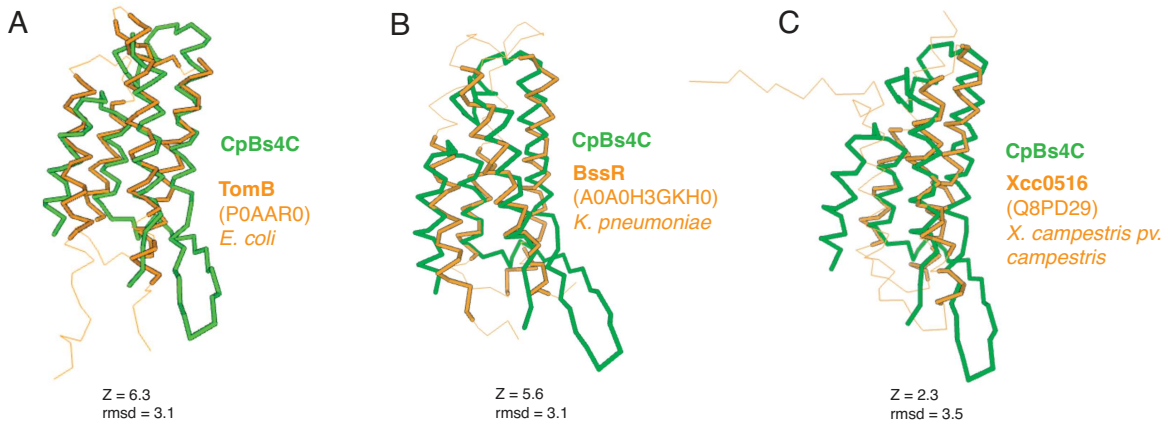

FIGURE 3.30. CpBs4C has structural homology to bacterial proteins.

Structural homology prediction using the DALI server. Green structure is CpBs4C and the orange structure is the predicted homologue, with the host organism, and the corresponding protein data bank reference. Z score is the DALI Z-score, and rmsd is the room mean square deviation.
A | CpBs4C structural similarity to TomB from *E. coli.*
B | CpBs4C structural similarity to BssR from *K. pneumoniae.*
C | CpBs4C structural similarity to Xcc0516 from *X. campestris pv. campestris.*

Specifically, there was structural homology to the *Escherichia coli* Hha toxicity modulatory protein TomB (PDB#: P0AAR0) with a Z=6.3 and rmsd=3.1 (Figure 3.30A), and also to the *Klebsiella pneumoniae* biofilm regulatory protein BssR (PDB#:A0A0H3GKH0) with a Z=5.6 and rmsd 3.1 (Figure 3.30B). There were other proteins that had structural homology to CpBs4C coming from bacteria, which have been outlined in Table 3.5. The proteins outlined in this table are the top 2 proteins from each species that had similar structures in addition to a high Z score.

Further investigation into TomB and BssR revealed that BssR actually had structural similarity to Xcc0516, a putative uncharacterized four-helix bundle coming from *Xanthomonas campestris* (Lin et al., 2006). Comparison of CpBs4C with Xcc0516 revealed a low Z-score (Z=2.3), but a similar rmsd score (rmsd=3.5) to the bacterial proteins listed in Table 3.5. While the Z score for comparing CpBs4C with Xcc0516 is relatively low, it is interesting that the plant pathogen *Xanthomonas campestris* has a somewhat similar structural homologue in Solanaceous plants, specifically *C. pubescens* (Figure 3.30C).

Table 3.5. Potential structural homologues of CpBs4C in bacteria.

Protein	PDB ID	Species	DALI score	RMSD Score
TomB, Hha toxicity modulator	P0AAR0	*Escherichia coli*	6.3	3.1
BssR, biofilm regulator	P0AAY1	*Escherichia coli*	5.6	4.1
Uncharacterized protein	A0A0H3GJ93	*Klebsiella pneumoniae*	6.2	3.2
BssR, biofilm regulator	A0A0H3GKH0	*Klebsiella pneumoniae*	5.6	3.1
UPF0344 protein	Q2FZT3	*Staphylococcus aureus*	5.4	3.5
Uncharacterized protein	Q2FVZ6	*Staphylococcus aureus*	5.3	3.0

PDB = protein databank, DALI = distance matrix alignment score, RMSD = root mean square deviation of atomic positions score.

In summary, it is evident that the executor *R* gene first identified in *C. pubescens, CpBs4C*, has structural homologues in many other Solanaceous species, including but not limited to *N. benthamiana*, *C. annuum*, and *S. lycopersicum* (Figure 3.3B), and that these structural homologues can be divided into two classes, cell death-inducing and non-cell death-inducing (Figure 3.4). While the non-cell death-inducing homologues do not produce a visible cell death response or reduce photosynthetic capacity, they still have a role in reducing bacterial proliferation upon their endogenous activation (Figure 3.8 and Figure 3.11), indicating that these homologues do indeed have a function that just has yet to be identified. Furthermore, CpBs4C was shown to have strong structural homology to the transmembrane region of neurotransmitter receptors (Figure 3.13) and with this, it was also found that CpBs4C can form a higher-order complex (Figure 3.16) and is able to bind to its homologues (Figure 3.17). CpBs4C was also found to utilise the movement of Ca^{2+} in its induction of cell death via Ca^{2+} channels (Figure 3.21), but this flow of Ca^{2+} does not follow the Ca^{2+} gradient by passively moving from the ER into the cytosol (Figure 3.22). These mechanistic insights bring us multiple steps closer to identifying the true function of CpBs4C and how it induces cell death *in planta*.

3.2. Genetically dissecting the CpBs4C signalling cascade

While we have presented many structural and functional insights into how CpBs4C might be inducing cell death, the identification of downstream signalling components could highlight the broader influence that CpBs4C has on the cell after its transcriptional activation.

3.2.1. The executor R protein CpBs4C from pepper induces growth arrest in Arabidopsis

CpBs4C has no known homologues in *Arabidopsis thaliana* (Arabidopsis hereafter) or any Brassicas for that matter. With the vast amount of resources that the Arabidopsis community has generated, it was logical to see if we could utilise this model species to further clarify how transcription of *CpBs4C* activates cell death. Seeing as CpBs4C activates cell death as soon as it is translated, an inducible promoter system was needed to see if CpBs4C can activate cell death in Arabidopsis. A T-DNA containing an epitope-tagged CpBs4C derivative under the transcriptional control of an estradiol inducible promoter (*Estr*) was generated and termed *Estr:CpBs4C-FLAG-GFP.* This T-DNA containing vector was put into *A. tumefaciens* and then used for Arabidopsis transformation. Wild-type Arabidopsis of the Columbia ecotype (Col-0 hereafter) was then transformed using this *Estr:CpBs4C-FLAG-GFP* containing *A. tumefaciens,* via the floral dip method (Zhang et al., 2006). Allowing the seeds to propagate, we inspected the seeds of multiple T2 lines to continue forward with the lines that had a visible estradiol dependent growth inhibition phenotype. These T2 seeds were placed under segregation analysis to identify lines that presumably only contained a single transgene insertion. Only lines with both a single T-DNA insertion and a strong estradiol dependent growth inhibition were used to generate large quantities of T3 seeds (the generation of transgenic lines and subsequent segregation analysis was performed by Dr. Robert Morbitzer and Markus Wunderlich). The selected T3 seeds were then analysed for *CpBs4C*-dependent growth inhibition. To do this, four-day old seedlings were put into liquid media containing or lacking estradiol for 10 days, and then analysed for seedling growth. It was found that in the presence of estradiol (but not in the absence) the *Estr:CpBs4C-FLAG-GFP* seedlings were severely stunted in their growth (Figure 3.31A). As an estradiol-inducible control, a transgenic line containing a *GUS-GFP* reporter was placed under the same estradiol-inducible promoter to generate *Estr:GUS-GFP* Arabidopsis plants. These *Estr:GUS-GFP* seedlings showed no signs of estradiol-dependent growth inhibition, therefore confirming that the growth inhibition seen in the *Estr:CpBs4C-FLAG-GFP* seedlings is entirely dependent on both the *CpBs4C*

transgene and estradiol together. Immunoblot analysis was also performed to show that both Arabidopsis lines generated a protein band at the expected sizes, in an estradiol-dependent fashion (Figure 3.31B). Taken together, these pieces of data illustrate that the executor R protein CpBs4C from pepper can induce cell death when expressed in Arabidopsis. The confirmation of functionality in this model plant positions us well to utilise the vast resources available for Arabidopsis, and specifically provides the basis for the genetic dissection of CpBs4C-dependent cell death in Arabidopsis.

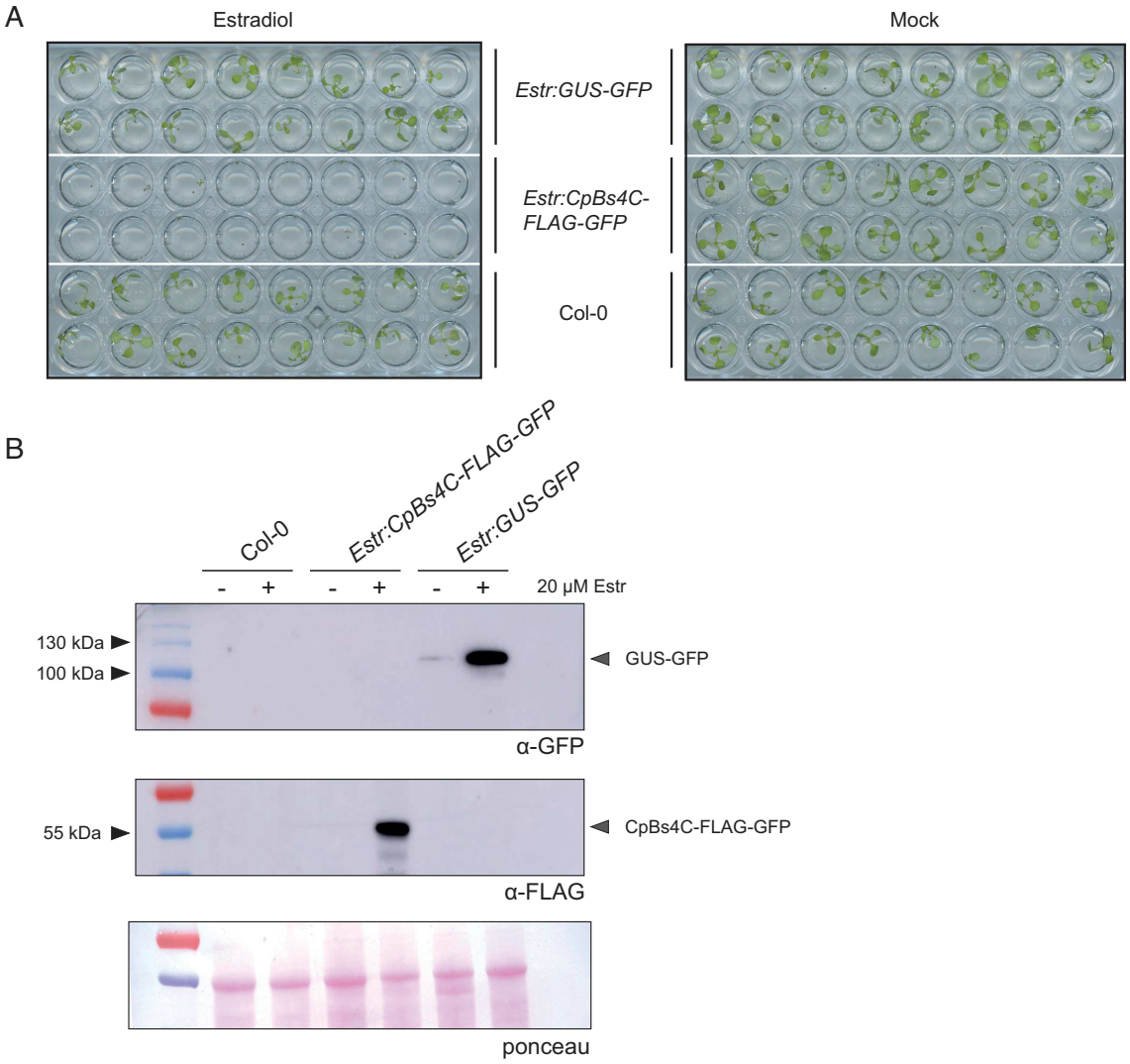

FIGURE 3.31. CpBs4C induces growth arrest in Arabidopsis.

A | Estradiol inducible transgene triggers seedling growth inhibition in Arabidopsis. Four-day old seedlings of the indicated genotypes were submerged in liquid media either containing estradiol or lacking estradiol (mock) and allowed to grow for 10 more days.

B | Immunoblot analysis of two-week-old Arabidopsis seedlings of indicated genotypes. Seedlings were submerged in liquid media either containing estradiol (Estr) or lacking estradiol (mock) for 24 hours. Two seedlings of each genotype and condition were pooled for protein analysis. Samples were run on a 10% SDS-PA gel. Anti-GFP-HRP or anti-FLAG antibody was used as indicated to detect protein. Ponceau stained membrane serves as a loading control. The numbers on the left side of each blot indicate the molecular weight (kDa) determined by a protein ladder.

3.2.2. A conditionally lethal screen in Arabidopsis identifies mutants that lack a CpBs4C dependent cell death

Approximately 10,000 *Estr:CpBs4C-FLAG-GFP* T3 seeds as mentioned above were treated with ethyl methanesulfonate (EMS) to randomly induce mutations across the Arabidopsis genome. These EMS treated seeds were termed the M0 generation. These M0 seeds were then sowed to soil and then transplanted into individual pots.

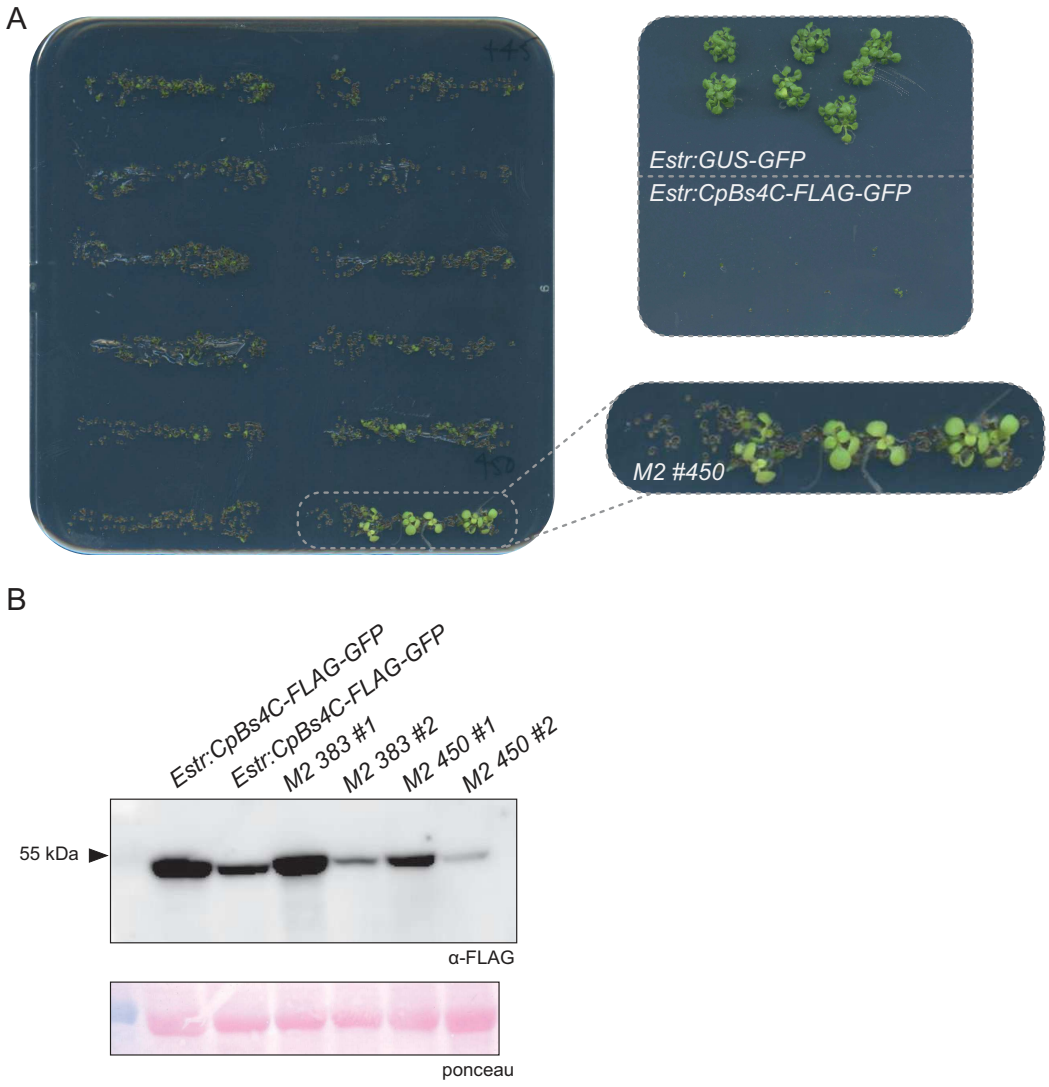

FIGURE 3.32. M2 mutant screening identifies *Estr:CpBs4C-FLAG-GFP* suppressors.

A | Approximately 100 seeds of each M2 family were placed on sterile media containing 20 µM estradiol, photos taken 14 days post germination. *Estr:GUS-GFP* and parental line *Estr:CpBs4C-FLAG-GFP* used as growth controls. Zoomed in image is of M2 family #450.
B | Immunoblot analysis of five-week-old Arabidopsis leaves after 24 hours of estradiol treatment. Samples were run on a 10% SDS-PA gel. CpBs4C protein was detected using an anti-FLAG antibody. Ponceau stained membrane serves as a loading control. The numbers on the left side of each blot indicate the molecular weight (kDa) determined by a protein ladder.

These plants were termed the M1 generation. Individual M1 plants were bagged and the resultant M2 seeds were harvested. This created 4,000 M2 families that were used for screening. Approximately 100 seeds from each M2 family were used as representatives for the entire M2 family, which equated to approximately 400,000 M2 seeds analysed in total. Seeds from each family were placed in rows on agar plates containing estradiol. The seeds were allowed to germinate and grow for approximately two weeks to identify families that inhibited CpBs4C-dependent cell death. After 14 days, the majority of the families' seedlings had stopped growing and neglected cotyledon emergence. M2 families containing individual M2 seedlings that survived on the estradiol medium were easily detectable, as they were large in size, had developed roots, and had true leaves that were matching the colour of *Estr:GUS-GFP* (Figure 3.32A). There were 46 M2 families which had individual plants that grew in a similar fashion to *Estr:GUS-GFP* plants on estradiol-containing plates. The low ratio of survivors vs. dead seedlings suggested a recessive inheritance of putative suppressor alleles. The survivors from each M2 family were transplanted from the estradiol plates to soil and allowed to mature, then tested for protein accumulation after transgene activation (Figure 3.32B). As it is a great deal of effort and resources to move forward with all 46 suppressing families, we decided to initially only test the first three families identified in the initial screen to suppress *CpBs4C*, M2 families #318, #383, and #450.

Two different types of mutations were expected from this forward genetic screen: mutations found within the putative signalling or regulatory components that are required for CpBs4C to induce cell death, and mutations found within the transgene which affect expression or functionality of CpBs4C. To check if there was any mutation within the *Estr:CpBs4C-FLAG-GFP* transgene, we extracted DNA from the leaves of mature M2 plants on soil, PCR amplified the *CpBs4C* coding sequence (CDS), and then sent it for Sanger sequencing. All three families had a WT CDS, so we next needed to check if there was CpBs4C expression. We tested many possibilities to check for CpBs4C-FLAG-GFP expression and found that induction of the transgene in young seedlings grown in sterile liquid culture had the most consistent success rate, therefore, we analysed the CpBs4C-FLAG-GFP expression in the seedlings of the M2 progeny (M3 generation). Suppression of the *CpBs4C-FLAG-GFP* transgene also needed to be tested in the M3 generation to confirm transgenerational inheritance. Four M2 plants from the surviving families were chosen at random and their progeny, the M3 seedlings, were tested for their seedling growth inhibition both in the presence and absence of estradiol. We found that in all M3 seedlings, the families were still able to suppress estradiol-dependent cell death (Figure 3.33A). Then the expression of CpBs4C-FLAG-GFP fusion protein was tested, and in all three suppressing families, signals matching the expected size of the fusion protein were detected, although some had varying signal levels (Figure 3.33B). Taken together, the WT

CDS in the *CpBs4C-FLAG-GFP* transgene and the expression of the CpBs4C-FLAG-GFP protein confirmed that the three suppressing families indeed harboured mutations within putative signalling or regulatory components required for CpBs4C execution of cell death.

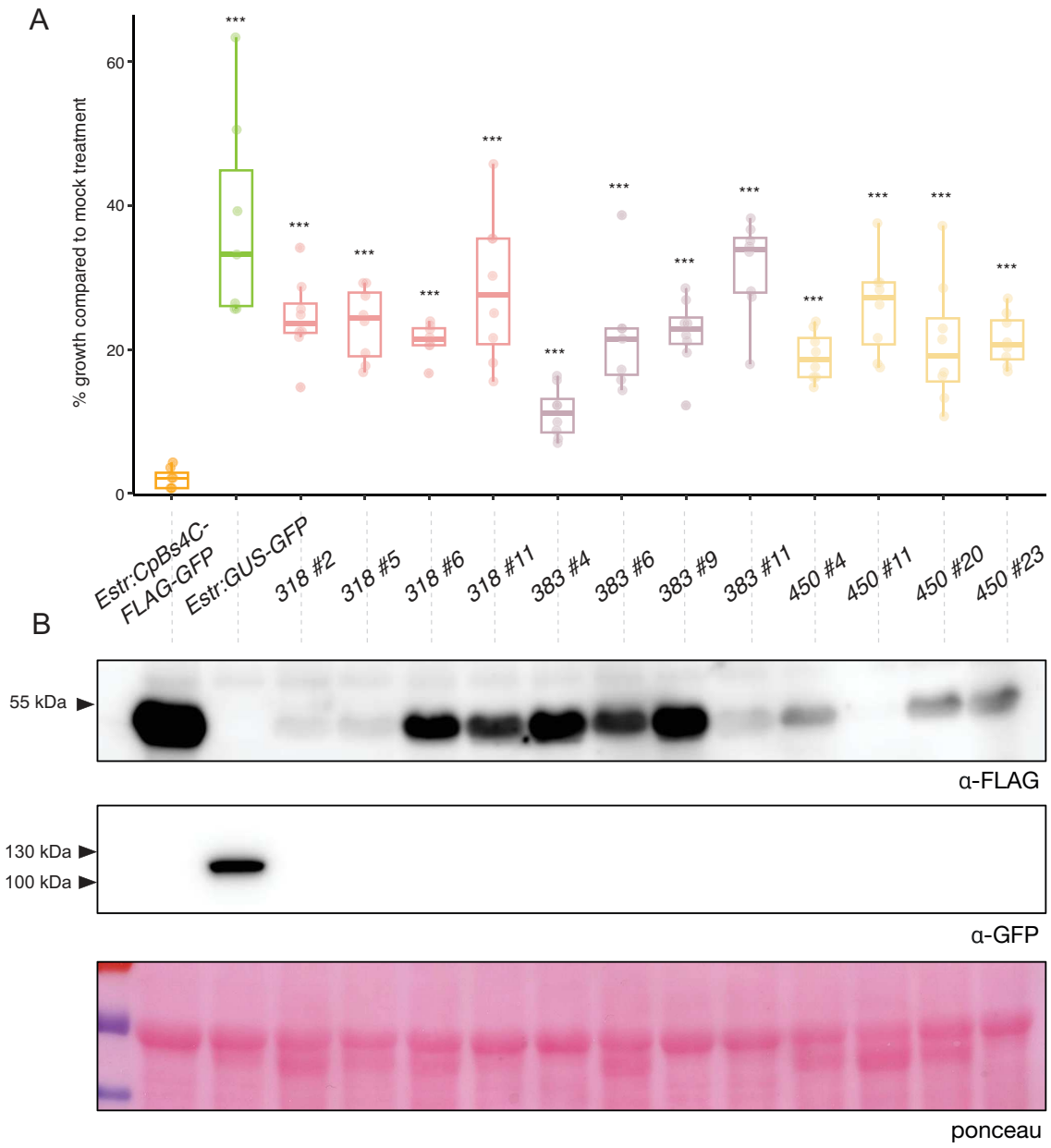

FIGURE 3.33. M3 generation still suppresses CpBs4C dependent growth inhibition.

A| Seedling growth inhibition of progeny of four individual M2 plants, as indicated by their number. Four-day-old seedlings were placed in liquid medium either containing or lacking estradiol and were allowed to grow for ten more days. Seedlings' fresh weight in inducing (estradiol containing) medium was compared to the growth in non-inducing medium (mock treatment) and set as a percentage. Bar and whisker plot to show variance of data points, n=8, statistical significance is compared to % growth of *Estr:CpBs4C-FLAG-GFP* and determined using a student's t-test, *** p<0.001.
B| Immunoblot analysis of two-week-old Arabidopsis seedlings after being submerged in estradiol for 24 hours. Samples were run on a 10% SDS-PA gel. Anti-GFP-HRP or anti-FLAG antibody was used as indicated to detect protein. Ponceau stained membrane serves as a loading control. The numbers on the left side of each blot indicate the molecular weight (kDa) determined by a protein ladder.

With the knowledge that all of the progeny in the M3 seedling growth inhibition assay suppressed the *CpBs4C* transgene in the presence of estradiol indicates that the mutation causing this suppression is likely a recessive allele in a homozygous fashion, and that segregation of this allele can be seen and tested in the M2 generation. There are two diploid cells in Arabidopsis M1 seeds that generate reproductive organs (inflorescence) of M1 plants, which are phenotypically evaluated in the subsequent generation (M2) (Jürgens et al., 1991; Page & Grossniklaus, 2002). Hypothetically, if mutagenesis via EMS induces random recessive mutations, the ratio of recessive mutants to WT gametes is 1:7 in the M1 generation (Bellini et al., n.d.). This would equate to 12.5% of the seeds of each suppressing M2 family surviving on estradiol-containing plates. Several hundred M2 seeds for each of the three suppressing families were put on estradiol-containing plates to observe their survival rates. 6.1% (45/734), 2.0% (17/833), and 5.1% (57/1114) were the survival rates for families 318, 383, and 450, respectively. It is unlikely that there was any phenotypic mis-scoring seeing as there is a very clear phenotype between alive and dead seedlings within the family. Given that we did not find 12.5% mutants to survive, the segregation is distorted. This is possibly the consequence of diplontic selection, whereby the mutagenized cells have a reduced proliferation to that of the WT cells (Gaul, 1965).

Regardless of the distorted segregation data mentioned above, the M2 plants that survived in the presence of estradiol and accumulated the correct protein, should, in theory, have a causal mutation in a homozygous configuration, assuming recessive inheritance. Therefore, we pooled together survivors from each individual M2 family on estradiol-containing medium and harvested their DNA in a pool to generate a bulked DNA profile of the survivors. Next-generation sequencing (NGS) detects the allele frequency for each EMS mutation within the survivor pool of one family when it is compared to the parental line *Estr:CpBs4C-FLAG-GFP*, which had no EMS mutagenesis. This has the potential to identify mutations that are homozygous across all survivors of one M2 family, which could possibly be the causal mutation for the suppression of *Estr:CpBs4C-FLAG-GFP* dependent cell death.

3.2.3. Three families harbour distinct mutations in *AtXRN4*

Whole genome sequencing was conducted first on the parental lines that were used for the EMS mutagenesis to generate the M0 population. This served as the control to identify which mutations were generated from the EMS mutagenesis. Survivors from the M2 families 318, 383, and 450 had their DNA harvested which generated 3 pools of DNA containing 38, 18, and 25 M2 survivors, respectively. Paired-end sequencing with a minimum depth of 150X

coverage was used to define EMS mutations and their respective allele frequencies. 60, 150, and 487 EMS-specific mutations were detected for M2 families 318, 383, and 450, respectively. The pooled genomes of the M2 survivors were scanned, and genomic regions with an increase in frequency of mutant alleles were highlighted. In all three of these M2 families, there was an increased and locally fixed allele frequency on chromosome 1, with a stable and average allele frequency of around 0.5 on all other chromosomes (Figure 3.34). Numerous mutations were found within the genomic regions with an increase in allele frequency, which can be seen in Table 3.6.

The search for causal mutations was constricted by only considering EMS mutations with an allele frequency of 0.95 or higher, indicating that at least 95% of the pooled DNA contained that specific EMS mutation at that position. The search was also limited by only considering hallmark base pair changes of EMS-induced mutations (C to T or G to A). Lastly, mutations that were found either to induce synonymous mutations (different base pair codon generating the same amino acid residue) in the coding regions or mutations found in non-coding regions (non-translated regions or intronic) were excluded from consideration. This allowed us to focus solely on non-synonymous mutations within the coding regions that potentially impacted the function of the gene. Using these stringent parameters, the search was narrowed down to one candidate gene in M2 families 318 and 383 (*At1g54490*), and three candidate genes in M2 family 450 (*At1g54490*, *At1g52940*, and *At1g5510*).

318

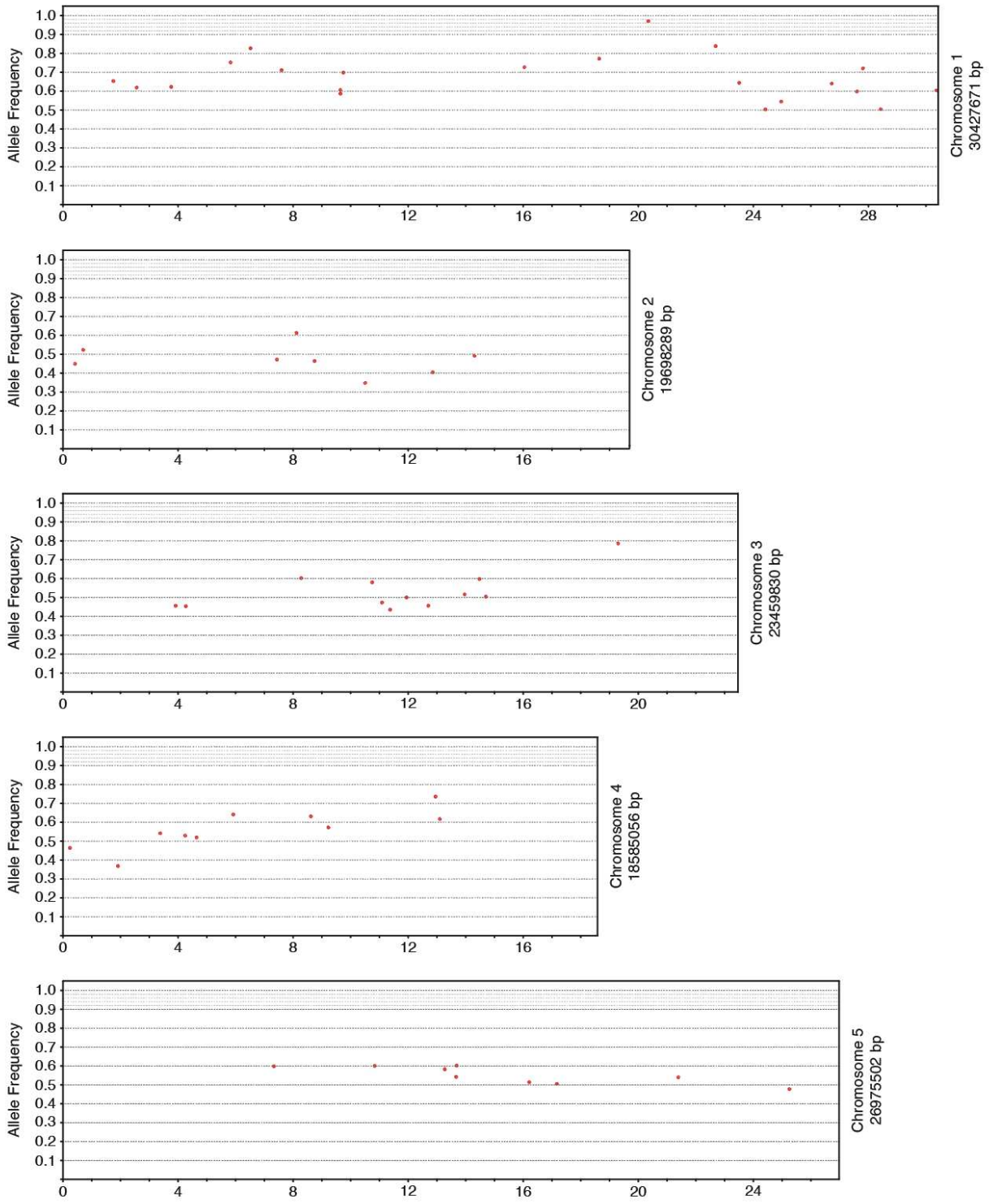
Allele Frequency
1.0
0.9
0.8
0.7
0.6
0.5
0.4
0.3
0.2
0.1
0
4
8
12
16
20
24
28
Chromosome 1
30427671 bp
Chromosome 2
19698289 bp
Chromosome 3
23459830 bp
Chromosome 4
18585056 bp
Chromosome 5
26975502 bp

383

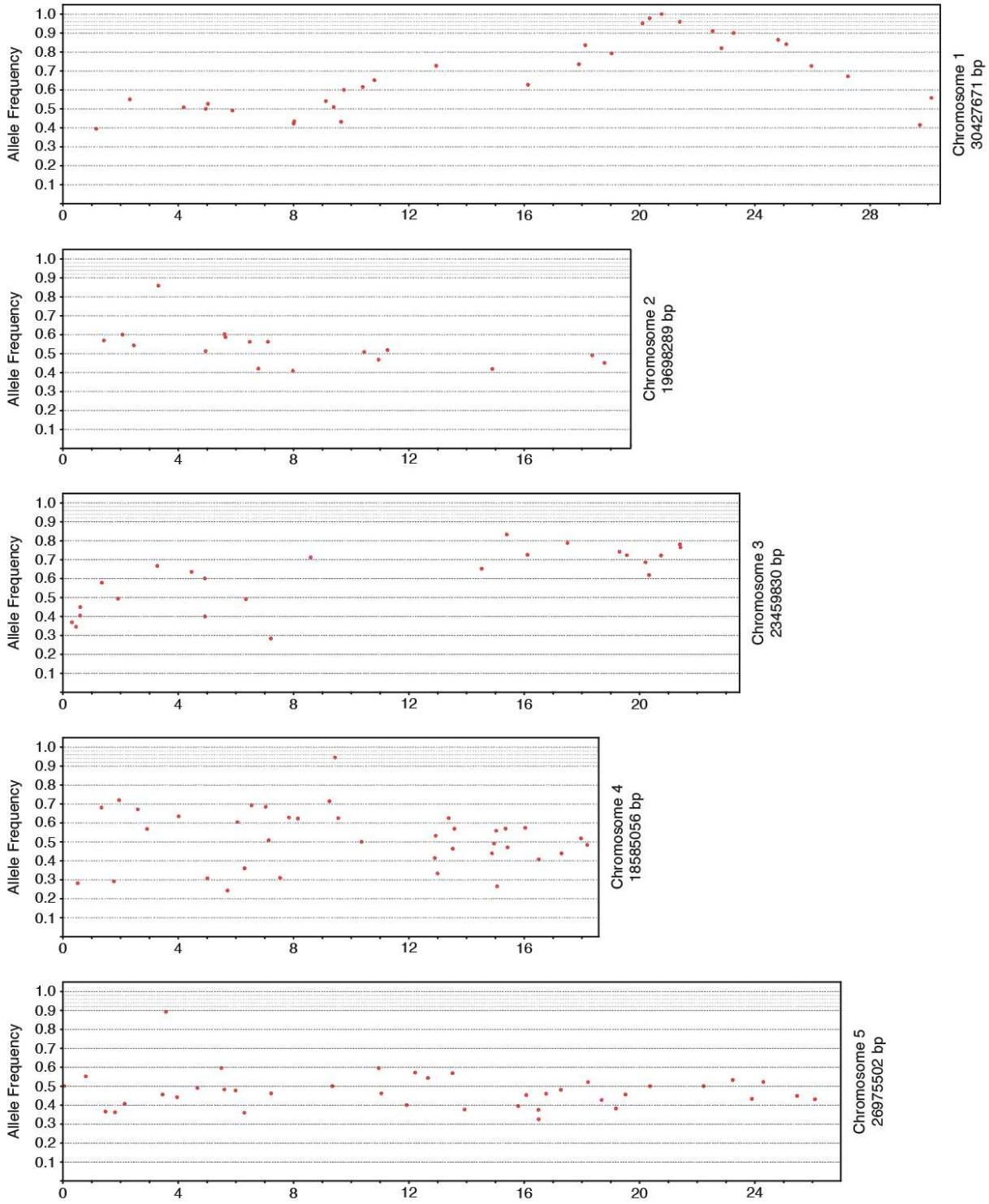
Allele Frequency
1.0
0.9
0.8
0.7
0.6
0.5
0.4
0.3
0.2
0.1
0
4
8
12
16
20
24
28
Chromosome 1
30427671 bp
Chromosome 2
19698289 bp
Chromosome 3
23459830 bp
Chromosome 4
18585056 bp
Chromosome 5
26975502 bp

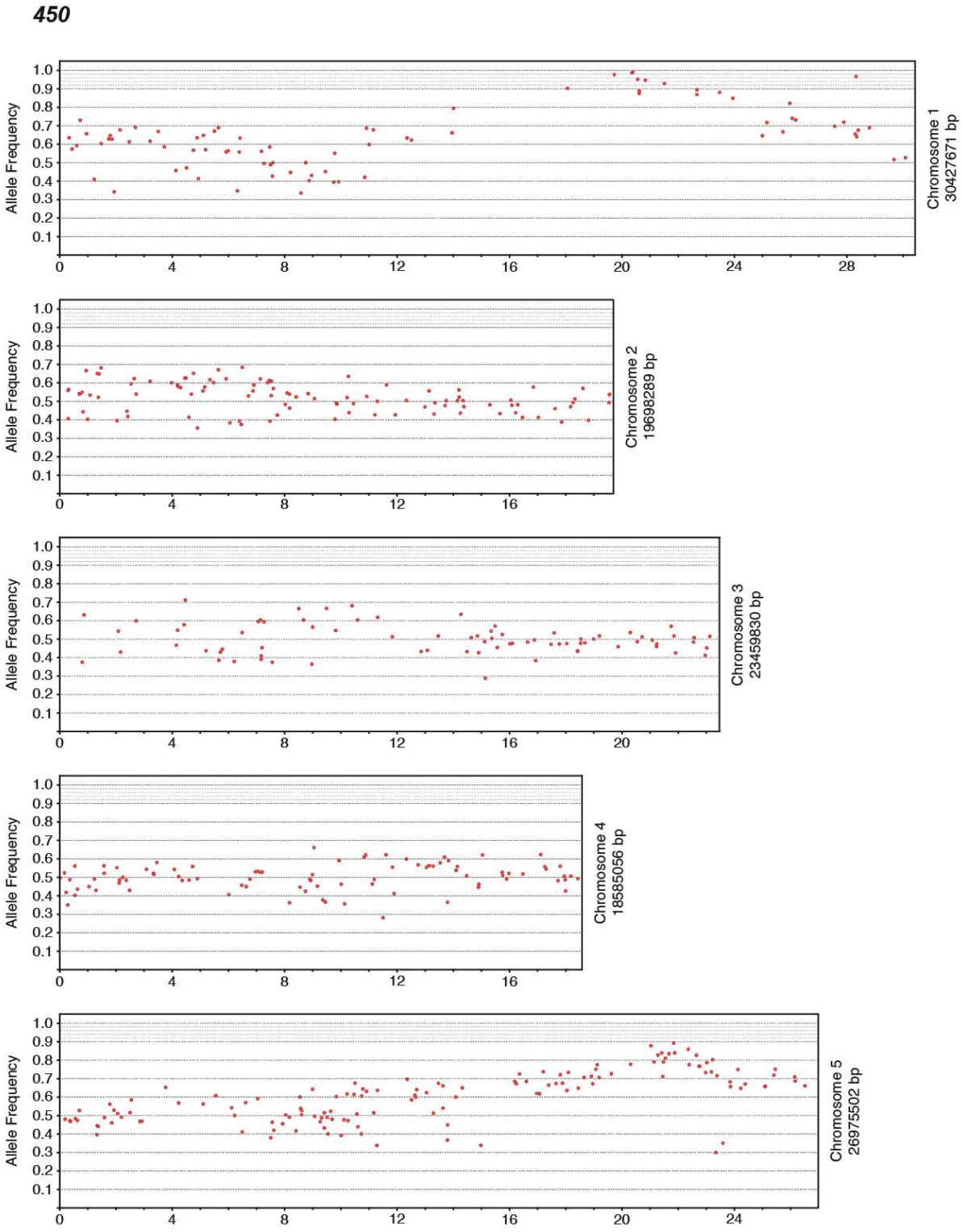

FIGURE 3.34. Allele frequency distribution of M2 families 318, 383, and 450.

The red dots specify the location of EMS-induced mutations on chromosomes 1-5 as indicated on the right side and their allele frequency (x-axis), within each M2 family. The name of each M2 family is written at the top of the page. Figure created by Dr. Thomas Lahaye.

Table 3.6. Allele frequencies of SNPs induced via EMS in three M2 families.

Family	Chr.	Position	Ref./ Alt.	Cover	Allele freq.	Gene ID	Region	CDS position	Effect	AA change
318	1	18 ,641,436	G/A	81	0.77	--	intergenic			
	1	20,352,190	G/A	98	0.97	**At1g54490.1**	CDS	706	Nonsyn	D/N
383	1	18,117,826	G/A	61	0.85	At1g48970.1	5' UTR			
	1	19,031,508	G/A	61	0.87	--	intergenic			
	1	20,105,279	G/A	59	0.97	At1g53850.1	intronic			
	1	20,105,279	G/A	59	0.97	At1g53850.2	intronic			
	1	20,352,595	G/A	44	0.98	**At1g54490.1**	CDS	911	Nonsyn	W/*
	1	20,765,374	G/A	59	1	At1g55580.1	CDS	1269	Syn	Q/Q
	1	21,402,987	G/A	47	0.96	--	intergenic			
450	1	18,062,237	C/T	101	0.9	At1g48840.1	intronic			
	1	19,722,708	C/T	129	0.98	At1g52940.1	CDS	478	Nonsyn	H/Y
	1	20,351,467	C/T	146	0.99	**At1g54490.1**	CDS	329	Nonsyn	A/V
	1	20,386,527	C/T	102	0.99	--	intergenic			
	1	20,560,738	C/T	139	0.95	At1g55110.1	CDS	1036	Nonsyn	E/K
	1	20,613,630	C/T	98	0.88	--	intergenic			
	1	20,616,883	C/T	96	0.89	--	intergenic			
	1	20,830,617	C/T	123	0.95	At1g55720.1	5' UTR			
	1	21,512,799	C/T	130	0.93	At1g58100.1	CDS	1087	Nonsyn	G/S
	1	21,512,799	C/T	130	0.93	At1g58100.2	CDS	1015	Nonsyn	G/S

SNPs identified through NGS of pooled M2 families (Family) on chromosome (Chr) 1. Stating the position of the mutation, the reference base (Ref.), the altered base (Alt.), the coverage (Cover), the frequency of that allele (Allele freq.), the Gene ID annotated from Tair10, the region within the gene, the position within the coding sequence (CDS position), the effect induced by the mutation, and the amino acid resulting from the mutation (AA change). Bold font with underline indicates the gene that had a mutation identified in all three of the M2 families. SNPs having an allele frequency below 0.77 were not listed.

At1g54490, which encodes the EXORIBONUCLEASE 4 (XRN4) protein, and is alternatively referred to as ETHYLENE INSENSITIVE 5 (EIN5) protein (Gazzani et al., 2004; Potuschak et al., 2006; Souret et al., 2004), was found to be mutated across all three M2 families, all with distinct mutations, perhaps suggesting that the mutations generated within the *XRN4* CDS have a functional impact. These distinct mutations harboured within the three families were all

found within the first half of the gene, with the 318 mutation found within the sixth exon, changing the wildtype aspartate to an asparagine (D to N), the 383 mutation generated an early stop codon within the eighth exon from a tryptophan (W to *), and the 450 mutation was found to lie within the third exon, altering the parental alanine to a valine (A to V) (Figure 3.35).

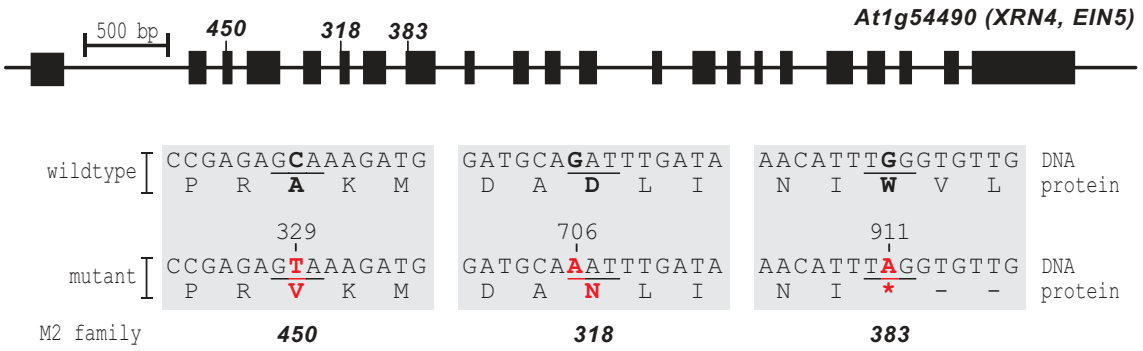

FIGURE 3.35. Three distinct mutations were found in *At1g54490*.

Gene schematic of EMS-induced mutations of M2 families 318, 383, and 450 within *At1g54490*. Black boxes indicate exons and black lines in between indicate introns. In the lower panel, bold font indicates a change in base pair or amino acid, black bold font represents the wildtype, and red bold font indicates mutation made by EMS and the induced change at the amino acid level.

There are two commonly used *xrn4* mutant alleles in the literature that are used as *XRN4* knockout plants, *xrn4-3* (SALK_014209) and *xrn4-5* (SAIL_681_E01) (Gazzani et al., 2004; Souret et al., 2004), and these T-DNA insertions are in the latter half of the gene, while the EMS-induced mutations found herein, are at the beginning half of the gene (Figure 3.36).

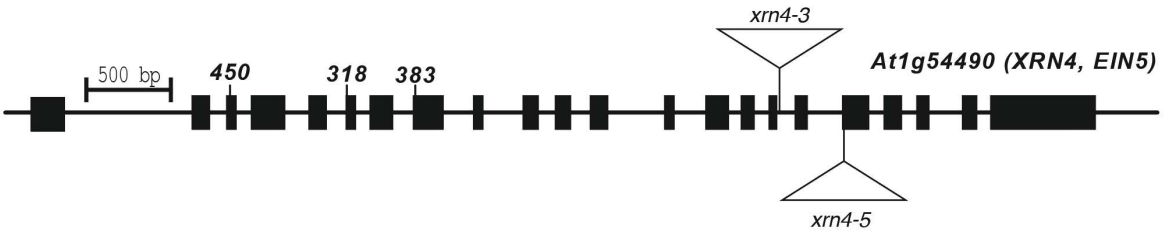

FIGURE 3.36. TDNA insertions and EMS mutations found within *At1g54490*.

Gene schematic of both EMS-induced mutations from above and T-DNA insertion alleles in *At1g54490*. Black boxes indicate exons and black lines in between indicate introns. White triangles indicate T-DNA insertion, *xrn4-3* is SALK_014209 and *xrn4-5* is SAIL_681_E01. T-DNA insertion size is not to scale.

Both *xrn4* mutant allele plants have a very striking phenotype in the adult leaves with a jagged edge of leaf compared to the smooth-edged leaves of a Col-0 mature plant. Interestingly, this phenotype of jagged edges can be observed in M3 individual plants from each of the M2 families (Figure 3.37), which is consistent with the fact that all three of these families were found to have non-synonymous mutations in the coding region of *XRN4*.

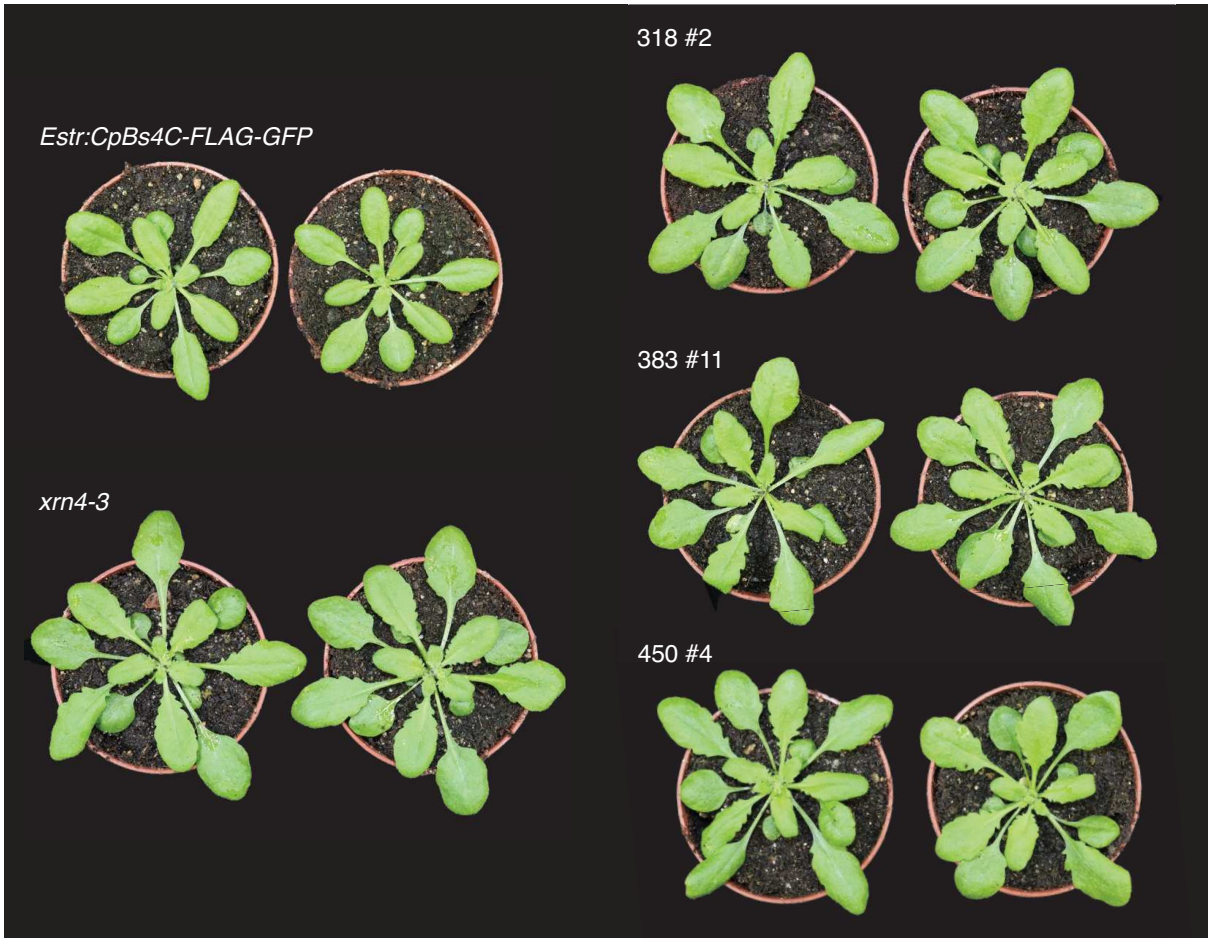

FIGURE 3.37. M3 individuals have a similar rosette phenotype to *xrn4-3*.

Rosette phenotypes of two M3 individuals of the indicated genotype. Photos taken at four weeks post germination. *Estr:Bs4C* is used as the parental control.

It is worth noting that the selection of the plants for the rosette phenotype was random, and that all M3 individuals (from 318 #2, 318 #5, 318 #6, 318 #11, 383 #4, 383 #6, 383 #9, 383 #11, 450 #4, 450 #11, 450 #20, and 450 #23) had the same rosette phenotype.

3.2.4. The *xrn4-5* mutant allele suppresses *CpBs4C* cell death in Arabidopsis

With EMS mutagenesis screens, there are two commonly used methods to verify if the mutation that was found in the screen is indeed causal. The first method is to complement the identified mutant with the WT copy of that gene to see if the original phenotype is restored. The second method is to identify or generate an independent mutant allele in the same gene as the mutation under investigation and test if the mutant phenotype can be reproduced with this independent mutant allele. Seeing as we had *xrn4-3* seeds in hand, we crossed it to the *Estr:CpBs4C-FLAG-GFP* parental line used for EMS mutagenesis that has a WT *AtXRN4*

allele to test if segregants containing loss of function *AtXRN4* alleles show consistently no estradiol dependent *CpBs4C* growth arrest. Unfortunately, however, we were unable to find segregants that were homozygous for the *xrn4-3* T-DNA and homozygous for the *Estr:CpBs4C-FLAG-GFP* transgene, possibly due to the fact that there could be an unknown mutation linked to the *xrn4-3* allele causing its progeny to be dwarfed and not able to produce seeds.

After this, we looked towards the other well-used *xrn4* mutant allele, *xrn4-5*, which can be seen in Figure 3.36, to see if it would suppress estradiol-dependent *CpBs4C* growth arrest. Instead of using the conventional crossing method, we transformed *xrn4-5* with the same *Estr:CpBs4C-FLAG-GFP* construct used to generate the parental line used for EMS, using the floral dip method. The T1 generation was sterilized and placed on kanamycin plates to select for plants containing the *Estr:CpBs4C-FLAG-GFP* transgene. These plants were then transplanted to soil and allowed to mature, and genotyped for the transgene to confirm the transformation, and their progeny was collected. Due to a limited time frame, we decided to move forward and work with the T2 generation because we were able to select for the *Estr:CpBs4C-FLAG-GFP* transgene by plating the seeds on kanamycin selective plates. The surviving T2 seedlings from the kanamycin plates were then placed in estradiol-containing medium on day five and left to grow for a total of 14 days. On day 14, the fresh weight of the seedlings grown in estradiol-containing medium and non-estradiol containing medium (mock) were recorded, and the growth in the estradiol medium was compared to the mock control. Using two T2 lines, *xrn4-5//Estr:CpBs4C-FLAG-GFP* #2 and *xrn4-5//Estr:CpBs4C-FLAG-GFP* #3, we found that the *xrn4-5* allele was able to suppress the estradiol dependent *CpBs4C* growth arrest in Arabidopsis (Figure 3.38A). Furthermore, we were able to confirm that both T2 lines were able to express the CpBs4C-FLAG-GFP protein and that the *xrn4-5* allele did not hinder protein accumulation, and there was even a visible increase in the amount of CpBs4C-FLAG-GFP protein in both *xrn4-5//Estr:CpBs4C-FLAG-GFP* #2 and #3 T2 individuals (Figure 3.38B). We also transformed the *xrn4-5* parental line with *Estr:GUS-GFP* as a control for a non-cell-death-inducing transgene. For this, we used two T2 lines, *xrn4-5//Estr:GUS-GFP* #2 and *xrn4-5//Estr:GUS-GFP* #3, and found that in *xrn4-5//Estr:CpBs4C-FLAG-GFP* #2, there was more GUS-GFP protein being produced after 24 hours of estradiol treatment than the parental *Estr:GUS-GFP* (Figure 3.38C), and there was little impact on growth when placed in estradiol containing medium for 14 days (Figure 3.38A).

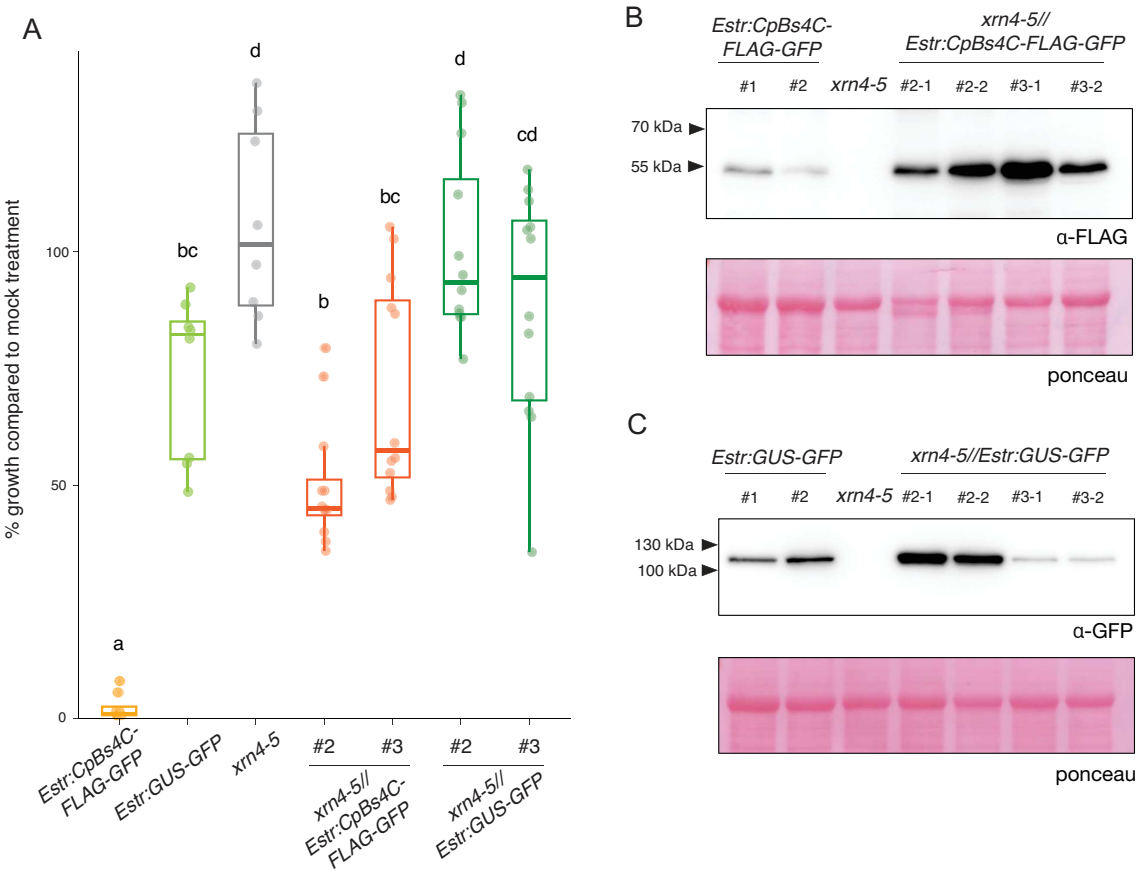

Figure 3.38. *xrn4-5* supresses *CpBs4C* growth arrest in Arabidopsis.

A| Seedling growth inhibition of selected T2 individuals of the indicated genotype. Five-day-old seedlings grown on kanamycin-containing medium were placed in liquid medium either containing or lacking estradiol and were allowed to grow for nine more days. Seedlings' fresh weight in inducing (estradiol-containing) medium was compared to the growth in non-inducing medium (mock treatment) and set as a percentage. Bar and whisker plot to show variance of data points, n=12, statistically significant groups ($p<0.05$) are presented with letters resolved by a one-way ANOVA with post hoc Tukey's test.
B| Immunoblot analysis of individual two-week-old Arabidopsis seedlings grown on kanamycin-containing medium, after being submerged in estradiol for 24 hours. Samples were run on a 10% SDS-PA gel. Anti-GFP-HRP or anti-FLAG antibody was used as indicated to detect protein. Ponceau stained membrane serves as a loading control. The numbers on the left side of each blot indicate the molecular weight (kDa) determined by a protein ladder.

Seeing as we were working in the T2 generation, the *Estr:CpBs4C-FLAG-GFP* and *Estr:GUS-GFP* transgenes were still segregating, we took individual plants grown on kanamycin-containing medium to use for immunoblot to see if there was variation in protein accumulation between individuals in the T2 generation, which was not obvious in the *xrn4-5//Estr:GUS-GFP* T2 lines, and could be argued for the *xrn4-5//Estr:CpBs4C-FLAG-GFP* T2 lines (Figure 3.38B and Figure 3.38C). Taken together, this confirms that the *xrn4-5* mutant allele does indeed suppress the growth arrest of CpBs4C in Arabidopsis, and that a functional *XRN4* allele is required for the mechanism of CpBs4C to induce growth arrest.

3.2.5. Novel knockout alleles of XRN4 could not be generated

We wanted to further confirm the results in Figure 3.38 by exhibiting that another *xrn4* mutant allele can suppress CpBs4C. As we were unable to generate proper *xrn4-3* x *Estr:CpBs4C-FLAG-GFP* lines, we decided to generate new mutations using CRISPR. As can be seen in Figure 3.35, the positions of the mutations are quite diverse, with the EMS point mutations within the first half of the gene and the T-DNA insertions being within the latter half of the gene. Our goal was to generate a mutation that was in a similar location along the genes as our EMS point mutations. Therefore, guides were designed and generated to create mutations or even a large deletion in the same area within the gene that the EMS-induced mutations were found in *XRN4*. A CRISPR plasmid containing Cas9 under the control of an Arabidopsis egg-cell-specific promoter was used, as it had the highest efficiency at the time of this transformation (Decaestecker et al., 2019). The Arabidopsis *Estr:CpBs4C-FLAG-GFP* parental line was used as the background for this CRISPR transformation, however, there were no survivors in the T1 selection. We also tried to generate CRISPR mutant alleles of *XRN4* in *N. benthamiana*, using guides designed in similar locations to that of the guides designed for the Arabidopsis *XRN4*, using the pDGE CRISPR plasmid system from Dr. Johannes Stuttman (Stuttmann et al., 2021). Two independent transformations of this plasmid using WT *N. benthamiana* generated zero transformants. Dr. J. Stuttman also generated an additional independent plasmid with newly designed guide RNAs at various positions along the gene, not just limited to the first half as we had. Dr. J. Stuttman performed two independent transformations of his plasmid using WT *N. benthamiana*. Similar to our outcome, his two independent rounds of transformation produced zero transformants. Ultimately, new alleles of *XRN4* in both Arabidopsis and *N. benthamiana* with mutations in the first half of the gene were unable to be generated.

3.2.6. Analysis of remaining M2 families uncovers more mutations in *AtXRN4*

After NGS results of M2 families 318, 383, and 450, screening of the remaining M2 families went underway. The suppressing families were further tested for their CpBs4C-FLAG-GFP expression and the *CpBs4C* CDS of the transgene was PCR amplified and sent for sequencing. Only families that had more than one M2 individual survive on estradiol and transplanted to soil, had sufficient CpBs4C expression, and had a WT transgene, were considered for NGS. These stringent measures ensured that only the families that had true second-site suppression were sent for sequencing. While none of the M2 families that had their transgene sequenced had a mutation within the CDS, there were many suppressing

families that did not have CpBs4C expression, for example, families 1902, 1920, 1988, 2013, and 2018 (Figure 3.39). Unfortunately, the membrane was not stained with ponceau for a loading control, therefore a comparison in the quantity of protein cannot be commented on, only that there is either a presence or absence of protein within each lane.

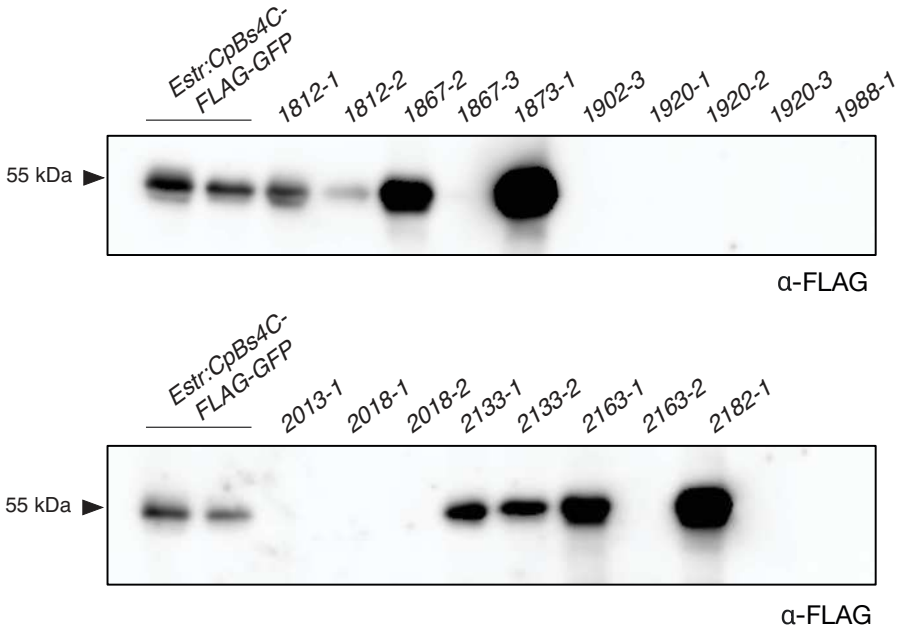

FIGURE 3.39. Immunoblot of individuals in additional M2 families.

Immunoblot analysis of five-week-old Arabidopsis leaves after 24 hours of estradiol treatment. CpBs4C protein was detected using an anti-FLAG antibody. The numbers on the left side of each blot indicate the molecular weight (kDa) determined by a protein ladder.

In total, 46 families suppressed CpBs4C dependent cell death, 46 families had a WT *CpBs4C* CDS in the transgene, 16 families had some level of CpBs4C expression detectable via immunoblot (this includes families where only some of the individuals had expression, and also individuals that had weak expression). Ultimately, 11 M2 families were sent for sequencing. Out of the eight families that were sent for NGS during the second round, only six families had a decent sequencing readout, and as such, the other two families' sequencing data was discarded. It would be worthwhile in the future to go back to these families and re-generate a bulked M2 DNA pool and re-send for NGS.

Table 3.7. Allele frequencies of SNPs induced via EMS in M2 family 1812.

Family	Chr.	Position	Ref/Alt	Cover	Allele freq	Gene ID	Region	GENE	CDS position	Effect	AA change
1812	2	13081230	G/A	73	1	AT2G30695.2	5' UTR				
	2	13081230	G/A	73	1	AT2G30695.1	intronic				
	2	13926520	G/A	60	1	AT2G32820.1	CDS	TFIIS	484	Nonsyn	E/K
	2	14204785	G/A	66	1	AT2G33540.1	CDS	CPL3	3274	Nonsyn	Q/*
	2	13022365	G/A	67	0.99	AT2G30575.1	intronic	GAUT5			
	2	12200571	G/A	64	0.98	AT2G28510.1	intronic	DOF 2.1			
	2	13048392	G/A	53	0.98	AT2G30630.1	intronic				
	2	13048392	G/A	53	0.98	AT2G30630.2	intronic				
	2	13194892	G/A	64	0.98	AT2G31010.1	5' UTR				
	2	13194892	G/A	64	0.98	AT2G31010.2	5' UTR				
	2	15650419	G/A	53	0.98	AT2G37280.1	CDS	PDR9	20	Nonsyn	S/N
	2	16249949	G/A	48	0.98	AT2G38920.1	intronic				
	2	16249949	G/A	48	0.98	AT2G38920.2	intronic				
	2	16249949	G/A	48	0.98	AT2G38920.3	intronic				
	2	10799205	G/A	58	0.97	AT2G25350.1	CDS		874	Nonsyn	G/R
	2	15611170	G/A	56	0.97	AT2G37160.1	intronic				
	2	15611170	G/A	56	0.97	AT2G37160.2	intronic				
	2	16714811	G/A	34	0.97	AT2G40030.1	intronic				
	2	12752257	G/A	59	0.95	AT2G29910.1	CDS		574	Nonsyn	P/S
	2	12752257	G/A	59	0.95	AT2G29910.2	CDS		574	Nonsyn	P/S
	2	12756385	G/A	67	0.94	AT2G29930.1	3' UTR				
	2	12756385	G/A	67	0.94	AT2G29930.2	3' UTR				
	2	12756385	G/A	67	0.94	AT2G29930.3	3' UTR				
	2	16085982	G/A	61	0.94	AT2G38400.2	intronic	AGT3			
	2	16085982	G/A	61	0.94	AT2G38400.1	3' UTR	AGT3			
	2	11524742	G/A	65	0.93	AT2G27000.1	CDS	CYP705A8	354	Syn	L/L
	2	15874555	G/A	77	0.93	AT2G37930.1	CDS		1189	Nonsyn	V/M
	2	16183215	G/A	54	0.93	AT2G38700.1	intronic	MDD1			
	2	17322316	G/A	53	0.93	AT2G41520.1	CDS		3075	Syn	K/K
	2	17322316	G/A	53	0.93	AT2G41520.2	CDS		2982	Syn	K/K
	2	9449356	G/A	60	0.92	AT2G22210.1	intronic				
	2	14915576	G/A	48	0.92	AT2G35500.1	CDS	SKL2	919	Nonsyn	E/K
	2	10172099	G/A	69	0.91	AT2G23890.1	CDS		935	Nonsyn	G/D
	2	10840584	G/A	74	0.91	AT2G25470.1	CDS		1511	Nonsyn	G/E
	2	12666921	G/A	62	0.91	AT2G29628.1	CDS		37	Nonsyn	L/F
	2	9638463	G/A	58	0.89	AT2G22670.1	3' UTR				
	2	9638463	G/A	58	0.89	AT2G22670.2	3' UTR				
	2	9638463	G/A	58	0.89	AT2G22670.3	3' UTR				
	2	9638463	G/A	58	0.89	AT2G22670.4	3' UTR				
	2	8927473	G/A	64	0.88	AT2G20710.1	CDS		1224	Nonsyn	W/*
	2	8927473	G/A	64	0.88	AT2G20710.2	CDS		939	Nonsyn	W/*
	2	16008356	G/A	39	0.87	AT2G38220.1	CDS		159	Syn	S/S
	2	9172865	G/A	53	0.84	AT2G21430.1	CDS		437	Nonsyn	P/L
	2	17539103	G/A	51	0.82	AT2G42030.1	CDS	MUSE2	1244	Nonsyn	S/F
	2	10840584	G/A	74	0.91	AT2G25470.1	CDS		1511	Nonsyn	G/E

SNPs identified through NGS of pooled remaining M2 families. Stating the chromosome on which the mutation was found (Chr.), the position of the mutation, the reference base (Ref.), the altered base (Alt.), the coverage (Cover), the frequency of that allele (Allele freq.), the Gene ID annotated from Tair10, the common gene name (GENE), the region within the gene, the position within the coding sequence (CDS position), the effect induced by the mutation, and the amino acid resulting from the mutation (AA change). Font with underline indicates gene that had a mutation identified in all three of the M2 families. SNPs having an allele frequency below 0.8 were not listed.

Table 3.8. Allele frequencies of SNPs induced via EMS in M2 families 2133, 3182, 3594, and 3761.

Family	Chr.	Position	Ref/Alt	Cover	Allele freq	Gene ID	Region	GENE	CDS position	Effect	AA change
2133	1	15778420	C/T	39	0.89	AT1G42260.1	intronic				
	1	10741044	C/T	54	0.87	AT1G30410.1	intronic				
	1	13195857	C/T	60	0.87	AT1G35660.1	CDS		2509	Nonsyn	L/F
	1	17712552	C/T	66	0.87	AT1G48010.1	CDS		109	Nonsyn	E/K
	1	19462184	C/T	64	0.85	AT1G52260.1	CDS	PDI3	1048	Nonsyn	L/F
	1	20556671	C/T	80	0.85	AT1G55090.1	CDS		1205	Nonsyn	P/L
	1	16199808	C/T	67	0.83	AT1G43060.1	intronic				
	1	20351493	C/T	46	0.82	**AT1G54490.1**	CDS	XRN4	355	Nonsyn	R/C
	1	9023556	C/T	63	0.8	AT1G26100.1	CDS		302	Nonsyn	G/E
	1	13632003	C/T	47	0.8	AT1G36270.1	intronic				
3182	1	20352703	G/A	70	1	**AT1G54490.1**	CDS	XRN4	1019	Nonsyn	G/D
	1	21401287	G/A	55	1	AT1G57777.1	3' UTR	ECA1			
	1	22691794	G/A	80	0.94	AT1G61500.1	CDS		1088	Nonsyn	S/F
	1	17434311	G/A	70	0.9	AT1G47500.1	CDS		1125	Nonsyn	W/*
	1	17326582	G/A	61	0.84	AT1G47270.1	5' UTR				
	1	17326582	G/A	61	0.84	AT1G47270.2	intronic				
	1	13563159	G/A	66	0.81	AT1G36185.1	intronic				
	1	15157297	G/A	51	0.81	AT1G40109.1	intronic				
3594	3	4066848	G/A	56	1	AT3G12810.1	Splice site	PIE1	3	4066848	G/A
3761	3	4068919	C/T	57	1	AT3G12810.1	CDS	PIE1	1693	Nonsyn	L/F
	3	4926072	C/T	50	1	AT3G14660.1	CDS		779	Nonsyn	A/V
	3	3660560	C/T	66	0.99	AT3G11590.1	intronic				
	3	3457948	C/T	36	0.97	AT3G11030.1	CDS	TBL32	972	Syn	K/K
	3	9652727	G/A	48	0.83	AT3G26340.1	intronic				
	3	233844	C/T	43	0.81	AT3G01610.1	intronic	EMB1354			

SNPs identified through NGS of pooled remaining M2 families. Stating the chromosome on which the mutation was found (Chr.), the position of the mutation, the reference base (Ref.), the altered base (Alt.), the coverage (Cover), the frequency of that allele (Allele freq.), the Gene ID annotated from Tair10, the common gene name (GENE), the region within the gene, the position within the coding sequence (CDS position), the effect induced by the mutation, and the amino acid resulting from the mutation (AA change). Font with underline indicates gene that had a mutation identified in all three of the M2 families. SNPs having an allele frequency below 0.8 were not listed.

Numerous mutations were found within the genomic regions with an increase in allele frequency of these remaining six families, which can be seen in Table 3.7 and Table 3.8. The same stringent parameters used in Table 3.6. were used in Table 3.7 and Table 3.8. Notably, there are two families within these six families that have non-synonymous mutations within *At1g54490*, at a very high allele frequency. In total, out of these 11 families that were sent for sequencing, five had independent non-synonymous mutations within the gene *At1g54490* (Figure 3.40), with an allele frequency ranging from 0.83 to 1.0. Both new mutations in M2 families 2133 and 3182 in the second round of sequencing were both found to be located in similar locations to that of the previous mutations found in M2 families 450 and 383.

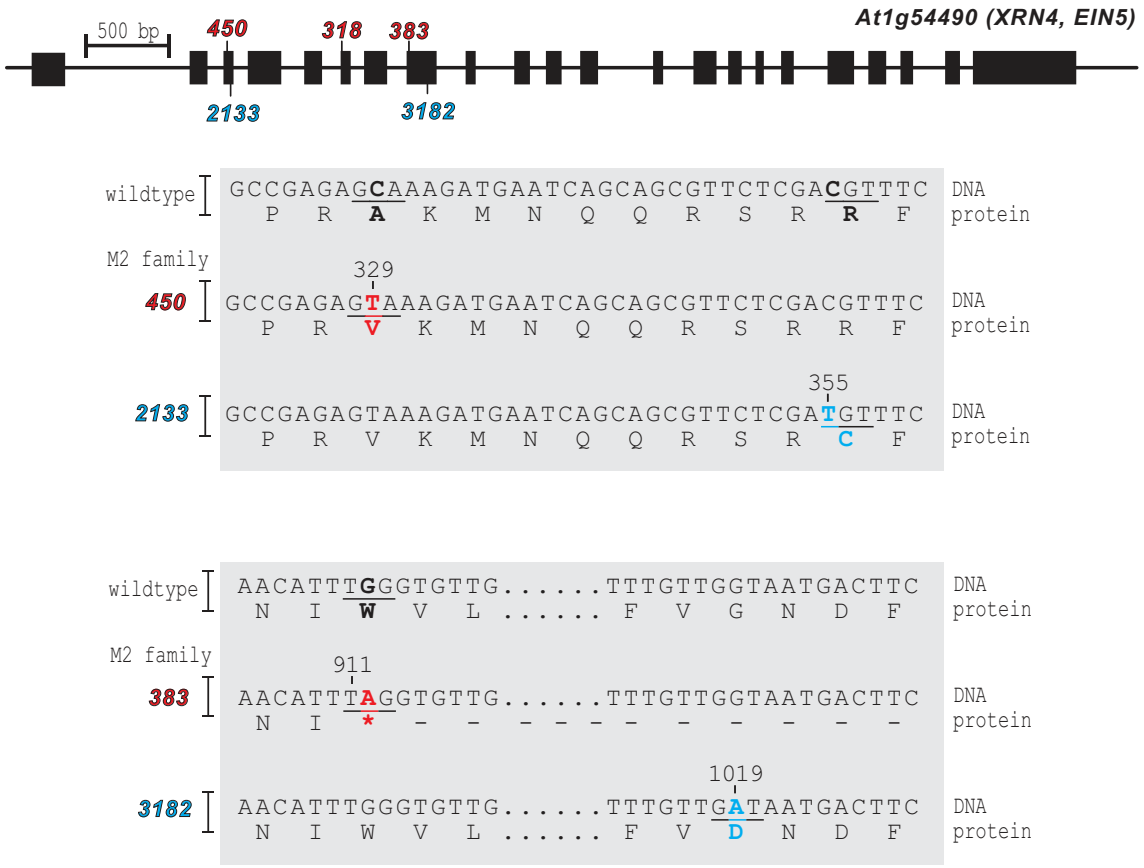

FIGURE 3.40. Five distinct mutations found in *At1g54490*.

Gene schematic of EMS-induced mutations of M2 families 318, 383, 450, 2133, and 3182 within *At1g54490*. Black boxes indicate exons and black lines in between indicate introns. In the lower panel, bold font indicates a change in base pair or amino acid, black bold font represents the wildtype, and red bold font indicates mutation made by EMS in the first round of sequencing, blue bold font indicates mutations made by EMS in the second round of sequencing.

While there were two families that contained non-synonymous mutations within *At1g54490*, there were four families that had genomic sections with an increased allele frequency that were not located within chromosome one. Notably, family 1812 had several non-synonymous mutations within the coding regions of annotated genes, and those might be interesting to look at in the future as potential additional suppressors of *CpBs4C* growth arrest.

Therefore, with all the aforementioned data, it is clear that the M2 mapping technique is efficient in identifying causal alleles in an Arabidopsis EMS screen, saving a large amount of time from the initiation of the screen (EMS mutagenesis of seeds) to the identification of causal allele (NGS sequencing). It is also evident that *XRN4* is a downstream signalling component of CpBs4C-mediated growth arrest in Arabidopsis, and that when *XRN4* is mutated, CpBs4C growth arrest is inhibited.

4. DISCUSSION

4.1. The native function of *CpBs4C* utilises calcium and likely lies outside resistance to *Xanthomonas*

There is great diversity among executor R proteins from different species both in subcellular localisation and predicted function after their activation (Römer et al., 2007; Strauß et al., 2012; Wang et al., 2015; Wang et al., 2017, 2018). We wanted to characterise the molecular function of CpBs4C-induced cell death and to also see how many other CpBs4C homologues there are in other species and if these similar proteins also elicited a cell death reaction.

4.1.1. Homologues of *CpBs4C* were found in other Solanaceous species

After a comprehensive search, we found multiple potential homologues of CpBs4C (Table 3.1). The homologues we moved forward with due to experimental accessibility had a wide range of amino acid per cent similarities between homologues (Figure 3.1). Looking both between species and within species, it was evident that the per cent similarity within a species is higher than the per cent similarity between species. For example, within the *Capsicum annuum* homologues, the per cent similarity ranges from 54.76% to 82.14%. The highest similarity between the homologues from *Capsicum pubescens, C. annuum*, *Solanum lycopersicum*, and *Nicotiana benthamiana* was between NbBs4C.2 and NbBs4C.3, with a similarity of 89.63% at the amino acid level. The high similarity between homologues in a species could suggest that they evolved by duplication within a given species and therefore could be paralogues of one another. In support of this, *S. lycopersicum* has only one potential homologue identified. It could be possible that the emergence of multiple *Bs4C* genes in other species resulted from gene duplications, creating multiple copies of *Bs4C* in other species, like *C. annuum*, and *N. benthamiana*. Hereafter, *Bs4C* homologues within the same species will be referred to as paralogues.

None of the Bs4C homologues identified have been annotated within their genome or found in the publicly available plant transcriptome database (Carpenter et al., 2019). It would be understandable if the cell death-inducing homologues could not be found in these transcriptomic databases, seeing that they initiate a cell death reaction as soon as they are expressed. However, even the transcripts of the non-cell death-inducing homologues could not be found. This lack of transcript discovery could indicate that the Bs4C homologues are

expressed extremely tightly, both spatially and temporally. Taking together the absence of annotation combined with the indication of tight spatiotemporal control is most likely why no Bs4C homologue transcript has been identified, besides *CpBs4C*.

The only reason that *CpBs4C* was identified in the first place as a functional gene was that it was activated by AvrBs4 in *C. pubescens* accession PI235047, which contains a *Bs4C*-allele preceded by an AvrBs4-compatible effector binding element (*EBE*), in an artificial environment (Sahin & Miller, 1998; Strauß et al., 2012). *C. pubescens* was initially found only in the highlands of Central and South America, having an average altitude of 2780 m with an average temperature of 12 ^{o}C, while other *Xanthomonas* host *Capsicum* species, like *C. annuum*, were initially found between 0 – 300 m of altitude, and grow in temperatures ranging from 21 – 27 ^{o}C (De Swart et al., 2006). While typical *Capsicum* species are cold-sensitive, *C. pubescens* seems cold-adapted. Moreover, *Xanthomonas* grows optimally between 25 – 30 ^{o}C, and the optimal *Xanthomonas* growth temperature range does not overlap with the optimal growth temperature of *C. pubescens* (Esgalhado et al., 1995). Therefore, building off the hypothesis from Nowack et al., 2022, it seems unlikely that the typical evolutionary arms race between bacteria and its host could be at play here. The notion is therefore raised that the only AvrBs4-compatible *Bs4C* allele was found in a pepper species that is likely not infected by *Xanthomonas*. Ultimately, this is inconsistent with the assumption that TALE-recognising alleles are a consequence of evolutionary pressure, and that the native function of *CpBs4C* lies outside of resistance to *Xanthomonas.*

This notion can further be supported by the fact that two different *C. pubescens* accessions PI 235047 and PI 585270 each have a *Bs4C* gene, with nearly identical coding sequences, *Bs4C-R* and *Bs4C-S* respectively, with only *Bs4C-R* being AvrBs4 inducible (Strauß et al., 2012). Bs4C-R and Bs4C-S both induce cell death when ectopically expressed under the control of a *35S* promoter. The 1 kb upstream sequences of *Bs4C-R* and *Bs4C-S* are also highly similar, however, *Bs4C-R* has a two base-pair alteration within the AvrBs4 *EBE* that is absent in the *Bs4C-S* upstream sequence, which allows for the activation of the downstream *Bs4C-R* in presence of AvrBs4, and the absence of activation of *Bs4C-S* in the presence of AvrBs4. It is therefore conceivable that the AvrBs4 compatible *EBE* in the 1 kb upstream region of *Bs4C-R* is there by chance and that these genes are acting in a different context. Additionally, some of the species identified to have a *CpBs4C* homologue are not native hosts to *Xanthomonas*, like, for example, *N. benthamiana*. We only use the *Xanthomonas – N. benthamiana* pathosystem as a proxy to study the function of *NbBs4C* gene's impact on bacterial growth in a non-host resistance context. Taken together, it therefore seems likely that the native function of *Bs4C* homologues lies outside resistance to *Xanthomonas.*

It would be both unlikely and energetically taxing for plants to have genes that are not beneficial, especially such genes that can cause very severe damage in the context of cell death if upstream mutations cause leaky expression. All these points lead towards the assumption that there is a native function of these genes; it just has yet to be identified.

4.1.2. Tomato *Bs4C* might be involved in developmental processes

The tight transcriptional regulation of *Bs4C* transcripts combined with the rapid cell death initiation both have similarities to other pathways that utilise cell death, and more specifically programmed cell death (PCD). The processes that use PCD are primarily development and biotic and abiotic stress responses (Williams & Dickman, 2008). Developmental PCD (dPCD) typically occurs in cells with vital organs, for example, root cap cells, which protect the root apical meristem during root growth and germination, vasculature where dPCD aids in cell elongation and helps with water transportation, and abscission where tightly controlled cell death is responsible for the shedding of organs, such as leaves, flowers, and ripe fruits (Daneva et al., 2016).

Seeing as there was no indication from the publicly available plant transcriptome database where and when *Bs4C* homologue transcripts might be present due to non-existent annotation, we sought out collaborators to check raw RNA-seq datasets. Collaborators had completed extensive RNA-seq experiments to try and get a whole transcriptomic profile of the entire tomato fruit at all stages of development (Shinozaki et al., 2018). There was only one identified *Bs4C* homologue from *S. lycopersicum*, *SlBs4C*, which narrowed down the search for transcript presence. It was found that *SlBs4C* transcripts were elevated during the earlier stages of fruit ripening, during mature green and breaker stages, specifically in the stem/top part of the fruit in the total pericarp, the septum, and the columella tissues (Figure 3.29). The part of the fruit where the *SlBs4C* transcripts were identified is a location within the fruit that does indeed undergo dPCD. The pericarp/columella is a section of the fruit where cell death occurs to prepare the fruit to fall away from the stem so that the two regions can separate (Daneva et al., 2016). This cell death process becomes more evident as the tomato ripens, going into the red ripe stage, and when the fruit and the stem disassociate, the stem of the columella leaves what is called a stem scar, a healing process which is regulated by abscisic acid (ABA) (Leide et al., 2012). As of yet, there has been no indication of a connection between Bs4C function and ABA signalling, however, it would be easy to check if ABA signalling is induced upon Bs4C expression, by checking for transcript levels of ABA-responsive genes. Furthermore, it would be relatively simple to corroborate if *SlBs4C* is indeed transcribed at the

mature green and breaker stages of tomato development in the pericarp, septum, and columella of the stem end of the fruit by collecting this tissue at these specific stages and checking transcript level.

As mentioned in section 3.1.1, we were unable to express SlBs4C ectopically *in planta*, so we are unable to definitively comment on whether or not SlBs4C induces cell death. However, looking at Figure 3.1, the highest % identity that SlBs4C has to any of the other Bs4C homologues, is to CpBs4C (34.48%) and NbBs4C.1 (46.24%), both of which induce a strong cell death reaction. To definitively test if SlBs4C causes cell death, we could activate the *SlBs4C* gene endogenously, as was done for the *NbBs4C* homologues in Figure 3.6, by designing a dTALE to bind upstream of the *SlBs4C* gene and activate it (Morbitzer et al., 2010). However, *S. lycopersicum* has a nucleotide-binding domain leucine-rich repeat (NLR) resistance gene, *Bs4*, which can sense the repeat region of TALEs, and subsequently activate a cell death response, hindering any result we might have (Schornack et al., 2004). Therefore, a previous PhD student in the lab, Dr. Kyrylo Schenstnyi, generated a *bs4* knockout tomato plant so that TALE-mediated studies could be conducted in *S. lycopersicum* (Schenstnyi et al., 2022). Using this *bs4* knockout plant, infiltrating the dTALE targeting *SlBs4C* would quickly tell us whether the activation of the gene induces a cell death response. Taking further inspiration from Dr. K. Schenstnyi's *bs4* knockout tomato plants, a definitive way to see if *SlBs4C* is involved in fruit development would be to knock out the *SlBs4C* coding sequence. Once this gene is knocked out, one could phenotype the fruit at the mature green or breaker stage and see if there are any visible developmental defects on the pericarp/septum/columella at the stem end of the fruit.

Working under the assumption that all Bs4C cell death-inducing homologues work in a similar fashion, then it could be possible that we could see a developmental defect in a plant that has multiple Bs4C homologues knocked out. However, as mentioned in section 3.1.3, there were no obvious developmental phenotypes observed in the *ΔNbBs4C.1-3* triple *nbbs4c* knockout mutant, although only the above-ground tissue was analysed. It could perhaps be that *ΔNbBs4C.1-3* has a phenotype that cannot be seen with the naked eye. The raw tomato RNA-seq finding in Figure 3.29 is the only indication of where *Bs4C* transcripts might be acting. While these transcripts could also be found in the reproductive organs of *N. benthamiana*, they could additionally be found in organs that we have not analysed yet, for example the roots, or at a particular developmental stage that has yet to be examined. Therefore, fusing the *NbBs4Cs* 5' upstream sequence to the RUBY reporter (He et al., 2020) would be an excellent solution for identifying specifically where and when each *NbBs4C* paralogue is transcribed. Taking *ΔNbBs4C.1-3* and performing individual transformations of each of the

NbBs4C paralogue upstream sequences driving RUBY expression would make it possible to potentially see where and when each of these genes are individually expressed. Specifically for *N. benthamiana*, with the *SlBs4C* transcriptomic data in mind, it would be wise to inspect the seed pod region, perhaps while it is still green and not yet turned brown, as this is the most parallel developmental organ and stage between *N. benthamiana* and *S. lycopersicum*. Taken together, it is plausible that *SlBs4C* is somehow involved in fruit development, and that the location of expression of the other *Bs4C* homologues could potentially be identified using stable reporter lines.

4.1.3. Bs4C could have evolved from a bacterial ancestor

CpBs4C is a short gene that lacks introns. Similarly, all homologues identified do not have any obvious intron-containing regions. Lacking introns is a hallmark characteristic of prokaryotic genes, mainly due to the fact that both transcription and translation are coupled in prokaryotic gene expression (Irastortza-Olaziregi & Amster-Choder, 2020), unlike the separate transcription and translation in eukaryotes, which can be differentially controlled on each level. While intronless genes can be found in eukaryotes, they comprise a much smaller proportion of genes when compared to intron-containing genes. For example, intronless genes only comprise 19.9% and 21.7% of rice and *Arabidopsis thaliana* (Arabidopsis hereafter) genomes, respectively (Jain et al., 2008). The majority of intron-less or intron-poor genes found within plant genomes are typically genes that need to be translated into proteins relatively quickly, requiring little to no splicing. For example, *AP2* genes, which partake in broad developmental changes of both reproductive and vegetative organs due to stresses, like drought and salt stress (Liu et al., 2021). *CpBs4C* after its activation induces cell death at a rather rapid speed compared to the other *Capsicum* executor *Bs3*, which has two introns (visible cell death of *CpBs4C* can start around 12 hpi of *Xanthomonas*, but *Bs3* cell death starts after 20 hpi of *Xanthomonas* (Römer et al., 2007; Strauß et al., 2012)). Perhaps lacking an intron might aid in the speed at which *CpBs4C* induces cell death. The problem also arises that if the *CpBs4C* promoter is somehow leaky or being activated inappropriately, this would be detrimental to the plant, as a cell death-inducing gene is activated and does not have an additional level of control to subdue any negative impact. It is possible that the energetic toll and potential risk that lacking an intron has on plants containing *CpBs4C* is overshadowed by the rapid response that CpBs4C undertakes. The benefits of being able to act more quickly without the secondary level of regulation outweigh the risks of having a cell death-inducing gene be potentially leaky, and speed could be a vital component of the yet-to-be-elucidated native function of *CpBs4C*.

CpBs4C has strong structural homology to the $GABA_A$ receptor, nicotinic receptor, and serotonin receptor, as seen in Figure 3.13, specifically in the transmembrane domains. These neurotransmitter receptors belong to the large superfamily of pentameric ligand-gated ion channels, or pLGICs. pGLICs are composed of five different subunits encircling a central pore that is selectively permeable to either cations or anions depending on the receptor. Using the $GABA_A$ receptor as inspiration, we also found that CpBs4C could form a putative pentamer resembling the $GABA_A$ receptor pentameric structure *in silico* (Figure 3.14). Furthermore, we showed that CpBs4C can associate with itself (Figure 3.15 and Figure 3.17), and it can form a higher-order complex (Figure 3.16 and Figure 4.2). However, while CpBs4C is structurally very similar to the transmembrane domains of the $GABA_A$ subunits, the $GABA_A$ receptor localises to the plasma membrane (PM) of the cell (Glykys & Mody, 2007), while CpBs4C and its homologues localise to the endoplasmic reticulum (ER). One interesting thing worth noting is that when the $GABA_A$ subunits homodimerize, they are stuck in the ER (Connolly et al., 1996), which is reminiscent of CpBs4C forming a complex and staying within the ER. We also see the GABA chimeras, where the CpBs4C, NbBs4C.1, and NbBs4C.2 C-terminal tails are fused to the transmembrane domain regions of the $GABA_A$ receptor subunit α, are also localised to the ER (Figure 3.28). An interesting follow-up experiment to this observation would be to perform coIP analysis on the GABA chimeras to see if they self-associate when expressed in *N. benthamiana*. Furthermore, it might be interesting to see if CpBs4C can associate with the GABA chimeras, which would show whether or not it is truly the structure of the transmembrane regions of CpBs4C that are associating with the other Bs4C homologues. The original idea behind generating the GABA-Bs4C chimeras was to see if the $GABA_A$ subunit α, which has the closest homology to CpBs4C, was able to induce cell death in *N. benthamiana* when overexpressed. However, we ultimately found that none of the GABA-Bs4C chimeras induced cell death (Figure 3.27), but perhaps co-expressing all of the different $GABA_A$ subunits might result in a cell death phenotype, or even a different subcellular localisation. If all the $GABA_A$ subunits were to be present, then perhaps the complex could localise to the PM and become functional, however, that is purely speculative at this point.

Another point linking Bs4C homologues and neurotransmitter receptors is that in a family of receptor subunits, say for example the $GABA_A$ receptors, there is ~70% sequence identity between the different subunits of each family, and between members of the different families there is anywhere between ~20-50% identity (Olsen & Tobin, 1990). We see a similar pattern between the Bs4C homologues (Figure 3.1). Between the NbBs4C paralogues, we see up to an 89.63% amino acid similarity, specifically between NbBs4C.2 and NbBs4C.3 (Figure 3.1). Furthermore, between the CaBs4C paralogues, in addition to all of the homologues found in the *C. annuum*, *C. pubescens*, *C. baccatum*, and *C. chinense*, we see anywhere from 48.15%

similarity to 78.53% similarity (Figure 3.1, Supplementary Table 6.4). The two lowest % similarities that we see between the homologues from *C. pubescens*, *N. benthamiana, S. lycopersicum*, and *C. annuum* is 21.35% identity between CaBs4C.1 and NbBs4C.2, and 21.58% identity between CpBs4C and NbBs4C.2. Seeing as NbBs4C.2 is coming from a different species than either CpBs4C and CaBs4C.1, it is reminiscent to the lower range of % identity between different neurotransmitter receptor families.

In a review article from 1995, Ortells and Lunt outlined their perspective on how pentameric ligand-gated ion channels likely evolved. Their most notable speculations were that the ancestor of pLGICs was probably homo-oligomeric, that the transmembrane region and the extracellular region probably evolved independently and then came together, and that the transmembrane region of pLGICs is most likely derived from a toxin-like related protein (Ortells & Lunt, 1995). These speculations conveniently align with the structural and functional characteristics of CpBs4C. We have shown that CpBs4C can form homo-oligomers, as seen in Figure 3.15 and 3.17, we show that CpBs4C has only structural homology to the transmembrane domains of the neurotransmitter receptors and not the extracellular domain, as seen in Figure 3.13, and also that CpBs4C is a protein that induces cell death, or as Ortells and Lunt put it, a “toxin-like related protein”, which can be seen in Figure 3.4 and in Strauß et al. 2012. Furthermore, there are many similarities between Bs4C homologues and neurotransmitter receptors, which makes the idea of Bs4C homologues evolving from a common ancestor conceivable. CpBs4C’s striking structural homology both to the single subunit α of the $GABA_A$ receptor and also as a putative pentameric ring compared to the $GABA_A$ receptor (Figure 3.13 and Figure 3.14), CpBs4C can form a higher-order complex as can neurotransmitter receptors (Figure 3.16), the Bs4C homologues can both homo- and hetero-associate (Figure 3.17 and Figure 3.18) similarly to the $GABA_A$ receptor, and they both use ions to execute their intended function, with CpBs4C likely using calcium (Ca^{2+} hereafter) (Figure 3.21), $GABA_A$ receptor using Cl^- (Kaila et al., 1989), and both nicotinic and serotonin receptors being permeable to Na^+, K^+, and sometimes Ca^{2+} (Changeux & Paas, 2009; Wu et al., 2015).

While we did not see the single $GABA_A$ receptor subunit α chimera induce cell death in *N. benthamiana*, it would be interesting to reciprocally test if CpBs4C could induce cell death both in HeLa cells, as well as in bacterial cells. While bacteria do not contain an ER, and the ultimate localisation of CpBs4C when expressed in bacteria is unknown, it would be interesting if it could induce cell death in bacteria. If it does indeed induce cell death in both bacteria and HeLa cells, then the mechanism with which CpBs4C induces cell death would be conserved all the way from bacteria to metazoans. However, the obvious point that bacteria do not

contain an ER is probable enough to speculate that CpBs4C would indeed not induce cell death in bacterial cells.

Along this line, CpBs4C structural homologues were found in bacterial species, specifically the Hha toxicity modulator TomB from *E. coli*, and the biofilm regulatory protein BssR from *K. pneumoniae* (Figure 3.30), supporting the notion that Bs4C homologues could have evolved from an earlier ancestor. This finding also supports the Ortells and Lunt 1995 hypothesis that the transmembrane domains of the neurotransmitter receptors evolved from a toxin-like related protein. In their 1995 review, Ortells and Lunt elaborate on the original observation in Unwin, 1993 that the transmembrane region of pLGICs looks similar to the two bacterial toxins heat-labile enterotoxin and verotoxin. The structures of enterotoxin and verotoxin from *E. coli* are now available due to the unveiling of the mass number of protein structures (Lin et al., 2022), and with a crude comparison, one can see that the structure of both enterotoxin (PDB#: A0A854AC01) and verotoxin (PDB#: A0A141AZM3) look nothing like the structure of CpBs4C (Supplementary Information S6). While the specific bacterial toxins that were observed in 1993 by Unwin do not have any close structural homology to CpBs4C, the hypothesis by Ortells and Lunt in 1995 is still supported by our finding of CpBs4C having structural homology to the bacterial proteins TomB and BssR (Figure 3.30).

One could speculate on the role of TomB in the toxin-antitoxin system within bacteria (Marimon et al., 2016) or the biofilm regulatory role of BssR (Domka et al., 2006) and how each could have evolved into a toxic compound in plants. However, further investigation into BssR revealed that BssR and to an extent CpBs4C, actually have slight structural similarity to the *Xanthomonas campestris pv. campestris* protein Xcc0516. Xcc0516 is a cytosolic protein that assembles into a homomeric pentamer that forms a central channel (Lin et al., 2006). There is not much known about the function of Xcc0516 and what it does, aside from its predicted localisation in the cytosol, therefore it would be interesting to see if this pentameric structure does indeed form a channel of some sort. The similarities between the CpBs4C predicted pentamer and the pentameric Xcc0516 are not spectacular, however, they do indicate a structurally similar bacterial protein that forms a homomeric pentamer. This pentameric ring structure not only aligns with CpBs4C, but also resembles the pentameric ring structure of the neurotransmitter receptors, ultimately supporting Ortells and Lunt's 1995 hypothesis of a bacterial protein being the ancestor of neurotransmitter receptor transmembrane domains.

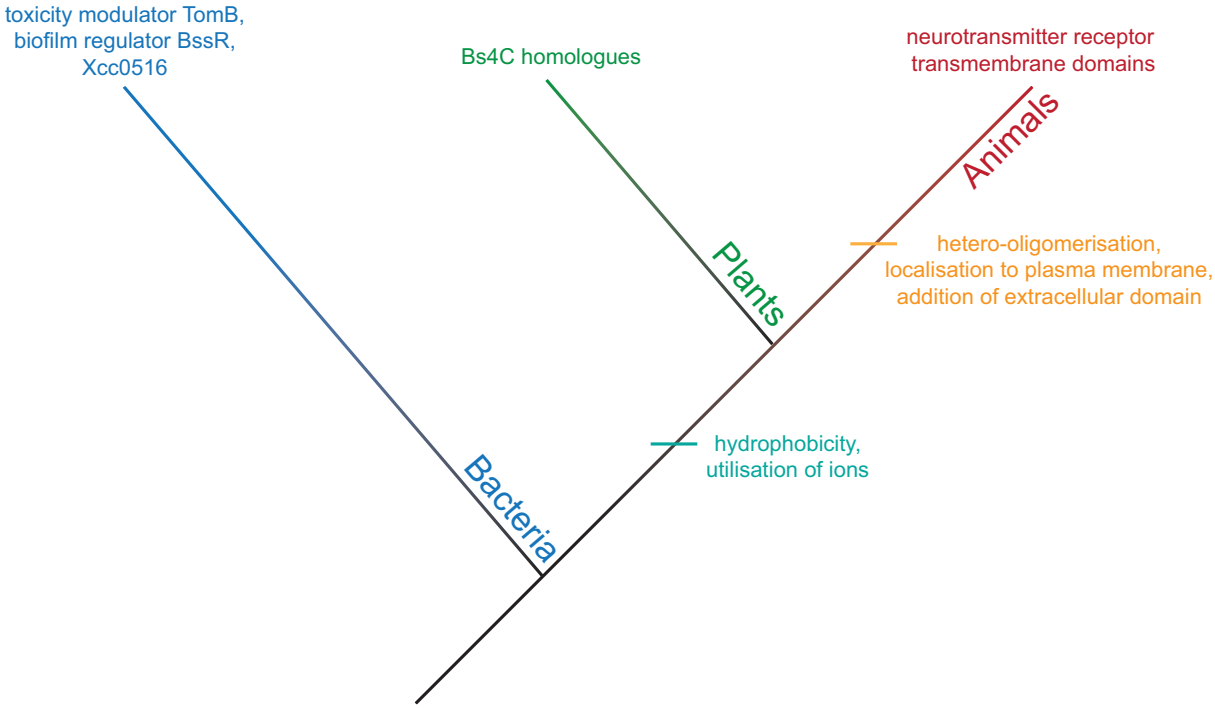

FIGURE 4.1. Bs4C homologues and neurotransmitter receptors could share a common bacterial ancestor.

Generation of a hypothetical phylogenetic tree whereby the bacterial proteins gained hydrophobicity and the utilisation of ions to differentiate into Bs4C homologues in plants, and then further distinguish themselves into neurotransmitter receptor transmembrane domains by gaining hetero-oligomerization capabilities, localising to the plasma membrane and the addition of the extracellular ligand binding domain.

Therefore, with CpBs4C and neurotransmitter receptors sharing so many traits and the resemblance of the bacterial pentameric formation, it seems possible that Bs4C homologues and neurotransmitter receptors have a common ancestor. It is entirely possible that this bacterial protein (1) gained the ability to form a pentameric structure, with the evidence of the Xcc0516. Then (2) differentiated and gained hydrophobicity, as Xcc0516 is localised to the cytoplasm and TomB and Bssr have no predicted membrane domains and the Bs4C homologues localise to the ER membrane. Subsequently (3) started utilising ions for activity, which is what we see in plants as CpBs4C utilises the movement of Ca^{2+} to induce cell death (Figure 3.21), and (4) further started to hetero-oligomerise and locate to the PM, which is what we see in metazoans as neurotransmitter receptor transmembrane domains (Figure 4.1). Taken together, it seems reasonable to speculate that the Bs4C homologues and neurotransmitters could have evolved from a common bacterial ancestor.

4.1.4. Non-cell death-inducing *Bs4C* homologues have an elusive function

While we only found NbBs4C.1 to induce cell death and reduce photosynthetic capacity when ectopically expressed (Figure 3.4), we saw that all three *NbBs4C* paralogues impacted bacterial growth (Figure 3.8). We initially hypothesised that the dTALE activating *NbBs4C.1* would be the only gene out of the *N. benthamiana* paralogues to impact bacterial growth, seeing as it had such a dramatic cell death phenotype and photosynthetic reduction when activated by a dTALE (Figure 3.6). While we did see that the activation of *NbBs4C.*1 during bacterial growth consistently had the most dramatic reduction of bacterial growth, we also found that the activation of *NbBs4C.2* and *NbBs4C.3* had a significant impact on bacterial growth (Figure 3.8). The *Xanthomonas* strain activating *NbBs4C.2* and *NbBs4C.3* significantly reduced growth over six days compared to the empty vector strain. This finding means that the cell death phenotype and photosynthetic measurements showing that NbBs4C.2 and NbBs4C.3 had a similar phenotype to AvrBs4 or non-infiltrated samples, is not an entirely accurate picture. Figure 3.6 shows that solely in the context of cell death and photosynthetic capacity, *NbBs4C.2* and *NbBs4C.3* do not have a phenotype. While this is true, it is not the entire story of what these non-cell death-inducing paralogues are doing within the cell, and that *NbBs4C.2* and *NbBs4C.3* are indeed doing something, and whatever their mechanism(s) might be, it seems to have an impact on bacterial proliferation and makes the cell somewhat unfavourable for bacteria.

The idea that *NbBs4C.2* and *NbBs4C.3* have a yet-to-be-determined function is further confirmed in the bacterial growth analysis when comparing the WT *N. benthamiana* to the *nbbs4c* triple knockout mutant, *ΔNbBs4C.1-3*. In every bacterial strain using a dTALE to activate an *NbBs4C* paralogue, the bacterial growth is increased in *ΔNbBs4C.1-3,* and in the case of dT779 and dT780 in *ΔNbBs4C.1-3* (the dTALEs activating *nbbs4c.1* and *nbbs4c.2*, respectively), it is higher than empty vector levels (Figure 3.11). Ultimately this confirms that these genes can independently impact bacterial growth, and they do not need to be acting in concert with one another, which is proven by their lack of dTALE cross-activation (Figure 3.10). It would be worthwhile to test if there is an additive effect on bacterial growth if the *NbBs4C* paralogues were activated together, as it could indicate if these genes might be working together. We know that when *NbBs4C.1* is activated with either *NbBs4C.2* or *NbBs4C.3,* there is a cell death reaction, and when *NbBs4C.2* and *NbBs4C.3* are activated together, there is no cell death reaction (Figure 3.19). However, it would be interesting to test if activating *NbBs4C.1* with *NbBs4C.2* or *NbBs4C.3* during bacterial growth would cause a similarly dramatic reduction in bacterial growth to that of *NbBs4C.1*, if it would have a reduction in growth similar to the level of *NbBs4C.2* or *NbBs4C.3*, or if it would have a bacterial growth

reduction greater than the level of *NbBs4C.1*. Furthermore, if strains activating *NbBs4C.2* and *NbBs4C.3* were to be co-infiltrated, would this have an additive effect and cause the bacterial growth to be reduced greater than *NbBs4C.2* or *NbBs4C.3* individually, or would the bacterial growth be similar to the reduction when *NbBs4C.2* and *NbBs4C.3* are activated individually? It is conceivable that an additive effect would be the result of co-activating *NbBs4C.2* and *NbBs4C.3* because the transcript levels of these two genes are significantly higher when the dTALEs are co-expressed, rather than expressed individually (Figure 3.19B).

Therefore, it is safe to assume that while *NbBs4C.2* and *NbBs4C.3* do not have a direct role in visible cell death or harming the cell so much to the point of limiting photosynthetic capacity, they do somehow make the plants challenging for the bacteria to proliferate. Ultimately, this means that all paralogues of *Bs4C* in *N. benthamiana* have a function, it just has yet to be elucidated.

4.1.5. Different cell death phenotypes are a result of the different amino acid composition within the N-terminal body

When the protein structures of all the chosen homologues were predicted and compared, it was shown that they all had a similar core structure, and the C-terminal tail of each homologue varied (Figure 3.3). While all the homologues had the same core structure, they had two different classes of phenotypes, cell death-inducing and non-cell death-inducing. Specifically for the homologues from *N. benthamiana* where the paralogue with the closest per cent identity between *N. benthamiana* and CpBs4C was NbBs4C.1, which when overexpressed ectopically, had a similar cell death phenotype, and a similar reduction in photosynthetic ability compared to an uninfiltrated sample (Figure 3.4). The other two paralogues, NbBs4C.2 and NbBs4C.3, when ectopically overexpressed, had no cell death phenotype and had no reduction in photosynthetic ability when compared to an uninfiltrated sample. This was interesting because these were the proteins that had such a strikingly similar core structure but had a vastly diverse phenotype.

When looking more closely at the structures of each of the proteins, their C-terminal tail was very different, which is what initially caused some issues in the comparison of all homologues (Figure 3.2). The initial hypothesis was that the different C-terminal tails were likely to be the deciding factor in whether a homologue induced cell death or not because it was the only part of the proteins that were structurally different from one another. After first determining that the C-terminal tail is needed for adequate protein accumulation (Figure 3.23), we generated

chimeras with NbBs4C.1 and NbBs4C.2 to swap the C-terminal tail to determine if the C-terminal tail conferred cell death. Surprisingly, it was actually the amino acid composition of the conserved N-terminal body of NbBs4C.1 that conferred cell death, and not the C-terminal tail (Figure 3.24). It would be worthwhile to confirm the hypothesis that the N-terminal body of a cell death-inducing Bs4C homologue is what actually confers cell death, and not the C-terminal tail, by generating additional chimeras of cell death-inducing and non-cell death-inducing homologues. For example, generating a chimera with the N-terminal body of CpBs4C and the C-terminal tail of NbBs4C.2 or NbBs4C.3, and seeing if this chimera is still able to induce a cell death response.

The next step was to take a closer look into the composition of the N-terminal body to see if any insights could be made into the function of the transmembrane region. Taking inspiration from the $GABA_A$ receptor from Kim et al. 2020, a putative pentamer of CpBs4C was modelled (Figure 3.14). Even though the modelling was done with the N-terminal body of CpBs4C, all homologues have the same conserved N-terminal body, so it stands to reason that all of the homologues could be modelled in a similar pentameric ring. Looking more closely at the pentameric ring, there is an alpha-helix that lines the inside of what could be the putative pore. The $GABA_A$ receptor is a cation channel, with indicative negatively charged amino acids within its pore-lining helices (Kaila et al., 1989). Furthermore, as outlined in section 1.2.1, the NLRs ZAR1, NRG1.1, and ADR1 all have a negatively charged amino acid within the inner ring of the central pore (Bi et al., 2021; Jacob et al., 2021). We thought that perhaps if the cell death-inducing Bs4C homologues are acting as ion channels, then there would be an indicative charge within the pore-lining helix of the cell death-inducing Bs4C homologues. We found that none of the Bs4C homologues from *C. pubescens* or *N. benthamiana* had any amino acids with a charge (either positive or negative) within this pore-lining helix (Figure 3.25), thus not giving any indication as to whether or not Bs4C is acting as a passive channel that is permeable to ions.

Regardless of the lack of an indicative charge, we still wanted to see if this pore-lining alpha-helix had an impact on the induction of cell death, so we swapped this alpha-helix between NbBs4C.1 and NbBs4C.2. None of the pore-swapped chimeras were found to induce a cell death reaction, although they did accumulate protein (Figure 3.24). This led us to believe that the integrity of the last two alpha helices together is important for the induction of cell death. We know that it is the last two alpha helices because when we swapped the C-terminal tail, one of the chimeras induced cell death, but when the pore-lining helix was swapped, there was protein accumulation, but none of the chimeras induced cell death. Narrowing down the specific region of the N-terminal body that is responsible for the induction of cell death in future

studies could provide valuable insight into the functional mechanism with which Bs4C homologues utilise to induce cell death.

4.1.6. Pepper and rice executors likely function in different manners

Previously, predictions using older transmembrane domain prediction software (TMHMM-2.0) determined that CpBs4C, Xa10, and Xa23 all had close structural homology with each other and three to four transmembrane domains that were all predicted to lie within the ER (Nowack et al., 2022; Wang et al., 2018). However, the structures that were resolved in Figure 3.12 clearly show that CpBs4C is not a structural homologue of Xa10 or Xa23, and that Xa10 and Xa23 are closer to each other in their structural topology than they are to CpBs4C. While CpBs4C, Xa10, and Xa23 might all act in the same subcellular compartment, that being the ER, they likely have distinct mechanisms with which they execute cell death. It was shown by Wang et al. 2018 that putting CpBs4C into *Oryza sativa* under control of the Xa10 promoter confers AvrXa10-dependent resistance when inoculated with *Xanthomonas oryzae* pv. *oryzae* (*Xoo*). This was likely done to show that CpBs4C acts in a similar manner to that of Xa10, but also to show that CpBs4C resistance can be transferred from the dicot *C. pubescens* to the monocot plant *O. sativa*. However, all that can be inferred from this is that *CpBs4C* can impede the proliferation of *Xoo*, and that the mechanism that *CpBs4C* uses to limit *Xoo* in *O. sativa* is likely the same mechanism that *CpBs4C* uses to limit *Xe* in *C. pubescens*, and that this mechanism is conserved across dicots and monocots.

One thing worth noting is that in Wang et al. 2018, the authors also identify and use a singular CpBs4C homologue from the *C. annuum* cultivar CM344 and called it CaBs4C. Upon comparison, their CaBs4C is actually the CaBs4C.1 homologue shown in Figure 3.1, 3.2, and 3.3. While CaBs4C.1 was unable to be ectopically expressed with a tag, a previous PhD student in the Lahaye lab, J. Elsaesser, was able to see a visible cell death reaction when CaBs4C.1 was ectopically expressed under control of the 35S promoter with no tag (Supplementary Information S1). Furthermore, Dr. Robert Morbitzer created a dTALE to activate *CaBs4C.1* in *C. annuum* via *Xe* delivery, and a strong cell death reaction can be observed (data not shown). While there was no immunoblot to confirm that CaBs4C.1 was expressed at the appropriate size, taking the visible cell death reaction observed from J. Elsaesser, the dTALE activation from Dr. R. Morbitzer, the localisation of CaBs4C.1 to the ER from Wang et al. 2018, and the striking structural homology and % amino acid similarity CaBs4C.1 has to CpBs4C in Figure 3.1 and 3.3, it stands to reason that CaBs4C.1 could induce cell death in a similar manner to both CpBs4C and NbBs4C.1.

Another aspect of *CpBs4C* that differentiates itself from its rice executor neighbours is the higher-order complex formation. In Tian et al., 2014 the authors show similar methods used herein to exhibit that Xa10 can homo-oligomerize and form a higher-order complex, primarily using FLIM-FRET, coIP, and BN-PAGE. While all of the assays in Tian et al. 2014 are missing the appropriate sub-cellular controls and the results need to be digested accordingly, they show that in FLIM-FRET experiments, the lifetime of Xa10-eGFP is reduced when it is co-expressed with Xa10-mCherry, that a laddering effect emerges in the coIP inferring multiple denatured complexes, in addition to higher order bands in the BN-PAGE. In the BN-PAGE, however, the authors highlight two bands between 66 and 146 kDa, indicating a hexameric formation and a slightly higher 'oligomer 2'. These sizes of the Xa10 complex do not coalesce with the pentameric prediction of CpBs4C and its complex size that we saw in Figure 3.16, further supporting the notion that while Xa10 and CpBs4C localise to a similar sub-cellular compartment, they likely act in a different manner to induce cell death.

It is possible, however, that while they are clearly structurally distinct, they could potentially be utilising a common secondary messenger to execute cell death. Ca^{2+} plays a fundamental role in signal transduction across all living organisms and is subsequently implicated in myriad physiological processes. We found that CpBs4C might be using Ca^{2+} to initiate cell death. Specifically, we found in our IP-MS proteomic analysis that frequent potential binding partners of CpBs4C were Ca^{2+}-transporting ATPases, both ER and PM-like (Table 3.4), and we also found that the Ca^{2+} channel inhibitor, $LaCl_3$, suppresses CpBs4C cell death (Figure 3.21). Moreover, we found that CpBs4C does not induce an increase of $[Ca^{2+}]_{cyt}$, unlike Bs3 (Figure 3.22). This is the exact opposite of what was found for Xa10 in Tian et al. 2014, where Xa10 caused an increase in $[Ca^{2+}]_{cyt}$, using the cytosolic Ca^{2+} indicator YC3.60 in FLIM-FRET studies. While this does not experimentally show that there is a depletion of Ca^{2+} from the ER, it is a logical assumption, as outlined in section 1.2.1 and 1.2.2, that the ER is a Ca^{2+} store, and the flux of Ca^{2+} from the ER into the cytoplasm is a hallmark of cell death initiation. A confirmatory experiment whereby the $[Ca^{2+}]_{cyt}$ is analysed side-by-side with Xa10 and CpBs4C would definitively show that Xa10 and CpBs4C utilise different movements of Ca^{2+} in the cell to induce cell death.

4.1.7. CpBs4C forms a high molecular weight complex and could be disrupting calcium homeostasis in the cell

After seeing the striking similarity of the structure of CpBs4C compared to the neurotransmitter receptors, both in their individual subunits (Figure 3.13) and as a putative pentamer (Figure 3.14), it seemed logical to test experimentally if CpBs4C does indeed form a pentamer. First,

we found that all of the Bs4C homologues from *C. pubescens* and *N. benthamiana* can homo-associate through coIP and FLIM-FRET (Figure 3.15 and Figure 3.17). Following this, we also found that CpBs4C can form a higher-order complex weighing at least 670 kDa (Figure 3.16). If this peak is solely CpBs4C-mCherry, this molecular weight could mean that the CpBs4C-mCherry complex is either forming at least a singular 15-mer complex, or 3 pentamers coming together (Figure 4.2B-C). Figure 3.16B was performed atypically using crude *N. benthamiana* extract and running it through a size exclusion column (SEC). A peak starting after 670 kDa was found to be the CpBs4C-mCherry complex, however, it could be entirely possible that this CpBs4C-mCherry complex could contain other binding partners that is making it heavier than the actual size of the complex. For example, many Ca^{2+}-ATPases were found to be potential binding partners of CpBs4C *in planta* (Table 3.4). One of the ER-type Ca^{2+}-ATPases found in Table 3.4 is Ca^{2+}-transporting ATPase 4, endoplasmic reticulum-type-like (NbD018366.1) and has a molecular weight of ~120 kDa. If one or many Ca^{2+}-ATPases are binding to the CpBs4C complex, then this is what could be potentially adding a large amount of weight to the complex (Figure 4.2D). Furthermore, the size of the complex seen via Blue Native PAGE (BN-PAGE) in Figure 3.16A displays a much larger complex than the one seen via SEC in Figure 3.16B and might even align with the first peak of the bi-modal peak found in the SEC, although this needs to be confirmed with additional protein standards at a higher molecular weight. This complex found in the BN-PAGE in Figure 3.16A could potentially be displaying a high molecular weight due to the added weight of binding partners. Typically, for SEC, the target protein is expressed, either in *E. coli*, insect cells, or *in planta*, then the protein is purified and then run through the column. This ensures that only your target protein is running through the system and that the size-specific eluates are specific to your purified protein. Performing the size exclusion using a crude extraction method *in planta* means that no purification step was taken, and that the size-specific eluates contained everything within the plant tissue at that specific molecular weight, making downstream analysis not possible. To definitively determine if this CpBs4C complex has binding partners that give it a higher molecular weight than a pure CpBs4C complex, one could enrich the CpBs4C complex from *N. benthamiana* using immunoprecipitation, to clear away any of the non-CpBs4C complex binding partners, and then run this CpBs4C enriched sample through the SEC column. The fractions that have a CpBs4C-specific peak could then be sent for mass spectrometry (MS) analysis to identify peptides or proteins that are coming down with CpBs4C. A cross-comparison with the potential *in planta* binding partners found in Table 3.4 and Figure 3.20 could potentially help to confirm the specific binding partners of CpBs4C *in planta*.

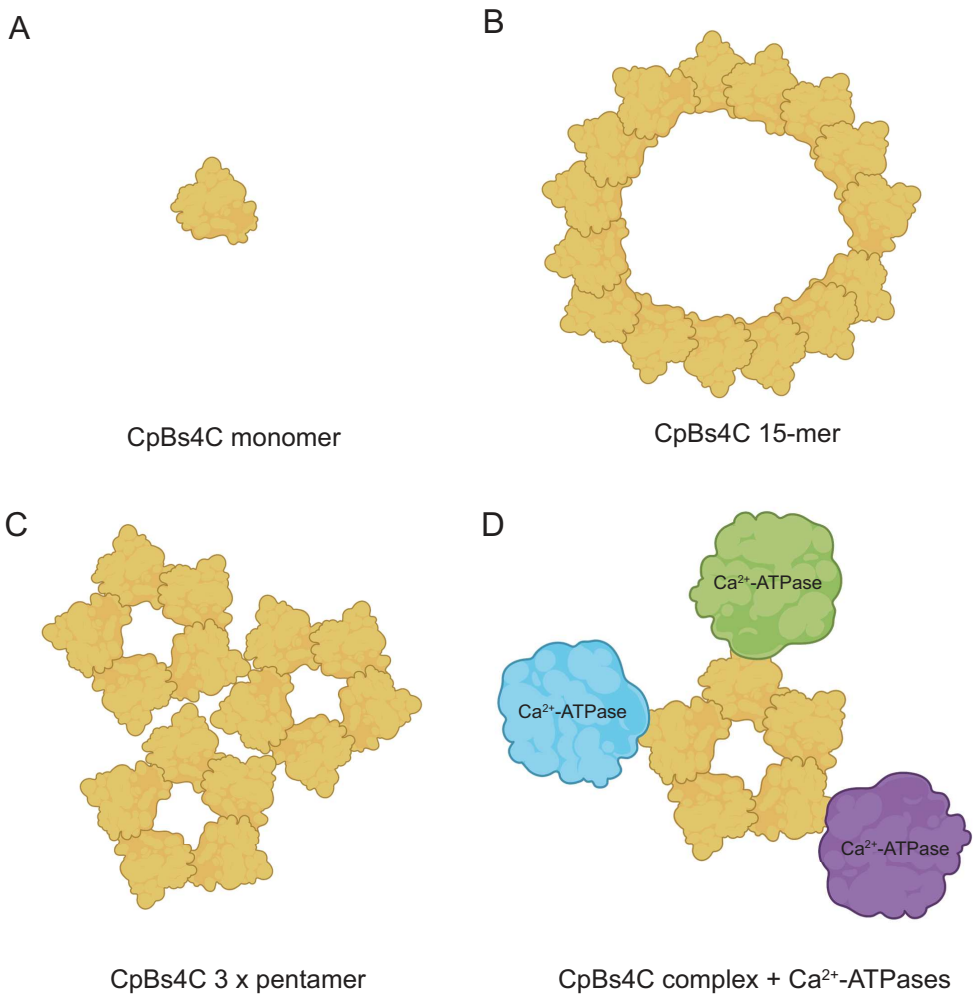

FIGURE 4.2. CpBs4C forms a high molecular weight complex.

A | Graphical depiction of a singular monomer unit of CpBs4C.
B | Top-down view of a graphical depiction of a putative 15-mer CpBs4C complex
C | Top-down view of a graphical depiction of a putative 3 x pentamer CpBs4C complex.
D | Top-down view of a hypothetical depiction of a CpBs4C complex with Ca^{2+}-ATPases as potential binding partners.
Images created using BioRender.com.

Furthermore, only CpBs4C was tested for the size of the potential complex. We know that both CpBs4C and NbBs4C.1 induce cell death and are localized to a similar sub-cellular compartment (Figure 3.4 and Figure 3.5), so it would be interesting to see if NbBs4C.1 forms a complex of similar size to CpBs4C in both SEC and BN-PAGE experiments. If they are similar, then it is possible that they either have the same number of subunits coming together to form the complex and/or NbBs4C.1 has similar binding partners to CpBs4C to aid in the induction of cell death. With this in mind, there are the two non-cell death-inducing homologues, NbBs4C.2 and NbBs4C.3, that also localize to similar subcellular compartments as CpBs4C and NbBs4C (Figure 3.4 and Figure 3.5). It could be that a differentiating factor between the two groups (cell death and non-cell death) could be either the size of their

complex or the potential binding partners of the Bs4C homologues. Testing both the size of the complexes of NbBs4C.1, NbBs4C.2, and NbBs4C.3 and sending their enriched SEC fractions for MS analysis, in addition to sending all of the NbBs4C paralogues for IP-MS analysis could provide valuable insight into the similarities or differences between all of the Bs4C homologues and could highlight a possible mechanism of action for these proteins.

We identified that CpBs4C is likely involved in the transmembrane transport of ions (Figure 3.20) and that Ca^{2+}-transporting ATPases were potential binding partners of CpBs4C (Table 3.4). Future experiments should test these potential binding partners with CpBs4C to validate the proteomics dataset, either using TurboID, coIP, or FLIM-FRET as experimental approaches. With the potential Ca^{2+}-transporting ATPases information, we took the recent findings of the ZAR1 resistosome and helper immune receptors being Ca^{2+}-permeable cation channels as inspiration for identifying if CpBs4C could be using Ca^{2+} channels to induce cell death (Bi et al., 2021; Jacob et al., 2021). Indeed, we found that CpBs4C cell death was suppressed when co-infiltrated with the Ca^{2+} channel inhibitor $LaCl_3$ (Figure 3.21) indicating that CpBs4C somehow uses Ca^{2+} channels to execute cell death. In all cases, the NbBs4C paralogues had their protein accumulation dramatically reduced in the presence of $LaCl_3$, and CpBs4C had a small visible reduction in protein accumulation with $LaCl_3$ (Figure 3.21B). The reduction of NbBs4C.1 protein in the presence of $LaCl_3$ is likely why we do not see any cell death, but the reduction of protein in the non-cell death-inducing paralogues, NbBs4C.2 and NbBs4C.3, in the presence of $LaCl_3$ is peculiar. In the majority of cases of $LaCl_3$ being co-infiltrated with CpBs4C there is no reduction in protein accumulation, however in a few instances, which is represented in Figure 3.21B, there is a slight reduction in the accumulation of CpBs4C when it is co-infiltrated with $LaCl_3$. It seems across all tested Bs4C homologues, that $LaCl_3$ has some sort of effect on the accumulation of the protein. Further investigation to see how and why the protein is being limited in its accumulation would be interesting, in addition to seeing if the limitation of Bs4C protein accumulation is a common response to other broad Ca^{2+} channel blockers like gadolinium (III) chloride ($GdCl_3$) or nifedipine (NFD) (De Vriese et al., 2018), or if it is specific to $LaCl_3$. Identifying how $LaCl_3$ is affecting these homologues could provide further insight into their mechanisms of action, and potentially further uncover the role of Ca^{2+} movement in the induction of cell death.

The ER is a major intracellular Ca^{2+} store, with Ca^{2+} being released from the ER and increasing $[Ca^{2+}]_{cyt}$ upon a variety of biotic and abiotic stresses, including osmotic stress, salt stress, and immunity (Costa et al., 2018). Increases in $[Ca^{2+}]_{cyt}$ upon stress are typically mediated by cyclic nucleotide-gated channels, Ca^{2+}-ATPases, two-pore Ca^{2+} channels, and glutamate receptors (Wilkins et al., 2016). The rice executor, Xa10, causes an increase in $[Ca^{2+}]_{cyt}$, depleting the

ER of its Ca^{2+} stores (Tian et al., 2014). To our surprise, however, there was no increase in $[Ca^{2+}]_{cyt}$ when CpBs4C was expressed, and the $[Ca^{2+}]_{cyt}$ was similar to the $[Ca^{2+}]_{cyt}$ when GFP was expressed, 24 hours after infiltration (Figure 3.22). This was rather unexpected, seeing as there was mounting evidence to suggest that CpBs4C uses Ca^{2+} in some way to induce cell death. Even more strange was the fact that Bs3 had an increase in $[Ca^{2+}]_{cyt}$, even though Bs3 cell death could not be suppressed by $LaCl_3$ (Figure 3.21). A possible explanation for this could be that CpBs4C could somehow be causing an influx of Ca^{2+} into the ER, therefore suggesting that the ER functions as a sink, and the cytosol acts as the source, moving against the electrochemical gradient of $[Ca^{2+}]$. The movement of ions against an electrochemical gradient is an active process that requires the use of ATP, like for example, with ATPases, which were found in our IP-MS analysis (Table 3.4).

ER Ca^{2+}-ATPases are active members in the process of the transfer of cytosolic Ca^{2+} into the ER (Ren et al., 2021). Specifically, after there is an increase in $[Ca^{2+}]_{cyt}$ after a stimulus, the $[Ca^{2+}]_{cyt}$ within the cell needs to be restored, if there is no cell death induction, and this is done through the use of ER Ca^{2+}-ATPases moving Ca^{2+} from the cytosol into the ER to return each organelle to its basal $[Ca^{2+}]$ (Brini & Carafoli, 2011). Ca^{2+}-ATPases use active transport to push Ca^{2+} ions against the electrochemical gradient (Inesi, 1985). Therefore, it is possible that CpBs4C could potentially be using ER-type Ca^{2+}-ATPases to transfer Ca^{2+} from the cytosol, or other sources, into the ER. In human cells, when the $[Ca^{2+}]_{ER}$ is overloaded, protein synthesis is impaired, and if the appropriate stress responses cannot be activated (the unfolded protein response and ER-associated degradation), then cell death is initiated (Paschen, 2004). After the translation of CpBs4C, a similar mechanism could possibly be occurring, whereby the ER is overwhelmed with too much Ca^{2+}, causing too great stress on the ER, leading to cell death (Figure 4.3).

We can rule out that CpBs4C could be acting as a channel for Ca^{2+} ions because this would be a passive process. Ca^{2+} permeable channels, like for example the ZAR1 resistosome, work passively when activated to move Ca^{2+} ions from a place with a high Ca^{2+} concentration to a place with a lower Ca^{2+} concentration (Bi et al., 2021; Gadsby, 2009). If CpBs4C was working as a channel, then we would expect a charged amino acid residue within the pore-lining helix indicating selectivity towards an ion, specifically negatively charged amino acids like glutamic acid (E) or aspartic acid (D) for Ca^{2+} selectivity, which we do not (Figure 3.26). Secondly, if CpBs4C was working as a channel, then when it is expressed, we would see a passive movement of Ca^{2+} from a location of high Ca^{2+} concentration (the ER) to a location of lower Ca^{2+} concentration (the cytosol), yet we see no increase in $[Ca^{2+}]_{cyt}$ upon CpBs4C expression (Figure 3.22). Taking both of these findings, combined with the observation that $LaCl_3$ inhibits

CpBs4C cell death, as seen in Figure 3.21, the most likely explanation is that CpBs4C is sequestering Ca^{2+}-ATPases within the cell and utilising their active transport capabilities to pump Ca^{2+} from the cytosol into the ER, ultimately disrupting the ER Ca^{2+} homeostasis, leading to cell death (Figure 4.3).

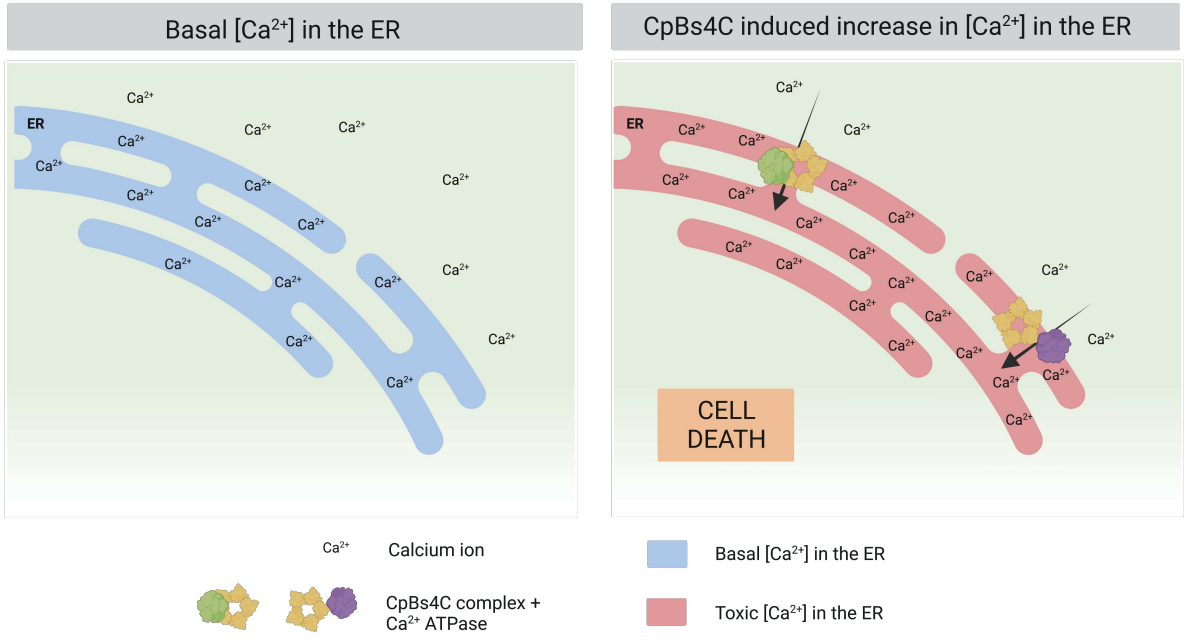

FIGURE 4.3. CpBs4C might be using Ca^{2+}-ATPases to pump Ca^{2+} into the ER.

Graphical depiction of how CpBs4C (yellow) might sequester ER localised Ca^{2+}-ATPases (purple and green) to actively pump Ca^{2+} into the ER, ultimately overloading the ER with Ca^{2+}, leading to cell death. Image created using BioRender.com.

While there are different types of Ca^{2+}-ATPases, the plant ER-type 2B Ca^{2+}-ATPases were found in our proteomic data set (Table 3.4). Plant-type ER-resident Ca^{2+}-ATPases can be specifically inhibited pharmacologically by cyclopiazonic acid (CPA) (Bonza et al., 2013; Liang & Sze, 1998). We can test if these ER Ca^{2+}-ATPases are a major player in CpBs4C-induced cell death by co-infiltrating CpBs4C and CPA and see if this somehow alters or suppresses CpBs4C cell death. $LaCl_3$ is a non-selective Ca^{2+} channel blocker, which can broadly target cation channels, Ca^{2+}-ATPases, Ca^{2+}-permeable channels, most Ca^{2+} binding sites, calmodulin (CaM), in addition to many other Ca^{2+} related transporting proteins, and is typically reported to be inhibitory for PM localised Ca^{2+} transporting mechanisms (De Vriese et al., 2018). However, the use of CPA, a specific ER Ca^{2+}-ATPase antagonist, would more explicitly highlight if CpBs4C utilises Ca^{2+}-ATPases localised at the ER to induce cell death. Furthermore, we could utilise an ER-localised Ca^{2+} sensor (Resentini et al., 2021) to determine if after CpBs4C is translated, there is an increase in $[Ca^{2+}]_{ER}$. The ER-localised Ca^{2+} sensor in

combination with the CPA inhibition could allow us to determine if the movement of Ca^{2+} against the electrochemical gradient into the ER via Ca^{2+}-ATPases is the mechanism that CpBs4C is using to induce cell death.

The discovery of CpBs4C homologues in multiple other solanaceous species led the way for the identification of the different phenotypes of Bs4C homologues, the conclusion that the native function of Bs4C homologues likely lies outside of *Xanthomonas* resistance, and ultimately allowed for the resolution of the structure of CpBs4C and the other homologues. After the structure was resolved, we were able to make larger conclusions about not only the potential origins of the Bs4C homologues but also the part of the protein that was responsible for cell death, as well as justifiable speculations about the molecular mechanism that CpBs4C employs to induce cell death.

4.2. Mapping in the M2 generation identifies *XRN4* as a downstream signalling component of *CpBs4C* in Arabidopsis

Once a potential mechanism of action was established for CpBs4C (Section 4.1.6), the next step was to determine vital signalling components for CpBs4C to induce cell death. We pursued this through the generation of a novel genetic mapping technique that was oriented towards identifying causal mutations in a reduced time frame compared to traditional methods.

4.2.1. *CpBs4C* is the foundation for a conditionally lethal screen in Arabidopsis

The majority of work performed in the effort to narrow down the function of CpBs4C and its homologues was done by working transiently in *N. benthamiana*. This method is relatively easy and quite efficient, however, the complexity and ambiguous nature of the *N. benthamiana* genome, in that it is a tetraploid species, makes it challenging to use for genetic dissection. We found that *CpBs4C* can induce growth arrest in Arabidopsis using an inducible promoter system (Figure 3.31), indicating that *CpBs4C* utilises a mechanism to execute cell death which is conserved in Arabidopsis. Due to the genetic simplicity (diploid species) and wealth of resources and information that is available in the Arabidopsis community, we used this conditionally lethal *CpBs4C* Arabidopsis line as the basis for a forward genetic screen to identify downstream signalling components of CpBs4C-induced cell death.

4.2.2. Causal EMS mutations can be identified in the M2 generation, saving over 8 months in time and resources

In traditional forward genetic screens, the parental seeds are mutagenized, generating an M0 population. This M0 population is sowed out on soil, producing M1 plants and these plants are allowed to mature and self-pollinate. The M1 plants are then bulked together and collected for seed in a large M2 population. This M2 population is then sowed out and individual plants are analysed for suppression of the phenotype found in the parental line. These individual M2 plants are then isolated, and their progeny is collected, generating an M3 population. In the past, the M3 plants are then sowed out and the phenotype observed in the M2 population is confirmed. Once this phenotype is confirmed, an individual plant from the M3 population is crossed to the original parental line, to generate an F1 population, and then subsequently a segregating F2 population. Assuming that the causal EMS mutation is recessive, the individuals within the F2 population are bulked together and their DNA is pooled and sent for

next-generation sequencing (NGS) (Kim et al., 2006; Qu & Qin, 2014) (Figure 4.4). Considering the average generation time (seed to seed) of Arabidopsis is at least eight weeks, the traditional method of isolating a causal EMS mutation would be at least 32 weeks (or eight months), but typically takes at least one year.

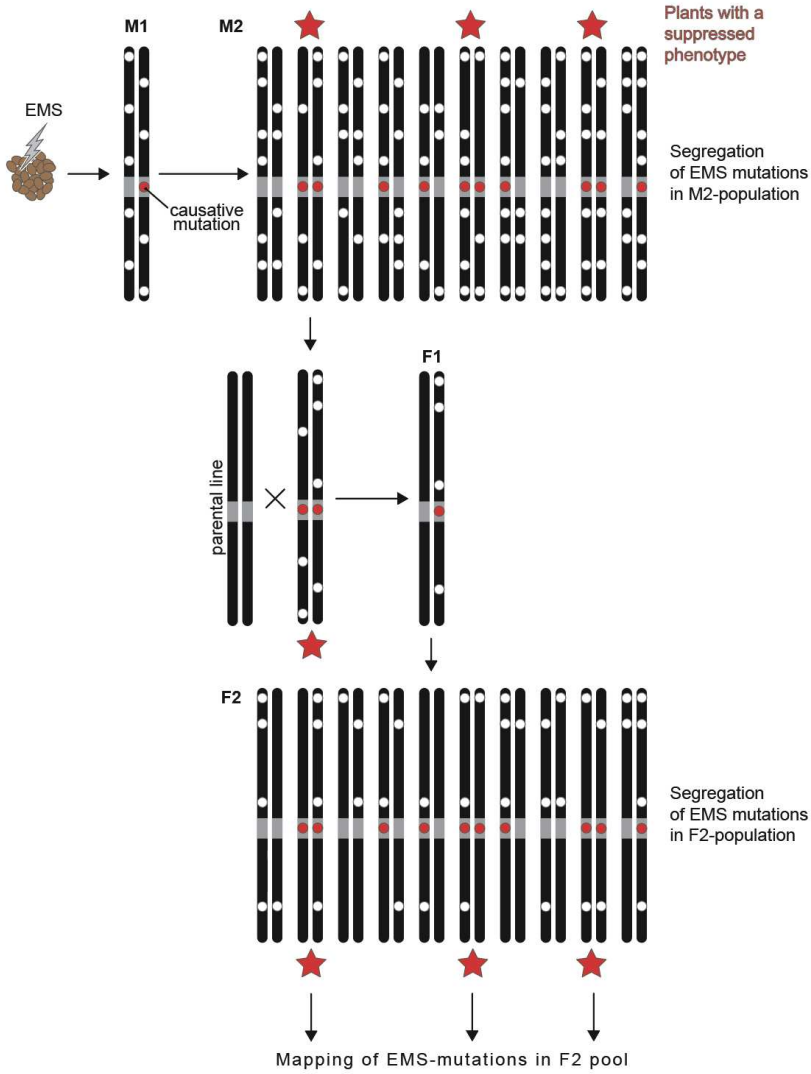

FIGURE 4.4. Traditional method of identifying a causal mutation in an EMS mutagenesis forward genetic screen in Arabidopsis, by backcrossing and performing bulk segregant analysis in the F2 generation.

Pairs of long black lines represent a pair of chromosomes. White circles indicate mutations generated via EMS. Red circles indicate causative mutations caused by EMS. Red star indicates a suppression in the parental phenotype. Figure has been adapted from the original figure made by Dr. Thomas Lahaye.

In 2020, a new method, “Mutagenomics”, was proposed to negate this backcrossing, and identify causal mutations within the M3 generation (Hodgens et al., 2020). This was performed using the same beginning steps as previously mentioned, by bulking the M1 plants together, producing a large M2 population, then selecting the individual M2 plant and collecting its

progeny, generating the M3. In Hodgens et al. 2020, the authors analysed the M3 population and took the plants with their suppression phenotype (Affected in the Response to Cytokinin) and bulked them together to create a DNA pool to send for NGS. Performing NGS in the M3 population abolished the need for a backcross to the parental line, and effectively eliminated 16 weeks of time needed to identify the causal mutation (Figure 4.5).

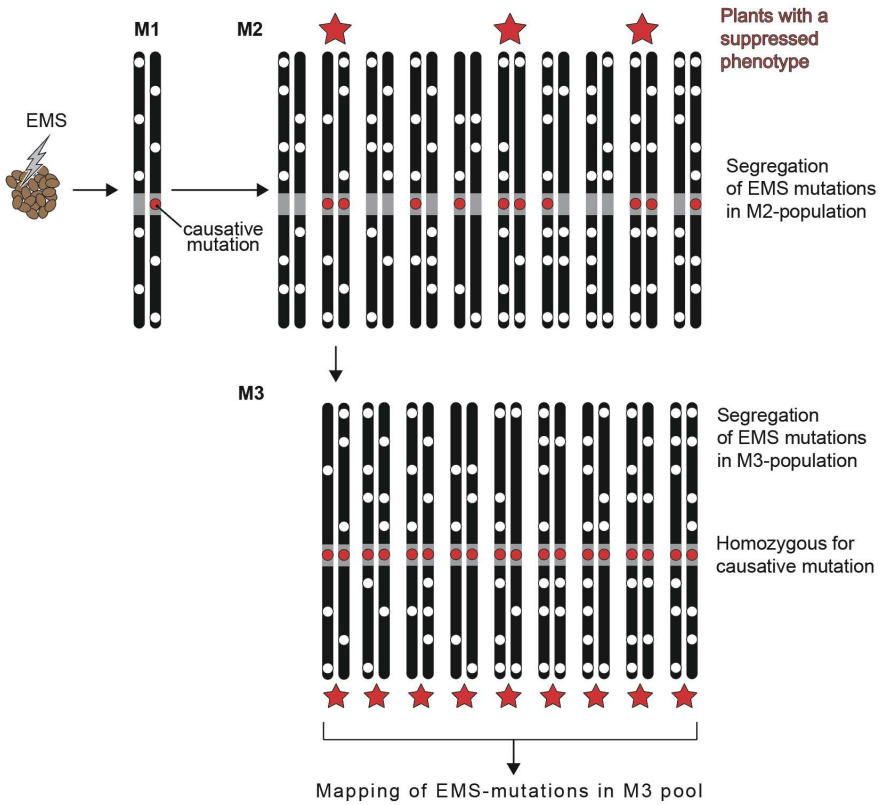

FIGURE 4.5. 'Mutagenomics' approach to identify a causal mutation in an EMS mutagenesis forward genetic screen in Arabidopsis, by mapping in the M3 generation.

Pairs of long black lines represent a pair of chromosomes. White circles indicate mutations generated via EMS. Red circles indicate causative mutations caused by EMS. Red star indicates a suppression in the parental phenotype. Figure has been adapted from the original figure made by Dr. Thomas Lahaye.

Our new method of identifying a causal mutation in the M2 generation takes an additional eight weeks off the newly minted "Mutagenomics" method described in Hodgens et al. 2020. Our method diverges from the two previously mentioned methods, by individually collecting the plants at the M1 stage, rather than the M2 stage. Individually collecting the plants at the M1 stage already generates a segregating population of the EMS mutations, as the EMS generates a mutation on only one strand of DNA (Koornneeff et al., 1982), effectively making a potentially causal mutation in a heterozygous configuration in the M1, and would create a monohybrid segregation pattern in the M2 (Figure 4.6). Furthermore, when using our method, only mutant M2 families that have multiple individuals suppressing the parental genotype are

considered. This ultimately reduces the possibility that a single mutant plant might be mis-scored, which is often found to be the case in the alternative methods.

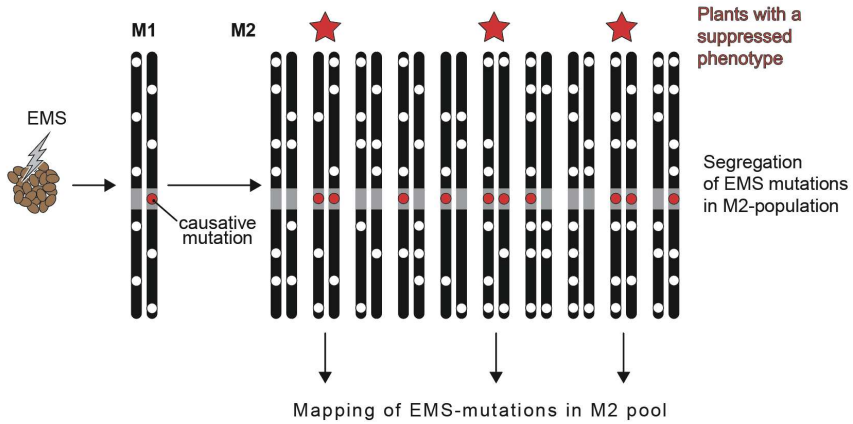

FIGURE 4.6. Novel method of identifying a causal mutation in the M2 generation of an EMS mutagenesis forward genetic screen in Arabidopsis.

Pairs of long black lines represent a pair of chromosomes. White circles indicate mutations generated via EMS. Red circles indicate causative mutations caused by EMS. Red star indicates a suppression in the parental phenotype. Figure has been adapted from the original figure made by Dr. Thomas Lahaye.

This novel method of mapping in the M2 generation promises to be a fast and efficient way of identifying EMS-induced causal mutations. While this method was developed in Arabidopsis, it can be easily applicable to any diploid plant species. This expedited method could help to screen and identify novel mutations in crop species faster than traditional methods. For example, in an effort to identify new resistance (*R*) genes that can be rapidly deployed in agriculture to create resilient crops in record time.

4.2.3. *xrn4* suppresses *CpBs4C* growth arrest in Arabidopsis

By using this fast-forward approach in sending the pooled M2 generation for NGS, we were able to identify five different M2 families that each harboured an independent non-synonymous mutation with the gene *At1g54490*, encoding the protein EXORIBONUCLEASE 4 (XRN4) (Figure 3.40). XRN4 is the functional plant orthologue of the mammalian and yeast XRN1 (also known as Pacman) and catalyses the degradation of mRNA in a 5’ to 3’ fashion within the cytoplasm (Kastenmayer & Green, 2000). XRN4 has been implicated in numerous different pathways, including the ethylene response pathway, development, heat stress, antiviral defence and plant immunity (Carpentier et al., 2020; Li & Wang, 2018; Potuschak et al., 2006; Tong et al., 2022; Yu et al., 2019). In the context of plant immunity, upon the activation of MAMP-triggered immune responses, decapping protein DCP1, is phosphorylated, which

enhances its interaction with XRN4 in processing bodies (P-bodies) to downregulate genes that negatively regulate immunity (Yu et al., 2019). The mRNA decapping complex that DCP1 is a part of decaps the 5' end of targeted mRNA to make it available for 5' to 3' degradation by XRN4 (Carpentier et al., 2020). XRN4 has also been found to obstruct several RNA viruses in plants, including Arabidopsis, *N. benthamiana*, and *O. sativa* by directly binding to and inhibiting HC-Pro, a viral silencing suppressor (Cheng et al., 2007; Jaag & Nagy, 2009; Jiang et al., 2018; Li & Wang, 2018; Peng et al., 2011). With a well-established role in numerous difference pathways, it is conceivable that XRN4 could be a shared regulator of basal bacterial immunity, viral defence, development, and cell death.

Ultimately, we were able to confirm that the mutant allele *xrn4-5* was able to suppress *CpBs4C*-induced growth arrest in Arabidopsis (Figure 3.38), validating the mapping results that identified five independent mutations in *XRN4* (Figure 3.40). In the past, one of the biggest concerns with the identification of *XRN4* in an EMS screen is that it can limit the expression of the main protein or transcript for which you are trying to identify suppressors (Li et al., 2019). We prove in both the M2 generation of EMS-induced *XRN4* mutations and in the independent T-DNA allele of *xrn4-5* in the T2 generation, that CpBs4C-FLAG-GFP protein is expressed at adequate levels, and in some instances even more than the parental control line, negating any concerns over mutations in *XRN4* limiting CpBs4C protein expression (Figure 3.32B and Figure 3.38B).

It would be interesting to see if the other cell death-inducing homologues of CpBs4C also require *XRN4* to induce cell death. We were unable to generate a new allele of *XRN4* in Arabidopsis via CRISPR mutagenesis, and we were unable to generate a stable knockout of *XRN4* in *N. benthamiana.* The inability to generate new alleles could have something to do with the position of the guide RNAs along the *XRN4* gene. As indicated in Figure 3.36, our EMS-induced mutations are found within the first half of the gene, and the T-DNA insertions are within the latter have of the gene. It could be that the generation of large deletions or very early stop codons within the coding sequence of *XRN4* is lethal for the plant. Therefore, a transient approach by silencing *XRN4* using VIGS (virus-induced gene silencing) would be a better alternative approach (Hayward et al., 2011). Using this method, we would be able to test if the transient ectopic overexpression of NbBs4C.1 is able to produce cell death in the *XRN4* silenced *N. benthamiana*. Furthermore, it would be interesting to see if the non-cell death-inducing Bs4C homologues from *N. benthamiana* are also affected by silencing *XRN4*, as activation of these genes still limits bacterial growth (Figure 3.8). This could be tested through silencing *XRN4* in *N. benthamiana*, and then performing *Xanthomonas* growth curves using the dTALEs activating *NbBs4C.2* and *NbBs4C.3* from Figure 3.7 and Figure 3.8.

Ultimately, as we can biologically confirm using one T-DNA allele that *XRN4* supresses *CpBs4C*-dependent growth arrest in Arabidopsis, this new M2 mapping technique is the fastest method of identifying EMS-induced mutations so far, with the shortest number of generations from EMS induction to isolating causal mutations. Future studies should explore additional knock-out alleles of *XRN4* to independently validate that *xrn4* suppresses CpBs4C-FLAG-GFP induced cell death.

4.2.4. *XRN4* could potentially be degrading a negative regulator of CpBs4C cell death

As previously mentioned, *XRN4* is a well-known integral component in the ethylene response pathway (Potuschak et al., 2006). Ethylene is also the direct key regulator in the ripening of climacteric fruit like tomato (Pech et al., 2012). At the onset of ripening, there is a surge in the production of ethylene, and in particular, at the mature green and breaker stages of tomato fruit development (Giovannoni, 2004; Karlova et al., 2014), which are the exact time points when *SlBs4C* was found to be expressed in RNA-seq experiments. More specifically, *SlBs4C* seems to be expressed in the top third of the tomato fruit in the pericarp, at the beginning of ripening in the mature green and breaker stages (Figure 3.29). However, the ethylene induction at the onset of fruit ripening is what differentiates climacteric and non-climacteric fruits (Karlova et al., 2014). Tomatoes are climacteric fruits, and their ripening process in response to ethylene is well documented (Pech et al., 2012). Other species where Bs4C homologues are found, like *Capsicum* species, which have in the past been labelled as producing non-climacteric fruits, have been found to have a limited partial requirement of ethylene perception for fruit ripening to occur (Aizat et al., 2013). However, *N. benthamiana*, where there were three Bs4C homologues identified, do not produce fruit, perhaps limiting the possibility that Bs4C homologues could be using *XRN4* in a fruit specific, ethylene-dependent developmental context.

XRN4 has been found to influence different stages of development, particularly in the later stage of development of the Arabidopsis stamen, and the development of young seedlings, both through the mechanism of mRNA decay (Carpentier et al., 2020; Rymarquis et al., 2011). The function of *XRN4* in the ethylene response pathway is to reduce the transcript level of two transcriptional regulators this pathway, EIN3 BINDING F-BOX PROTEIN1 (EBF1) and EBF2, allowing for the activation of ethylene-responsive genes (Potuschak et al., 2006). With all three of these examples of XRN4 regulating development and hormone pathways with the decay of

specific transcripts, combined with the finding that *XRN4* degrades negative regulators of Arabidopsis immunity (Yu et al., 2019), it stands to reason that *XRN4* could be degrading a transcript that is potentially a negative regulator of CpBs4C induced cell death (Figure 4.7).

Recalling from Section 4.1.6, the working model is that CpBs4C is sequestering ER-Ca^{2+}-ATPases to actively transport Ca^{2+} from the cytosol into the ER, and potentially overloading the ER with Ca^{2+}, leading to an imbalance of $[Ca^{2+}]_{ER}$, and inducing cell death. If we take this working model and apply it to the finding that *XRN4* is required for CpBs4C cell death in Arabidopsis, it is purely speculative, yet conceivable, that *XRN4* could be degrading the transcript of Ca^{2+}-ATPase inhibitor, allowing the Ca^{2+}-ATPase to be active in a normal setting. When *XRN4* is mutated and non-functional, it could be possible that the Ca^{2+}-ATPase inhibitor transcript over-accumulates, rendering the Ca^{2+}-ATPase non-functional, ultimately not allowing CpBs4C to induce cell death.

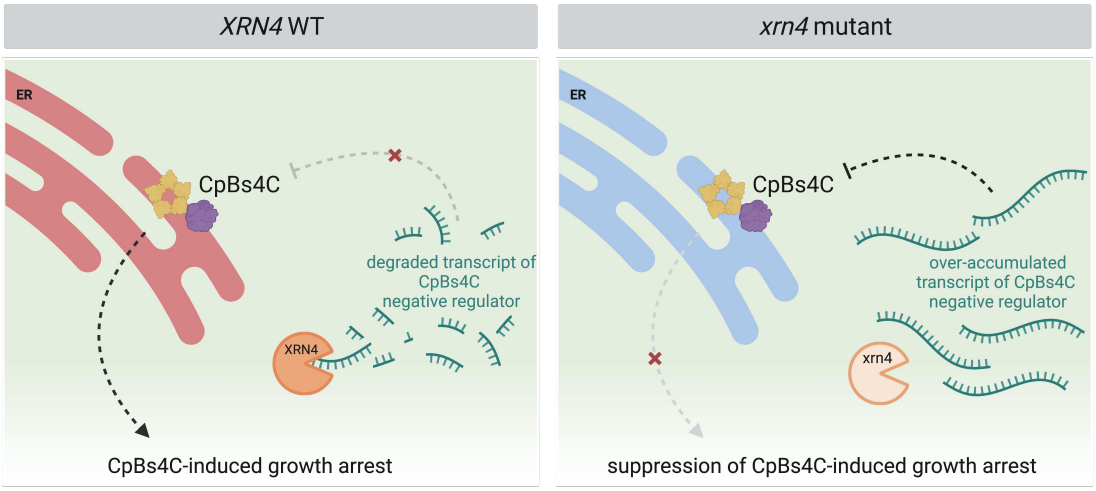

FIGURE 4.7. *xrn4* mutant could over-accumulate transcripts of negative regulators of CpBs4C-induced growth arrest.

Left panel schematic depicts the potential scenario in Arabidopsis, where *XRN4* wildtype (WT) (orange) degrades the mRNA transcripts of a CpBs4C negative regulator, allowing CpBs4C (yellow complex with purple Ca^{2+}-ATPase in the ER) to induce growth arrest.
Right panel schematic depicts the potential scenario in Arabidopsis, where a mutant *xrn4* (faded orange) is unable to degrade the mRNA transcripts of a CpBs4C negative regulator, allowing these transcripts to accumulate, and suppress the function of CpBs4C (yellow complex with purple Ca^{2+}-ATPase in the ER), not allowing for the induction of growth arrest.
Images created using BioRender.com.

In Arabidopsis, AtACA2, an ER localised Ca^{2+}-ATPase which was a close homologue of the *N. benthamiana* Ca^{2+}-ATPase found in our proteomic dataset (Table 3.4), is inhibited in its activity when it is phosphorylated in its regulatory domain by a Ca^{2+}-dependent protein kinase (Hwang et al., 2000). Therefore, if this negative regulator of the Ca^{2+}-ATPase over-

accumulates, then the Ca^{2+}-ATPase would be constitutively inhibited. It could be possible that there is an inhibitory mechanism working on the ER-localised Ca^{2+}-ATPases found to potentially be binding partners of CpBs4C in Table 3.4, and that *XRN4* is regulating the transcripts of these inhibitory elements. A possible way to test this would be to perform RNA-seq on both the *Estr:CpBs4C-FLAG-GFP* Arabidopsis lines after estradiol induction, and compare it to the *xrn4-5//Estr:CpBs4C-FLAG-GFP* after estradiol induction. If there are transcript(s) that are upregulated in the *xrn4-5//Estr:CpBs4C-FLAG-GFP* lines and downregulated in the *Estr:CpBs4C-FLAG-GFP* line, then these transcripts could potentially be the negative regulators of CpBs4C induced growth arrest in Arabidopsis.

In five of the six M2 families that we sent for sequencing that had a decent readout, we found a non-synonymous mutation with *At1g54490, XRN4* (Figure 3.40). In the last remaining M2 family that had a good sequencing readout, family 1812, the identified mutations were found on chromosome two, as opposed to the other five families, which mainly found mutations on chromosome one, where *At1g54490*, *XRN4* is located. In the future, the M2 family 1812 should be further investigated. There are many interesting genes that were found to have mutations in this family, for example, there was a non-synonymous mutation at an allele frequency of 1.00 in *At2g32820*, which encodes for *TRANSCRIPTION ELONGATION FACTOR II or TFIIS*, a non-synonymous mutation at an allele frequency of 0.98 in *At2g37280*, a gene encoding for *PLEIOTROPIC DRUG RESISTANCE 5* or *PDR5*, and a non-synonymous mutation inducing an early stop codon with an allele frequency of 1.00 in *At2g33540*, which encodes *C-TERMINAL DOMAIN PHOSPHATASE-LIKE3*, or *CPL3* (Table 3.7). Further investigation either through independent CRISPR generated or T-DNA alleles combined with complementation analysis would help to decipher if *TFIIS*, *PDR5*, or *CPL3* are involved in CpBs4C mediated cell death, and could potentially highlight another signalling node in the CpBs4C growth arrest signalling cascade.

In conclusion, we have shown that the novel mapping method can not only identify causal mutations in the M2 population, saving months of time and effort, but we were also able to biologically and functionally validate this method, by showing that *XRN4* is indeed involved in the pathway that induces CpBs4C dependent growth arrest in Arabidopsis. Furthermore, we have displayed that there are numerous homologues of CpBs4C in Solanaceous species and shown evidence that suggests the native function of these Bs4C homologues likely does not lie in immunity against *Xanthomonas*, and that these homologues could have arisen from a bacterial ancestor. We further discovered that CpBs4C utilises the movement of Ca^{2+} to induce cell death and underscored that future studies building upon these findings will allow for the elucidation of the true and native purpose of *Bs4C* genes in plants.

5. LITERATURE CITED

Adlung, N., Prochaska, H., Thieme, S., Banik, A., Blüher, D., John, P., Nagel, O., Schulze, S., Gantner, J., Delker, C., Stuttmann, J., & Bonas, U. (2016). Non-host Resistance Induced by the Xanthomonas Effector XopQ Is Widespread within the Genus Nicotiana and Functionally Depends on EDS1. *Frontiers in Plant Science*, *7*, 1796.

Aizat, W. M., Able, J. A., Stangoulis, J. C. R., & Able, A. J. (2013). Characterisation of ethylene pathway components in non-climacteric capsicum. *BMC Plant Biology*, *13*, 191.

Arabidopsis Genome Initiative. (2000). Analysis of the genome sequence of the flowering plant Arabidopsis thaliana. *Nature*, *408*(6814), 796–815.

Arisha, M. H., Shah, S. N. M., Gong, Z.-H., Jing, H., Li, C., & Zhang, H.-X. (2015). Ethyl methane sulfonate induced mutations in M2 generation and physiological variations in M1 generation of peppers (Capsicum annuum L.). *Frontiers in Plant Science*, *6*, 399.

Bajar, B. T., Wang, E. S., Zhang, S., Lin, M. Z., & Chu, J. (2016). A Guide to Fluorescent Protein FRET Pairs. *Sensors* , *16*(9).

Ballvora, A., Pierre, M., van den Ackerveken, G., Schornack, S., Rossier, O., Ganal, M., Lahaye, T., & Bonas, U. (2001). Genetic mapping and functional analysis of the tomato Bs4 locus governing recognition of the Xanthomonas campestris pv. vesicatoria AvrBs4 protein. *Molecular Plant-Microbe Interactions: MPMI*, *14*(5), 629–638.

Bashan, Y., Azaizeh, M., Diab, S., Yunis, H., & Okon, Y. (1985). Crop loss of pepper plants artificially infected with Xanthomonas campestris pv. vesicatoria in relation to symptom expression. *Crop Protection* , *4*(1), 77–84.

Basu, S. K., & De, A. K. (2003). Capsicum: historical and botanical perspectives. In *Capsicum* (1st Edition, pp. 21–35). CRC Press.

Bellini, C., Barbier-Brygoo, H., & Ephritikhine, G. (n.d.). Module 4: Mutagenesis and mutant analysis in Arabidopsis thaliana. In *Practical Course on Genetic and Molecular Analysis of Arabidopsis* (pp. 1–10).

Bezrutczyk, M., Yang, J., Eom, J.-S., Prior, M., Sosso, D., Hartwig, T., Szurek, B., Oliva, R., Vera-Cruz, C., White, F. F., Yang, B., & Frommer, W. B. (2018). Sugar flux and signaling in plant-microbe interactions. *The Plant Journal: For Cell and Molecular Biology*, *93*(4), 675–685.

Bi, G., Su, M., Li, N., Liang, Y., Dang, S., Xu, J., Hu, M., Wang, J., Zou, M., Deng, Y., Li, Q., Huang, S., Li, J., Chai, J., He, K., Chen, Y.-H., & Zhou, J.-M. (2021). The ZAR1 resistosome is a calcium-permeable channel triggering plant immune signaling. *Cell*, *184*(13), 3528-3541.e12.

Blanco, A., & Blanco, G. (2017). Chapter 25 - Biochemical Basis of Endocrinology (I) Receptors and Signal Transduction. In A. Blanco & G. Blanco (Eds.), *Medical Biochemistry* (pp. 547–572). Academic Press.

Boch, J., Scholze, H., Schornack, S., Landgraf, A., Hahn, S., Kay, S., Lahaye, T., Nickstadt, A., & Bonas, U. (2009). Breaking the code of DNA binding specificity of TAL-type III effectors. *Science*, *326*(5959), 1509–1512.

Bogdanove, A. J., Schornack, S., & Lahaye, T. (2010). TAL effectors: finding plant genes for disease and defense. *Current Opinion in Plant Biology*, *13*(4), 394–401.

Bonas, U., Schulte, R., Fenselau, S., Minsavage, G. V., Staskawicz, B. J., & Stall, R. E. (1991). Isolation of a gene cluster from Xanthomonas campestris pv. vesicatoria that determines pathogenicity and the hypersensitive response on pepper and tomato. *Molecular Plant-Microbe Interactions: MPMI*, *4*(1), 81–88.

Bonas, U., Stall, R. E., & Staskawicz, B. (1989). Genetic and structural characterization of the avirulence gene avrBs3 from Xanthomonas campestris pv. vesicatoria. *Molecular & General Genetics: MGG*, *218*(1), 127–136.

Bonza, M. C., Loro, G., Behera, S., Wong, A., Kudla, J., & Costa, A. (2013). Analyses of Ca2+ accumulation and dynamics in the endoplasmic reticulum of Arabidopsis root cells using a genetically encoded Cameleon sensor. *Plant Physiology*, *163*(3), 1230–1241.

Boudsocq, M., Willmann, M. R., McCormack, M., Lee, H., Shan, L., He, P., Bush, J., Cheng, S.-H., & Sheen, J. (2010). Differential innate immune signalling via Ca(2+) sensor protein kinases. *Nature*, *464*(7287), 418–422.

Bresson, J., Bieker, S., Riester, L., Doll, J., & Zentgraf, U. (2018). A guideline for leaf senescence analyses: from quantification to physiological and molecular investigations. *Journal of Experimental Botany*, *69*(4), 769–786.

Brini, M., & Carafoli, E. (2011). The plasma membrane Ca^2+ ATPase and the plasma membrane sodium calcium exchanger cooperate in the regulation of cell calcium. *Cold Spring Harbor Perspectives in Biology*, *3*(2).

Büttner, D., & He, S. Y. (2009). Type III protein secretion in plant pathogenic bacteria. *Plant Physiology*, *150*(4), 1656–1664.

Carpenter, E. J., Matasci, N., Ayyampalayam, S., Wu, S., Sun, J., Yu, J., Jimenez Vieira, F. R., Bowler, C., Dorrell, R. G., Gitzendanner, M. A., Li, L., Du, W., K Ullrich, K., Wickett, N. J., Barkmann, T. J., Barker, M. S., Leebens-Mack, J. H., & Wong, G. K.-S. (2019). Access to RNA-sequencing data from 1,173 plant species: The 1000 Plant transcriptomes initiative (1KP). *GigaScience*, *8*(10).

Carpentier, M.-C., Deragon, J.-M., Jean, V., Be, S. H. V., Bousquet-Antonelli, C., & Merret, R. (2020). Monitoring of XRN4 Targets Reveals the Importance of Cotranslational Decay during Arabidopsis Development. *Plant Physiology*, *184*(3), 1251–1262.

Changeux, J.-P., & Paas, Y. (2009). Nicotinic Acetylcholine Receptors. In L. R. Squire (Ed.), *Encyclopedia of Neuroscience* (pp. 1129–1133). Academic Press.

Chen, S., Novick, P., & Ferro-Novick, S. (2013). ER structure and function. *Current Opinion in Cell Biology*, *25*(4), 428–433.

Chen, X., Liu, P., Mei, L., He, X., Chen, L., Liu, H., Shen, S., Ji, Z., Zheng, X., Zhang, Y., Gao, Z., Zeng, D., Qian, Q., & Ma, B. (2021). Xa7, a new executor R gene that confers durable and broad-spectrum resistance to bacterial blight disease in rice. *Plant Communications*, *2*(3), 100143.

Cheng, C.-P., Jaag, H. M., Jonczyk, M., Serviene, E., & Nagy, P. D. (2007). Expression of the Arabidopsis Xrn4p 5'-3' exoribonuclease facilitates degradation of tombusvirus RNA and promotes rapid emergence of viral variants in plants. *Virology*, *368*(2), 238–248.

Cheng, C.-Y., Krishnakumar, V., Chan, A. P., Thibaud-Nissen, F., Schobel, S., & Town, C. D. (2017). Araport11: a complete reannotation of the Arabidopsis thaliana reference genome. *The Plant Journal: For Cell and Molecular Biology*, *89*(4), 789–804.

Choi, J. K., Bae, J.-B., Lyu, J., Kim, T.-Y., & Kim, Y.-J. (2009). Nucleosome deposition and DNA methylation at coding region boundaries. *Genome Biology*, *10*(9), R89.

Connolly, C. N., Krishek, B. J., McDonald, B. J., Smart, T. G., & Moss, S. J. (1996). Assembly and Cell Surface Expression of Heteromeric and Homomeric γ-Aminobutyric Acid Type A Receptors. *The Journal of Biological Chemistry*, *271*(1), 89–96.

Cook, A. A., & Guevara, Y. G. (1984). Hypersensitivity in Capsicum chacoense to race 1 of the bacterial spot pathogen of pepper. *Plant Disease*, *68*(4), 329.

Cook, A. A., & Stall, R. E. (1963). Inheritance of resistance in pepper to bacterial spot. *Phytopathology*, *53*, 1060–1062.

Costa, A., Navazio, L., & Szabo, I. (2018). The contribution of organelles to plant intracellular Calcium signalling. *Journal of Experimental Botany*, *69*(7), 4175–4193.

Couto, D., & Zipfel, C. (2016). Regulation of pattern recognition receptor signalling in plants. *Nature Reviews Immunology*, *16*(9), 537–552.

Daneva, A., Gao, Z., Van Durme, M., & Nowack, M. K. (2016). Functions and Regulation of Programmed Cell Death in Plant Development. *Annual Review of Cell and Developmental Biology*, *32*, 441–468.

Dangl, J. L., & Jones, J. D. G. (2019). A pentangular plant inflammasome. *Science*, *364*(6435), 31–32.

De Vriese, K., Costa, A., Beeckman, T., & Vanneste, S. (2018). Pharmacological Strategies for Manipulating Plant Ca2+ Signalling. *International Journal of Molecular Sciences*, *19*(5), 1506.

Decaestecker, W., Buono, R. A., Pfeiffer, M. L., Vangheluwe, N., Jourquin, J., Karimi, M., Van Isterdael, G., Beeckman, T., Nowack, M. K., & Jacobs, T. B. (2019). CRISPR-TSKO: A Technique for Efficient Mutagenesis in Specific Cell Types, Tissues, or Organs in Arabidopsis. *The Plant Cell*, *31*(12), 2868–2887.

DeFalco, T. A., Bender, K. W., & Snedden, W. A. (2009). Breaking the code: Ca2+ sensors in plant signalling. *Biochemical Journal*, *425*(1), 27–40.

Demidchik, V., Shabala, S., Isayenkov, S., Cuin, T. A., & Pottosin, I. (2018). Calcium transport across plant membranes: mechanisms and functions. *The New Phytologist*, *220*(1), 49–69.

Dodd, A. N., Kudla, J., & Sanders, D. (2010). The language of calcium signaling. *Annual Review of Plant Biology*, *61*, 593–620.

Domka, J., Lee, J., & Wood, T. K. (2006). YliH (BssR) and YceP (BssS) regulate Escherichia coli K-12 biofilm formation by influencing cell signaling. *Applied and Environmental Microbiology*, *72*(4), 2449–2459.

Doyle, E. L., Booher, N. J., Standage, D. S., Voytas, D. F., Brendel, V. P., Vandyk, J. K., & Bogdanove, A. J. (2012). TAL Effector-Nucleotide Targeter (TALE-NT) 2.0: tools for TAL effector design and target prediction. *Nucleic Acids Research*, *40*(W1), W117-22.

Dubiella, U., Seybold, H., Durian, G., Komander, E., Lassig, R., Witte, C.-P., Schulze, W. X., & Romeis, T. (2013). Calcium-dependent protein kinase/NADPH oxidase activation circuit is required for rapid defense signal propagation. *Proceedings of the National Academy of Sciences of the United States of America*, *110*(21), 8744–8749.

El Kasmi, F., Chung, E.-H., Anderson, R. G., Li, J., Wan, L., Eitas, T. K., Gao, Z., & Dangl, J. L. (2017). Signaling from the plasma-membrane localized plant immune receptor RPM1 requires self-association of the full-length protein. *Proceedings of the National Academy of Sciences*, *114*(35), E7385–E7394.

Elsaesser, J. (2014). *Functional characterisation of Bs4C-R*.

Esgalhado, M. E., Roseiro, J. C., & Collaço, M. T. A. (1995). Interactive Effects of pH and Temperature on Cell Growth and Polymer Production by Xanthomonas campestris. *Process Biochemistry*, *30*(7), 667–671.

Evans, R., O'Neill, M., Pritzel, A., Antropova, N., Senior, A., Green, T., Žídek, A., Bates, R., Blackwell, S., Yim, J., Ronneberger, O., Bodenstein, S., Zielinski, M., Bridgland, A., Potapenko, A., Cowie, A., Tunyasuvunakool, K., Jain, R., Clancy, E., Kohli, P., Jumper, J., & Hassabis, D. (2022). Protein complex prediction with AlphaFold-Multimer. In *bioRxiv* (p. 2021.10.04.463034).

Feng, Z., Zhang, B., Ding, W., Liu, X., Yang, D.-L., Wei, P., Cao, F., Zhu, S., Zhang, F., Mao, Y., & Zhu, J.-K. (2013). Efficient genome editing in plants using a CRISPR/Cas system. *Cell Research*, *23*(10), 1229–1232.

Flor, H. H. (1955). Host-parasite interaction in flax rust - Its genetics and other implications. *Phytopathology*, *45*, 680–685.

Gadsby, D. C. (2009). Ion channels versus ion pumps: the principal difference, in principle. *Nature Reviews Molecular Cell Biology*, *10*(5), 344–352.

García Bossi, J., Kumar, K., Barberini, M. L., Domínguez, G. D., Rondón Guerrero, Y. D. C., Marino-Buslje, C., Obertello, M., Muschietti, J. P., & Estevez, J. M. (2020). The role of P-type IIA and P-type IIB Ca2+-ATPases in plant development and growth. *Journal of Experimental Botany*, *71*(4), 1239–1248.

Garcia, V., Bres, C., Just, D., Fernandez, L., Tai, F. W. J., Mauxion, J.-P., Le Paslier, M.-C., Bérard, A., Brunel, D., Aoki, K., Alseekh, S., Fernie, A. R., Fraser, P. D., & Rothan, C. (2016). Rapid identification of causal mutations in tomato EMS populations via mapping-by-sequencing. *Nature Protocols*, *11*(12), 2401–2418.

Gaul, H. (1965). *Selection in M1 generation after mutagenic treatment of barley seeds*. Publishing House of the Czechoslovak Academy of Sciences.

Gazzani, S., Lawrenson, T., Woodward, C., Headon, D., & Sablowski, R. (2004). A link between mRNA turnover and RNA interference in Arabidopsis. *Science*, *306*(5698), 1046–1048.

Giovannoni, J. J. (2004). Genetic regulation of fruit development and ripening. *The Plant Cell*, *16 Suppl*(Suppl), S170-80.

Gitaitis, R., & Walcott, R. (2007). The epidemiology and management of seedborne bacterial diseases. *Annual Review of Phytopathology*, *45*, 371–397.

Glykys, J., & Mody, I. (2007). Activation of GABAA receptors: views from outside the synaptic cleft. *Neuron*, *56*(5), 763–770.

Greenberg, J. T. (1997). Programmed cell death in plant-pathogen interactions. *Annual Review of Plant*, *48*, 525–545.

Gu, K., Yang, B., Tian, D., Wu, L., Wang, D., Sreekala, C., Yang, F., Chu, Z., Wang, G.-L., White, F. F., & Yin, Z. (2005). R gene expression induced by a type-III effector triggers disease resistance in rice. *Nature*, *435*(7045), 1122–1125.

Hayward, A., Padmanabhan, M., & Dinesh-Kumar, S. P. (2011). Virus-Induced Gene Silencing in Nicotiana benthamiana and Other Plant Species. In A. Pereira (Ed.), *Plant Reverse Genetics: Methods and Protocols* (pp. 55–63). Humana Press.

He, Y., Zhang, T., Sun, H., Zhan, H., & Zhao, Y. (2020). A reporter for noninvasively monitoring gene expression and plant transformation. *Horticulture Research*, *7*(1), 152.

Higgins, B. B. (1922). The bacterial spot of pepper. *Phytopathology*, *12*, 501–517.

Hodgens, C., Chang, N., Schaller, G. E., & Kieber, J. J. (2020). Mutagenomics: A Rapid, High-Throughput Method to Identify Causative Mutations from a Genetic Screen. *Plant Physiology*, *184*(4), 1658–1673.

Holm, L., & Sander, C. (1993). Protein structure comparison by alignment of distance matrices. *Journal of Molecular Biology*, *233*(1), 123–138.

Holm, Liisa. (2020). Using Dali for Protein Structure Comparison. In Z. Gáspári (Ed.), *Structural Bioinformatics: Methods and Protocols* (pp. 29–42). Springer US.

Holm, Liisa. (2022). Dali server: structural unification of protein families. *Nucleic Acids Research*, *50*(W1), W210–W215.

Holsters, M., Silva, B., Van Vliet, F., Genetello, C., De Block, M., Dhaese, P., Depicker, A., Inzé, D., Engler, G., & Villarroel, R. (1980). The functional organization of the nopaline A. tumefaciens plasmid pTiC58. *Plasmid*, *3*(2), 212–230.

Huang, Y.-P., Huang, Y.-W., Chen, I.-H., Shenkwen, L.-L., Hsu, Y.-H., & Tsai, C.-H. (2017). Plasma membrane-associated cation-binding protein 1-like protein negatively regulates intercellular movement of BaMV. *Journal of Experimental Botany*, *68*(17), 4765–4774.

Huysmans, M., Lema A, S., Coll, N. S., & Nowack, M. K. (2017). Dying two deaths - programmed cell death regulation in development and disease. *Current Opinion in Plant Biology*, *35*, 37–44.

Hwang, I., Sze, H., & Harper, J. F. (2000). A calcium-dependent protein kinase can inhibit a calmodulin-stimulated Ca^{2+} pump (ACA2) located in the endoplasmic reticulum of *Arabidopsis*. *Proceedings of the National Academy of Sciences of the United States of America*, *97*(11), 6224–6229.

Inesi, G. (1985). Mechanism of calcium transport. *Annual Review of Physiology*, *47*, 573–601.

Irastortza-Olaziregi, M., & Amster-Choder, O. (2020). Coupled Transcription-Translation in Prokaryotes: An Old Couple With New Surprises. *Frontiers in Microbiology*, *11*, 624830.

Jaag, H. M., & Nagy, P. D. (2009). Silencing of Nicotiana benthamiana Xrn4p exoribonuclease promotes tombusvirus RNA accumulation and recombination. *Virology*, *386*(2), 344–352.

Jacob, P., Kim, N. H., Wu, F., El Kasmi, F., Chi, Y., Walton, W. G., Furzer, O. J., Lietzan, A. D., Sunil, S., Kempthorn, K., Redinbo, M. R., Pei, Z.-M., Wan, L., & Dangl, J. L. (2021). Plant 'helper' immune receptors are Ca2+-permeable nonselective cation channels. *Science*, *373*(6553), 420–425.

Jain, M., Khurana, P., Tyagi, A. K., & Khurana, J. P. (2008). Genome-wide analysis of intronless genes in rice and Arabidopsis. *Functional & Integrative Genomics*, *8*(1), 69–78.

Janeway, C. A., Jr, Travers, P., Walport, M., & Shlomchik, M. J. (2001). *Principles of innate and adaptive immunity*. Garland Science.

Ji, Z., Guo, W., Chen, X., Wang, C., & Zhao, K. (2022). Plant Executor Genes. *International Journal of Molecular Sciences*, *23*(3), 1524.

Jiang, S., Jiang, L., Yang, J., Peng, J., Lu, Y., Zheng, H., Lin, L., Chen, J., & Yan, F. (2018). Over-expression of Oryza sativa Xrn4 confers plant resistance to virus infection. *Gene*, *639*, 44–51.

Jinek, M., Chylinski, K., Fonfara, I., Hauer, M., Doudna, J. A., & Charpentier, E. (2012). A programmable dual-RNA-guided DNA endonuclease in adaptive bacterial immunity. *Science*, *337*(6096), 816–821.

Jones, J. B., Lacy, G. H., Bouzar, H., Stall, R. E., & Schaad, N. W. (2004). Reclassification of the xanthomonads associated with bacterial spot disease of tomato and pepper. *Systematic and Applied Microbiology*, *27*(6), 755–762.

Jones, J. B., Minsavage, G. V., Roberts, P. D., Johnson, R. R., Kousik, C. S., Subramanian, S., & Stall, R. E. (2002). A Non-Hypersensitive Resistance in Pepper to the Bacterial Spot Pathogen Is Associated with Two Recessive Genes. *Phytopathology*, *92*(3), 273–277.

Jones, J. D. G., & Dangl, J. L. (2006). The plant immune system. *Nature*, *444*(7117), 323–329.

Jones, J. D. G., Vance, R. E., & Dangl, J. L. (2016). Intracellular innate immune surveillance devices in plants and animals. *Science*, *354*(6316).

Jumper, J., Evans, R., Pritzel, A., Green, T., Figurnov, M., Ronneberger, O., Tunyasuvunakool, K., Bates, R., Žídek, A., Potapenko, A., Bridgland, A., Meyer, C., Kohl, S. A. A., Ballard, A. J., Cowie, A., Romera-Paredes, B., Nikolov, S., Jain, R., Adler, J., Back, T., Petersen, S., Reiman, D., Clancy, E., Zielinski, M., Steinegger, M., Pacholska, M., Berghammer, T., Bodenstein, S., Silver, D., Vinyals, O., Senior A. W., Kavukcuoglu, K., Kohli, P., & Hassabis, D. (2021). Highly accurate protein structure prediction with AlphaFold. *Nature*, *596*(7873), 583–589.

Jürgens, G., Mayer, U., Ramon A., T. R., Berleth, T., & Miséra, S. (1991). Genetic analysis of pattern formation in the Arabidopsis embryo. *Development* , *113*(Supplement_1), 27–38.

Kaila, K., Pasternack, M., Saarikoski, J., & Voipio, J. (1989). Influence of GABA-gated bicarbonate conductance on potential, current and intracellular chloride in crayfish muscle fibres. *The Journal of Physiology*, *416*, 161–181.

Karlova, R., Chapman, N., David, K., Angenent, G. C., Seymour, G. B., & de Maagd, R. A. (2014). Transcriptional control of fleshy fruit development and ripening. *Journal of Experimental Botany*, *65*(16), 4527–4541.

Kastenmayer, J. P., & Green, P. J. (2000). Novel features of the XRN-family in Arabidopsis: evidence that AtXRN4, one of several orthologs of nuclear Xrn2p/Rat1p, functions in the cytoplasm. *Proceedings of the National Academy of Sciences of the United States of America*, *97*(25), 13985–13990.

Kim, B. S., & Hartmann, R. W. (1985). Inheritance of a gene (Bs3) conferring hypersensitive resistance to Xanthomonas campestris pv. vesicatoria in pepper (Capsicum annuum). *Plant Disease*, *69*, 233–235.

Kim, J. J., Gharpure, A., Teng, J., Zhuang, Y., Howard, R. J., Zhu, S., Noviello, C. M., Walsh, R. M., Jr, Lindahl, E., & Hibbs, R. E. (2020). Shared structural mechanisms of general anaesthetics and benzodiazepines. *Nature*, *585*(7824), 303–308.

Kim, Y., Schumaker, K. S., & Zhu, J.-K. (2006). EMS Mutagenesis of Arabidopsis. In J. Salinas & J. J. Sanchez-Serrano (Eds.), *Arabidopsis Protocols* (pp. 101–103). Humana Press.

Kimbrell, D. A., & Beutler, B. (2001). The evolution and genetics of innate immunity. *Nature Reviews Genetics*, *2*(4), 256–267.

Klement, Z. (1982). Hypersensitivity. *Phytopathogenic Prokaryotes*, *2*, 149–177.

Klement, Z., & Goodman, R. N. (1967). The Hypersensitive Reaction to Infection by Bacterial Plant Pathogens. *Annual Review of Phytopathology*, *5*(1), 17–44.

Knight, M. R., Campbell, A. K., Smith, S. M., & Trewavas, A. J. (1991). Transgenic plant aequorin reports the effects of touch and cold-shock and elicitors on cytoplasmic calcium. *Nature*, *352*(6335), 524–526.

Koebnik, R. (2023, February 17). *Type III Effectors from Xanthomonas*. EuroXanth. https://euroxanth.ipn.pt/doku.php?id=bacteria:t3e:t3e

Koornneeff, M., Dellaert, L. W. M., & van der Veen, J. H. (1982). EMS- and relation-induced mutation frequencies at individual loci in Arabidopsis thaliana (L.) Heynh. *Mutation Research/Fundamental and Molecular Mechanisms of Mutagenesis*, *93*(1), 109–123.

Köster, P., DeFalco, T. A., & Zipfel, C. (2022). Ca2+ signals in plant immunity. *The EMBO Journal*, *41*(12), e110741.

Kourelis, J., Kaschani, F., Grosse-Holz, F. M., Homma, F., Kaiser, M., & van der Hoorn, R. A. L. (2019). A homology-guided, genome-based proteome for improved proteomics in the alloploid Nicotiana benthamiana. *BMC Genomics*, *20*(1), 722.

Kourelis, J., & van der Hoorn, R. A. L. (2018). Defended to the Nines: 25 Years of Resistance Gene Cloning Identifies Nine Mechanisms for R Protein Function. *The Plant Cell*, *30*(2), 285–299.

Krogh, A., Larsson, B., von Heijne, G., & Sonnhammer, E. L. (2001). Predicting transmembrane protein topology with a hidden Markov model: application to complete genomes. *Journal of Molecular Biology*, *305*(3), 567–580.

Krönauer, C. (2019). *Functional and biochemical analysis of the Capsicum annuum resistance protein Bs3* (T. Lahaye, Ed.) [Doctorate of Natural Sciences]. Eberhard Karls Universität Tübingen.

Krönauer, C., Kilian, J., Strauß, T., Stahl, M., & Lahaye, T. (2019). Cell Death Triggered by the YUCCA-like Bs3 Protein Coincides with Accumulation of Salicylic Acid and Pipecolic Acid But Not of Indole-3-Acetic Acid. *Plant Physiology*, *180*(3), 1647–1659.

Kufareva, I., & Abagyan, R. (2012). Methods of protein structure comparison. *Methods in Molecular Biology* , *857*, 231–257.

Kuhn, L., Vincent, T., Hammann, P., & Zuber, H. (2023). Exploring Protein Interactome Data with IPinquiry: Statistical Analysis and Data Visualization by Spectral Counts. In T. Burger (Ed.), *Statistical Analysis of Proteomic Data: Methods and Tools* (pp. 243–265). Springer US.

Leide, J., Hildebrandt, U., Hartung, W., Riederer, M., & Vogg, G. (2012). Abscisic acid mediates the formation of a suberized stem scar tissue in tomato fruits. *The New Phytologist*, *194*(2), 402–415.

Li, F., & Wang, A. (2018). RNA decay is an antiviral defense in plants that is counteracted by viral RNA silencing suppressors. *PLoS Pathogens*, *14*(8), e1007228.

Li, T., Natran, A., Chen, Y., Vercruysse, J., Wang, K., Gonzalez, N., Dubois, M., & Inzé, D. (2019). A genetics screen highlights emerging roles for CPL3, RST1 and URT1 in RNA metabolism and silencing. *Nature Plants*, *5*(5), 539–550.

Liang, F., & Sze, H. (1998). A high-affinity Ca2+ pump, ECA1, from the endoplasmic reticulum is inhibited by cyclopiazonic acid but not by thapsigargin. *Plant Physiology*, *118*(3), 817–825.

Lin, L.-Y., Ching, C.-L., Chin, K.-H., Chou, S.-H., & Chan, N.-L. (2006). Crystal structure of the conserved hypothetical cytosolic protein Xcc0516 from Xanthomonas campestris reveals a novel quaternary structure assembled by five four-helix bundles. *Proteins*, *65*(3), 783–786.

Lin, Z., Akin, H., Rao, R., Hie, B., Zhu, Z., Lu, W., Smetanin, N., Verkuil, R., Kabeli, O., Shmueli, Y., dos Santos Costa, A., Fazel-Zarandi, M., Sercu, T., Candido, S., & Rives, A. (2022). Evolutionary-scale prediction of atomic level protein structure with a language model. In *bioRxiv* (p. 2022.07.20.500902). https://www.biorxiv.org/content/10.1101/2022.07.20.500902v3.full

Liu, H., Lyu, H.-M., Zhu, K., Van de Peer, Y., & Max Cheng, Z.-M. (2021). The emergence and evolution of intron-poor and intronless genes in intron-rich plant gene families. *The Plant Journal: For Cell and Molecular Biology*, *105*(4), 1072–1082.

Luo, D., Huguet-Tapia, J. C., Raborn, R. T., White, F. F., Brendel, V. P., & Yang, B. (2021). The Xa7 resistance gene guards the rice susceptibility gene SWEET14 against exploitation by the bacterial blight pathogen. *Plant Communications*, *2*(3), 100164.

M. De Swart, E. A., Marcelis, L. F. M., & Voorrips, R. E. (2006). Variation in relative growth rate and growth traits in wild and cultivated Capsicum accessions grown under different temperatures. *The Journal of Horticultural Science & Biotechnology*, *81*(6), 1029–1037.

Marimon, O., Teixeira, J. M. C., Cordeiro, T. N., Soo, V. W. C., Wood, T. L., Mayzel, M., Amata, I., García, J., Morera, A., Gay, M., Vilaseca, M., Orekhov, V. Y., Wood, T. K., & Pons, M. (2016). An oxygen-sensitive toxin-antitoxin system. *Nature Communications*, *7*, 13634.

Minsavage, G. V., Dahlbeck, D., Whalen, M. C., Kearney, B., Bonas, U., Staskawicz, B. J., & Stall, R. E. (1990). Gene-for-gene relationships specifying disease resistance in Xanthomonas campestris pv. vesicatoria-pepper interactions. *Molecular Plant-Microbe Interactions: MPMI*, *3*(1), 41–47.

Mirdita, M., Schütze, K., Moriwaki, Y., Heo, L., Ovchinnikov, S., & Steinegger, M. (2022). ColabFold: making protein folding accessible to all. *Nature Methods*, *19*(6), 679–682.

Morbitzer, R., Römer, P., Boch, J., & Lahaye, T. (2010). Regulation of selected genome loci using de novo-engineered transcription activator-like effector (TALE)-type transcription factors. *Proceedings of the National Academy of Sciences of the United States of America*, *107*(50), 21617–21622.

Moscou, M. J., & Bogdanove, A. J. (2009). A simple cipher governs DNA recognition by TAL effectors. *Science*, *326*(5959), 1501.

Nomura, K., Debroy, S., Lee, Y. H., Pumplin, N., Jones, J., & He, S. Y. (2006). A bacterial virulence protein suppresses host innate immunity to cause plant disease. *Science*, *313*(5784), 220–223.

Nowack, M. K., Holmes, D. R., & Lahaye, T. (2022). TALE-induced cell death executors: an origin outside immunity? *Trends in Plant Science*, *27*(6), 536–548.

Olsen, R. W., & Tobin, A. J. (1990). Molecular biology of GABAA receptors. *FASEB Journal: Official Publication of the Federation of American Societies for Experimental Biology*, *4*(5), 1469–1480.

Olvera-Carrillo, Y., Van Bel, M., Van Hautegem, T., Fendrych, M., Huysmans, M., Simaskova, M., van Durme, M., Buscaill, P., Rivas, S., Coll, N. S., Coppens, F., Maere, S., & Nowack, M. K. (2015). A Conserved Core of Programmed Cell Death Indicator Genes Discriminates Developmentally and Environmentally Induced Programmed Cell Death in Plants. *Plant Physiology*, *169*(4), 2684–2699.

Ortells, M. O., & Lunt, G. G. (1995). Evolutionary history of the ligand-gated ion-channel superfamily of receptors. *Trends in Neurosciences*, *18*(3), 121–127.

Osdaghi, E., Jones, J. B., Sharma, A., Goss, E. M., Abrahamian, P., Newberry, E. A., Potnis, N., Carvalho, R., Choudhary, M., Paret, M. L., Timilsina, S., & Vallad, G. E. (2021). A centenary for bacterial spot of tomato and pepper. *Molecular Plant Pathology*, *22*(12), 1500–1519.

Page, D. R., & Grossniklaus, U. (2002). The art and design of genetic screens: Arabidopsis thaliana. *Nature Reviews. Genetics*, *3*(2), 124–136.

Pain, C., Kriechbaumer, V., Kittelmann, M., Hawes, C., & Fricker, M. (2019). Quantitative analysis of plant ER architecture and dynamics. *Nature Communications*, *10*(1), 984.

Paschen, W. (2004). Endoplasmic reticulum dysfunction in brain pathology: critical role of protein synthesis. *Current Neurovascular Research*, *1*(2), 173–181.

Pech, J.-C., Purgatto, E., Bouzayen, M., & Latché, A. (2012). Ethylene and Fruit Ripening. *Annual Plant Reviews, 44,* 275–304.

Penella, C., & Calatayud, A. (2018). Pepper Crop under Climate Change: Grafting as an Environmental Friendly Strategy. In *Climate Resilient Agriculture - Strategies and Perspectives* (pp. 129–155).

Peng, J., Yang, J., Yan, F., Lu, Y., Jiang, S., Lin, L., Zheng, H., Chen, H., & Chen, J. (2011). Silencing of NbXrn4 facilitates the systemic infection of Tobacco mosaic virus in Nicotiana benthamiana. *Virus Research*, *158*(1–2), 268–270.

Pettersen, E. F., Goddard, T. D., Huang, C. C., Meng, E. C., Couch, G. S., Croll, T. I., Morris, J. H., & Ferrin, T. E. (2021). UCSF ChimeraX: Structure visualization for researchers, educators, and developers. *Protein Science: A Publication of the Protein Society*, *30*(1), 70–82.

Pirayesh, N., Giridhar, M., Ben Khedher, A., Vothknecht, U. C., & Chigri, F. (2021). Organellar calcium signaling in plants: An update. *Biochimica et Biophysica Acta, Molecular Cell Research*, *1868*(4), 118948.

Potnis, N., Minsavage, G., Smith, J. K., Hurlbert, J. C., Norman, D., Rodrigues, R., Stall, R. E., & Jones, J. B. (2012). Avirulence proteins AvrBs7 from Xanthomonas gardneri and AvrBs1.1 from Xanthomonas euvesicatoria contribute to a novel gene-for-gene interaction in pepper. *Molecular Plant-Microbe Interactions: MPMI*, *25*(3), 307–320.

Potnis, N., Timilsina, S., Strayer, A., Shantharaj, D., Barak, J. D., Paret, M. L., Vallad, G. E., & Jones, J. B. (2015). Bacterial spot of tomato and pepper: diverse Xanthomonas species with a wide variety of virulence factors posing a worldwide challenge. *Molecular Plant Pathology*, *16*(9), 907–920.

Potuschak, T., Vansiri, A., Binder, B. M., Lechner, E., Vierstra, R. D., & Genschik, P. (2006). The exoribonuclease XRN4 is a component of the ethylene response pathway in Arabidopsis. *The Plant Cell*, *18*(11), 3047–3057.

Qu, L.-J., & Qin, G. (2014). Generation and Identification of Arabidopsis EMS Mutants. In J. J. Sanchez-Serrano & J. Salinas (Eds.), *Arabidopsis Protocols* (pp. 225–239). Humana Press.

Raffeiner, M., Üstün, S., Guerra, T., Spinti, D., Fitzner, M., Sonnewald, S., Baldermann, S., & Börnke, F. (2022). The Xanthomonas type-III effector XopS stabilizes CaWRKY40a to regulate defense responses and stomatal immunity in pepper (Capsicum annuum). *The Plant Cell*, *34*(5), 1684–1708.

Rahman, M. M., Teng, J., Worrell, B. T., Noviello, C. M., Lee, M., Karlin, A., Stowell, M. H. B., & Hibbs, R. E. (2020). Structure of the Native Muscle-type Nicotinic Receptor and Inhibition by Snake Venom Toxins. *Neuron*, *106*(6), 952-962.e5.

Ranty, B., Aldon, D., Cotelle, V., Galaud, J.-P., Thuleau, P., & Mazars, C. (2016). Calcium Sensors as Key Hubs in Plant Responses to Biotic and Abiotic Stresses. *Frontiers in Plant Science*, *7*, 327.

Ren, H., Zhao, X., Li, W., Hussain, J., Qi, G., & Liu, S. (2021). Calcium Signaling in Plant Programmed Cell Death. *Cells* , *10*(5), 1089.

Resentini, F., Grenzi, M., Ancora, D., Cademartori, M., Luoni, L., Franco, M., Bassi, A., Bonza, M. C., & Costa, A. (2021). Simultaneous imaging of ER and cytosolic Ca2+ dynamics reveals long-distance ER Ca2+ waves in plants. *Plant Physiology*, *187*(2), 603–617.

Römer, P., Hahn, S., Jordan, T., Strauss, T., Bonas, U., & Lahaye, T. (2007). Plant pathogen recognition mediated by promoter activation of the pepper Bs3 resistance gene. *Science*, *318*(5850), 645–648.

Ryan, R. P., Vorhölter, F.-J., Potnis, N., Jones, J. B., Van Sluys, M.-A., Bogdanove, A. J., & Dow, J. M. (2011). Pathogenomics of Xanthomonas: understanding bacterium-plant interactions. *Nature Reviews Microbiology*, *9*(5), 344–355.

Rymarquis, L. A., Souret, F. F., & Green, P. J. (2011). Evidence that XRN4, an Arabidopsis homolog of exoribonuclease XRN1, preferentially impacts transcripts with certain sequences or in particular functional categories. *RNA* , *17*(3), 501–511.

Sahin, F., & Miller, S. A. (1998). Resistance in Capsicum pubescens to Xanthomonas campestris pv. vesicatoria Pepper Race 6. *Plant Disease*, *82*(7), 794–799.

Salari, R., Murlidaran, S., & Brannigan, G. (2014). Pentameric Ligand-gated Ion Channels: Insights from Computation. *Molecular Simulation*, *40*(10–11), 821–829.

Schenstnyi, K., Straußß, A., Dressel, A., Morbitzer, R., Wunderlich, M., Andrade, A. G., Phan, T.-T.-T., de Los Angeles Aguilera, P., Brancato, C., Berendzen, K. W., & Lahaye, T. (2022). The tomato resistance gene Bs4 suppresses leaf watersoaking phenotypes induced by AvrHah1, a transcription activator-like effector from tomato-pathogenic xanthomonads. *The New Phytologist*. https://doi.org/10.1111/nph.18456

Schindelin, J., Arganda-Carreras, I., Frise, E., Kaynig, V., Longair, M., Pietzsch, T., Preibisch, S., Rueden, C., Saalfeld, S., Schmid, B., Tinevez, J.-Y., White, D. J., Hartenstein, V., Eliceiri, K., Tomancak, P., & Cardona, A. (2012). Fiji: an open-source platform for biological-image analysis. *Nature Methods*, *9*(7), 676–682.

Schneeberger, K., Ossowski, S., Lanz, C., Juul, T., Petersen, A. H., Nielsen, K. L., Jørgensen, J.-E., Weigel, D., & Andersen, S. U. (2009). SHOREmap: simultaneous mapping and mutation identification by deep sequencing. *Nature Methods*, *6*(8), 550–551.

Schornack, S., Ballvora, A., Gürlebeck, D., Peart, J., Baulcombe, D., Ganal, M., Baker, B., Bonas, U., & Lahaye, T. (2004). The tomato resistance protein Bs4 is a predicted non-nuclear TIR-NB-LRR protein that mediates defense responses to severely truncated derivatives of AvrBs4 and overexpressed AvrBs3. *The Plant Journal: For Cell and Molecular Biology*, *37*(1), 46–60.

Schultink, A., Qi, T., Lee, A., Steinbrenner, A. D., & Staskawicz, B. (2017). Roq1 mediates recognition of the Xanthomonas and Pseudomonas effector proteins XopQ and HopQ1. *The Plant Journal: For Cell and Molecular Biology*, *92*(5), 787–795.

Seppelt, R., Klotz, S., Peiter, E., & Volk, M. (2022). Agriculture and food security under a changing climate: An underestimated challenge. *iScience*, *25*(12), 105551.

Seybold, H., Trempel, F., Ranf, S., Scheel, D., Romeis, T., & Lee, J. (2014). Ca2+ signalling in plant immune response: from pattern recognition receptors to Ca2+ decoding mechanisms. *The New Phytologist*, *204*(4), 782–790.

Sharma, A., Li, J., Wente, R., Minsavage, G. V., Gill, U. S., Ortega, A., Vallejos, C. E., Hart, J. P., Staskawicz, B. J., Mazourek, M. R., Stall, R. E., Jones, J. B., & Hutton, S. F. (2023). Mapping of the bs5 and bs6 non-race-specific recessive resistances against bacterial spot of pepper. *Frontiers in Plant Science*, *14*, 1061803.

Shinozaki, Y., Nicolas, P., Fernandez-Pozo, N., Ma, Q., Evanich, D. J., Shi, Y., Xu, Y., Zheng, Y., Snyder, S. I., Martin, L. B. B., Ruiz-May, E., Thannhauser, T. W., Chen, K., Domozych, D. S., Catalá, C., Fei, Z., Mueller, L. A., Giovannoni, J. J., & Rose, J. K. C. (2018). High-resolution spatiotemporal transcriptome mapping of tomato fruit development and ripening. *Nature Communications*, *9*(1), 364.

Shu, C. H., & Yang, S. T. (1990). Effects of temperature on cell growth and xanthan production in batch cultures of Xanthomonas campestris. *Biotechnology and Bioengineering*, *35*(5), 454–468.

Souret, F. F., Kastenmayer, J. P., & Green, P. J. (2004). AtXRN4 degrades mRNA in Arabidopsis and its substrates include selected miRNA targets. *Molecular Cell*, *15*(2), 173–183.

Stael, S., Wurzinger, B., Mair, A., Mehlmer, N., Vothknecht, U. C., & Teige, M. (2012). Plant organellar calcium signalling: an emerging field. *Journal of Experimental Botany*, *63*(4), 1525–1542.

Stall, R. E., Jones, J. B., & Minsavage, G. V. (2009). Durability of resistance in tomato and pepper to xanthomonads causing bacterial spot. *Annual Review of Phytopathology*, *47*, 265–284.

Staskawicz, B. J. (2001). Genetics of plant-pathogen interactions specifying plant disease resistance. *Plant Physiology*, *125*(1), 73–76.

Steinegger, M., & Söding, J. (2017). MMseqs2 enables sensitive protein sequence searching for the analysis of massive data sets. *Nature Biotechnology*, *35*(11), 1026–1028.

Stephenson, J. L. M., & Hawes, C. R. (1986). Stereology and stereometry of endoplasmic reticulum during differentiation in the maize root cap. *Protoplasma*, *131*(1), 32–46.

Strauß, T., van Poecke, R. M. P., Strauß, A., Römer, P., Minsavage, G. V., Singh, S., Wolf, C., Strauß, A., Kim, S., Lee, H.-A., Yeom, S.-I., Parniske, M., Stall, R. E., Jones, J. B., Choi, D., Prins, M., & Lahaye, T. (2012). RNA-seq pinpoints a *Xanthomonas* TAL-effector activated resistance gene in a large-crop genome. *Proceedings of the National Academy of Sciences of the United States of America*, *109*(47), 19480–19485.

Streubel, J., Pesce, C., Hutin, M., Koebnik, R., Boch, J., & Szurek, B. (2013). Five phylogenetically close rice SWEET genes confer TAL effector-mediated susceptibility to Xanthomonas oryzae pv. oryzae. *The New Phytologist*, *200*(3), 808–819.

Stuttmann, J., Barthel, K., Martin, P., Ordon, J., Erickson, J. L., Herr, R., Ferik, F., Kretschmer, C., Berner, T., Keilwagen, J., Marillonnet, S., & Bonas, U. (2021). Highly efficient multiplex editing: one-shot generation of 8× Nicotiana benthamiana and 12× Arabidopsis mutants. *The Plant Journal: For Cell and Molecular Biology*, *106*(1), 8–22.

Sun, H., & Schneeberger, K. (2015). SHOREmap v3.0: Fast and Accurate Identification of Causal Mutations from Forward Genetic Screens. In J. M. Alonso & A. N. Stepanova (Eds.), *Plant Functional Genomics: Methods and Protocols* (pp. 381–395). Springer New York.

Suzek, B. E., Wang, Y., Huang, H., McGarvey, P. B., Wu, C. H., & UniProt Consortium. (2015). UniRef clusters: a comprehensive and scalable alternative for improving sequence similarity searches. *Bioinformatics* , *31*(6), 926–932.

Thor, K. (2019). Calcium-Nutrient and Messenger. *Frontiers in Plant Science*, *10*, 440.

Thor, K., Jiang, S., Michard, E., George, J., Scherzer, S., Huang, S., Dindas, J., Derbyshire, P., Leitão, N., DeFalco, T. A., Köster, P., Hunter, K., Kimura, S., Gronnier, J., Stransfeld, L., Kadota, Y., Bücherl, C. A., Charpentier, M., Wrzaczek, M., MacLean, D., Oldroyd, G. E. D., Menke, F. L. H., Roelfsema, M. R. G., Hedrich, R., & Zipfel, C. (2020). The calcium-permeable channel OSCA1.3 regulates plant stomatal immunity. *Nature*, *585*(7826), 569–573.

Tian, D., Wang, J., Zeng, X., Gu, K., Qiu, C., Yang, X., Zhou, Z., Goh, M., Luo, Y., Murata-Hori, M., White, F. F., & Yin, Z. (2014). The rice TAL effector-dependent resistance protein XA10 triggers cell death and calcium depletion in the endoplasmic reticulum. *The Plant Cell*, *26*(1), 497–515.

Tian, W., Hou, C., Ren, Z., Wang, C., Zhao, F., Dahlbeck, D., Hu, S., Zhang, L., Niu, Q., Li, L., Staskawicz, B. J., & Luan, S. (2019). A calmodulin-gated calcium channel links pathogen patterns to plant immunity. *Nature*, *572*(7767), 131–135.

Tong, J., Ren, Z., Sun, L., Zhou, S., Yuan, W., Hui, Y., Ci, D., Wang, W., Fan, L.-M., Wu, Z., & Qian, W. (2022). ALBA proteins confer thermotolerance through stabilizing HSF messenger RNAs in cytoplasmic granules. *Nature Plants*, *8*(7), 778–791.

Tornero, P., Chao, R. A., Luthin, W. N., Goff, S. A., & Dangl, J. L. (2002). Large-scale structure-function analysis of the Arabidopsis RPM1 disease resistance protein. *The Plant Cell*, *14*(2), 435–450.

Tran, T. T., Doucouré, H., Hutin, M., Jaimes Niño, L. M., Szurek, B., Cunnac, S., & Koebnik, R. (2018). Efficient enrichment cloning of TAL effector genes from Xanthomonas. *MethodsX*, *5*, 1027–1032.

United Nations. (n.d.). *Population | United Nations*. Retrieved 1 April 2023, from https://www.un.org/en/global-issues/population

Unwin, N. (1993). Nicotinic acetylcholine receptor at 9 Å resolution. *Journal of Molecular Biology*, *229*(4), 1101–1124.

Vogel, S. S., van der Meer, B. W., & Blank, P. S. (2014). Estimating the distance separating fluorescent protein FRET pairs. *Methods* , *66*(2), 131–138.

Waadt, R., Krebs, M., Kudla, J., & Schumacher, K. (2017). Multiparameter imaging of calcium and abscisic acid and high-resolution quantitative calcium measurements using R-GECO1-mTurquoise in Arabidopsis. *The New Phytologist*, *216*(1), 303–320.

Wallrabe, H., & Periasamy, A. (2005). Imaging protein molecules using FRET and FLIM microscopy. *Current Opinion in Biotechnology*, *16*(1), 19–27.

Wang, Chunlian, Zhang, X., Fan, Y., Gao, Y., Zhu, Q., Zheng, C., Qin, T., Li, Y., Che, J., Zhang, M., Yang, B., Liu, Y., & Zhao, K. (2015). XA23 is an executor R protein and confers broad-spectrum disease resistance in rice. *Molecular Plant*, *8*(2), 290–302.

Wang, Congying, Chen, S., Feng, A., Su, J., Wang, W., Feng, J., Chen, B., Zhang, M., Yang, J., Zeng, L., & Zhu, X. (2021). Xa7, a Small Orphan Gene Harboring Promoter Trap for AvrXa7, Leads to the Durable Resistance to Xanthomonas oryzae Pv. oryzae. *Rice* , *14*(1), 48.

Wang, Jizong, Hu, M., Wang, J., Qi, J., Han, Z., Wang, G., Qi, Y., Wang, H.-W., Zhou, J.-M., & Chai, J. (2019). Reconstitution and structure of a plant NLR resistosome conferring immunity. *Science*, *364*(6435).

Wang, Jun, Tian, D., Gu, K., Yang, X., Wang, L., Zeng, X., & Yin, Z. (2017). Induction of Xa10-like Genes in Rice Cultivar Nipponbare Confers Disease Resistance to Rice Bacterial Blight. *Molecular Plant-Microbe Interactions: MPMI*, *30*(6), 466–477.

Wang, Jun, Zeng, X., Tian, D., Yang, X., Wang, L., & Yin, Z. (2018). The pepper Bs4C proteins are localized to the endoplasmic reticulum (ER) membrane and confer disease resistance to bacterial blight in transgenic rice. *Molecular Plant Pathology*, *19*(8), 2025–2035.

White, F. F., Potnis, N., Jones, J. B., & Koebnik, R. (2009). The type III effectors of Xanthomonas. *Molecular Plant Pathology*, *10*(6), 749–766.

Wilkins, K. A., Matthus, E., Swarbreck, S. M., & Davies, J. M. (2016). Calcium-Mediated Abiotic Stress Signaling in Roots. *Frontiers in Plant Science*, *7*, 1296.

Williams, B., & Dickman, M. (2008). Plant programmed cell death: can't live with it; can't live without it. *Molecular Plant Pathology*, *9*(4), 531–544.

Wittig, I., Braun, H.-P., & Schägger, H. (2006). Blue native PAGE. *Nature Protocols*, *1*(1), 418–428.

Wu, L., Goh, M. L., Sreekala, C., & Yin, Z. (2008). XA27 depends on an amino-terminal signal-anchor-like sequence to localize to the apoplast for resistance to Xanthomonas oryzae pv oryzae. *Plant Physiology*, *148*(3), 1497–1509.

Wu, Z.-S., Cheng, H., Jiang, Y., Melcher, K., & Xu, H. E. (2015). Ion channels gated by acetylcholine and serotonin: structures, biology, and drug discovery. *Acta Pharmacologica Sinica*, *36*(8), 895–907.

Yu, X., Li, B., Jang, G.-J., Jiang, S., Jiang, D., Jang, J.-C., Wu, S.-H., Shan, L., & He, P. (2019). Orchestration of Processing Body Dynamics and mRNA Decay in Arabidopsis Immunity. *Cell Reports*, *28*(8), 2194-2205.e6.

Yuan, M., Ngou, B. P. M., Ding, P., & Xin, X.-F. (2021). PTI-ETI crosstalk: an integrative view of plant immunity. *Current Opinion in Plant Biology*, *62*, 102030.

Zhang, B., Han, X., Yuan, W., & Zhang, H. (2022). TALEs as double-edged swords in plant-pathogen interactions: Progress, challenges and perspectives. *Plant Communications*, 100318.

Zhang, J., Yin, Z., & White, F. (2015). TAL effectors and the executor R genes. *Frontiers in Plant Science*, *6*, 641.

Zhang, X., Henriques, R., Lin, S.-S., Niu, Q.-W., & Chua, N.-H. (2006). Agrobacterium-mediated transformation of Arabidopsis thaliana using the floral dip method. *Nature Protocols*, *1*(2), 641–646.

Zhang, Y., Dijkman, P. M., Zou, R., Zandl-Lang, M., Sanchez, R. M., Eckhardt-Strelau, L., Köfeler, H., Vogel, H., Yuan, S., & Kudryashev, M. (2021). Asymmetric opening of the homopentameric 5-HT3A serotonin receptor in lipid bilayers. *Nature Communications*, *12*(1), 1074.

Zhu, X., Caplan, J., Mamillapalli, P., Czymmek, K., & Dinesh-Kumar, S. P. (2010). Function of endoplasmic reticulum calcium ATPase in innate immunity-mediated programmed cell death. *The EMBO Journal*, *29*(5), 1007–1018.

6. APPENDIX

6.1. Materials used

Table 6.1. List of plasmids used.		
Plasmid	**Resistance**	**Reference/Made by**
35S:GFP	Spectinomycin	Christina Krönauer
35S:Bs3-HA	Spectinomycin	Christina Krönauer
35S:Bs3-GFP	Spectinomycin	Krönauer et al., 2019
35S:CpBs4C-HA	Spectinomycin	*This study*, Danalyn R. Holmes
35S:CpBs4C-GFP	Spectinomycin	*This study*, Danalyn R. Holmes
35S:CpBs4C-mCherry	Spectinomycin	*This study*, Danalyn R. Holmes
35S:NbBs4C.1-HA	Spectinomycin	*This study*, Danalyn R. Holmes
35S:NbBs4C.1-GFP	Spectinomycin	*This study*, Danalyn R. Holmes
35S:NbBs4C.1-mCherry	Spectinomycin	*This study*, Danalyn R. Holmes
35S:NbBs4C.2-HA	Spectinomycin	*This study*, Danalyn R. Holmes
35S:NbBs4C.2-GFP	Spectinomycin	*This study*, Danalyn R. Holmes
35S:NbBs4C.2-mCherry	Spectinomycin	*This study*, Danalyn R. Holmes
35S:NbBs4C.3-HA	Spectinomycin	*This study*, Danalyn R. Holmes
35S:NbBs4C.3-GFP	Spectinomycin	*This study*, Danalyn R. Holmes
35S:NbBs4C.3-mCherry	Spectinomycin	*This study*, Danalyn R. Holmes
35S:NbBs4C-1N2C-HA	Spectinomycin	*This study*, Danalyn R. Holmes
35S:NbBs4C-2N1C-HA	Spectinomycin	*This study*, Danalyn R. Holmes
35S:NbBs4C-1n2p1c-HA	Spectinomycin	*This study*, Danalyn R. Holmes
35S:NbBs4C-2n1p2c-HA	Spectinomycin	*This study*, Danalyn R. Holmes
pSKX1_dTALE779	Gentamycin	*This study*, Robert Morbitzer
pSKX1_dTALE780	Gentamycin	*This study,* Robert Morbitzer
pSKX1_dTALE782	Gentamycin	*This study,* Robert Morbitzer
35S:GABA-CpBs4C-Ctail-GFP	Spectinomycin	*This study*, Danalyn R. Holmes
35S:GABA-NbBs4C.1-Ctail-GFP	Spectinomycin	*This study*, Danalyn R. Holmes
35S:GABA-NbBs4C.2-Ctail-GFP	Spectinomycin	*This study*, Danalyn R. Holmes
pBs3:dT779EBE_RUBY	Spectinomycin	*This study*, Danalyn R. Holmes
pBs3:dT780EBE_RUBY	Spectinomycin	*This study*, Danalyn R. Holmes
pBs3:dT782EBE_RUBY	Spectinomycin	*This study*, Danalyn R. Holmes
pER10:CpBs4C-FLAG-GFP	Spectinomycin	Holmes et al., 2020
pER10:GFP-GUS	Spectinomycin	Holmes et al., 2020
pUBQ10:HDEL-mCherry	Kanamycin	AG Üstün
pUBQ10:HDEL-GFP	Kanamycin	AG Üstün
pUBQ10:R-GECO1-mTurquoise	Kanamycin	Waadt et al., 2017

Table 6.2. List of primers used.

Primer name	Primer sequence (5' to 3')	Primer use	Reference
DHo009_LBb1.3	ATTTTGCCGATTTCGGAAC	Genotyping	http://signal.salk.edu/tdnaprimers.2.html
DHo010_LB1	GCCTTTTCAGAAATGGATAAATAGCCTTGCTTCC	Genotyping	http://signal.salk.edu/tdnaprimers.2.html
DHo102_35S_F	CATCGTGGAAAAAGAACAC	Cloning	C. Krönauer
DHo103_GFP_R	GTCAGCTTGCCGTAGGT	Cloning	C. Krönauer
DHo120_Estrpro1_F	CCATGTAATATGCTCGACTC	Genotyping	*This study*, D.R. Holmes
DHo121_Estrpro2_F	TTCATTTGGAGAGGACAC	Genotyping	*This study*, D.R. Holmes
DHo122_GFPtag1_R	GATACGGACGAAAGCTGG	Genotyping	*This study*, D.R. Holmes
DHo123_GFPtag1_R	TACTTGTACAGCTCGTCC	Genotyping	*This study*, D.R. Holmes
DHo135_xrn4-3_F	AGGTGTATGCTCTTGGCAATG	Genotyping	Gazzani et al., 2004
DHo136_xrn4-3_R	AACTGCCATGAAAACTGATGG	Genotyping	Gazzani et al., 2004
DHo317_318/339_F	ACCATAACCCTGGCTGGA	Genotyping	*This study*, D.R. Holmes
DHo318_318/339_R	CTCGCAACACCCAAATGT	Genotyping	*This study*, D.R. Holmes
DHo319_318/339seq_R	CCAGGGCAATCTGAAGCA	Genotyping	*This study*, D.R. Holmes
DHo320_383_F	CTGATTTCCACCCCTACG	Genotyping	*This study*, D.R. Holmes
DHo321_383_R	CCCACAGATATAATGCAG	Genotyping	*This study*, D.R. Holmes
DHo322_383seq_R	CAGCAAGTTTATAGCCCC	Genotyping	*This study*, D.R. Holmes
DHo323_450_F	GGCTGTGTGTATTTTGTTC	Genotyping	*This study*, D.R. Holmes
DHo322_450_R	TCCCGGAACATTTGAATC	Genotyping	*This study*, D.R. Holmes
DHo323_450seq_F	CGTGTTATGGTGATACTTG	Genotyping	*This study*, D.R. Holmes
DHo336_NbActin_q_F	GATGAAGATACTCACAGAAAGA	qPCR	(Huang et al., 2017)
DHo337_NbActin_q_R	GTGGTTTCATGAATGCCAGCA	qPCR	Huang et al., 2017
DHo416_NbBs4C.1_geno_F	GAAAACTGAAGAACCATTGCG	Genotyping	*This study*, D.R. Holmes
DHo417_NbBs4C.1_geno_R	GTACCAATATAACACTTGAGGG	Genotyping	*This study*, D.R. Holmes
DHo418_NbBs4C.1_seq_R	AGTCCCAAAAACGGTTGC	Sequencing	*This study*, D.R. Holmes
DHo419_NbBs4C.2_geno_F	CAGGCATTGAGGGAGACAT	Genotyping	*This study*, D.R. Holmes
DHo420_NbBs4C.2_seq_R	TCTGAAGGAAACAAATGGTG	Sequencing	*This study*, D.R. Holmes
DHo421_NbBs4C.3_geno_F	ACCCTTATGCTCTTTTGTTCC	Genotyping	*This study*, D.R. Holmes
DHo422_NbBs4C.3_geno_R	GGTTTAGATTGGCAGTGGC	Genotyping	*This study*, D.R. Holmes
DHo423_NbBs4C.3_seq_R	GGCAAGCCAAGTATAATTCA	Sequencing	*This study*, D.R. Holmes
DHo425_pUbi_F	GGCTTGCGATGTAGATCTATG	Cloning	*This study*, D.R. Holmes
DHo438_CpBs4C_CACC_F	TTTGGTCTCTCACCATGGAGTTTGATCTCAGAT ACTTGA	Cloning	*This study*, D.R. Holmes
DHo439_CpBs4C_Nbod_TTCA_R	AAAGGTCTCATGAAGAAAGTGCAATGATAATGA CG	Cloning	*This study*, D.R. Holmes
DHo440_NbBs4C.2_Ctail_TTCA_F	TTTGGTCTCTTTCAATGAATTATACTTGGCTTG CCAAGA	Cloning	*This study*, D.R. Holmes
DHo441_NbBs4C.1_Nbod_TTCA_R	AAAGGTCTCATGAAATTAATGAAGAAAGTATAA TAGTAATGAAGAAAATG	Cloning	*This study*, D.R. Holmes
DHo442_NbBs4C.1_Ctail_TTCA_F	TTTGGTCTCTTTCATGTTATTGGGTTTCTAATA CATGC	Cloning	*This study*, D.R. Holmes
DHo443_NbBs4C.2_Nbod_TTCA_R	AAAGGTCTCATGAAATCAATATGATCATGGGAT ATGC	Cloning	*This study*, D.R. Holmes
DHo444_CpBs4C_Ctail_TTCA_F	TTTGGTCTCTTTCATGTTCTTCTTGGATTGGCA ATA	Cloning	*This study*, D.R. Holmes
DHo445_CpBs4C_AAGG_R	AAAGGTCTCACCTTGACGAGCAGGCGATTTGT	Cloning	*This study*, D.R. Holmes
DHo447_NbBs4C.1_noC_AAGG_R	AAAGGTCTCACCTTTGAAATTAATGAAGAAAGT ATAATAGT	Cloning	*This study*, D.R. Holmes
DHo448_CpBs4C_noC_AAGG_R	AAAGGTCTCACCTTTGAGGAAAGTGCAATGAT AATGAC	Cloning	*This study*, D.R. Holmes
DHo450_CpBs4C_Nbod_TTCA_R	GTCATTATCATTGCACTTTCCTCAATGAGACC TTT	Cloning	*This study*, D.R. Holmes
DHo453_ccdB_F	GGTTTACACCTATAAAAGAGAGAGC	Cloning	*This study*, D.R. Holmes
DHo454_ccdB_R	CCGATATGCACCACCGGGTAAAGTTC	Cloning	*This study*, D.R. Holmes
DHo455_M13_F	GTTGTAAAACGACGGCCAG	Cloning	
DHo456_M13_R	CAGGAAACAGCTATGACCATG	Cloning	
DHo467_NbBs4C.2_noC_AAGG_R	AAAGGTCTCCCTTATGAAATCAATATGATCAT GGGATATGCATA	Cloning	*This study*, D.R. Holmes
DHo468_NbBs4C.1_Nbod_ACCA_R	AAAGGTCTCATGGTATTACAAATGAGGCTAG	Cloning	*This study*, D.R. Holmes
DHo469_NbBs4C.2_Nbody_ACCA_R	AAAGGTCTCATGGTACTACCAGACAGACCAG	Cloning	*This study*, D.R. Holmes
DHo470_CpBs4C_Nbody_ACCA_R	AAAGGTCTCATGGTAGTAGAAGAGAAGCTAGA C	Cloning	*This study*, D.R. Holmes
DHo471_NbBs4C.1_pore_ACCA_F	ACCACAAGTGTTATATTGGTACATTTTCTTCA TTACTATTATACTTTCTTCATTAAT	Cloning	*This study*, D.R. Holmes
DHo472_NbBs4C.1_pore_TTCA_R	TGAAATTAATGAAGAAAGTATAATAGTAATGA AGAAAATGTACCAATATAACACTTG	Cloning	*This study*, D.R. Holmes
DHo473_NbBs4C.2_pore_ACCA_F	ACCAAAATTTATATTTTGGTATGCATATCCCA TGATCATATTGAT	Cloning	*This study*, D.R. Holmes
DHo474_NbBs4C.2_pore_TTCA_R	TGAAATCAATATGATCATGGGATATGCATACC AAAATATAAATTT	Cloning	*This study*, D.R. Holmes
DHo475_CpBs4C_pore_ACCA_F	ACCACAAATGTTGTTCTGGTACTTTTTCGTCA TTATCATTGCACTTTC	Cloning	*This study*, D.R. Holmes
DHo476_CpBs4C_pore_TTCA_R	TGAAGAAAGTGCAATGATAATGACGAAAAAGTA CCAGAACAACATTTG	Cloning	*This study*, D.R. Holmes
DHo482_Nb1_q2_F	AGCCTCATTTGTAATCCCTCAA	qPCR	*This study*, D.R. Holmes
DHo483_Nb1_q2_R	GAATAGTGGAGAGTATGCCCAG	qPCR	*This study*, D.R. Holmes
DHo486_Nb2_q2_F	TGGTGACCATTGATCATCTTGA	qPCR	*This study*, D.R. Holmes
DHo487_Nb2_q2_R	GGAACTGCTACAACGTTGAAC	qPCR	*This study*, D.R. Holmes
DHo490_Nb3_q2_F	TCTCAAATCTGGAATTGGACCT	qPCR	*This study*, D.R. Holmes
DHo491_Nb3_q2_R	AAGGAGAAGATGATGAACGTGA	qPCR	*This study*, D.R. Holmes
DHo503_xrn4-5_F	GTTTCTTGGTTGTTGCAGCTC	Genotyping	Souret et al., 2004
DHo504_xrn4-5_R	TCATGACGAATTCCTTTGAGG	Genotyping	Souret et al., 2004
DHo520_dT779EBE_F	CACCTGCGTCACCTTCCACTTCC	Cloning	*This study*, D.R. Holmes
DHo521_dT779EBE_R	CCAGGGAAGTGGAAGGTGACGCA	Cloning	*This study*, D.R. Holmes
DHo522_dT780EBE_F	CACCTAGTATTACACCTGTTATG	Cloning	*This study*, D.R. Holmes
DHo523_dT780_EBE_R	CCAGCATAACAGGTGTAATACTA	Cloning	*This study*, D.R. Holmes
DHo524_dT782_EBE_F	CACCTGTTCCTACCACTACCTAG	Cloning	*This study*, D.R. Holmes
DHo525_dT782_EBE_R	CCAGCTAGGTAGTGGTAGGAACA	Cloning	*This study*, D.R. Holmes

Table 6.3. Arabidopsis thaliana genotypes used.			
Species	**Genotype**	**Mutation type**	**Reference**
Arabidopsis thaliana	Col-0	WT	(Arabidopsis Genome Initiative, 2000)
Arabidopsis thaliana	*Estr:CpBs4C-FLAG-GFP*	T-DNA insertion	Holmes et al., 2020
Arabidopsis thaliana	*Estr:GUS-GFP*	T-DNA insertion	Holmes et al., 2020
Arabidopsis thaliana	*xrn4-3* (SALK_014209)	T-DNA insertion	Gazzani et al., 2004
Arabidopsis thaliana	*xrn4-5* (SAIL_681_E01)	T-DNA insertion	Souret et al., 2004
Arabidopsis thaliana	*xrn4-5//Estr:CpBs4C-FLAG-GFP #2*	T-DNA insertion	*This study*
Arabidopsis thaliana	*xrn4-5//Estr:CpBs4C-FLAG-GFP #3*	T-DNA insertion	*This study*
Arabidopsis thaliana	*xrn4-5//Estr:GUS-GFP #2*	T-DNA insertion	*This study*
Arabidopsis thaliana	*xrn4-5//Estr:GUS-GFP #3*	T-DNA insertion	*This study*
Nicotiana benthamiana	WT	WT	
Nicotiana benthamiana	ΔNbBs4C.1-3	CRISPR-induced	*This study*

6.2. Sequences used

Genomic DNA sequences of genes used herein. Grey highlight indicates coding sequence (CDS). Bold font indicates the start and stop codon.

>CpBs4C (Bs4C from Capsicum pubescens)

TAAATTAAACTAGTTAATTAAAAAAGAAGCAACTCTATCCACTGCCGCCGCAGTATCTTTTAGGGATTGTTTAGT
GTGAGGTATAAGTAATTCTGGGATAAAATATAAAGATCAATTTATCCCATGTTTGATCAGAGGGATTAATCAGTG
GTGAGATAACTTATCCCCCTATTACACCATAGTGATGGAATAACTTATCCCATATTCACAGTGAGATAAGTTATC
CCAAAAAAATCCCAATATTAATTATCCAAAAATAATAATTTCCCAACCAAACGAACCCTTTTAAGTTAAGAGACTA
TAGGAAACGCAAAGATTGACTTATGGAGAGTTCTAAGTCCGAAATTGTTTTGTCAAATGGGGCCTACGAAAAACA
TTATTTCTTCGCAGGAACACAACTAGCTTGACTACACTAACGTCCCAGTGGAAAAGTACCTTCATGCAGCAGTAT
GGTACAATATTATTAAAGCGCTGGAACATTTTAATAtaAAAAATAGTCCTCTCAGCCCTTAGACAAGCAGGAATA
AAATTATTCTAAATCAACTTTCGGATTTGGATACTTCGAGGAAAGAGCACCATCTTAAAATGACAGTGTCTATAA
ATAAATACACAACCAGCATACTACACCCAACCATAGAATTTTAGGAAAAGATTCAAAAGAATAGA**ATG**GAGTTTG
ATCTCAGATACTTGATCTTGATTTTGGCTAACATGCTCAAATCAATATTATCCATTTCTGATAACTGGGATCCTT
TCCATATATTTCATGACCATCCCAGTTTCATCGTGTTCATCAATAAGCTCTTCTTTCTTTTCATATTTTCCTTTA
TTTTCTCCATCACTCGTATAACACTTCATCATCCAAATATACGAATACGTGTACGTACTACTACTTCAGCAGATC
TCTCCAAGTCCTTTAATATCTTGTGTCTAGCTTCTCTTCTACTCCCACAAATGTTGTTCTGGTACTTTTTCGTCA
TTATCATTGCACTTTCCTCATGTTCTTCTTGGATTGGCAATACATGGGCTAGTTTTCGACAACGGATTCTGCATA
TTTTCTCAACAATAATATTTCCAGCAGTCAGCATTTTCATCAATGTGGAGTTTGACAGAAATAATGTGAGCCAGC
AACATGAAACTCAAACAAATCGCCTGCTCGTC**TAG**

>NbBs4C.1 (Bs4C homologue from Nicotiana benthamiana)

AAAGCCAGAACAAGTTTAAAAAATGATGTATCCAACCATATAAAAGATTAATTATTTCCAAATATTTATATATAT
TGCTTATAGAAAAATATTTGCAACTTCTATAACAATTATCATAGCGGAAAAAAGTTTATTAAAATTAAAATTAAA
ATTTTATTCAAGACCAATACTGTCTAAAAAAATTAAATAGAGTAATTTTGTATTTATAAATTTTAAGACAAATTT
GGGGCCTCTTATTGAAGTTTGGCTTTAGGCCACCAACTTTATTGAGCCGACCCAAGGGGCATAAAACACCTTGTA
TTTATAGTGTAGACACTTTATTCTAATAGTAATATTAATGATTATTTATATGATTTGAACTCGTAACTTATATAC
CGGCAATACACTATTGTTTCGAAGCTTTCTTCTACCTTTGATAATAGGAGTAATATAACTCCAATAACATAATAA
CCCAAGGGTAACACAAGGTTTAAAAATGTTATAGTACGTCAGCCTACTTTTGTTATAATATAAGTATTTGTTATT
TTAATTTTTAACCGGAAAAAAAGTGCTTCAGCAGAAAAAGATGAGGAAAACTGAAGAACCATTGCGTCACCTTCC
ACTTCCATATCCAAACCCCACCAATCTTTTCTCCTTCCTTATAAATTCAAGTGAGATAAAACTTATTTTTTGAAC
AAACCAAAAAAGAAGAAGAAAAGAA**ATG**AGATTGGTAGAGCTAAGGTACATTATATTGATGTTAATCAACATCTT
CAAATCTATGATGGGATCATCTTCTGATTGGGATCCTTTCCACATATTAAACCATAATTCTTTTCCAAGTTTCAT
TAATAAAATCCTTTTTCTTTTATTATTTTCCTTTATTTTCTCCATCACCTCTATAACAGTTGACACAACTACTCG
TCCTATCAGTATACACATTTGCATTGGAAATTTTTCCAAGTCCTTCAATGGTTTATTTCTAGCCTCATTTGTAAT
CCCTCAAGTGTTATATTGGTACATTTTCTTCATTACTATTATACTTTCTTCATTAATATCTTGTTATTGGGTTTC
TAATACATGCAACCGTTTTTGGGACTGCGCTCTGGGCATACTCTCCACTATTCCACTTCTTAAAATTTTCATCAA
TGCTGAAATTCACAGCAGTGGGAATGAAGACCAGCAGTCTCCAGTC**TAA**

>NbBs4C.2 (Bs4C homologue from Nicotiana benthamiana)

GGCGAAGACTAACTGTTGGGTAAGTAACCACATAGCCAAAGTCTACCTGTGAAGGTCACTATCAAAAAGCTAGAA
GCATTTGATGTGGGAGTCAACCTGAGAGGAGGCATTAAACCCTTAATTGCAGATTTATACAACCCAAAAACGCAC
AAAATGTTAAGTCAATATAATGTACTAGCAGTTTCTGTCGACCAGCTGCTCTATATTAGTTCTTTCTCCGTTTAA
TATTGTTTAAGCTAGTTTGATTCGGCGAGTTTAAGAAGAAAAAAAAAAGACTTTTGATCTTAAAAATTTAAAGAG
TAAAAAGTTTGTGATGTCATACCATTTGTGTGGATATAAAAACTTCTCATTGAGAGCAAAAATGGTAAAATAATT
AAAGAGTTTAAAGTTGTATTATTTCCAAATTTAAAAATGTATCATTTATTTTGAAACTGACTAAAAAAACATCTC
AACGGAGGAAGTAGTACCATTTTGTTTCAGCGACTTCACTTATGTAGTCAGTAGTCAGAAGTCAACATATACATG
TCCTTAAGTATCATAGGATTTGTAAGTTTTGACCCATAATGCTCTGTTATTCCTATCACCACCTTAACCTCATAG
TAGGAAAATTGGTAGTATTACACCTGTTATGATTTATATAAACTTGGAAAGATTAAGACATCTTCTACAATATCA
TCTACAGAGGTTCTGAAGGAAACAA**ATG**GTGACCATTGATCATCTTGATCTTAGGCACACTATGTTAGTGTTAGT
AAACATTCTCAAATCTGGAGTGGGACCTCCCTGGCAATGGAATCCGTTCAACGTTGTAGCAGTTCCTCACCAGTT
TACTTTAATGGAAGCTGTCATTCTTCTCTTCACGTTCATCATCTTCTCCTTCACCTCCATAAAAGTTCATCCCAG
AAGTGAGCAGTGGCAAATATGTATAAGACTTGGAGATTTCTCCACAAGTCTTACTCTATTATTGCTGGTCTGTCT
GGTAGTACCAAAATTTATATTTTGGTATGCATATCCCATGATCATATTGATATCCATGAATTATACTTGGCTTGC
CAAGACTTTCAATACTTTCCTGGATTGGCTACAAGGAATGTCTCCCTCAATGCCTGTTTTCAATAGTTTCGTCGT
AACAACACTTGCCACTACCAGTCCGGACCATGAAGATCAGCAACCTAGTTCAGGGCATGAAGCAGTT**TAA**

>NbBs4C.3 (Bs4C homologue from Nicotiana benthamiana)

TTATAATTTCTGGGTGGGCTAATTTTGGACCAATGTAAGTAGGCCACGTGTTTAAAAAACTTGAGGAAACCAGGT
TTAACGGTGGAAGGGTATATGTGGCCCGAATGTGTAACGGTGTGGGTATATTTGTCAAAGAATTCAAACGGAGTA
TAAATGTAGCTTATTTTGAATAGTACAAGGGCAAATCCGACCCTTAACCGTTTTAAATTTGATCTTTTTCTTGCC
AGCTACAGCAGTCGGAAAAGGCAAATATAGAGCAGAAGGCGAAGACTAACCGTTGGGTAAGTCAGAACCACATAG
CGAAAGTCTACCTATGAAGGTCACTGAAAAGAGTGTATCAAAAAGCTAGGAGCATTTGATGTGGGAGTCAACCTG
AGAGGAGGTATTAAGCCCTTAATTGTAGATTTATACAACCCAAAGACACATAAAGTCAATATAATGTTGCAGTTT
CTGTCGACCAGCCGCTCTTAGTTAACATTTTGCTTCAGCAACTTGACTTATGTAGTCAGTAGTCACAAGTCAACA
TATACATGTCCTTAAGTATCATAGGATTTGTAAGTTTTGACCCTTATGCTCTTTTGTTCCTACCACTACCTAGCC
TGCTAGTAGGAAAATTGGGATTGCACCTGTTATGATCTATATAAACTCGGAAAGGTTAAAACATCTTCTACAATA
TCTACGGAGATTCTGAAGGAAACAA**ATG**GTAACCATTGATAATTTTGATCTTAGGCACACTATCTTAGTGTTAGT
AAACATTCTCAAATCTGGAATTGGACCTCCCTGGCAATGGGATTCGTTCAATGTTGTAGCAGTTTCTCACCAGTT
TACTTTAATGGAAGCTGTCATTCTACTCTTCACGTTCATCATCTTCTCCTTCACCTCCATAAAAGTTCATCCCAG
AAGTGAGCAGTGGCAAATATGTATAAGAGTTGGAGATTTCTCCAGAAGTCTTACTCTATTATTGCTGGTCTGTCT
GGTAATACCAAAATATATATTTTGGTATGCATATCCCATGATCATATTGATTTCCATGAATTATACTTGGCTTGC
CAAGACTTTCAATACTTTCATGGATTGGCTACAAGGAATGTCTCCCTCAATGCCTGTTTTCAATATTTTCGTCGT
AACAACACTTGCCACTGCCAATCTAAACCATGAAGATCAGCAACCTAGTTCAGGGCATGAAGCAGTT**TAA**

>SlBs4C (Bs4C homologue from Solanum lycopersicum)

GAAAAGTAAAATTTGAATACAAATCATAATATAATATTGAGGAAAGAAAAAAATATCATTTTTTTAGAAAGTAAA
AAAAATAGAGAATTGAGTTAGAGTTAATTATCTAATTTTTTTTAAAAAAAACTCTATATTTGAAGAGTGAAATAT
AGAAAATAGAATCGAAAAATAGAGTACCATACAAAAATTTTAAGAGGCAAAAGCTAATAAATACCAAACATACCC
TAGTCATACAAGCTATATGGTGTTGGGATGAAAGAAACAGGTTGGTCGTCCCTATTAAGTCAACCTAAAAAGGTT
GATTTTGTGTGTTTTACGCGTCTATCTTTAGATCTTTGAAGTTTCCGCAACTTTATGTGTAAATACGAACTCAGT
ATATGTTAATACATTTGTCTTGATTTAAATATTTTGAATTATTAATTTTTATTATTTATAATACTTTTTATATAA
ATTTTAAATAATATATATTATTTCTTGTCCCAATTATGTGAACACATATAAAATTTTGAGCTAAAATTTTAATAT
GTTATTAGAATATTTTACATAGTTAATTATCGTCTTTTCTTTCTCTTTTGTAATTTTAAATAATAAATTTCACTC
TCTGTAAATTCTAAAATTTGATCCAAGCTCCTCTTTTATTCCCTTTATCGTAATTTTTGTAAAGAAAGTTCCCCT
TTTATAAATAATGAAATATAACCCTAAGTTCACTCTCTGTAAATTCTAAAATTTGATCCAAGCTCCTCTTTTATT
CCCTTTATCGTAATTTTTTTAAAAAAGTTCCCCTTTTATAAATAATGAAATTTAACCCTAAGCTCCTCTTTTTTC
CTCTTATTATATATAGAGAGAGAAAGAGAGAGAGAGAGATAGGAATCAACAATAATTTAATCAATAGATTGAACT
CAGAATATATTTCTTCGACAGTTCTTGAATTATTTGTCGAGGATCAATCAAAAACAATCCATCTCTCTGTAGCTG
GTTAAAAAATATAAGGGTAACTAGTC**ATG**AGAATCTTCGACTTGAGGTATATTATTTTGATGCTAATTAACATCT
TCAAATCCACTTCTTCTGATTGGGATCCTTTCCATTTATTATTATATTATGATTTTGATCCAATATTATTTAGTT
TCATCATACACATAAATAAAATTCTTTTACTCATATCACTTTCCTTTATTTTCTCCATCATTTCTATTAGAATAA
TCCACATGACTAATTATTCTAATCGTCCTATAAATATAAAAATACAATTTGGAACTTTTTCCAAGTTCTTTAAAA
TCTTATGTATAATCACACTTTTACTCCCACAAGTGTTGTTTTGGTATATTTTGTTCATTATTATTTTATTTTCTT
TATTGTTCATGTCTTGCCCTAATTGGATTTCTAATTTATGTGAATGGACTCTTCACATACTCTCAACAATTCCTG
TCCTTACAATTTTTATCTGTGCTCAACTTGATAACAATGATGAGAATTACCTACTACCAATTCACAGGACACAAC
CTACTATCACAGATGGCACTGACACAGGTATCGAG**TAA**

>CaBs4C.1 (Bs4C homologue from Capsicum annuum)

GGCGACTATGAAGCCTCCGACAAATGTTGTGAAAAGCTGAACGAACTTCACTATCTGCAATCATTCAGTATAAGA
TTATTTTCTGTTGGGTTCCTTTAAAAAAATAGACAAAGTTAAAAACATTAAAGATTAGGTTATCCAAACAATCTA
GGTATAAGAAATATCCAAACATTGTAAGTTAGGATTTTTAAATTATTCTAATTAGAAAAATGCAGACCAATGAAA
ATATGCCACTTCATTCATGAAATGTTTTTTTATTTATTTAATATTGGAAATGTTAAATAAAGGGTATTTTAGAGG
TCAAAGGTAGATGTGAAGGACATTTTGGAGTCCGAAGGTGGATGTGAAGGGCATTATAGAGCCAAAAGATGAATG
AGGGATATTTTTGCACTATTTTCAATAGATGAAGAACATTTTAGGACCTTTTCCAAAAAAATAAATGAAAAATAAA
TTTAATGGGTATATCTCAAATTAAATTTTCAAAAGGGGCTGTCATTGCAAATATTCTTGATTAAGTTACCCACAG
TCCACACCGACTATAGGAGAGTCAAGTCCGAAATTGTTTTATCAAATGGGGCCTACGAAAAACATTATTCCTAAT
TACACTAACGTCCCAGTGGAAAAGTACCTTCATGCAGTAGTATGGTACAATATTATTAAAGCGATGAAACTTTTT
AATACCAAAAATAGCCCTCCCAGCCTTCACCAATTAGGAATATAAAATTATTCTAAATCAACACTACTGGATAAA
ATTGGATATATTGACCTAATATACACTACTGGATAAAATTGGATATATTGACCTAATATACACTACTGGATAAAA
TTGGATATATTGACCTAATATATTTAACTATATTTATACTCTTTCCTCACTAAGCTTCGAGGAAAGATCGCGTAC
GTGATCTTAAAATGACTGTCTATAAATAAAATTAAAATGACACAACCAGCATACTATACCCAACCATATAATTTT
AGGAAAAGATTCAACAGAATATAAT**ATG**GAGTTTGATCTaAGATACTTCATCTTAATTTTGGCTAACATGCTCAA
ATCAATATTATCCATTTCTAATAACTGGGATCCTTTCCATATAATTGGTAACCCCATTCCAAGTTTCATGACATT
TATGAATAGGCTCTTCTTTCTTTTCATATTTTCCTTCATTTTCTCCATCACTCGTATGACACTTCATCATCCAAT
TATACGAATACGTGTAAGTATTACTTTCTCCAAGTCGTTTAATATCTTGTGCCTAGCTTCTCTTCTACTCCCACA
AATGTTGTTCTGGTACTTTTTCTTCATTATCATTACACTTTCCTTATGTTCTTCTTGGATTGGCAATACATGGGC

TAGTTTTCGACAACGGATTCTGCATATTTTCTCAACAATAATATTTCCAGCAGTTAGCATTTTCATCAATGTGGA
GTTTGATAGAAATAATGTCATCAGCCAGCAGCATGAAACTCAAACAAATCACCTGCTCTCTCTCGTC**TAG**

>CaBs4C.3 (Bs4C homologue from Capsicum annuum)
GTACAGATAGTTTTCGATCTGCATCTTCCAGAAACCAAAATCGGATCCATCAAACTTCTTGATTCCAAACTTCGA
TCCTTCCATCTTCAGTGATCGTGATGTCTCCCAAGCTTTGATACCAGTTGTTAGGATCGATTAGCAGTTCACGCA
CACTAAATCTGTGGAGAGGATGAAGAAAATTGGAGAGAGAGTTCTTTAGGAGAGAGAGAGAGAGAATTAATTTCG
TGGTAACACCCGTGGGTAACCTCCACGGGAGACAGGCTATTTATATTAATGACTGATAACACCAGTACACCAGAT
ATTAATCAGACTCCACAACCTAACAAGATTGAACGGTTAAGACTTAATAACTAAACTAAGATTTATTAGTCAAAT
CTATACCATTTATTTTGACTCAGGTCATGTATGTCTCCTCCAAGAAGGAAATTGAAAAAAATGGAGAGGAGCTCA
ATCCCTTTCGGTATATACCGCTGGGTCTGAGTGTGACACTTTTATTTTGACCACCTCACCAAACCAAACGTGATA
TTATGTATGTAATTGTGGACGATCTTTCCGATGCATGCAGTTGTCTTTTAGTGGACAAACTTTCCAATGGCATAA
AAATACATATATAGTTTTCTATGTAGTGGGCTAACTTTGCGATGGCATAGAACTTAGAAGTAGTAACTACATTAC
ATACATGGGCTGGTGTTTTTGGTTCAGCAATGAAAAAGTACCTTCATGCAGCAATAGGGTACAATATTATTAAAG
CGATGAAACAATTAAAATGCCAAAAATAGCCCTCCATGCTAGTAGACCAGCCATGACAACTATTGTAAAGCCGTT
CAATCTCGAGAAAAATTGGGCCCAACCTATTTATACACGCTCAACTTCGAGGAAAGAGCAGAATGTTAGAAATAT
AATTTTACGCGTAGATATAAATAATGAAAAACACAACCAGCAGGAAGCATTATACATTGCTATATAATCCACTCA
AAATTTTCAAAAAAGCTCAAGAAGA**ATG**GAGTTTGATCTTAGATACTTGATCTTAATTATAGTTAACATTCTCAA
ATCCATATCACCTTCTGAAAATTGGGATCCTTTCCATATATTTGGCAATCCCATTCCAAGTTTCATCACATTTAT
GAATAGGCTCGCCTTTCTTTTCTTATTTTCCTTCATTTTCTCCATCACTCGTACAACACTTCATCATCCAATTAT
ACGAATACGTATAAGTATTACTTTCTCCAAGTCCTTCATTTTCTCCATCACTCGTACAACACTTCATCATCCAAT
TATACGAATACGTATAAGTATTACTTTCTCCAAGTCGTTTAATATCTTGTGCCTAGCTTCTCTTCTACTCCCACA
AATGTTGTTCTGGTACTTTTTCTTCATCACCATTACACTTTCCTCATGTTCTTCTTGGATTGGCAATGCATGGGC
TAGTTTTCGACAACCGACTCTGCATATTTTCTCTACAATATTTCCAGCAGTTAGCATTTTCATCAATGTGGAGTT
TGACAGAAATACTGTGAGCCAGCAGCATGAAACTCAAACAACTCGCCTGCTCTCTCTCGTC**TAG**

>CaBs4C.4 (Bs4C homologue from Capsicum annuum)
TCATTAATGCATGCAACTTTTTTTTTTTCCTCTCATAAAATCTCTCCCATTTTTTTTTAAAATCGATTGATACAT
ATATAAATTTATTTAGTTATTCATACATCTTTATTTTTTTAATGGTGATTCATATGAATGATAAATATGATATCA
TTATATGGGTATTATGGTGATTCATACGATAAATACATTTTGTATGATTTTAACAGGTGATACATATGATATTAA
TGGGTGATACATATTGTATTATGGTGATTCATATGGTATATACAATTATTTATTTCAATTATTGGGTGATTCATA
TATATGATATTATGGTGATTCATTTGGTAGATACAATTATTTATTTCAATTATTGGGTGATTCGTATGATATTAA
TGGGTGATATATATAGTATTATGGGTGATTCATATGTTATTAATAAAAGGTAATGGTGCACTCAATGTAGAAAAC
AAAAGTAATAATATTTTTTTAAAAAAATACTAAAAGCAGAATTGAAACATAATTAAAATTAAATCTAAAAAAAGA
AAAAAATTAGATATCTTTCCTTAAATAAAAGAATACAATGAATAAAAGAGAGTCTATTATTTCCCTAAATAAATA
TCTTGTTAGTTTCAAATGTATCACTTTTTATATGTATCATCATATAACATATGTATCACATTTAAAAAAATCGGA
ATAAAATGTAATTAACAAAATAATCGATATTTTATGTAATATCACTTAAAAGTTAGGAATTTATGTAAGTTAATG
TTAATTTGTATCGAATCGATCGATACCCGATATGAAAGCCTATTTTAAGGTGAGCTTTTTCCCAACCAACAAAAA
ATATTCTTGGTTGTCCCTATTATGTTGGGTCTTTGTTGGCATGCAAACAACGTGGATGAGCAAAGCAATTTTACA
AAACATTATAGTAAAATGATAATTTTGCCTTTACTTGGTTGACTATCTTGTCTTTTGATTTTGTCTATCTATATA
TATTCATTTAGAAACAAAACAAAATATACTCAAACATAAAGATACAAAAGTTTACCAAGA**ATG**GAGTTTGATCTA
AGGTACACAATATTAATTATAGTTAACATTCTCAAATCAATATTTATTTCAAATGAATGGGATCCTTTTCATATA
TTTGTCCAACTCACTTTCATGGCATTTATGAATAGGCTTTTTCTTCTTCTATTGTTTTCTTTCATTTTCTCCATC
ACTAGTATAACAATTCATTATCCAATGAGAGTACATATAAGTTCAACATATTTCTCAAAGTCCTTTAATATATTA
TTTTTAACTTCATTTCTACTTCCACAAGTGTTATTTTGGTACATTTTCTTCATTACTATTATGACATTTCCTTCT
AATTGGATTTCCAATTTTAAGGAATGGTCTTTATATATTATTTCAATAATTCCAGGATTTAGTATTTTCATCAAT
GCTGAGCTTGATAGAAATAATGTGAATAACCAGCAGCCCCAAGCTCAAACAATTCACCTACTCCTTCCTGTC**TAA**

>$GABA_A$ subunit α, codon optimized for expression in N. benthamiana
ATGAATATTGGGTACTTCATTCTCCAAACGTATATGCCGTCTATTTTGATTACGATTCTGAGCTGGGTAAGTTTC
TGGATTAACTACGATGCCAGTGCAGCTCGCGTCGCATTAGGCATAACAACTGTTCTCACTATGACGACGATAAAT
ACTCACTTGAGAGAGACTTTGCCTAAAATTCCTTACGTCAAGGCCATCGATATGTATTTAATGGGTTGTTTCGTT
TTCGTATTCATGGCTTTACTCGAGTATGCCCTTGTTAATTACATATTCTTCTCTCAGCCCGCCCGGGCTGCGGCA
ATTGACAGATGGAGCCGCATCTTCTTTCCTGTGGTATTCTCTTTCTTCAATATTGTGTACTGGCTTTATTATGTG
AACGTCGACGGCAGCGGGGCAACAAATTTCTCATTGCTTAAGCAAGCGGGAGATGTGGAAGAGAATCCTGG

Amino acid sequences of the proteins used for structural analysis herein. Amino acids highlighted in orange were used for the C-tail chimera generation in Figure 3.23, Figure 3.24, and Figure 3.27. Underlined amino acids are the pore-lining helix used for pore-swap chimeras in Figure 3.25 and Figure 3.26.

>CpBs4C
MEFDLRYLILILANMLKSILSISDNWDPFHIFHDHPSFIVFINKLFFLFIFSFIFSITRITLHHPNIRIRVRTTT
SADLSKSFNILCLASLLLPQMLFWYFFVIIIALSSCSSWIGNTWASFRQRILHIFSTIIFPAVSIFINVEFDRNN
VSQQHETQTNRLLV*

>NbBs4C.1
MRLVELRYIILMLINIFKSMMGSSSDWDPFHILNHNSFPSFINKILFLLLFSFIFSITSITVDTTTRPISIHICI
GNFSKSFNGLFLASFVIPQVLYWYIFFITIILSSLISCYWVSNTCNRFWDCALGILSTIPLLKIFINAEIHSSGN
EDQQSPV*

>NbBs4C.2
MVTIDHLDLRHTMLVLVNILKSGVGPPWQWNPFNVVAVPHQFTLMEAVILLFTFIIFSFTSIKVHPRSEQWQICI
RLGDFSTSLTLLLLVCLVVPKFIFWYAYPMIILISMNYTWLAKTFNTFLDWLQGMSPSMPVFNSFVVTTLATTSP
DHEDQQPSSGHEAV*

>NbBs4C.3
MVTIDNFDLRHTILVLVNILKSGIGPPWQWDSFNVVAVSHQFTLMEAVILLFTFIIFSFTSIKVHPRSEQWQICI
RVGDFSRSLTLLLLVCLVIPKYIFWYAYPMIILISMNYTWLAKTFNTFMDWLQGMSPSMPVFNIFVVTTLATANL
NHEDQQPSSGHEAV*

>SlBs4C
MRIFDLRYIILMLINIFKSTSSDWDPFHLLLYYDFDPILFSFIIHINKILLLISLSFIFSIISIRIIHMTNYSNR
PINIKIQFGTFSKFFKILCIITLLLPQVLFWYILFIIILFSLLFMSCPNWISNLCEWTLHILSTIPVLTIFICAQ
LDNNDENYLLPIHRTQPTITDGTDTGIE*

>CaBs4C.1
MEFDLRYFILILANMLKSILSISNNWDPFHIIGNPIPSFMTFMNRLFFLFIFSFIFSITRMTLHHPIIRIRVSIT
FSKSFNILCLASLLLPQMLFWYFFFIIITLSLCSSWIGNTWASFRQRILHIFSTIIFPAVSIFINVEFDRNNVIS
QQHETQTNHLLSLV*

>CaBs4C.3
MEFDLRYLILIIVNILKSISPSENWDPFHIFGNPIPSFITFMNRLAFLFLFSFIFSITRTTLHHPIIRIRISITF
SKSFNILCLASLLLPQMLFWYFFFITITLSSCSSWIGNAWASFRQPTLHIFSTIFPAVSIFINVEFDRNTVSQQH
ETQTTRLLSLV*

>CaBs4C.4
MEFDLRYTILIIVNILKSIFISNEWDPFHIFVQLTFMAFMNRLFLLLLFSFIFSITSITIHYPMRVHISSTYFSK
SFNILFLTSFLLPQVLFWYIFFITIMTFPSNWISNFKEWSLYIISIIPGFSIFINAELDRNNVNNQHPQAQTIHL
LLPV*

>OsXa10
MQLMLTFCTGPLLFAVLLLMVYLKQLAAAACVDVLIIYLCRFLLLRGIIFSGDGKLRFRVKVAIGFLYISLSAIL
FYLSAAVMALPPWGAVAMWGMALVATELGYSFLCPYSCRCIGEDDEEISPV*

>OsXa23
MLHHLKELAAVAGIHMILIYLCRFLLRRSRNVLFTVSNSLRFRLKVLTVLLYICLSVMLFYLFGSIMPLPPWGLV
VGWVMALIAVELAYAFIFPYSFRYIADNDDDKMVILPV*

6.3. Supplementary information

S1. Bs4C-R-like proteins from *C. annuum* induces cell death in *N. benthamiana.* T-DNA constructs containing the indicated coding sequences, driven by the 35S promoter, were infiltrated into *N. benthamiana* leaves via *Agrobacterium tumefaciens*. Photos taken 3 days post infiltration. Leaves were cleared with ethanol for HR visualisation (indicated by the dark brown areas). Image taken by J. Elsaesser.

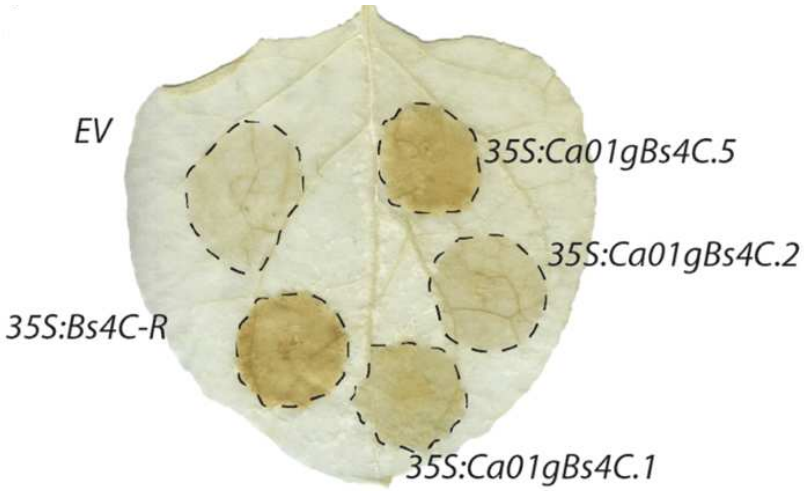

S2. Protein sequence alignment of all of the Bs4C homologues used for pairwise comparison in Figure 3.1. Black highlight indicates amino acid residues that are conserved across all homologues and grey highlight indicates similar amino acid residues that are similar between homologues.

```
NbBs4C.2 MVTIDHLDLRHTMLVLVNILKSGVGPPWQWNPFNVVAV-------PHQFTLMEAVILLFT  53
NbBs4C.3 MVTIDNFDLRHTILVLVNILKSGIGPPWQWDSFNVVAV-------SHQFTLMEAVILLFT  53
CaBs4C.4 ----MEFDLRYTILIIVNILKSI-FISNEWDPFHIFVQ-------LTFMAFMNRLFLLLL  48
CaBs4C.3 ----MEFDLRYLILIIVNILKSI-SPSENWDPFHIFGN-----PIPSFITFMNRLAFLFL  50
CpBs4C   ----MEFDLRYLILILANMLKSILSISDNWDPFHIFHD------HPSFIVFINKLFFLFI  50
CaBs4C.1 ----MEFDLRYFILILANMLKSILSISNNWDPFHIIGN-----PIPSFMTFMNRLFFLFI  51
NbBs4C.1 ---MRLVELRYIILMLINIFKSMMGSSSDWDPFHILNHNSFP-------SFINKILFLLL  50
SlBs4C   ---MRIFDLRYIILMLINIFKS---TSSDWDPFHLLLYYDFDPILFSFIIHINKILLLIS  54

NbBs4C.2 F-IIFSFTSIKVHPRSEQW----------------------QICIRLGDFSTSLTLLLL  89
NbBs4C.3 F-IIFSFTSIKVHPRSEQW----------------------QICIRVGDFSRSLTLLLL  89
CaBs4C.4 FSFIFSITSITIHYPMRVH-IS-------------------------STYFSKSFNILFL  82
CaBs4C.3 FSFIFSITRTTLHHPIIRIRISITFSKSFIFSITRTTLHHPIIRIRISITFSKSFNILCL 110
CpBs4C   FSFIFSITRITLHHPNIRIRVRTTT----------------------SADLSKSFNILCL  88
CaBs4C.1 FSFIFSITRMTLHHPIIRIRVSI-------------------------TFSKSFNILCL  85
NbBs4C.1 FSFIFSITSITV----DTTT-------------------RPISIHICIGNFSKSFNGLFL  87
SlBs4C   LSFIFSIISIRIIHMTNYSN-------------------RPINIKIQFGTFSKFFKILCI  95

NbBs4C.2 VCLVVPKFIFWYAYPMIILISM----NYTWLAKTFNTFLDWLQGMSPS--MPVFNSFVVT 143
NbBs4C.3 VCLVIPKYIFWYAYPMIILISM----NYTWLAKTFNTFMDWLQGMSPS--MPVFNIFVVT 143
CaBs4C.4 TSFLLPQVLFWYIFFITIMT-F----PSNWISNF----KE--WSLYIISIIPGFSIFINA 131
CaBs4C.3 ASLLLPQMLFWYFFFITITLSS----CSSWIGNAWASFRQPTLHIFST-IFPAVSIFINV 165
CpBs4C   ASLLLPQMLFWYFFVIIIALSS----CSSWIGNTWASFRQRILHIFSTIIFPAVSIFINV 144
CaBs4C.1 ASLLLPQMLFWYFFFIIITLSL----CSSWIGNTWASFRQRILHIFSTIIFPAVSIFINV 141
NbBs4C.1 ASFVIPQVLYWYIFFITIILSSLI--SCYWVSNTCNRFWDCALGILST--IPLLKIFINA 143
SlBs4C   ITLLLPQVLFWYILFIIILFSLLFMSCPNWISNLCE----WTLHILST--IPVLTIFICA 149

NbBs4C.2 TLATTSPDHEDQQPSSGHEAV*--------- 164
NbBs4C.3 TLATANLNHEDQQPSSGHEAV*--------- 164
CaBs4C.4 ELDRNNVNNQQPQAQTIHLLLPV*------- 154
CaBs4C.3 EFDRNTV-SQQHETQTTRLLSLV*------- 187
CpBs4C   EFDRNNV-SQQHETQTNRLLV*--------- 164
CaBs4C.1 EFDRNNVISQQHETQTNHLLSLV*------- 164
NbBs4C.1 EIHSSGNEDQQSPV*---------------- 157
SlBs4C   QLDNNDEN-YLLPIHRTQPTITDGTDTGIE* 178
```

S3. dTALE effector binding sites in the upstream sequences of the *NbBs4C* paralogues. Grey highlight indicates coding sequence (CDS). Bold font indicates the start and stop codon. Underline font indicates effector binding site.

>*NbBs4C.1* (dT779)
AAAGCCAGAACAAGTTTAAAAAATGATGTATCCAACCATATAAAAGATTAATTATTTCCAAATATTTATATATAT
TGCTTATAGAAAAATATTTGCAACTTCTATAACAATTATCATAGCGGAAAAAAGTTTATTAAAATTAAAATTAAA
ATTTTATTCAAGACCAATACTGTCTAAAAAAATTAAATAGAGTAATTTTGTATTTATAAATTTTAAGACAAATTT
GGGGCCTCTTATTGAAGTTTGGCTTTAGGCCACCAACTTTATTGAGCCGACCCAAGGGGCATAAAACACCTTGTA
TTTATAGTGTAGACACTTTATTCTAATAGTAATATTAATGATTATTTATATGATTTGAACTCGTAACTTATATAC
CGGCAATACACTATTGTTTCGAAGCTTTCTTCTACCTTTGATAATAGGAGTAATATAACTCCAATAACATAATAA
CCCAAGGGTAACACAAGGTTTAAAAATGTTATAGTACGTCAGCCTACTTTTGTTATAATATAAGTATTTGTTATT
TTAATTTTTAACCGGAAAAAAAGTGCTTCAGCAGAAAAAGATGAGGAAAACTGAAGAACCATTGCGTCACCTTCC
ACTTCCATATCCAAACCCCACCAATCTTTTCTCCTTCCTTATAAATTCAAGTGAGATAAAACTTATTTTTTGAAC
AAACCAAAAAAGAAGAAGAAAAGAA**ATG**AGATTGGTAGAGCTAAGGTACATTATATTGATGTTAATCAACATCTT
CAAATCTATGATGGGATCATCTTCTGATTGGGATCCTTTCCACATATTAAACCATAATTCTTTTCCAAGTTTCAT
TAATAAAATCCTTTTTCTTTTATTATTTTCCTTTATTTTCTCCATCACCTCTATAACAGTTGACACAACTACTCG
TCCTATCAGTATACACATTTGCATTGGAAATTTTTCCAAGTCCTTCAATGGTTTATTTCTAGCCTCATTTGTAAT
CCCTCAAGTGTTATATTGGTACATTTTCTTCATTACTATTATACTTTCTTCATTAATATCTTGTTATTGGGTTTC
TAATACATGCAACCGTTTTTGGGACTGCGCTCTGGGCATACTCTCCACTATTCCACTTCTTAAAATTTTCATCAA
TGCTGAAATTCACAGCAGTGGGAATGAAGACCAGCAGTCTCCAGTC**TAA**

>*NbBs4C.2* (dT780)
GGCGAAGACTAACTGTTGGGTAAGTAACCACATAGCCAAAGTCTACCTGTGAAGGTCACTATCAAAAAGCTAGAA
GCATTTGATGTGGGAGTCAACCTGAGAGGAGGCATTAAACCCTTAATTGCAGATTTATACAACCCAAAAACGCAC
AAAATGTTAAGTCAATATAATGTACTAGCAGTTTCTGTCGACCAGCTGCTCTATATTAGTTCTTTCTCCGTTTAA
TATTGTTTAAGCTAGTTTGATTCGGCGAGTTTAAGAAGAAAAAAAAAAGACTTTTGATCTTAAAAATTTAAAGAG
TAAAAAGTTTGTGATGTCATACCATTTGTGTGGATATAAAAACTTCTCATTGAGAGCAAAAATGGTAAAATAATT
AAAGAGTTTAAAGTTGTATTATTTCCAAATTTAAAAATGTATCATTTATTTTGAAACTGACTAAAAAAACATCTC
AACGGAGGAAGTAGTACCATTTTGTTTCAGCGACTTCACTTATGTAGTCAGTAGTCAGAAGTCAACATATACATG
TCCTTAAGTATCATAGGATTTGTAAGTTTTGACCCATAATGCTCTGTTATTCCTATCACCACCTTAACCTCATAG
TAGGAAAATTGGTAGTATTACACCTGTTATGATTTATATAAACTTGGAAAGATTAAGACATCTTCTACAATATCA
TCTACAGAGGTTCTGAAGGAAACAA**ATG**GTGACCATTGATCATCTTGATCTTAGGCACACTATGTTAGTGTTAGT
AAACATTCTCAAATCTGGAGTGGGACCTCCCTGGCAATGGAATCCGTTCAACGTTGTAGCAGTTCCTCACCAGTT
TACTTTAATGGAAGCTGTCATTCTTCTCTTCACGTTCATCATCTTCTCCTTCACCTCCATAAAAGTTCATCCCAG
AAGTGAGCAGTGGCAAATATGTATAAGACTTGGAGATTTCTCCACAAGTCTTACTCTATTATTGCTGGTCTGTCT
GGTAGTACCAAAATTTATATTTTGGTATGCATATCCCATGATCATATTGATATCCATGAATTATACTTGGCTTGC
CAAGACTTTCAATACTTTCCTGGATTGGCTACAAGGAATGTCTCCCTCAATGCCTGTTTTCAATAGTTTCGTCGT
AACAACACTTGCCACTACCAGTCCGGACCATGAAGATCAGCAACCTAGTTCAGGGCATGAAGCAGTT**TAA**

>*NbBs4C.3* (dT782)
TTATAATTTCTGGGTGGGCTAATTTTGGACCAATGTAAGTAGGCCACGTGTTTAAAAAACTTGAGGAAACCAGGT
TTAACGGTGGAAGGGTATATGTGGCCCGAATGTGTAACGGTGTGGGTATATTTGTCAAAGAATTCAAACGGAGTA
TAAATGTAGCTTATTTTGAATAGTACAAGGGCAAATCCGACCCTTAACCGTTTTAAATTTGATCTTTTTCTTGCC
AGCTACAGCAGTCGGAAAAGGCAAATATAGAGCAGAAGGCGAAGACTAACCGTTGGGTAAGTCAGAACCACATAG
CGAAAGTCTACCTATGAAGGTCACTGAAAAGAGTGTATCAAAAAGCTAGGAGCATTTGATGTGGGAGTCAACCTG
AGAGGAGGTATTAAGCCCTTAATTGTAGATTTATACAACCCAAAGACACATAAAGTCAATATAATGTTGCAGTTT
CTGTCGACCAGCCGCTCTTAGTTAACATTTTGCTTCAGCAACTTGACTTATGTAGTCAGTAGTCACAAGTCAACA
TATACATGTCCTTAAGTATCATAGGATTTGTAAGTTTTGACCCTTATGCTCTTTTGTTCCTACCACTACCTAGCC
TGCTAGTAGGAAAATTGGGATTGCACCTGTTATGATCTATATAAACTCGGAAAGGTTAAAACATCTTCTACAATA
TCTACGGAGATTCTGAAGGAAACAA**ATG**GTAACCATTGATAATTTTGATCTTAGGCACACTATCTTAGTGTTAGT
AAACATTCTCAAATCTGGAATTGGACCTCCCTGGCAATGGGATTCGTTCAATGTTGTAGCAGTTTCTCACCAGTT
TACTTTAATGGAAGCTGTCATTCTACTCTTCACGTTCATCATCTTCTCCTTCACCTCCATAAAAGTTCATCCCAG
AAGTGAGCAGTGGCAAATATGTATAAGAGTTGGAGATTTCTCCAGAAGTCTTACTCTATTATTGCTGGTCTGTCT
GGTAATACCAAAATATATATTTTGGTATGCATATCCCATGATCATATTGATTTCCATGAATTATACTTGGCTTGC
CAAGACTTTCAATACTTTCATGGATTGGCTACAAGGAATGTCTCCCTCAATGCCTGTTTTCAATATTTTCGTCGT
AACAACACTTGCCACTGCCAATCTAAACCATGAAGATCAGCAACCTAGTTCAGGGCATGAAGCAGTT**TAA**

S4. DNA alignment of the 700 bps upstream of the ATG of the *N. benthamiana Bs4C* paralogues. Black highlight indicates base pair that is conserved across all paralogues and grey highlight indicates similar base pairs that are similar between paralogues.

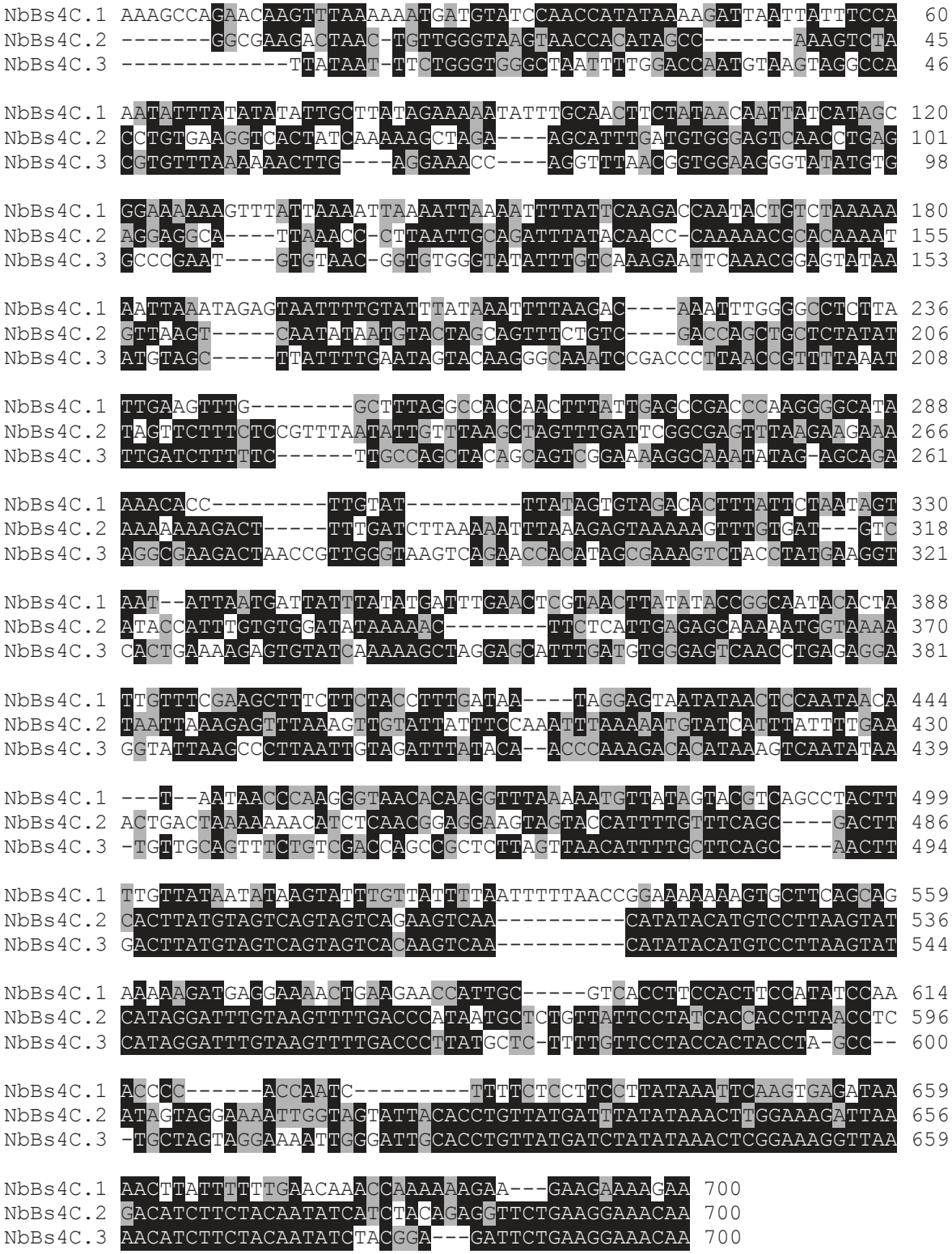

S5. Pairwise comparison of the 700 bps upstream of the ATG of the *N. benthamiana Bs4C* paralogues. Numbers in the box indicate the % identity between the two indicated upstream sequences.

		NbBs4C.1 700 bp upstream ATG	NbBs4C.2 700 bp upstream ATG	NbBs4C.3 700 bp upstream ATG
		1	2	3
NbBs4C.1 700 bp upstream ATG	1		38.90	35.86
NbBs4C.2 700 bp upstream ATG	2	38.90		56.83
NbBs4C.3 700 bp upstream ATG	3	35.86	56.83	

20% 60%

S6. Structural predictions of enterotoxin (PDB#: A0A854AC01) and verotoxin (PDB#: A0A141AZM3) from the AlphaFold Protein Structure Database (https://alphafold.ebi.ac.uk/).

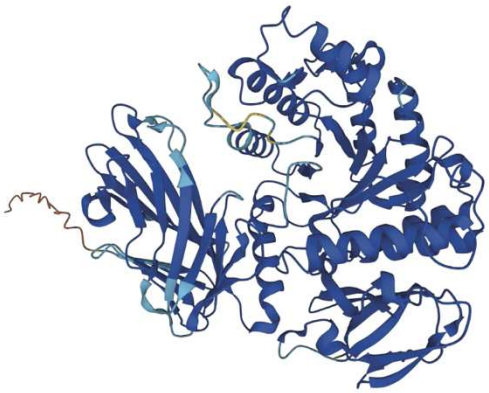

Enterotoxin
PDB# A0A854AC01
E. coli

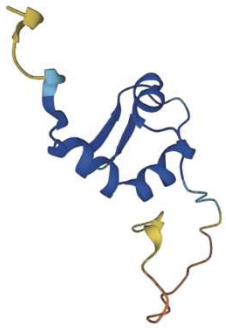

Verotoxin
PDB# A0A141AZM3
E. coli

Table 6.4. CpBs4C homologues found in Capsicum baccatum and Capsicum chinense.

Species	Chromosome	% identity to CpBs4C	Annotated in genome?
Capsicum baccatum	1	78.53%	No
Capsicum baccatum	7	48.15%	No
Capsicum baccatum	9	62.86%	No
Capsicum baccatum	11	68.57%	No
Capsicum baccatum	12	25.77%	No
Capsicum chinense	1	75.15%	No
Capsicum chinense	5	53.19%	No
Capsicum chinense	6	68.57%	No
Capsicum chinense	7	59.62%	No
Capsicum chinense	9	58.57%	No

CpBs4C homologues identified using tblastn on the *Capsicum baccatum* genome (assembly ASM227188v2) and the *Capsicum chinense* genome (assembly GCA_026120095.1). % identity refers to the percentage of amino acid identity similarity between the indicated protein and CpBs4C.

7. LIST OF FIGURES AND TABLES

7.1. List of Figures

7.2. List of Tables

8. ACKNOWLEDGEMENTS

First and foremost, I would like to thank Prof. Dr. Thomas Lahaye for being an exceptional supervisor, allowing me to run with this project and supporting me to follow the strange and peculiar leads that arose. Thank you for giving me the independence to make this project my own, and for always taking the time to discuss the experiments and the science.

Many thanks to Prof. Dr. Suayb Üstün for being an awesome mentor and committee member and for pushing me outside my comfort zone to explore new areas of molecular biology, and for reviewing this thesis. Thank you to Prof. Dr. Rosa Lozano-Durán and Dr. Farid El Kasmi for guiding aspects of this project, and for being on my committee and examination panel.

Thank you to all members of AG Lahaye, specifically Dr. Annett Strauß and Dr. Robert Morbitzer, for the fruitful scientific discussions, experimental advice, and practical help that they all gave so selflessly.

A huge thank you to all of the collaborators that made this work possible: Gautier Langin, Dr. Julien Gronnier, Kaltra Xhelilaj, Dr. Shouguang Huang, Dr. Rainer Heidrich, Dr. Hequan Sun, Dr. Korbinian Schneeberger, Dr. Johannes Stuttman, and Dr. Zangjun Fei.

A warm thank you to my closest friends who made this journey an enjoyable and memorable one.

Last but not least, a massive thank you to my parents and sister for their constant support and encouragement. This thesis would frankly not be possible without them or their unwavering commitment to helping me achieve my goals.